IMPERIAL COLLEGE OF SCIENCE TECHNOLOGY AND MEDICINE
UNIVERSITY OF LONDON

INSPECTION OF COMPLEX STRUCTURES USING GUIDED WAVES

by

Naresh Juluri

A thesis submitted to the University of London for the degree of
Doctor of Philosophy

Department of Mechanical Engineering
Imperial College London
London SW7 2AZ

February 2008

Dedication

This thesis is dedicated to

My
Parents

and my
PhD Supervisors

Prof Peter Cawley
And
Prof Mike Lowe

For their invaluable support during my research work

Abstract

Experimental observation has shown that a compression wave (similar to the Lamb wave S0) travelling along a weld between two plates is strongly guided by the weld and so does not decay as quickly as it would in a plain plate. This phenomenon is attractive for Non Destructive Evaluation (NDE) of welds because it may offer the potential to inspect long lengths of welds using a wave which travels along the weld and is guided by it. In order to understand the phenomenon, studies have been carried out on a variety of structures. Finite element, semi analytical finite element simulations and experimental measurements of waves propagating along these structures have revealed the physics behind the phenomenon.

Studies have been conducted on structures where a medium, in which the wave is slower, is embedded in a medium, in which the wave is faster, and from these studies it is understood that a trapped mode is generated in a medium when it is embedded in a faster medium. It is also understood that this trapped mode decays less than the S0 mode in a plain plate because of its one dimensional propagation, and can potentially be used to inspect long lengths of slower medium from a single location. Numerical and experimental studies proved that the trapped mode exists in the weld and in the region near the weld and therefore it is also possible to inspect defects in the region near the weld or heat affected zones using the trapped mode.

The trapped mode generated in the slower medium decays as it leaks bulk longitudinal and shear waves into the surrounding faster medium. The attenuation of the trapped mode in the slower medium increases as the impedance difference between the slower medium and the surrounding faster medium decreases and it shows zero attenuation at frequencies where the trapped mode is slower than both bulk longitudinal and shear waves.

This thesis discusses the nature of the trapping effect, illustrates the effects, and proposes its potential for practical NDE of welds and other geometric features where a slower medium is embedded in a faster medium.

Acknowledgements

I would like to thank Prof Peter Cawley and Prof Mike Lowe for their invaluable guidance and support throughout this research project, without whom the work could not have been accomplished.

I would like to thank Dr Michel Castaings, University of Bordeaux, France and Mr Zheng Fan, NDT Lab, Imperial College for their collaboration and support in the SAFE analysis.

I would also like to thank all members of the NDT Lab at Imperial College London and particularly to Dr. Prabhu Rajagopal for many useful discussions, technical and otherwise.

Contents

Chapter 4
Study of the trapped S0-like mode using Semi Analytical Finite Element method

Chapter 5
Application of the trapped S0-like mode for real welds

Chapter 6

Interaction of the trapped S0-like mode with defects in the weld and in the region near the weld

Chapter 7

Conclusions and Future work

List of Figures

Chapter 1
Introduction and Overview

1.1 Motivation

Routine maintenance of large structures, like storage tanks, in service usually requires implementation of Non-destructive testing (NDT) techniques. Conventional inspection is based on either visual inspection or one of the different non-destructive inspection methods developed in the mid-50s or earlier such as Radiography [1], Eddy current [2-4], Bulk wave ultrasound, Dye penetrants and Magnetic flux [5, 6]. Non-destructive testing and monitoring of these structures interrogate discrete points and are therefore very time consuming [7, 8]. Furthermore, there are many cases where the structure is inaccessible or it is often necessary to physically enter into hazardous areas and conventional inspection methods are no longer practicable. Alternate remote inspection methods would be highly desirable in these cases.

It is therefore useful to introduce at the very first stage of an inspection process a screening procedure which is fast and sufficiently accurate to identify the areas where there is a defect. When a preliminary fast screening test is performed, the use of conventional NDT techniques can focus on the classification of the severity of defects in the areas previously identified by the screening technique. Effectively, the implementation of a complementary fast screening technique enables the achievement of inspection against the conflicting goals of the reliable detection and sizing of defects and the reduction of the overall inspection costs.

Guided waves offer an attractive solution to this as they enable a large area of structure to be tested from a single transducer position, avoiding the time-

consuming point by point scanning required by conventional inspection methods. The technique is even more attractive when part of the structure is inaccessible.

Large plate structures are generally made by joining (welding) small or medium size plates together. This process results in long lengths of welds in the structure and any defects are mainly found in the welds and heat affected zones. An example of a long length of weld in an oil storage tank is shown in Figure 1.1. Sometimes the access to these welds is difficult (e.g. storage tanks and hull structures in ships and submarines) and it is often necessary to undertake an internal examination, requiring emptying of the tank and the entry of a person into a potentially hazardous area. Therefore an alternative remote method for assessing the health of the welded joints with restricted access, without emptying the tank, is sought. This thesis looks at guided wave screening methods for long lengths of welds.

1.2 Introduction and background to Guided Waves

A guided wave is an ultrasonic wave whose energy is concentrated near a boundary or between parallel boundaries and the direction of propagation is effectively parallel to these boundaries. A guided wave can be thought of as a superposition of shear and/or longitudinal waves that propagate in a structure and get reflected back and forth between the boundaries of the structure. A guided wave is described by the wave number projection onto the propagation direction and a mode shape. In contrast to bulk waves the propagation of these waves is dispersive ,i.e., wave length and propagation velocity depend on frequency.

Chapter 1
Introduction and Overview

The propagation of guided waves in free plates was first studied by Lamb [9] and guided waves in plates are called Lamb waves. For a given plate thickness and an acoustic frequency, there exists a number of propagating modes. Two types of modes are possible in a plate structure: symmetric and anti symmetric. Symmetric modes have a symmetric wave structure with respect to the mid plane of the plate and anti symmetric modes have an anti symmetric structure with respect to the mid plane of the plate.

Several methods exist for defining the characteristics of propagating guided waves in an elastic plate. The two most popular are the method of potentials and the partial wave technique[10, 11]. The following equations give the dispersion relations for guided waves obtained using the method of potentials[11].

$$\frac{\tan(qh)}{\tan(ph)} = -\frac{4pqk^2}{(q^2-k^2)^2} \qquad \text{for symmetric modes} \qquad (1.1)$$

$$\frac{\tan(qh)}{\tan(ph)} = -\frac{(q^2-k^2)^2}{4pqk^2} \qquad \text{anti-symmetric modes} \qquad (1.2)$$

$$p^2 = \frac{\omega^2}{c_L^2} - k^2 \qquad and \qquad q^2 = \frac{\omega^2}{c_T^2} - k^2$$

where

k – Wavenumber, ω - Angular frequency

c_L, c_T - Bulk longitudinal and bulk shear wave velocities

The value of the wave number k for these waves is found by solving the above equations numerically. DISPERSE[12, 13], a software package developed in the NDT lab, Imperial College, provides a useful tool to find these solutions.

A complete description of such propagation characteristics for plates is normally given in the form of a set of dispersion curves, illustrating the plate-mode phase velocity as a function of the frequency–thickness product. Each curve represents a specific mode, which is conventionally called A_0, S_0, A_1, S_1 etc. where A_n denotes antisymmetric modes and S_n symmetric modes [11]. Figure 1.2 shows wave number dispersion curves and Figure 1.3 shows phase velocity dispersion curves for a 1 mm thick steel plate. The red curves are dispersion curves for symmetric modes and blue curves are anti symmetric modes.

The use of ultrasonic waves is well established in non-destructive testing (NDT) in industry. Most standard tests for locating defects involve the excitation of a bulk wave in the material. Bulk waves are used more than guided waves in the industry because they offer the advantage of being easy to understand and easy to use. Only two types of waves can propagate in the bulk of the material: Shear and longitudinal. The velocity of these waves is constant with frequency. The measurements are performed by using transducers in two possible configurations, pulse echo when the emitter is used to receive the ultrasonic signal and pitch-catch when the receiver and emitter are two different units. Simple velocity and attenuation measurements can give accurate analysis of the health of the structure being monitored. The use of bulk waves in NDT is a well documented subject[14, 15].

The main difference between bulk and guided waves is that bulk waves travel in the bulk of the material, away from the source, and guided waves travel either at

the boundaries or between boundaries. The propagation of bulk waves is 3 dimensional whereas the propagation of guided waves is either one dimensional (e.g. pipes) or 2 dimensional (e.g. plates). Because of this property of guided waves, they can travel longer distances. Hence, a large area of the test structure can be inspected from a single location. However, guided wave inspection is complicated by the existence of at least two modes at any given frequency. In practice, it is difficult to generate a pure mode, particularly above the cut off frequency of the 'A1' mode. Therefore, the received signal generally contains more than one mode, and the proportions of the different modes present are modified by mode conversion at defects and other impedance changes. The modes are also generally dispersive, which means that the shape of a propagating wave changes with distance along the propagation path. This makes interpretation of signals difficult and also leads to signal-to-noise problems since the peak amplitude in the signal envelope decreases rapidly with distance if the dispersion is strong[16, 17]. All the above elements lead to complex response signals which are difficult to analyse and interpret.

Although Lamb produced the dispersion equation for acoustic wave propagation in plates in 1917[9], it was not until 1961 that Worlton [18] gave an experimental confirmation of Lamb waves at megacycle frequencies and that Lamb waves can be used for non-destructive testing purposes. Worlton [18] noted that Lamb waves effectively revealed sub surface laminar flaws and overcame some of the problems encountered in conventional ultrasonic testing such as near-surface defects. Since then much work has been carried out on the use of Lamb waves and other guided waves. A good review can be found in[8, 19-21].

In general, guided waves are used for two different purposes. Firstly, there is short range propagation, where guided waves may be used at relatively high frequencies in preference to conventional techniques. This purpose includes material characterisation [22] and the detection of defects close to interfaces[23, 24]. In these cases the dispersion is not of such importance as the wave propagates over short distances but the sensitivity is a key factor. The second purpose is in applications where the wave propagates over long distances.

A large number of workers have recognized the advantages of using guided waves for fast inspection[7, 25-27]. Guided waves have been widely applied for fast screening of pipe lines[27-30]. Guided waves have also been applied to inspection of plate structures and composites[31-33]. Due to the complexity of the guided wave propagation, the practical testing of plates needs to be optimised depending on the specific guided wave application. Many authors have reported on the optimization of the use of guided waves for detecting defects[21, 34, 35].

A fast screening technique for pipe testing using guided waves was developed in the NDT lab at Imperial College[36]. This is capable of screening long lengths of pipes. Cylindrical guided waves are excited at one axial location using an array of transducers distributed around the circumference of the pipe. These waves stress the whole pipe wall and propagate along the length of the pipe; they are partially reflected when they encounter features (such as welds, branches, drains, corrosion etc…) that locally change the geometry of the pipe. The technique is capable of detecting corrosion defects removing 5 to 10% of the total cross sectional area at any axial location.

A medium range plate inspection technique for detection of corrosion in large areas of thick plates without features has been developed at Imperial College[14]. This technique can be used for inspection of large structures such as storage tanks if the structure has no features like welded joints. However this technique, in its present stage, is not capable of inspecting plate structures with many features, which is the motivation for this thesis.

Experimental observation has shown that a compression wave (similar to the Lamb wave S0) travelling along a weld between two plates is strongly guided by the weld and so does not decay as quickly as it would in a plain plate[37]. This phenomenon is believed to occur principally because of the geometry: the compression wave in the weld is slower than that in the plate at the operating frequency even though there is no material property variation between the plate and the weld. Therefore the weld acts as a slower medium (in which the wave is slower than that in the plate) and the plate acts as a faster medium (in which the wave is faster than the weld) for the compression wave.

As the slower weld is embedded between two faster plates, some part of the energy is trapped in the weld, which is analogous to optical waveguides[38], resulting in a trapped guided mode within the weld. This trapped guided mode is guided by the weld and propagates along the weld. The trapped guided mode is expected to decay less than the S0 mode in a plain plate as the propagation of the trapped guided mode is one dimensional, along the weld, whereas the propagation of the S0 mode in a plain plate is two dimensional with cylindrical spreading. This trapped guided mode is very interesting for NDE of welds and

other joints where the wave in the joint is slower compared to the wave in the surrounding material, as it decays less than the S0 mode in a plain plate and thus can be used to inspect longer lengths of welds and joints from a single location. This thesis investigates the nature of the trapping effect, illustrates the effects, and proposes its potential for practical NDE of long lengths of welds and other geometric features.

1.3 Outline of thesis

Chapter 2 mainly concentrates on Finite Element modelling of large geometries. A large amount of time during my PhD work was spent on dealing with large 3D FE models, and this chapter discusses the difficulties encountered when dealing with large geometries and their solutions.

Chapter 3 presents experimental observations of energy trapping within the weld and explains the reasons for this energy trapping. Studies have been conducted to understand the characteristics of the trapped guided mode, over a range of possible test frequencies, in order to fully exploit the trapped guided mode for NDE of long lengths of welds. This chapter presents the attenuation characteristics of the trapped guided mode in idealized welds (simplified weld geometries), at different frequencies and the reasons for the attenuation of the trapped guided mode are discussed.

Chapter 4 presents the use of semi analytical finite element models with absorbing regions to study the trapped guided mode. The Semi Analytical Finite

Element (SAFE) method has been used as very large 3D FE models were not possible because of the computational limitations and analytical methods such as transfer matrix method and surface impedance matrix method cannot be used to find dispersion relations of guided modes in structures with an arbitrary cross section.

Chapter 5 concentrates on the applicability of the trapped guided mode for inspection of long lengths of real welds. The attenuation characteristics of the trapped guided mode in real welds are discussed and compared with the attenuation characteristics of the trapped guided mode in idealised welds explained in chapter 3.

Chapter 6 presents the interaction of the trapped guided mode with different kinds of target defects. Defects such as cracks, notches and circular defects are studied. The interaction of the trapped guided mode with defects both in the weld and in the region near the weld are studied and discussed. The conclusions of the thesis are presented in chapter 7.

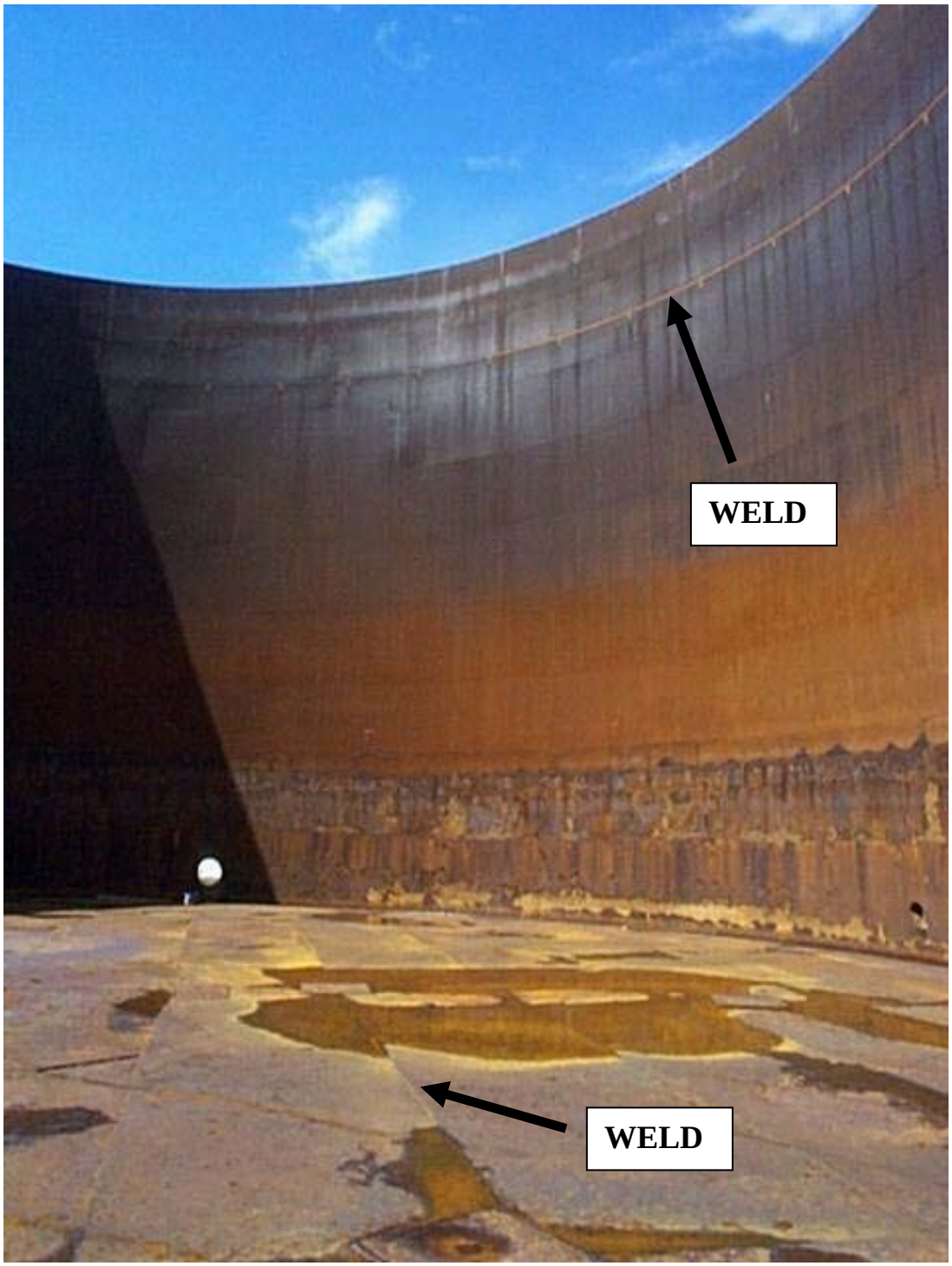

FIGURE 1.1: Long lengths of welds in an oil tank

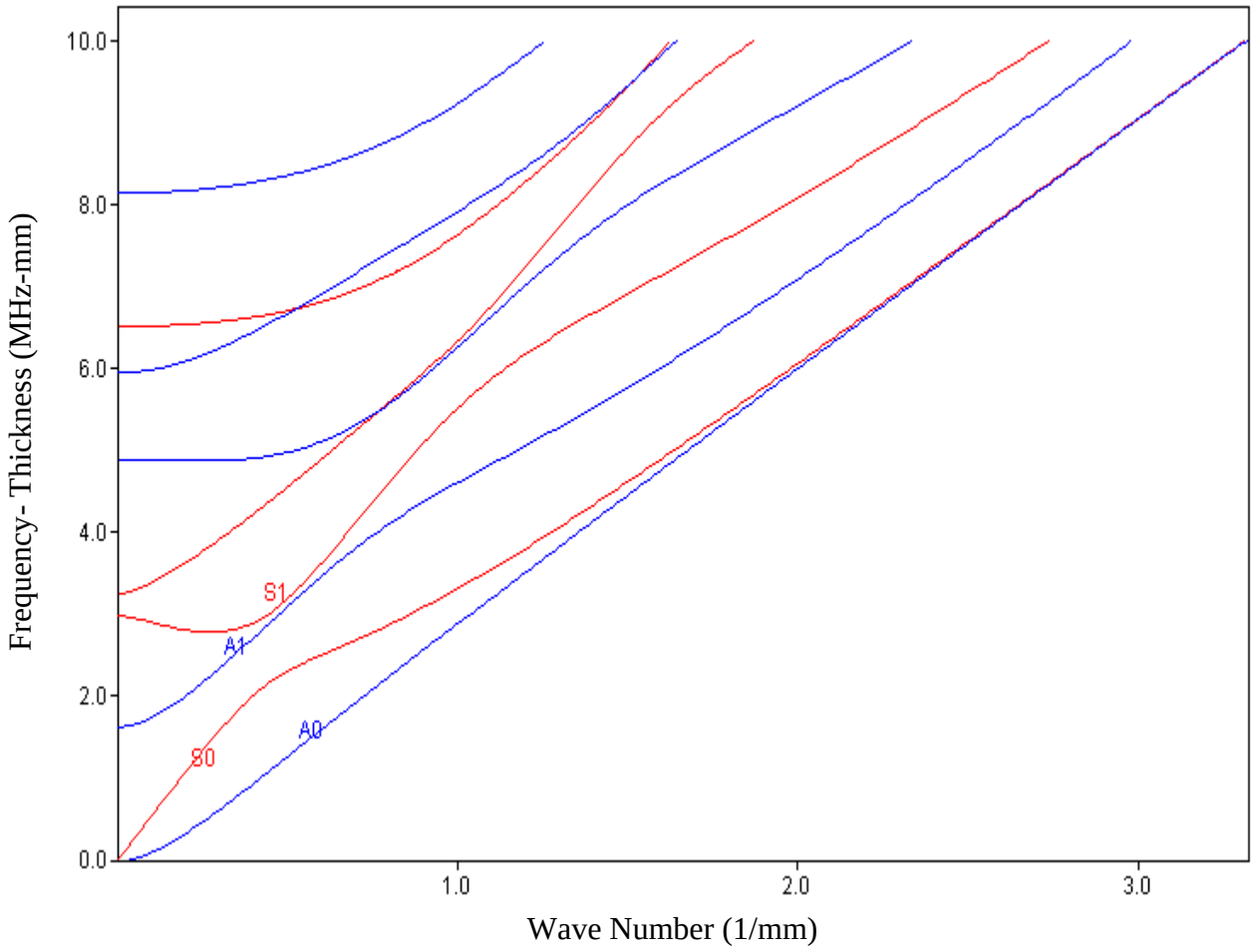

FIGURE 1.2: Wave number dispersion curves for a 1 mm steel plate

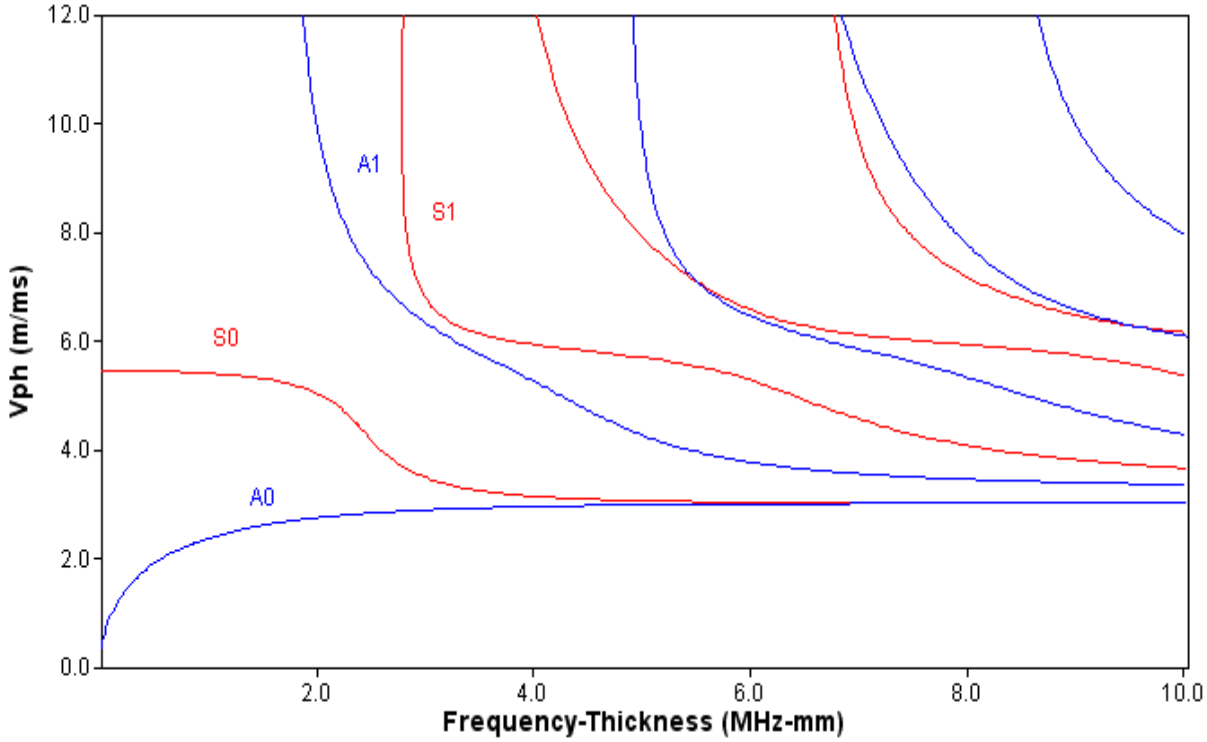

FIGURE 1.3: Phase velocity dispersion curves for a 1 mm steel plate

Chapter 2
Finite Element Modelling of Large Geometries

2.1 Introduction

One approach to modelling guided wave propagation phenomena is to solve the governing differential equations of motion and their associated boundary conditions analytically. However, these equations become intractable for complicated geometries. Another approach to this problem is a numerical solution; the main advantage of this approach is that the difficulties associated with complicated geometries and defects are much easier to handle numerically. Many numerical tools have been used in the past to study wave propagation in structures; Finite Difference[39], Boundary Element[40], Finite Element[41-44].

The Finite Difference (FD) method simplifies the problem of the solution of the differential equations of wave motion in a continuum by discretizing them into a set of difference equations, in which the field variables are defined at the nodal intersections of the grid. The Boundary Element (BE) method converts volume integrals into surface integrals with the aid of the Green's functions. In the boundary element method elements are placed over the boundary of the solid under investigation and over defects within the structure. In the Finite Element (FE) method, the structure is divided into a finite number of elements of finite size, which are connected to the rest of the structure by the boundaries of the elements.

The most attractive feature of the Finite Difference method is that it is very easy to implement. The Finite Difference method in its basic form is restricted to handle rectangular shapes and simple alterations. Another practical problem in the Finite Difference formulation is the difficulty in defining stress free boundary

conditions, which are very common in NDT. The BE method has the advantage that just the surface of the specimen needs to be discretised; the numerical problem itself is therefore reduced by one dimension. However, for many problems boundary element methods are significantly less efficient than volume-discretisation methods (Finite Element, Finite Difference, and Finite Volume)[46]. Handling of geometries in FEM is theoretically straightforward and another primary advantage of the FE method is that there are numerous commercial FE codes available, thus eliminating any need to develop actual code. These commercial FE codes have the additional advantages of being very user friendly, and providing sophisticated pre and post-processing options. Thus the FE method has been widely used in the past to study wave propagation[19, 47].

The time domain finite element model enables the wave propagation along a structure to be simulated. The temporal discretisation may be obtained using a finite difference approximation. Both implicit and explicit schemes can be used for this purpose [47]. In implicit schemes the dynamic equilibrium is satisfied at the end of each time step and the displacements are obtained by solving the wave equation. The main disadvantage of using this procedure is that the inversion of a matrix of the order of the number of degrees of freedom is needed; on the other hand large time steps are allowed. Explicit schemes solve the wave equation only at the beginning of the increment[43, 44]. In this scheme the mass matrix is diagonalized, thus the accelerations at the beginning of the time step are calculated simply by using the net mass and force acting on each element. Therefore this scheme does not require any large matrix inversion. The

accelerations are then integrated twice to obtain the displacement after a time step Δt. Since the method integrates constant accelerations, the time increments must be quite small for the method to produce accurate results, so that the accelerations are nearly constant during the increments.

The spatial and temporal discretization of the finite element model must be carefully assigned in order to ensure the convergence to the correct solution[48]. For the FE model (2D or 3D) to have a convergent solution, the time step must be chosen according to the following rule [48].

$$\Delta t < 0.8 \frac{\Delta x}{V_{\max}} \tag{2.1}$$

where $V_{\max}$ is the velocity of the fastest wave and Δx is the element size. In order to accurately model a wave it is necessary to have at least 8 elements for the shortest wavelength [48], within the bandwidth of the signal, of any waves which may travel in the waveguide.

One of the biggest problems of any FE analysis of wave propagation is the model size. Monitored signals are often complicated by the existence of more then one mode at any operating frequency and the reflections from boundaries and other geometrical features of the model. It is difficult to separate the signal of interest from other unwanted signals. This problem becomes worse if the structure is complicated with the presence of other geometrical features[16, 17, 49]. At low frequencies, guided waves have large wavelengths. For example the A0 mode at 20 kHz in a 1 mm steel plate, has a wavelength of 22 mm so a 5 cycles tone burst

occupies about 110 mm in space; S0 at 100 kHz in a 1mm steel plate, has a wavelength of about 50 mm so a 5 cycles tone burst occupies about 250 mm in space. The models must be large enough in order to separate the signal of interest from other unwanted modes and reflections from boundaries. At high frequencies, guided waves have smaller wavelengths. However it is still difficult to separate the signal of interest from other signals because of many modes present at these frequencies.

It is not possible to model very large geometries because of computational limitations. This has been the main limitation for previous studies found in the literature and that is why there is little literature available on modelling of 3D structures for wave propagation. Practically it is not possible to model large 3D geometries with "brick" elements with the available computational resources, though the available computers in the NDT lab at Imperial College are capable of dealing with models up to 25 million degrees of freedom. Our experience of working on large FE models suggests approximately that 'X' GB RAM is required in order to run a model with 'X' million degrees of freedom.

During the course of my PhD, the following techniques have been investigated to solve the above model size problem to some extent, as explained in the next few sections.

- Use of Shell elements for modelling of the A0 mode at low frequencies.
- Signal subtraction technique.
- Absorbing layers with increased damping to avoid reflections from far edges.

This study started with studying the applicability of the low frequency A0 mode for inspecting complex structures like ship structures and aircraft fuselages. During initial days of my work, The use of shell elements for modelling of the A0 mode at low frequencies to solve the size problems of FE models has been investigated. Shell elements can only be used for very low frequency A0 mode modelling and can not be used for modelling the S0 mode as explained in appendix 'A'. However the other two techniques, the signal subtraction technique and the Absorbing layers with increased damping, can be used to model any mode at any frequency. Subsequently low frequency A0 inspection has been omitted and the trapped guided mode was concentrated as it was found to be more promising because of its one dimensional propagation and zero decay at some frequencies. As the rest of the thesis talks about trapped guided modes, the details of shell element modelling are separated from this chapter and presented at the end of the thesis in appendix 'A'. The details provided in Appendix 'A' may be useful for people who work on modelling the low frequency A0 mode.

2.2 Signal subtraction technique

The signal subtraction technique is a technique where the signal of interest is separated by obtaining two signals from two separate FE models; one being the model studied and the other being a model with different dimensions where the signal of interest or the signal that interferes with the signal of interest is not present, and subtracting one signal from the other. The following two cases explain the signal subtraction technique with examples.

- Oblique incidence of A0 with an edge
- Oblique incidence of A0 with a weld

2.2.1 Oblique incidence of A0 with an edge

Figure 2.1(a) shows the FE model studied. This model has been used to study the reflection of A0 from an edge at oblique incidence. The model has been excited at point A, as shown in the figure, using a 5 cycle tone burst multiplied by a Hanning window with a centre frequency of 20 kHz, and different points on line B have been monitored to understand the amount of reflection from edge C. The model dimensions are chosen in such a way that the reflections from edge D and edge E do not interfere with the direct signal and reflection from edge C. A typical monitored signal, at a point on line 'B' in this case is shown in figure 2.1(b). The monitored signal on line B is composed of a direct signal from point A and the reflection from edge C, and these are not separated in time. It is necessary to model a very large geometry to avoid interference of reflections from all edges with the direct signal. The model shown in Figure 2.1(a) is not large enough in order to separate these signals in time and it was already at its computational limit.

In order to separate these signals, the method of signal subtraction has been used, employing a second model which is shown in figure 2.2(a). The point of excitation has been moved away from the edge 'C' in order to avoid the interference of the direct signal from the source and the reflection from the edge 'C'. The reflection from edge 'C' in this case interferes with reflections from

other far edges. This model has been excited at point A in exactly the same way as for model 1. However the difference is that the model dimensions are chosen in such a way that the reflections from edges do not interfere with the direct signal from point A. A typical monitored signal in this case is shown in figure 2.2(b). The monitored signal in this case is composed of the direct signal from point A and the reflections from edges but the direct signal is separated in time. A signal is obtained by subtracting the signals shown in Figure 2.1(b) and Figure 2.2(b) and is shown in figure 2.3(a). The reflection from edge C is thus separated in this signal and can be gated out for further processing.

In order to validate the signal subtraction technique, the reflection coefficients from edge 'C' have been compared with theoretical reflection coefficients of the A0 mode from an edge. A0 is the only anti-symmetric mode at the frequency of operation and therefore can not mode convert at a symmetric edge. Therefore the reflection coefficient is unity from theoretical understanding[11, 50, 51]. The FE reflected signals have then been normalized to account for distance travelled since the amplitude of a cylindrical wave decreases at a rate of $\frac{1}{\sqrt{r}}$ where r is the distance travelled. The reflection coefficients for different angles have been plotted in Figure 2.3(b). This confirms that the model correctly predicts a reflection coefficient of 1.0 for all angles.

Another case, where the reflection from a weld is separated from other signals using the signal subtraction technique is explained in the next section.

2.2.2 Oblique Incidence of A0 with a weld.

This section deals with the reflection of A0 from a weld for cases of angles of oblique incidence. Figure 2.4(a) shows the FE model used to study this. The plate is 1 mm thick and the weld is 1.25 mm thick. The weld shown in Figure 2.4(a) is a simplified weld. The model has been excited at point A as shown in the figure 2.4(a) using a 5 cycle tone burst multiplied by a Hanning window with a centre frequency of 20 kHz, and different points on line B have been monitored to understand the amount of reflection from the weld. The model dimensions are chosen in such a way that the reflections from far edges do not interfere with the reflection from the weld.

A typical monitored signal for reflection is shown in figure 2.4(b). This signal has a direct component from point A, and reflections from the weld and other edges. The reflections from far edges are separated in time but the direct signal and the reflection from the weld are not separated in time. It is not possible to separate these signals directly; in order to do this, the method described in the above section, signal subtraction, has been used. For this another model shown in figure 2.5(a) has been used. This model has the same dimensions of the model shown in Figure 2.4(a) and it has no weld. This model has been excited at point A. A typical monitored signal on line B is shown in figure 2.5(b), consisting of the direct signal from point A and reflection from far edges; the direct signal is separated in time from other signals. A signal for the weld reflection on its own is obtained by subtracting the signal shown in figure 2.5(b) from the signal shown in figure 2.4(b), and this is shown in figure 2.6. This signal shows the

reflection from the weld, and it is separated from all other signals, so can be taken for further processing. The results have not been presented as the purpose of this section is to explain the principle of the signal subtraction technique; the omission of the results helps to simplify the discussion

The signal subtraction technique can be used to separate the signal of interest from reflections from boundaries and other geometrical features. Computing power is increasing day by day and it might not take long before one would be able to model very large geometries. However, the guided wave signals change shape and size as the propagation distance increases because of their dispersive nature and it is desirable to monitor signals at locations not very far away from the source to avoid dispersion and dispersion related problems for signal processing. Therefore, the signal subtraction technique, along with FFT and dispersion compensation techniques, will be still attractive even with large geometries.

The signal subtraction technique can not be used where more than one mode is generated in the system and they need to be separated. In these cases we need long models to separate all modes in time, but long models are not possible because of computational limitations as explained before. Absorbing layers with increased damping (ALID) can be used to handle the problem to some extent and this is explained in the next section.

2.3 Absorbing layers with increased damping (ALID)

In this section, we explain the use of ALID [52, 53] in order to reduce the model size and avoid unwanted reflections from edges. We start this by taking an example model shown in Figure 2.7. This shows a plate with a thickened region in the middle. This model was studied to understand the attenuation of the trapped guided mode in the thickened region at different frequencies and the motivation for the model is explained in detail in chapter 3; this section only concentrates on the computational aspects of the model.

The plate is 6 mm thick and the thickened region is 18 mm thick and 16 mm wide. The plate has dimensions of 3 m x 1.5 m..These dimensions have been chosen in order to avoid the interference of the reflections from the far edges with the direct signal.. The trapped guided mode has characteristics similar to the S0 mode in a plain plate, explained in detail in chapter 3, and the wavelength of the S0 mode in plain plate has been taken as the reference to choose the element size for the FE models. The S0 mode in an 18 mm (thickness of the thickened region) steel plate has a wave length of 25 mm at frequency 150 kHz. Therefore an 8 node brick element of size 2 mm has been used to mesh the model in 3D for central frequencies up to 150 kHz, in order to have more than 8 to 10 elements per wavelength. The model has 4.5 million nodes and about 13.5 million degrees of freedom in total.

A finer mesh is needed at high frequencies (above 150 kHz) because of the smaller wavelength at these frequencies. The S0 mode in an 18 mm (thickness of the thickened region) steel plate has a wave length of 15 mm at frequency 200

kHz. Therefore an element size of 1.5 mm has been chosen between frequencies 150 kHz and 200 kHz. With elements of size 1.5 mm the model shown in figure 2.7(a) would have 10 million nodes and 30 million degrees of freedom, which was impossible to implement with the computational resources available and also the size limitations of ABAQUS. One of the solutions to this problem is to reduce the model dimensions, but the signal of interest interferes with other signals and reflections from the far edges in smaller models, and separating these signals in time is a difficult or impossible task.

The model dimensions can be reduced to some extent by using symmetric boundary conditions. Therefore a smaller model with symmetric boundary conditions as shown in Figure 2.7(b) has been used at frequencies above 150 kHz. An element size of 1 mm has been chosen above 200 kHz and this model has about 5.6 million nodes and 16.8 million degrees of freedom.

To study the attenuation of the trapped guided mode in the thickened region, The model has been excited at point ‘A’ in the in-plane direction and the trapped guided mode has been monitored at a series of nodes on the line ‘CC’ shown in Figure 2.7(a). The attenuation of the trapped guided mode in the thickened region has been calculated by monitoring two points on line ‘CC’ which are at different distances from the source. The decay as a function of frequency has been plotted in Figure 2.8. The blue curve shows attenuation calculated by monitoring two signals one at 300 mm from the source and one at 450 mm from the source. Similarly the red curve is obtained by monitoring two signals, one at 450 mm

and one at 600 mm from the source. The red, pink and black curves have been obtained in a similar way.

It would be expected that the signal loss (in dB) should be the same for any of these positions. However, Figure 2.8 shows that the decay rate greatly decreases with distance from the source. This is mainly due to near field effects and interference of the trapped guided mode in the thickened region with other modes. The near field effects are explained in chapter 3. In order to avoid all these near field effects and to separate the signal of interest from all other signals present in the system, it is necessary to model a very long plate and to monitor the signal at a location very far away from the source. Unfortunately this is not possible because of computational limitations. Therefore a model with no reflections from the lateral edges is sought.

Removing unwanted reflections in numerical wave propagation models is equivalent to representing total radiation outside the area of study. This topic has attracted many researchers in the last 25 years[54]. Well known techniques include infinite elements[55], boundary integral methods[56], non reflecting boundary conditions[57] and absorbing layers with increased damping[58-61].

These various techniques have proved successful in their context. Infinite elements are a special type of element with modified properties which can be used in conjunction with standard finite elements and which simulate an infinite space. A general presentation of the development of infinite elements can be found in [56]. A single row of infinite elements is positioned outside the

boundaries of the area of study. However previous research on guided waves showed that infinite elements are not suitable for high accuracy removal of unwanted reflections [62].

Non reflecting boundary conditions (NRBC) are special boundary conditions used in FE or finite difference (FD) methods to model wave propagation in unbounded media. The dimensions of the model are the same as the area of study; only the boundary conditions are changed. The modified boundary conditions generally use extra variables in order to approximate the infinite expanse of the medium. Many different methods have been developed for a wide range of fields. Early work in the ‘70s on NRBC was dominated by the use of the radiation condition given by Sommerfeld [63] but this method had limits as demonstrated in [64]. Other methods were developed such as the Engquist-Majda [65], Bayliss-Turkel [66] and are still widely used today. Exact non-local methods based on the Dirichlet-to-Neumann map [57, 67] or the difference potential method were developed from the late ‘80s. In the last 10 years, high order local NRBC have been developed for various cases[68]. These techniques were shown to work correctly but, as they require modification of the standard solving procedure, the development of specialist FE codes is required. Hence they were not investigated in this study to reduce the model dimensions.

Absorbing layers with increased damping (ALID) are finite regions “attached” at the extremities of a model. Their objective is to approximate the case of an unbounded problem by absorbing waves entering them. Small reflections from the absorbing region exist but these can be made acceptably small by correctly

defining the layer's parameters. A detailed discussion of ALID can be found in [59, 64].

The ALID can be better understood by taking the equation of equilibrium [59, 64]:

$$[M]\ddot{u} + [C]\dot{u} + [K]u = f \tag{2.1}$$

Where [M], [C] and [K], are mass, damping and stiffness matrices and *u* is displacement. With stiffness or mass proportional damping

$$[C] = C_M [M] + C_K [K] \tag{2.2}$$

where C_M and C_K are the mass and stiffness proportional damping coefficients.

In ALID with a boundary perpendicular to the x axis, the values of C_M *and* C_K are defined as follows.

$$C_M(x) = C_{M\max} . X(x)^p \qquad \textit{and} \qquad C_K(x) = C_{K\max} . X(x)^p \tag{2.3}$$

$C_{M\max}$ *and* $C_{K\max}$ are positive real numbers and *X(x)* varies from '0' at the interface between the ALID and the area of study to 1 at the end of the ALID region following a power law whose order is defined by *p*. In a time domain

model, $C_{M\max}$ and $C_{K\max}$ are constant and therefore do not vary with the frequency. This leads to a variation of the wave attenuation with frequency.

The target when defining layer parameters is to achieve a good approximation of unboundedness in the area of study with the smallest absorbing layer possible. It is essential to determine a sensible acceptability criterion for the approximation of unboundedness. For this work and as discussed in [62], a layer is considered acceptable when the amplitude of waves reflected from it is smaller than 0.1% (-60dB) of the amplitude of the incident wave entering it. A low percentage criterion (e.g. 0.1%) leads to a bigger absorbing layer than a high percentage one (e.g.5%). Hence, an adequately chosen criterion is the first step towards achieving computational efficiency.

The correct definition of the layer parameters (length of the layer *L*, variation of the attenuation parameter C_M and the power law *p*) is essential to achieve an efficient model. In FE models, as the space is discretized, the gradual increase of C_M occurs by steps. The ALID is defined as a series of sub layers having the same material properties but different values of C_M . It is preferable to minimize the change in C_M between two adjacent sub layers and therefore it is recommended to have one element thick sub layers [52]. Previous studies on absorbing layers suggest that the length of the absorbing region needs to be at least 3 times the wavelength of the wave to be absorbed [52] in order to satisfy the 60 dB criterion. The maximum value of the damping coefficient can be found

by analytical models or by trial and error. The previous research suggests that p = 2 gives accurate results.

In order to solve the computational problem explained in the previous section, a model with absorbing boundaries shown in Figure 2.9 has been used. This model is a quarter model of the model shown in Figure 2.7(a) with symmetric boundary conditions to represent the full model. An absorbing region is modelled as shown in the figure in order to suppress the reflections from the boundary 'B'.

The optimum length of the absorbing region depend on the projection of the wavelength on to the propagation direction [52] The maximum possible wavelength in the model is that of the S0 mode at the lowest frequency of interest. At 50 kHz the wavelength of the S0 mode in the plate is about 100 mm and its projection along the x axis will depend on the angle of incidence. Therefore, the optimum length of absorbing region is different for different angles of incidence. For angles of incidence close to 90^0, the projection of the wave length along the x-axis is close to infinity. As it is impossible to model infinite lengths of absorbing regions, because of computational limitations, it is also almost impossible to avoid reflections from the edge 'B' at large angles of incidence. These reflections again pollute the monitored signal at distances far away from the source.

The length of the absorbing region has been chosen in such a way that there are no significant reflections from the edge for angles of incidence between $0^o \; and \; 70^o$ where the projection of wavelength along the x-axis would be

between 100 mm and 300 mm. The length of the absorbing region was therefore set equal to 900 mm (three times maximum wave length). The width of the model was set to 1.5 m including the absorbing regions. The length of the model is 4.5 m. An 8 node brick element has been used to mesh the model in 3D and the element size was set to 2 mm for frequencies up to 150 kHz. 2 mm size elements give 50 elements per wave length at 50 kHz which is more than sufficient. The model has about 5 million nodes and 15 million degrees of freedom. A model with at least 30 million degrees of freedom would be required if ALID were not used.

Figure 2.10 shows attenuation of the trapped guided mode in the thickened region for different frequencies. Each decay curve has been calculated by monitoring two points on the thickened region which are at different distances from the excitation. The separation distance of the two points was 150mm in each case. The gaps between the sets of curves are because the results are obtained from two different FE runs, with two different centre frequencies, and plotted separately, otherwise the curves should be continuous. The curves are much closer in this case but they still do not overlap and even show negative attenuation at some frequencies. This is possibly due to small reflections at large angles of incidence that pollute the monitored signal at distances far away from the source. Even though small reflections from ALID are not avoidable at large angles of incidence, ALID still provides a valuable tool to deal with large FE models. Therefore ALID has been used in this thesis to deal with large FE models.

2.4 Conclusions:

This chapter discusses some techniques for optimizing large FE models. The signal subtraction technique provides a valuable tool to separate the signal of interest from reflections from the boundaries and other geometrical features. However signal subtraction may not be useful when more than one mode is generated in the system and it is necessary to separate one mode from others in time. In these cases the model must be long enough to separate different modes. Long models are possible by making the model long enough in one direction yet short in other directions and using ALID to avoid reflections from edges. The parameters of the absorbing region must be optimized in order to avoid unwanted reflections completely. The length of the absorbing region should be at least 3 times the maximum wave length of the wave to be absorbed and the optimum damping coefficient can be calculated using analytical models or by trial and error.

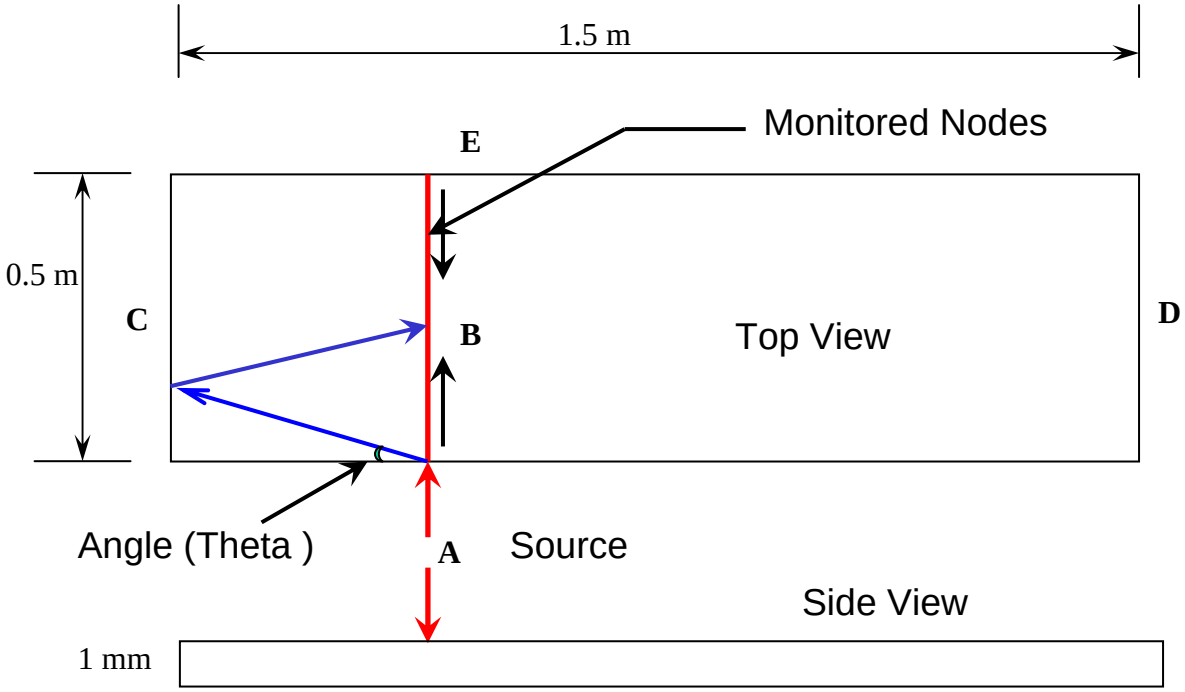

(a)

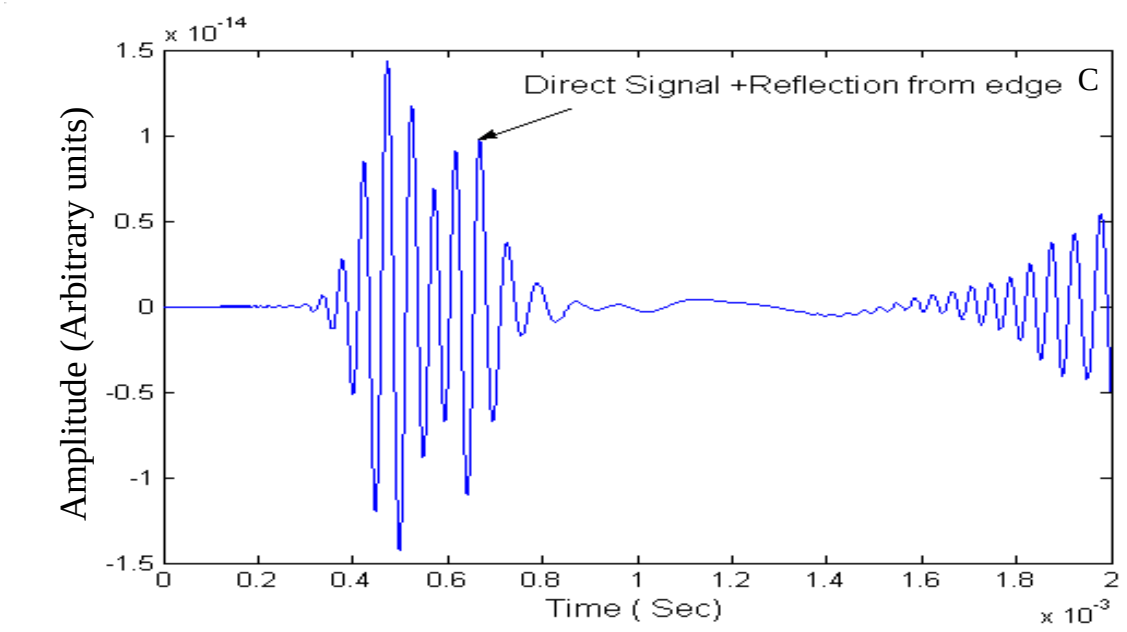

(b)

FIGURE 2.1: (a) FE model 1 used to separate reflection of A0 mode from an edge, for Oblique Incidence, (b) Typical time signal from FE model shown in figure 2.1(a) on line 'B'

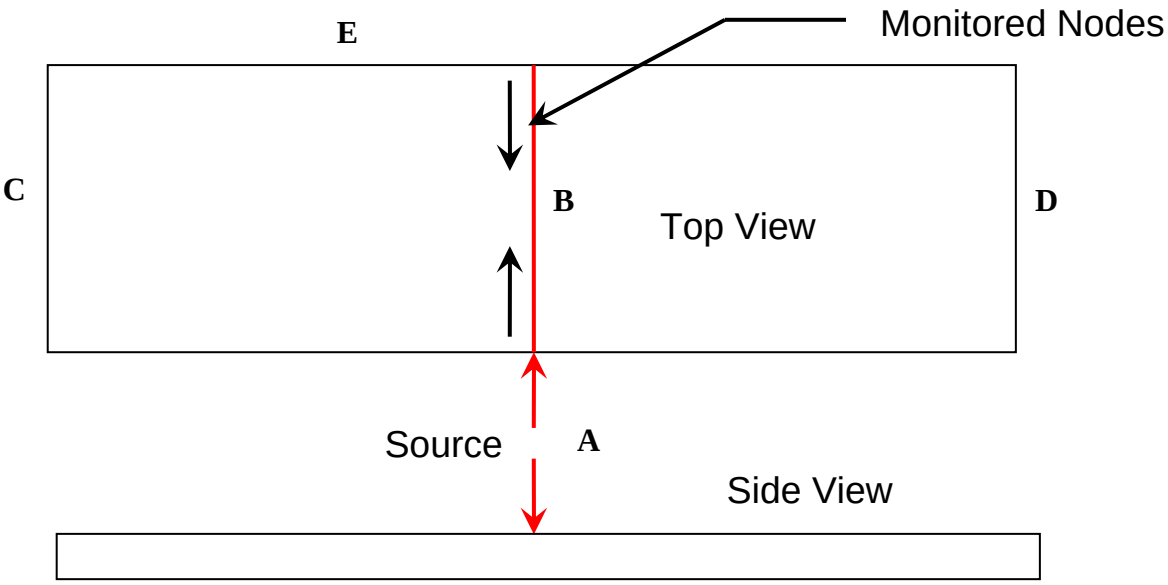

(a)

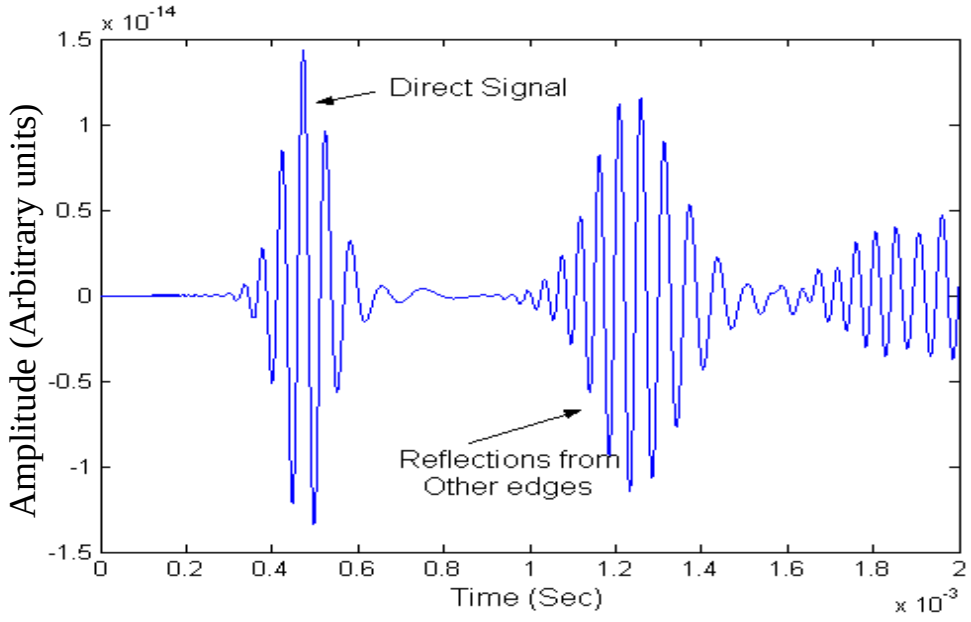

(b)

FIGURE 2.2: (a) FE model 2 used to study reflection of A0 mode from an edge for Oblique Incidence, (b) Typical time signal from FE model shown in figure 2.2(a), on line 'B'

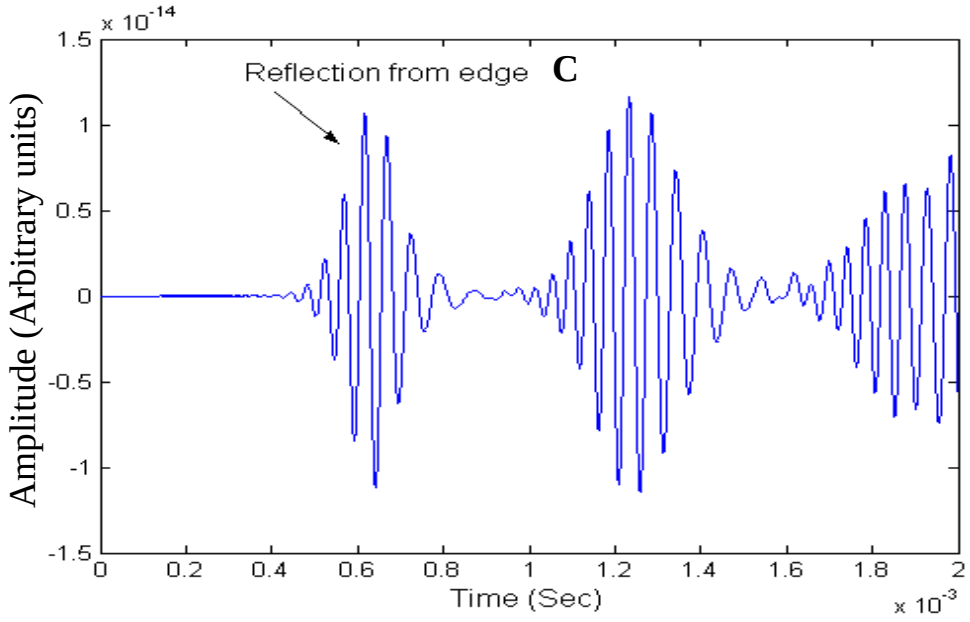

(a)

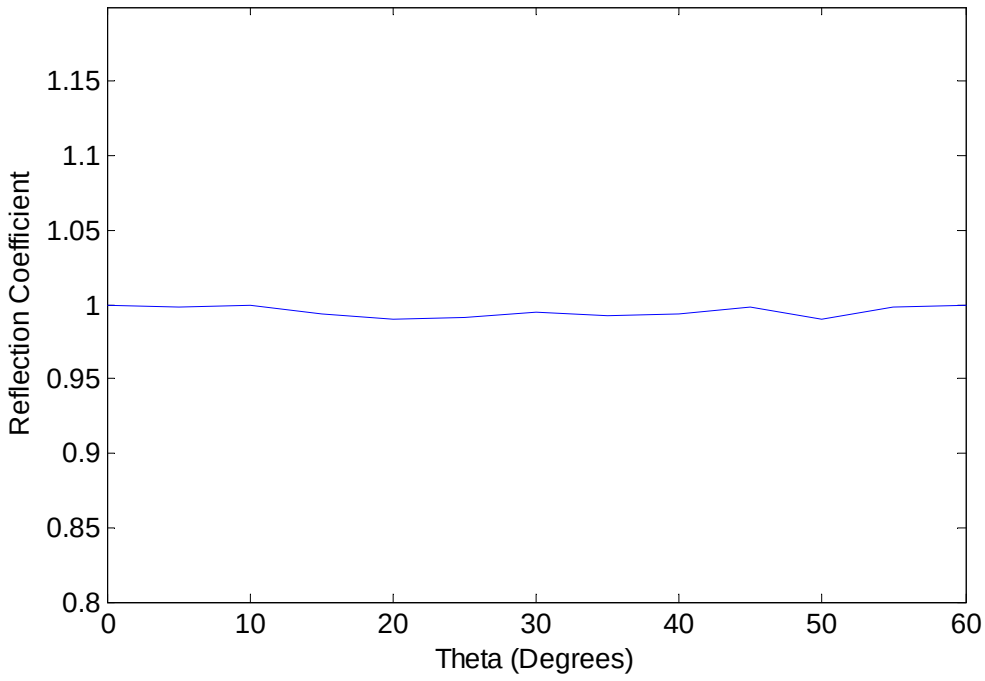

(b)

FIGURE 2.3: (a) Signal obtained by subtracting signals shown in figures 2.1(b) and 2.2(b), (b) Reflection coefficient of the A0 mode from an edge for different angles

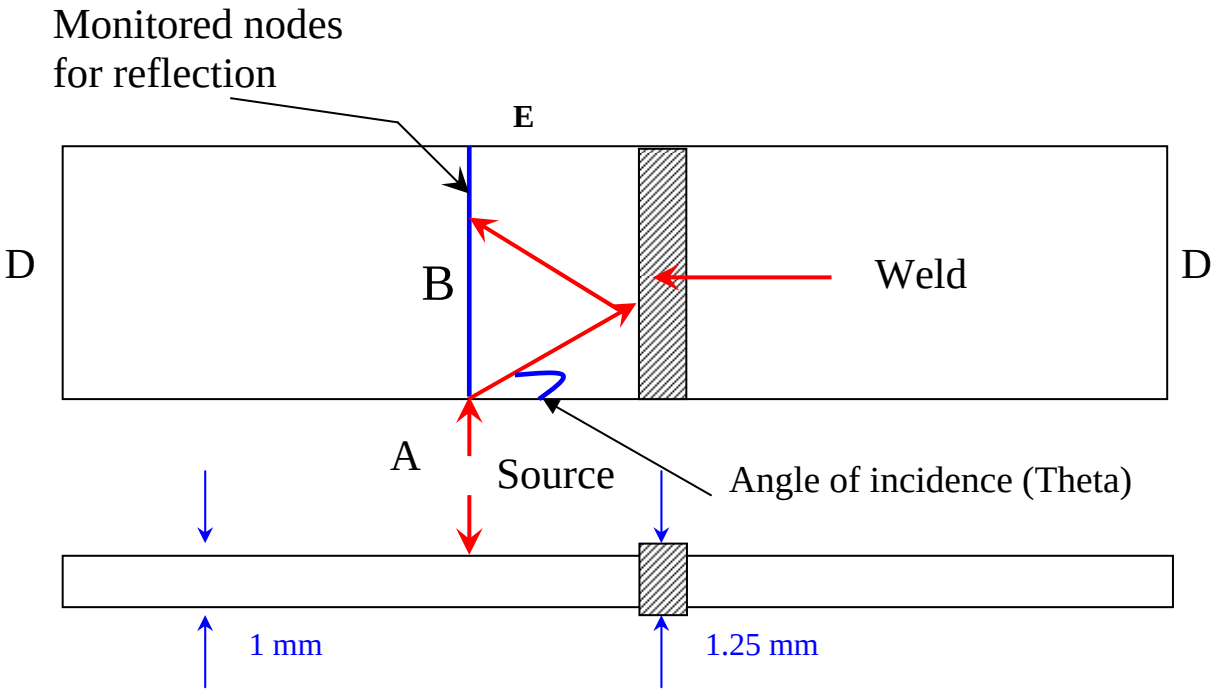

(a)

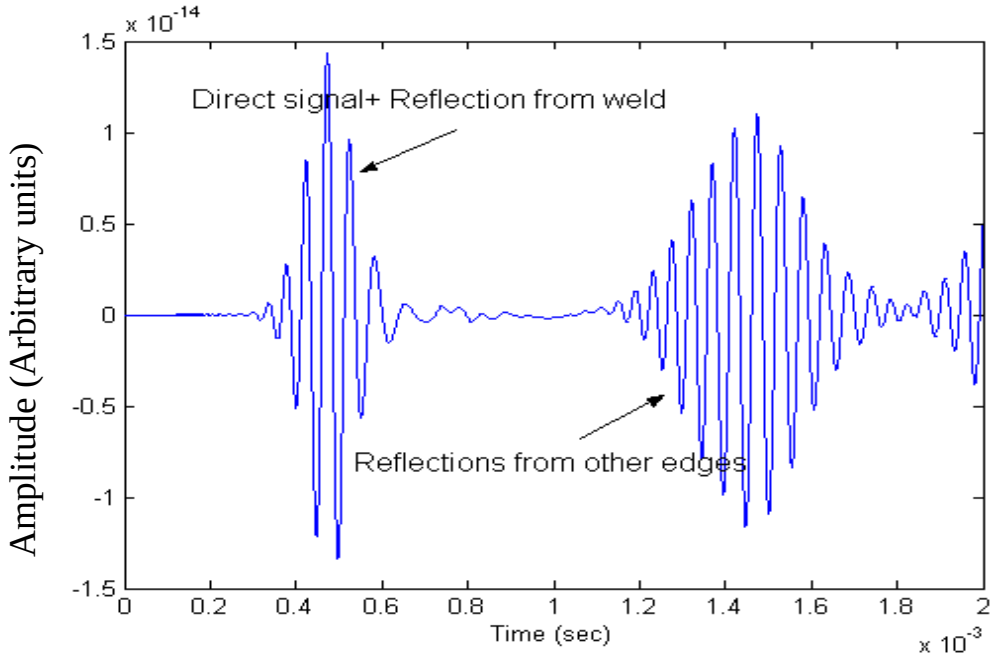

(b)

FIGURE 2.4: (a) FE model used to study reflection from weld

(b) Typical time signal measured on line B from FE model shown in figure 2.4 (a)

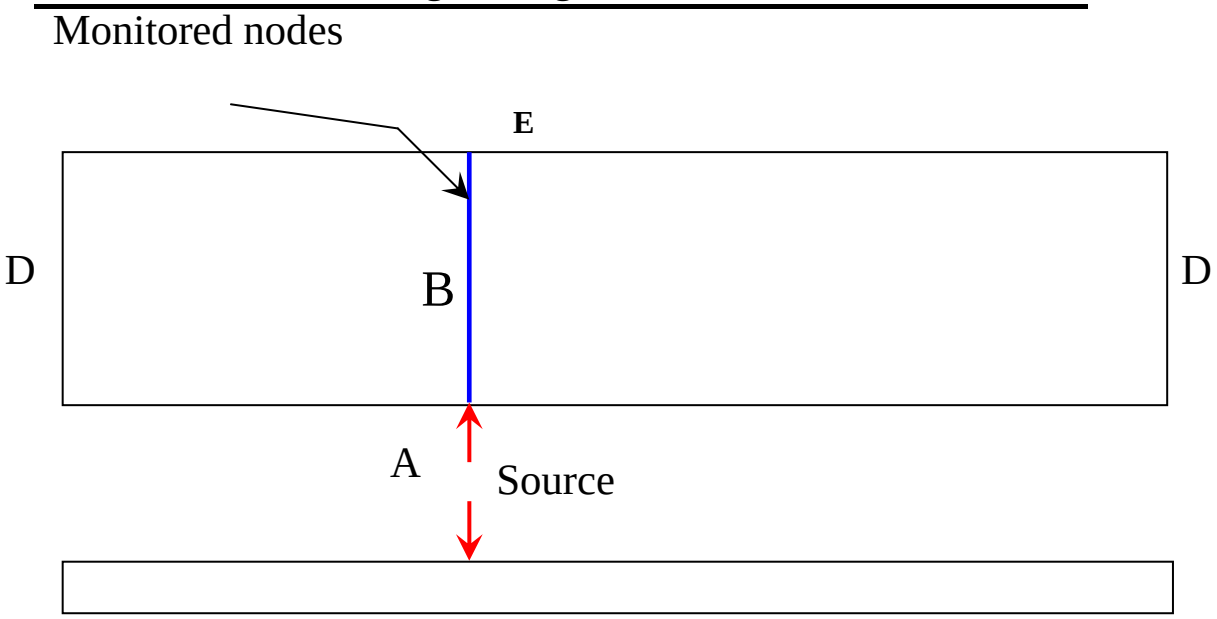

(a)

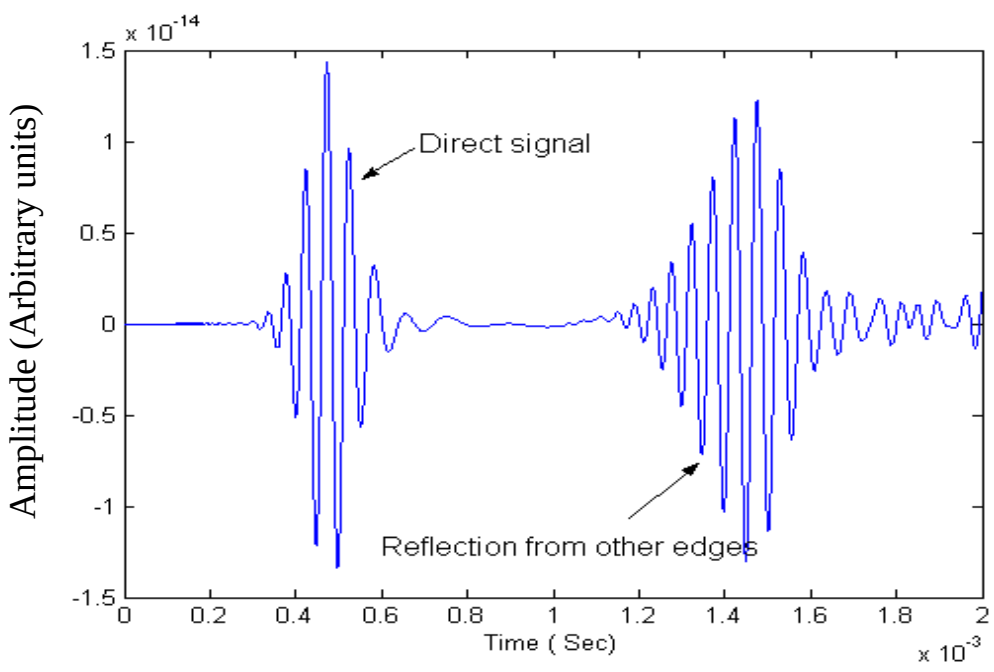

(b)

FIGURE 2.5: (a) FE model 2 used to study reflection from weld,

(b) Typical time signal measured on line B from FE model shown in figure 2.5(a)

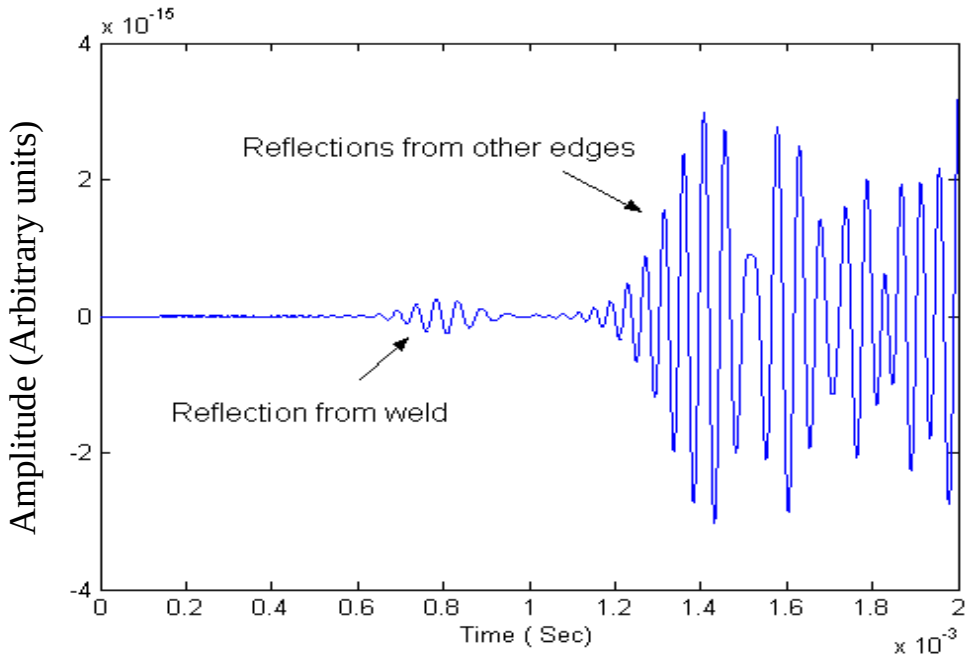

FIGURE 2.6: Signal obtained by subtracting signals shown in figures 2.5(b) and 2.4(b)

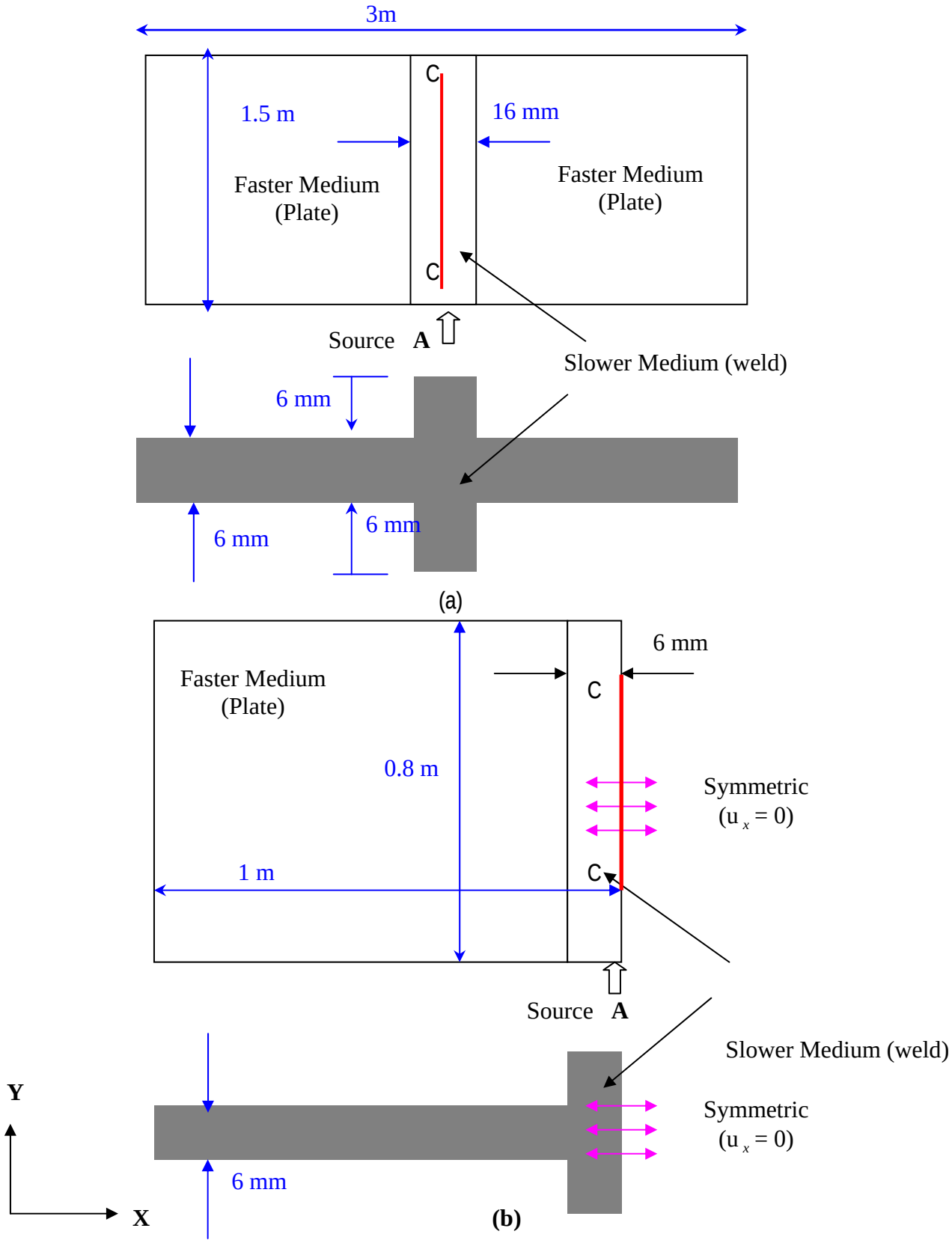

FIGURE 2.7: (a) Schematic diagram of system modelled (Not to scale); The trapped guided wave in the plate is faster than the trapped guided wave in the weld because the weld is thicker than the plate, (b). Schematic diagram of system modelled with symmetric boundary conditions for high frequencies (Not to scale),

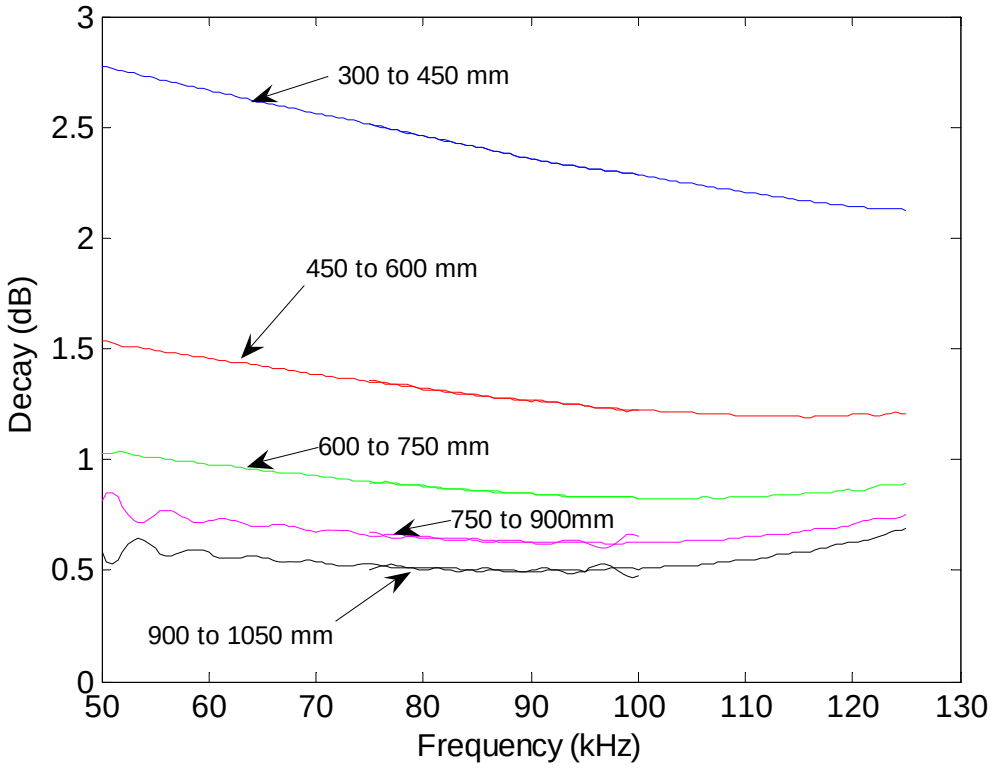

(b)

FIGURE 2.8: Attenuation of the trapped guided mode in the thickened region over a distance of 150 mm at different distances from the source.

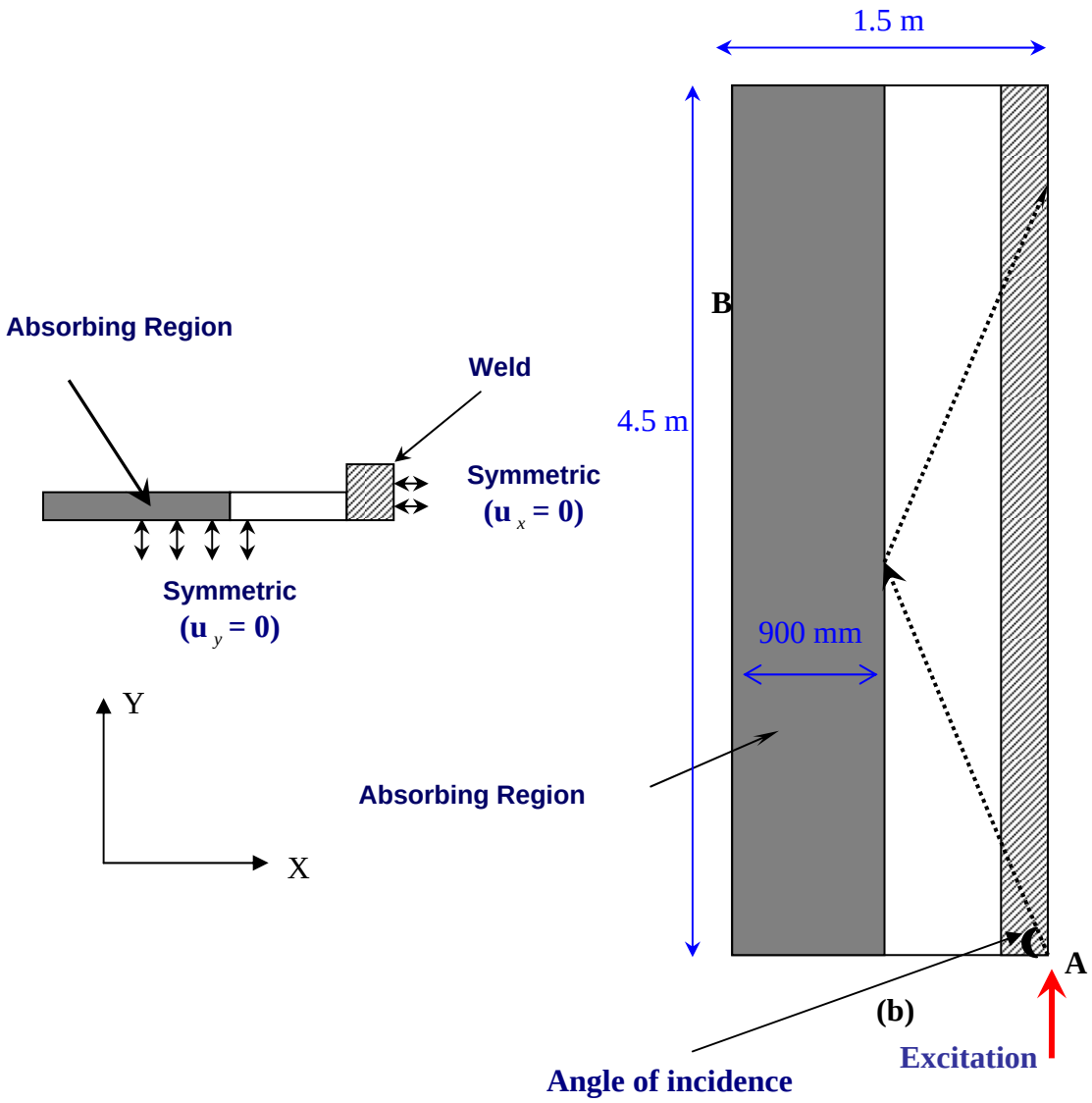

FIGURE 2.9: FE model with absorbing regions to study the attenuation of the trapped guided mode in the thickened region. (a) Side View, (b) Top View

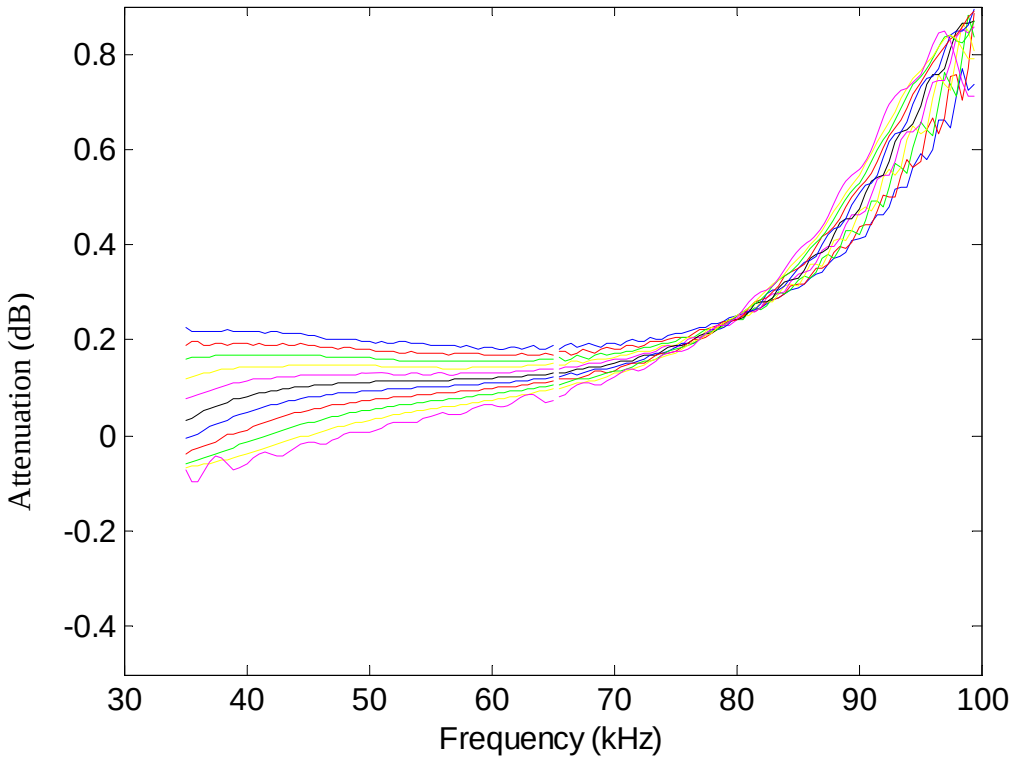

FIGURE 2.10: Attenuation of the trapped guided mode in the thickened region for different frequencies (Different curves show attenuations obtained when monitored signals are at different distances) (from 1950 mm to 3600 mm with 150 mm interval)

Chapter 3
Observation and illustration of Wave Trapping Phenomenon

3.1 Introduction

In this chapter we explain the experimental observation of trapping the S0 mode in the weld and how this phenomenon can potentially be used to inspect long lengths of welds and inaccessible regions of welds from a single transducer. Initial studies have been conducted on a variety of structures where a slower medium is embedded in a faster medium, to understand the phenomenon. Analytical and finite element studies on these structures reveal the physics behind the phenomenon. The properties of the trapped mode and its applicability to NDE of long lengths of welds over a range of possible test frequencies are discussed.

3.2 Experimental observation of guiding effect phenomenon

This phenomenon was observed when experiments were being conducted at the NDT Lab, Imperial College, London by Sargent [37]. Figure 3.1 shows the experimental setup. The test plate comprised two 1m x 2m x 6mm steel plates butt welded together to give a 2m square plate with a weld down the middle. The weld is approximately 12 mm wide and 10 mm thick. A flat bottomed hole (3mm deep part depth “defect” touching the weld) was located at a distance of 1.5m from the rear edge. The transducer which was used is a single element immersion transducer and it was mounted on the near edge of the plate as shown in Figure 3.1. The plate was excited as shown in Figure 3.1 in the in-plane direction using a 20 cycle tone burst multiplied by a Hanning window with a centre frequency of 200 kHz. Single pulse echo measurements were made at different locations on

the edge of the plate (from location ‘A’ to location ‘B’ as shown in Figure 3.1(d)) and the S0 reflections from the hole and the far edge of the plate were monitored.

Figure 3.2 shows typical time signals monitored when the plate was excited at different locations from point ‘A’ to point ‘B’ and point ‘B’ to point ‘C’. Point ‘A’ is at location X=900 mm, i.e. at a distance of 100 mm from the weld on the left side of the weld. Point ‘B’ is on the weld (X=1000 mm) and point ‘C’ is at location X=1060 mm, i.e. at a distance of 60 mm from the weld on the right side of the weld. The monitored signals show reflections from the defect and reflections from the far edge of the plate. The reflected signal from the far edge was observed to be both stronger and slower when the transducer was at or near the weld (location ‘B’). The reflections from the defect were also found to be stronger when the plate was excited at the weld compared to the reflections from the hole when the plate was excited away from the weld. Monitored time signals from ‘A’ to ‘B’ showed that the amplitude of the reflection from the defect and the amplitude of the reflection from the far edge of the plate increases as the transducer is bought near the weld[37], thus increasing the defect sensitivity.

This phenomenon is believed to occur principally because of the geometry: the S0 mode in the weld is slower than that in the plate at the operating frequency. Figure 3.3 shows phase velocity dispersion curves for the S0 mode for a plate with 10 mm thickness (maximum thickness of the weld in the structure) and for a plate with 6 mm thickness (thickness of plate in the structure). The phase velocity dispersion curves shown in Figure 3.3 show that at the operating frequency of 200 kHz the velocity of the S0 mode in the weld is slower than that

in the plate, as the weld is thicker than the plate. As the slower weld is embedded between two faster plates, some part of the energy is trapped in the weld, which is analogous to optical waveguides [38], resulting in a trapped guided mode within the weld. This trapped guided mode is expected to decay less than the S0 mode in a plain plate as the propagation of the trapped guided mode is one dimensional(propagation along the weld) whereas the propagation of the S0 mode in a plain plate is two dimensional (propagation in the plate with cylindrical spread). This trapped guided mode (S0 mode propagating along weld) is very interesting for the NDE of welds and other joints where the joint is slower compared to the surrounding material, as it decays less rapidly than the S0 mode in plain plate and can thus be used to inspect longer lengths of weld from a single location.

It is necessary to understand the principles behind the observed phenomenon and its governing characteristics over a range of possible test frequencies in order to be able to fully exploit it. Studies have been carried out on different model structures where a slower medium (a medium in which the wave is slower) is embedded in a faster medium (a medium in which the wave is faster) and they are reported in the next few sections.

3.3 Characteristics of S0 mode in a medium when the medium is embedded in a faster medium

Several methods based on the superposition of bulk waves, including, for example, the transfer matrix method or the surface impedance matrix method[32], have been developed in the past for the dispersion equation solution for simple geometries of waveguides such as plates or pipes. However, these methods cannot be used to find dispersion relations of guided modes in structures with arbitrary cross section. Therefore, a simplified multi layered model shown in Figure 3.4 has been used for initial studies. In this model, a slower plate, to represent the weld, is embedded between two faster media. The material properties of the faster media are taken to be those of steel ($C_l = 5960 m/s \ and \ C_s = 3260 m/s$) and the longitudinal and shear velocities of the slower plate are taken to be 90% of the longitudinal and shear velocities of steel ($C_l = 5364 m/s \ and \ C_s = 2934 m/s$) and the density to be 0.01 g/cm^3. The density of slower medium (0.01 g/cm^3) is a small percentage of the density of the surrounding medium (steel) and this makes the solution easier to find [32]. Both media are assumed to be perfectly elastic with no material damping to make the model simpler. The program DISPERSE[12, 13] has been used for these calculations.

Figure 3.5(a) shows the phase velocity dispersion curve of the S0 mode in the slower medium. When an elastic system is in vacuum, there is no mechanism for energy to be lost, so the attenuation is always zero. However, when the system is

surrounded by other materials, energy can leak from the system into the surrounding media, where it is free to propagate away in the form of bulk waves which travel to the infinite boundaries[32, 69]. The S0 mode in the slower medium leaks both longitudinal and shear waves into the faster media at all frequencies where the velocity of S0 in the slower medium is greater than the bulk longitudinal and shear velocities in the faster media (up to 2.6 MHz) as shown in figure 3.5(a). However, below the bulk longitudinal velocity of the surrounding media, the slower plate can only leak shear waves. The leakage results in the attenuation of S0 in the slower medium, Figure 3.5(b) shows the attenuation of S0 in the slower medium at different frequencies.

The variation in attenuation can be attributed to the changing amount of normal and in-plane displacements and stresses on the surface of the slower plate [69]. The displacements permit the energy to be coupled from the guided wave into the surrounding media. However when the phase velocity of S0 mode drops below the bulk shear velocity of the surrounding media, the attenuation becomes zero although there is still significant normal and in-plane displacement at the surface [69]. At higher frequencies (above 4 MHz as shown in Figure 3.5(a)) where S0 in the slower medium is slower than bulk shear waves in the faster media, there is no leakage and the mode has zero attenuation.

When the phase velocity of S0 in the slower medium crosses the bulk longitudinal velocity, there is a sudden jump. The cause of this jump is that at a phase velocity above the bulk longitudinal velocity of surrounding medium, it leaks both longitudinal and shear waves. However below the bulk longitudinal

velocity, the S0 mode in the weld can only leak shear waves which leads to a sudden jump. The jump phenomenon, when the phase velocity dispersion curve of a guided wave crosses a bulk longitudinal or shear velocity, is discussed in [69]. Effort has not been expended to study jumps in this particular case as the jump portion is very dispersive and not suitable for NDE.

Another case has been studied by changing the density of the slower medium from 0.01 g/cm^3 to 0.001 g/cm^3. Figure 3.6(a) shows the phase velocity dispersion curve of the S0 mode in the slower medium and Figure 3.6(b) shows attenuation. The attenuation values are much smaller here than the previous case. The smaller attenuation is mainly because the impedance difference between the slower medium and the surrounding medium is much higher in this case. Therefore, the guided wave that is propagating in the slower medium couples weakly to the bulk waves that are generated in the faster media. Figure 3.6(b) also shows zero attenuation when the velocity of the S0 mode in the slower medium is less than the shear velocity in the faster medium. One of the main limitations of guided wave inspection is the decay of the signal due to leakage into the surrounding material. Therefore, this S0 mode with zero attenuation could be used to inspect long lengths of slower embedded media.

The above studies explain the principles behind the trapping phenomenon. However, the geometries examined so far are highly simplified weld models. Trapping of S0 in the weld happens when the S0 mode in the weld is slower than the S0 mode in the plate. This condition can be achieved by two ways; one being the variation in the material properties between the weld and surrounding plates

and the other being the variation in geometry between the weld and the surrounding plates. In real welds, the trapping of S0 is caused by the variation in the geometry of the weld and the plates. The thicker weld makes the S0 wave slower even though there is no significant material property variation between the weld and the plate. In order to exploit the trapped guided mode for NDE of welds, it is necessary to fully understand the characteristics, mainly attenuation and defect sensitivity, of the trapped guided mode, in realistic welds, over a range of possible test frequencies. Therefore, the following two models are studied.

- Idealised weld 1: A simplified 3D weld model where the trapping of S0 is caused by material property variation between the weld and the surrounding plates.
- Idealised weld 2: A simplified 3D weld model where the trapping of S0 is caused by variation in the geometry between the weld and the surrounding plates. Here the geometry of the weld cap is greatly simplified.

The attenuation of the trapped guided mode in the above two 3D idealised cases has been studied both at low frequencies and high frequencies using 3D time domain finite element simulations. The program ABAQUS 6.5.1 [70] was used for these Finite Element calculations.

3.4 Study of Attenuation of the trapped guided mode in an Idealized weld where the trapping of S0 is caused by material property variation

3.4.1 Geometry, material properties and FE input data

A model plate system consisting of a slower plate, to represent the weld, between two faster plates as shown in Figure 3.7(a) has been studied. The material properties of faster media are taken to be exactly equal to the properties of steel. The slower medium is defined by taking the values of young's modulus and poisson's ratio equal to steel with an increased density equal to 12000 kg/m^3. The increased density makes the waves slower in that medium. Both media are assumed to be perfectly elastic with no material damping.

The model dimensions are chosen in such a way that the reflections from the far edges of the plate and direct signals from the source do not interfere. The plate has dimensions of 2m x 1m with 6 mm thick and the idealized weld is 12 mm wide as shown in Figure 3.7(a). The plate was excited at point 'A', as shown in the figure, in the in-plane direction using a five cycle Hanning-windowed tone burst, to generate the S0 mode in the system. An explicit central difference scheme was employed to perform the time marching solution, the time step being chosen to be less than the time taken for the fastest wave to travel between two adjacent nodes. To study the properties at different frequencies from the low frequency region to the high frequency region, the model was excited with tone bursts of centre frequencies 100 kHz, 150 kHz, 200 kHz and 250 kHz.

An 8 node brick element of size 2 mm has been used to mesh the model in 3D when the model was excited with tone bursts of centre frequencies up to 200 kHz, giving more than 10 elements per wavelength. The model has two million nodes and about 6 million degrees of freedom in total. The wave length of the S0 mode in the slower medium (weld) at 200 kHz is 22 mm. A finer mesh is needed at high frequencies (above 200 kHz) because of the smaller wavelength at these frequencies. Therefore an element size of 1 mm has been chosen at frequencies above 200 kHz. With elements of size 1mm the model shown in figure 3.7(a) would have 14 million nodes and 42 million degrees of freedom which was impossible to implement with the computational resources available. Therefore a smaller model with symmetric boundary conditions as shown in Figure 3.7(b) has been used at frequencies above 200 kHz.

The model shown in Figure 3.7(b) is a half model with symmetric boundary conditions ($u_x = 0$) on surface 'D'. This model has about 2.1 million nodes and 6.3 million degrees of freedom. The analysis was run twice: once with the weld (slower embedded medium) as described, and the second time with a plain plate without weld, for comparison.

3.4.2 Results

A series of points on line BB, shown in Figure 3.7(a), 200 mm from the source were monitored to see what is happening near the weld and what is happening away from the weld. The maximum amplitudes of displacements the S0 mode at these monitored nodes have been plotted in Figure 3.8. The red curve in Figure 3.8 shows maximum amplitudes for the with-weld case and the blue curve shows maximum amplitudes for a plain plate case. Figure 3.8 shows that the strain energy is concentrated in and around the weld region in the presence of the weld. The strain energy concentration occurs principally because the S0 mode in the weld is slower than that in the plate at the operating frequency. As the slower weld is embedded between two faster plates, some part of the strain energy is trapped in the weld, resulting in energy concentration in and around the weld region.

Figure 3.9 shows the magnitude of the resultant displacement at two instants in time during the finite element simulation, which clearly shows the trapped guided mode which is guided along the weld along with the other modes. Figure 3.9(a) shows the resultant displacement at one instant in time and Figure 3.9(b) shows resultant displacement at a later instant in time. The following modes are found in the structure:

- A trapped guided mode which is guided along the weld.
- S0 in the plate
- SH0 in the plate
- A leaky wave from the trapped guided mode.

From figure 3.9 we can see that the trapped guided mode is slower than the S0 mode in the plate. The mode shapes of the trapped guided mode have been obtained by monitoring nodes through the thickness and are shown in Figure 3.10. Figure 3.10(a) shows out-of-plane displacement and Figure 3.10(b) shows in-plane displacement. These mode shapes suggest that the trapped guided mode, which is guided along the weld, is a symmetric mode and has mode shape close to that of the S0 mode. Even tThe phase velocity dispersion curve of the trapped guided mode is close to that of the S0 mode and this will be explained in the next chapter. Therefore we call this mode trapped S0-like mode in the rest of this thesis.

The S0 and SH0 modes in the plate are generated by the excitation. The velocity of the trapped S0-like mode is greater than the velocity of SH0 in the plate and less than S0 in the plate. Therefore, the trapped S0-like mode can only leak SH0 into the plate. The velocity and mode shapes of the leaky wave have been obtained and this has confirmed that the leaky wave is the SH0 wave. Figure 3.9 shows that the trapped S0-like mode is also present in the region adjacent to the weld, which suggests that the trapped S0-like mode can also potentially be used to inspect heat affected zones.

To be able to improve the inspection capabilities of long lengths of welds using the trapped S0-like mode, the attenuation of the trapped S0-like mode has to be less than the attenuation of the S0 mode in a plain plate at the operating frequency. To check this, the trapped S0-like mode has been monitored at a series of nodes on line ‘CC’, shown in Figure 3.11(a). The log of the maximum

amplitudes of these signals in the frequency domain have been plotted and a straight line is fitted connecting these points as shown in Figure 3.11(b). The red curve is a fitted curve for the with-weld case and the blue curve is a fitted curve for the without-weld case. Figure 3.11(b) shows an increasing gap between amplitudes for with weld and without weld cases as the distance from the source increases. The attenuation of the trapped S0-like mode depends on the impedance difference between the slower medium and the surrounding faster medium. The attenuation values decrease as the impedance difference increases.

To study the attenuation of the trapped S0-like mode quantitatively, at different frequencies, the model was excited with tone bursts with centre frequencies 100 kHz, 150 kHz, 200 kHz and 250 kHz and the attenuation has been calculated for frequencies from 75 kHz to 275 kHz using the following equation.

$$Decay = 20\log(\frac{A2}{A1}) \qquad (3.1)$$

where '*A2*' and '*A1*' are the amplitudes of the trapped S0-like mode in the frequency domain, at the two monitored nodes on line 'CC'. The values of attenuation for different frequencies are shown in Figure 3.12(a). The gaps/ discontinuities in the attenuation curve are only because the attenuation values are calculated from four different FE runs with different centre frequencies, otherwise the curve should be continuous.

The trapped S0-like mode attenuates as it leaks SH0 in to the plate. The change in attenuation can be attributed to the change in velocity differences between the trapped S0-like mode and the SH0 wave in the plate. The velocity difference between S0 in the weld and SH0 in the plate is shown in Figure 3.12(b). When the velocity difference is higher at low frequencies, the acoustic impedance difference, for the S0 mode, between the weld and the plate is higher, which results in less leakage into the plate and less attenuation of the trapped S0-like mode in the weld. At high frequencies where the velocity difference is low, the acoustic impedance difference is low and results in high attenuation of the trapped S0-like mode in the weld.

From the studies conducted on simplified geometries, explained in the previous sections, it would be expected that at high frequencies, where the trapped S0-like mode is slower than the SH0 mode in the plate, the trapped S0-like mode cannot leak SH0 and so will show no attenuation. To check this, the model, with an element size of 0.5 mm, was excited with a 12 cycle Hanning windowed tone burst with a centre frequency of 500 kHz and a typical monitored signal on line 'CC' is shown in Figure 3.13. The monitored signal is complicated by the presence of many modes at this frequency.

Only symmetric modes are possible in the structure as the structure, shown in Figure 3.7, is symmetric and the excitation is symmetric. The S1 mode is separated in time but the trapped S0-like mode and S2 modes are not separated in time. In fact even the S1 and S2 modes could be trapped but these modes are considered simple S1 and S2 modes in order not to complicate the discussion.

The only mode of interest in this thesis is the trapped S0-like mode. A very large FE model is needed in order to separate these signals in time and this large model was not possible with the available computational resources.

Therefore, a finite element study has been carried out for a case in which the density of the slower medium was set to 30000 kg/m^3. The phase velocity dispersion curve of a plain plate with such properties (E=216.9 GPa, μ = 0.2865 and density = 30000 kg/ m^3) is shown in Figure 3.14. Figure 3.14 shows that the phase velocity of the S0 mode in the slower medium (weld) is less than the phase velocity of SH0 mode in the plate at all frequencies. Therefore the trapped S0-like mode in the slower medium cannot leak SH0 into the plate and is expected to show zero attenuation at all frequencies.

The plate was excited at point 'A' as shown in Figure 3.15(a) in the in plane direction using a five cycle Hanning-windowed tone burst with a centre frequency of 100 kHz. Figure 3.15(b) shows the contour of magnitude of the resultant displacement, at an instant during the simulation, for this case. The following modes are found in the structure.

- Trapped S0-like mode which is guided along the weld.
- S0 in the plate
- SH0 in the plate

From Figure 3.15(b), we can clearly see that the trapped S0-like mode is slower than the SH0 mode in the plate and we can also see that there is no SH0 leaking from the weld and thus the guided wave experiences zero decay.

3.5 Study of Attenuation of the trapped S0-like mode in a 3D Idealized weld where the trapping is caused by variation in the geometry between the weld and the surrounding plates.

3.5.1 Geometry, material properties and FE input data

In this section, the case where the trapping of S0 is caused by the variation in the geometry between the weld and the surrounding plates is explained and the propagation and attenuation of the trapped S0-like mode over a range of possible test frequencies from low frequencies to high frequencies is discussed. A plate system consisting of a thickened rectangular cross section to represent the weld, shown in Figure 3.16 has been studied. The plate is 6 mm thick and the idealized weld is 18 mm thick and 16 mm wide. The model dimensions are optimized in such a way that the reflections from the far edges of the plate and direct signals do not interfere. The plate has dimensions of 3m x 1.5m.

The phase velocity dispersion curves for an 18 mm (thickness of weld in the model) steel plate are shown in Figure 3.17. The S0 mode in an 18 mm steel plate has a wave length of 25 mm at frequency 150 kHz. Therefore an 8 node brick element of size 2 mm has been used to mesh the model in 3D for central frequencies up to 150 kHz, in order to have more than 10 elements per

wavelength. The model has 4.5 million nodes and about 13.5 million degrees of freedom in total. A finer mesh is needed at high frequencies (above 150 kHz) because of the smaller wavelength at these frequencies. Therefore an element size of 1.5 mm has been chosen between frequencies 150 kHz and 200 kHz. With elements of size 1.5 mm the model shown in figure 3.16(a) would have 10 million nodes and 30 million degrees of freedom, which was impossible to implement with the computational resources available. Therefore a smaller model with symmetric boundary conditions as shown in Figure 3.16(b) has been used at frequencies above 150 kHz. An element size of 1 mm has been chosen above 200 kHz and this model has about 5.6 million nodes and 16.8 million degrees of freedom.

The plate was excited at point ‘A’ as shown in the figure in the in plane direction using a five cycle Hanning-windowed tone burst. At high frequencies (between 100 kHz and 200 kHz) the S0 mode is very dispersive as shown in Figure 3.17, and it is very difficult to separate it from other signals present in the system. So, the plate was excited with 12 cycle Hanning-windowed tone burst at some frequencies where it was necessary. From Figure 3.17, we can see that the Phase velocity of S0 in the weld is greater than the phase velocity of SH0 in the plate at frequencies up to 180 kHz. Therefore, the trapped S0-like mode would be expected to leak SH0 wave in the plate for frequencies up to 180 kHz and will show attenuation. At frequencies above 180 kHz, where the trapped S0-like mode is slower than SH0 mode in the plate, an attenuation of zero would be expected.

3.5.2 Results

To study the attenuation of the trapped S0-like mode, the trapped S0-like mode has been monitored at a series of nodes on line 'CC' shown in Figure 3.16(a). A typical monitored signal, when the model was excited with a 12 cycle Hannng-windowed tone burst with a centre frequency of 100 kHz, at a distance of 500 mm from the source has been shown in Figure 3.18. The monitored signal has two modes: trapped S0-like and S1 and these modes are separated in time. The attenuation of the trapped S0-like mode has been calculated using equation (3.1) by monitoring two points on line 'CC' which are at different distances from the source, where *'A2'* and *'A1'* are the amplitudes of the signals, in frequency domain, monitored at the two points on line 'CC'. The separation distance of the two points was 150 mm.

The contour of magnitude of resultant displacement at a chosen time during the simulation is shown in Figure 3.19(a). The decay for different frequencies has been plotted in Figure 3.19(b). The blue curve shows attenuation calculated by monitoring two signals one at 300 mm from the source and one at 450 mm from the source. Similarly the red curve is obtained by monitoring two signals one at 450 mm and one at 600 mm from the source. The red, pink and black curves have been obtained in a similar way.

It would be expected that the signal loss (in dB) should be the same for any of these positions as the propagation is one dimensional. However, Figure 3.19(b) shows that the decay rate greatly decreases with distance from the source. This is

believed to be mainly due to the interference of the trapped S0-like mode with the S0 mode generated in the system because of the excitation. The velocity difference between the trapped S0-like mode and S0 mode in the system depends on the thickness of the weld and the operating frequency. The thicker the weld, the higher the velocity difference. In order to separate the trapped S0-like mode from the S0 mode in the plate because of excitation, in time, it is necessary to model a very long plate and to monitor the signal at a location very far away from the source. Unfortunately this is not a trivial exercise because of the computational limitations.

In order to solve the above problem, a model with absorbing boundaries shown in Figure 3.20 has been used. This model is a quarter model of the model shown in Figure 3.16(a) with symmetric boundary conditions to represent the full model. An absorbing region is modelled as shown in the figure in order to suppress the reflections from the boundary 'B'. The absorbing region has been optimized as explained in chapter 2.

The maximum possible wave length in the model is that of the S0 mode at the lowest frequency of interest. At 50 kHz the wavelength of the S0 mode in the plate is about 100 mm and its projection along the x axis will depend on the angle of incidence. Therefore, the optimum length of absorbing region is different for different angles of incidence. For angles of incidence close to 90^0, the projection of the wave length along the x-axis is close to infinity. As it is impossible to model infinite lengths of absorbing regions, because of computational limitations, it is also almost impossible to avoid reflections from

the edge 'B' at large angles of incidence. These reflections again pollute the monitored signal at distances far away from the source.

The length of the absorbing region has been chosen in such a way that there are no reflections from the edge for angles of incidence between 0^o *and* 70^o where the projection of wavelength along the x-axis would be between 100 mm and 300 mm. The length of the absorbing region was therefore set equal to 900 mm (three times maximum wave length). The width of the model was set equal to 1.5 m including the absorbing regions. The length of the model is 4.5 m.

An 8 node brick element has been used to mesh the model in 3D and the element size was set equal to 2 mm for frequencies up to 150 kHz. 2 mm size elements give 50 elements per wave length at 50 kHz which is very much sufficient. The wave length decreases as the frequency increases and becomes less than 10 mm above 150 kHz. Therefore the model dimensions have been changed and finer meshing is used at high frequencies. At high frequencies the model has been meshed with 1 mm brick elements and the model has approximately 25 million degrees of freedom, which is the current largest model possible with the available computational resources in the lab.

The model was excited at point 'A' in the in-plane direction as shown in Figure 3.20. The trapped S0-like mode has been monitored at a distance very far away from the source (from 1950 mm to 3600 mm with 150 mm interval) and the attenuation has been calculated using the equation 3.1. Figure 3.21 shows attenuation of the trapped S0-like mode for different frequencies. Each decay

curve has been calculated by monitoring pairs of points on the weld which are at different distances from the excitation. The separation distance of each pair of points was 150mm. The gaps between curves are because the results are obtained from two different FE runs, with two different centre frequencies, and plotted separately; otherwise the curves should be continuous.

The decay curves are much closer in this case than in the previous model but they still do not overlap and even show negative attenuation at some frequencies. This is thought to be due to small reflections at large angles of incidence that pollute the monitored signal at distances far away and also the interference of the trapped S0-like mode with S0 mode in the plate. An average of these curves has been taken as the best measure of the decay of the trapped S0-like mode to nullify the error generated because of noise and has been plotted in Figure 3.22. The attenuation increases as the frequency increases as expected because of the increase in shear leakage as the velocity difference of the trapped S0 mode and SH0 in the plate decreases. This observation is similar to the observations in the previous section.

At frequencies above 250 kHz the trapped S0-like mode is expected to show zero attenuation as the velocity of the trapped S0-like mode at these frequencies is less than the SH0 wave in the plate. Therefore, the analysis was run at frequencies above 250 kHz. Figure 3.23 show typical monitored signals with a central frequency of 250 kHz, at different distances. Figure 3.24 shows the attenuation at different frequencies from 250 kHz to 320 kHz. Different curves in Figure 3.24 are obtained by monitoring signals at different distances, e.g. the

blue curve is obtained by monitoring two signals one at 1000 mm and the other at 1100 mm. Figure 3.23 and Figure 3.24 show no attenuation of the trapped S0 mode, as expected.

The above studies show that the trapped S0-like mode decays less than the S0 mode would in a plain plate. Therefore this trapped S0-like mode can potentially be used to inspect long lengths of welds provided it is sensitive to target defects. To check the defect sensitivity of the trapped S0-like mode, defects have been introduced in the weld and this is explained in the next section.

3.6 Defect sensitivity of the trapped S0-like mode

An initial defect study has been carried out in order to check whether the trapped S0-like mode can be used advantageously to inspect welds. In real welds, defects are arbitrary in geometry, size, orientation and position within the weld. However, in the Finite Element study reported here, through-thickness square "defects" were investigated as an initial trial as they are easier to model than defects with arbitrary geometry. A through-thickness square defect (6 mm x 6 mm) has been introduced in the weld as shown in Figure 3.25(a). The defect is at a distance of 200 mm from the source. The defect has been modelled by removing the elements from the weld. The analysis was run twice: once with the weld as described, and the second time with a plain plate without weld, for comparison. The defect was the same in both cases.

The model was excited at point ‘A’ as shown in the figure using a five cycle Hanning windowed tone burst with a centre frequency of 150 kHz and the reflections from the defect were monitored at point B. Figure 3.25(b) shows a monitored signal. The faster signal in the figure is the monitored signal for a plain plate. The slower signal is the monitored signal for the plate with the idealised weld. The first part of the signal shows the incident signal from the source and the second part shows the reflection coming back from the defect. From the first part of the signal we can see that the wave in the weld is slower than the wave in the plate. From the second part of the figure we can clearly see that the defect reflection is stronger in the weld case. This initial defect study reveals the potential use of the trapped S0-like mode for the inspection of welds.

3.7 Conclusions

From the studies on simple structures, it is understood that a trapped S0-like mode is generated in a medium when it is embedded in a faster medium. It is also understood that this trapped S0-like mode decays less than S0 in plain plate because of its one dimensional propagation, and can potentially be used to improve inspection capabilities of long lengths of welds. The trapped S0-like mode in the slower medium decays because of leakage into the surrounding medium. The amount of leakage depends upon the velocity difference between the trapped S0-like mode in the slower medium and the leaky wave in the surrounding medium. Initial studies on simplified weld geometries were successful and indicated the potential of the method.

The finite element studies on idealized welds show that the attenuation of the trapped S0-like mode increases as the frequency increases because of the decrease in velocity difference between the trapped S0-like mode and the SH0 mode in the surrounding plates. However the attenuation becomes zero at high frequencies where the trapped S0-like mode is slower than SH0 in the plate. The initial defect studies have confirmed the potential applicability of the trapped S0-like mode for NDE of long lengths of welds. The trend of the attenuation curve shown in Figure 3.22 is convincing qualitatively but may not be accurate quantitatively because of the uncertainties related to the performance of the absorbing region at large angles of incidence and also the interference of the trapped S0-like mode with the S0 mode in the plate. Therefore semi analytical finite element (SAFE) models have been used to study the attenuation of the trapped S0 mode quantitatively and also to compare the FE results, and have been explained in the next chapter.

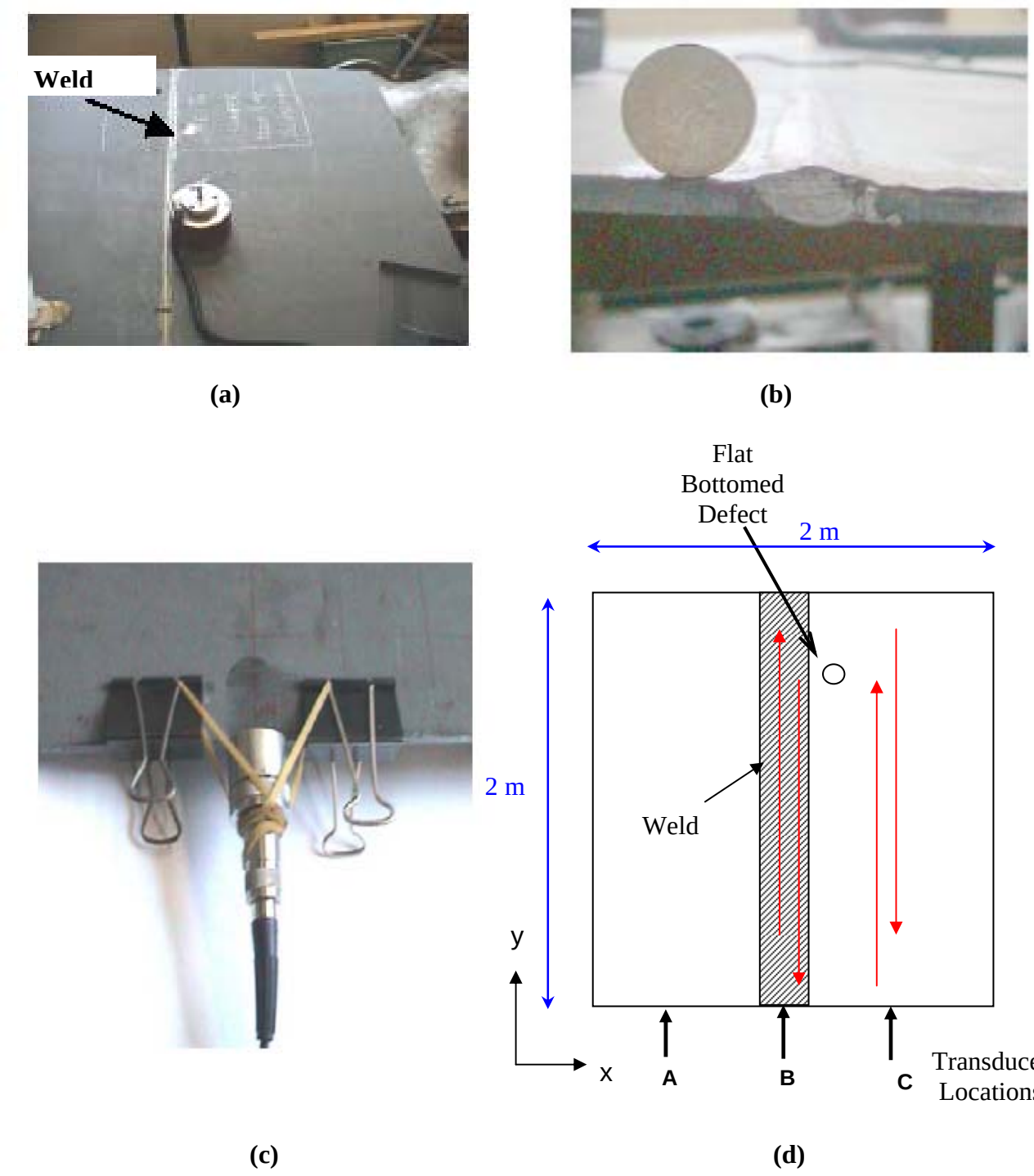

FIGURE 3.1. Experimental Setup, (a) Plate with a butt weld in the middle, (b) Edge of the plate with butt weld, (c) Transducer mounted on the edge of the plate, (d) Schematic diagram of the plate used for experiments [Ref].

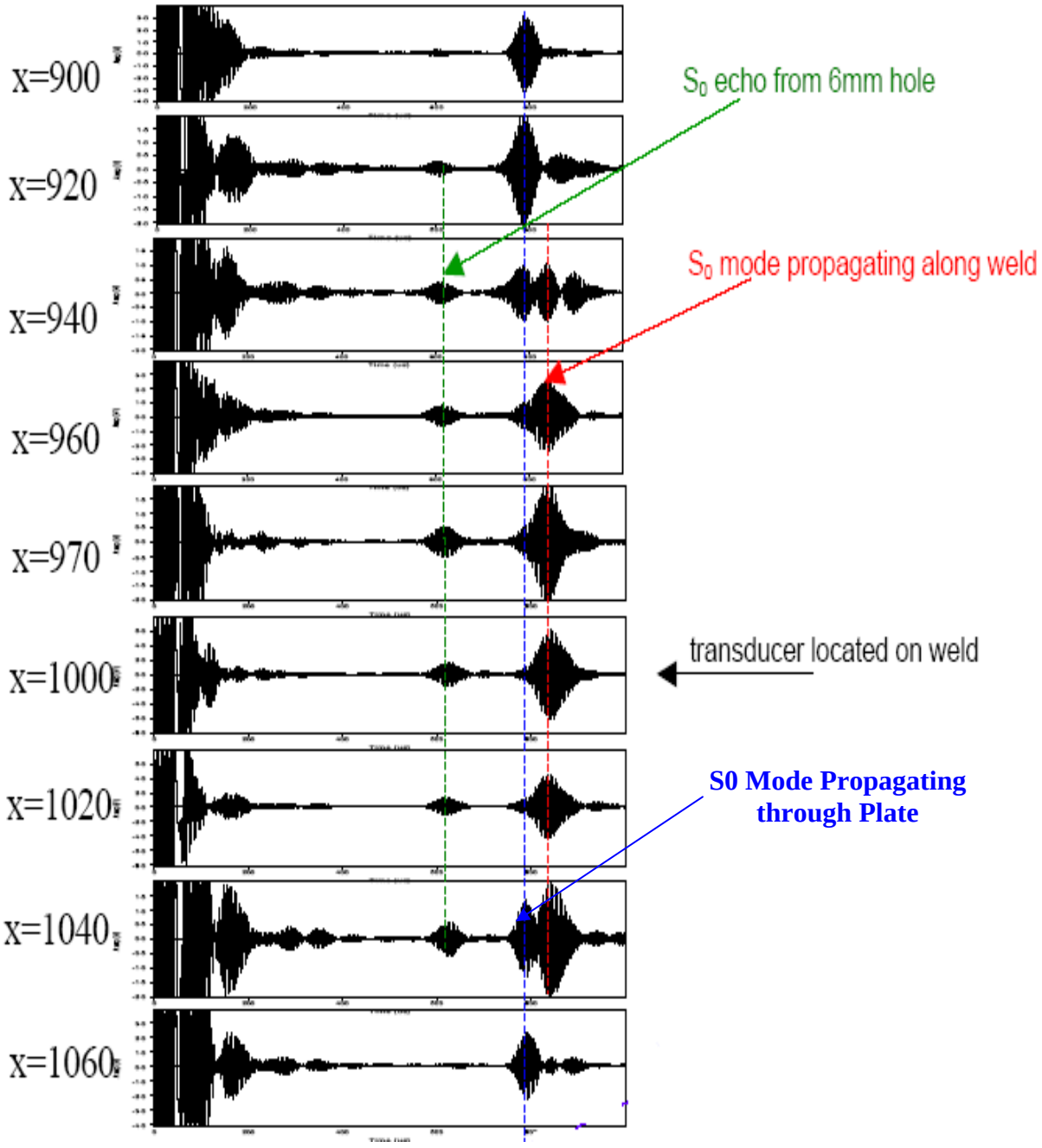

FIGURE 3.2: Typical time signals monitored at different distances from the weld [Ref]

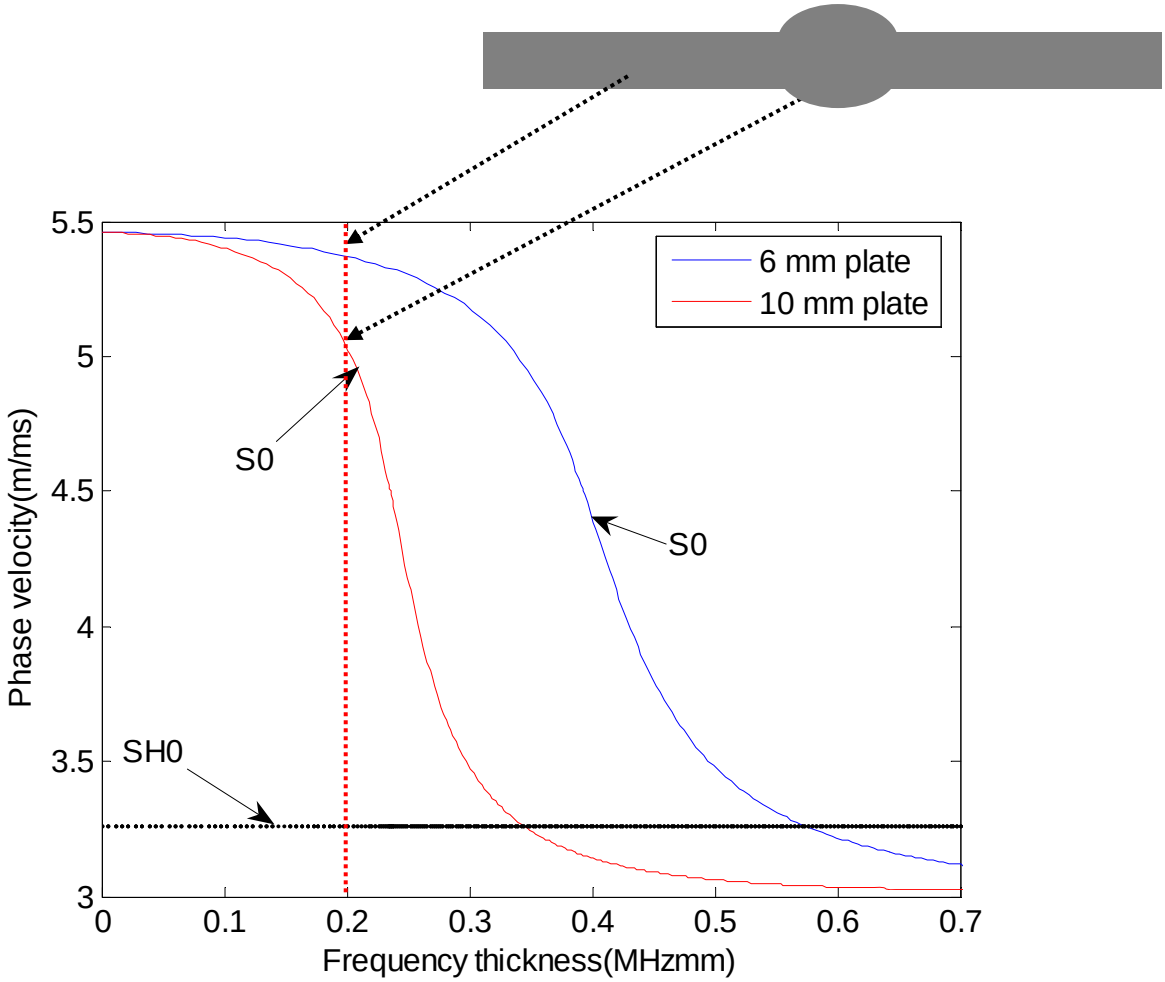

FIGURE 3.3: Phase velocity dispersion curves of S0 mode in 6 mm thick and 10 mm thick steel plates

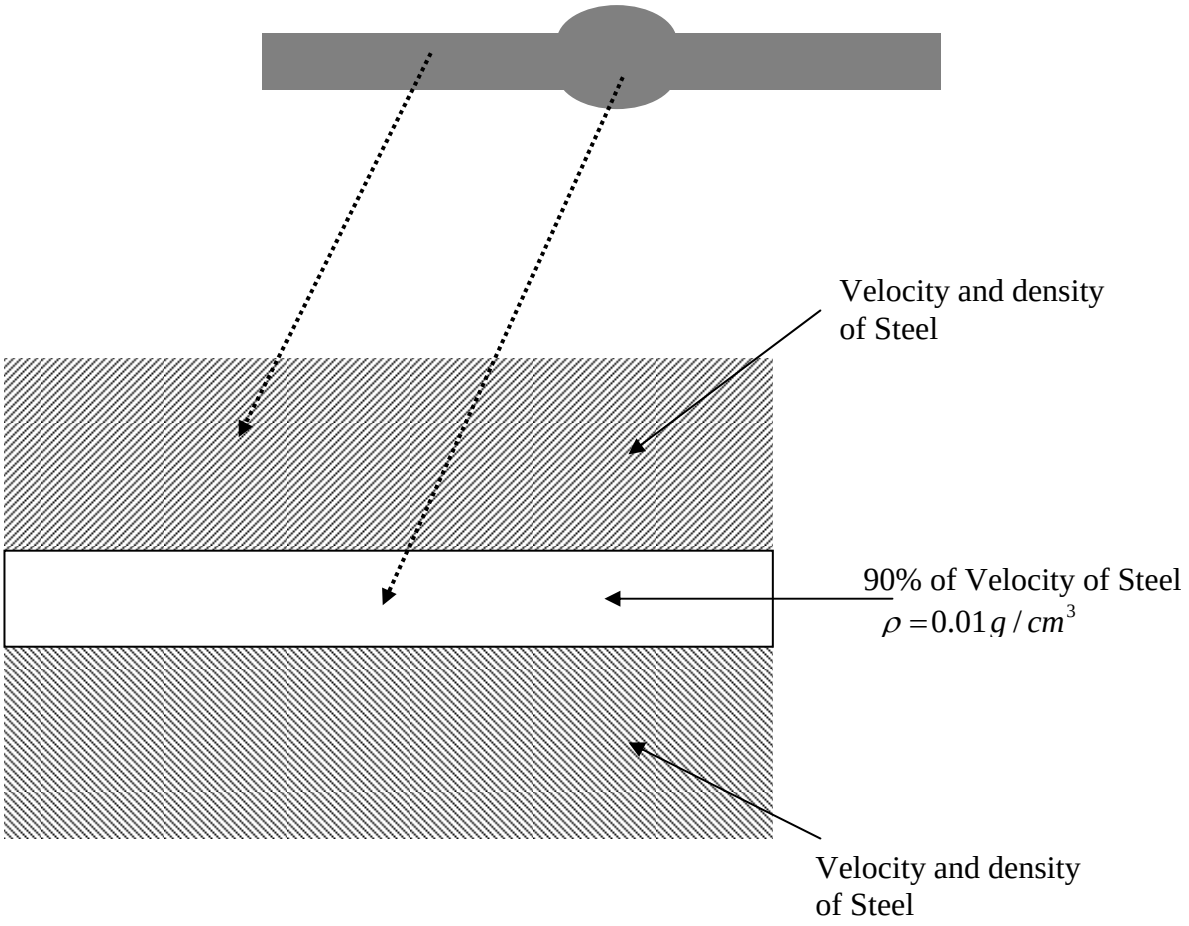

FIGURE 3.4: A model system, where a slower medium is embedded between two faster media, to represent the slower weld between two faster plates

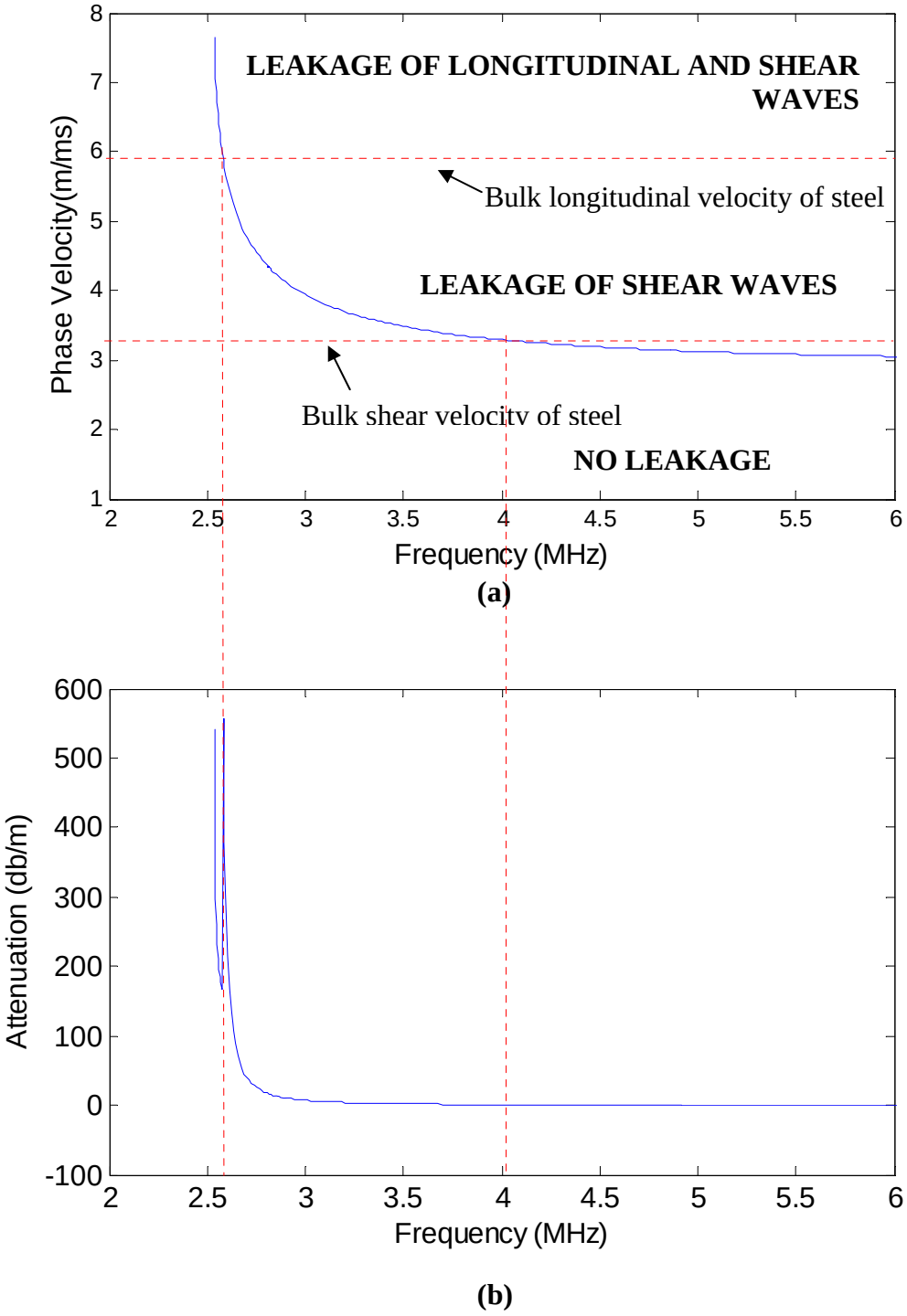

FIGURE 3.5: Dispersion curves of S0 mode in the model shown in Figure 3.4 when

$$C_l = 5.36\, m/ms,\ C_s = 2.93\, m/ms,\ \rho = 0.01\, g/cm^3$$

(a) Phase velocity, (b) Attenuation

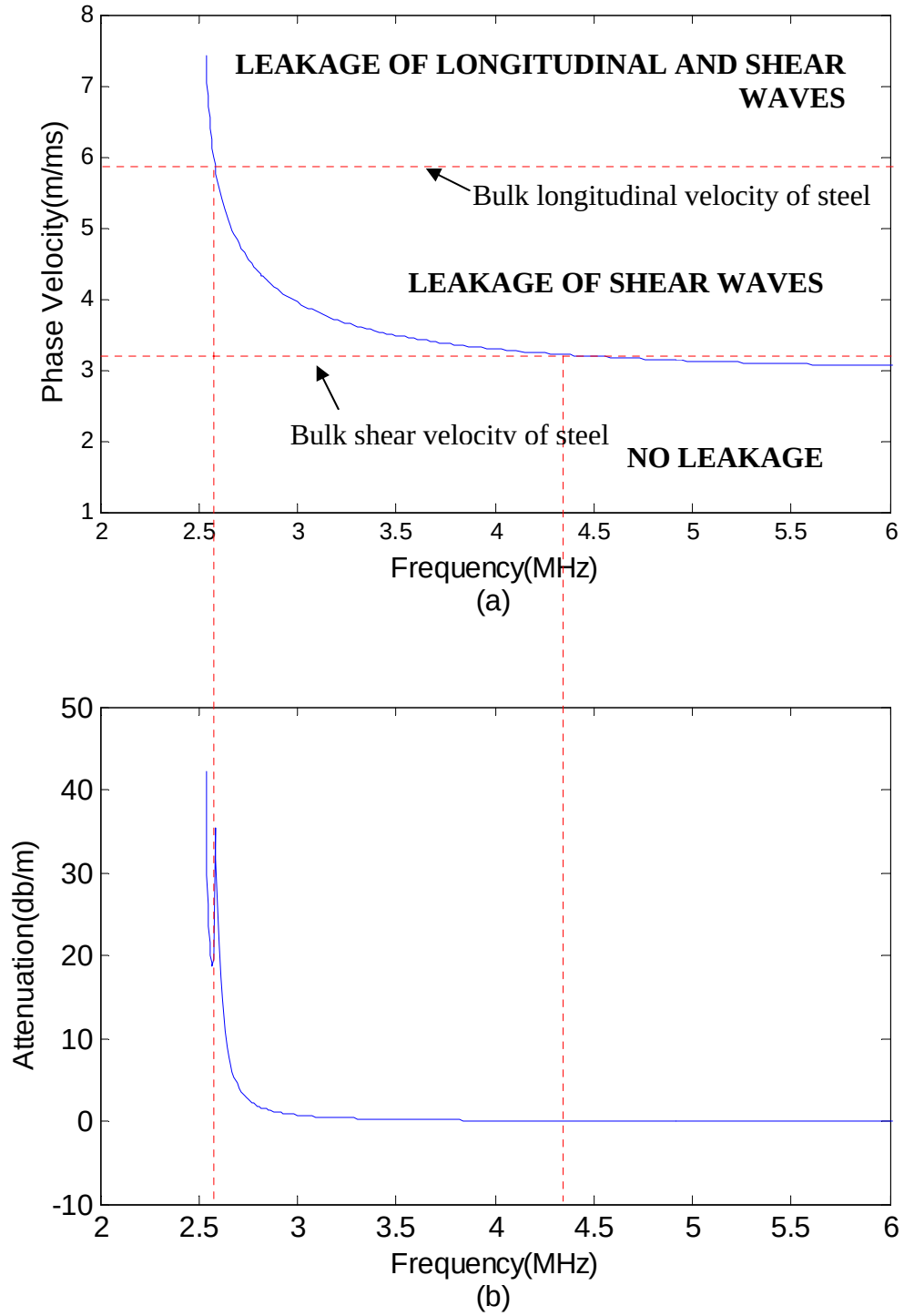

FIGURE 3.6: Dispersion curves of S0 mode in the model shown in Figure 3.4 when

$$C_l = 5.36\, m/ms,\ C_s = 2.93\, m/ms,\ \rho = 0.001\, g/cm^3$$

(a) Phase velocity, (b) Attenuation

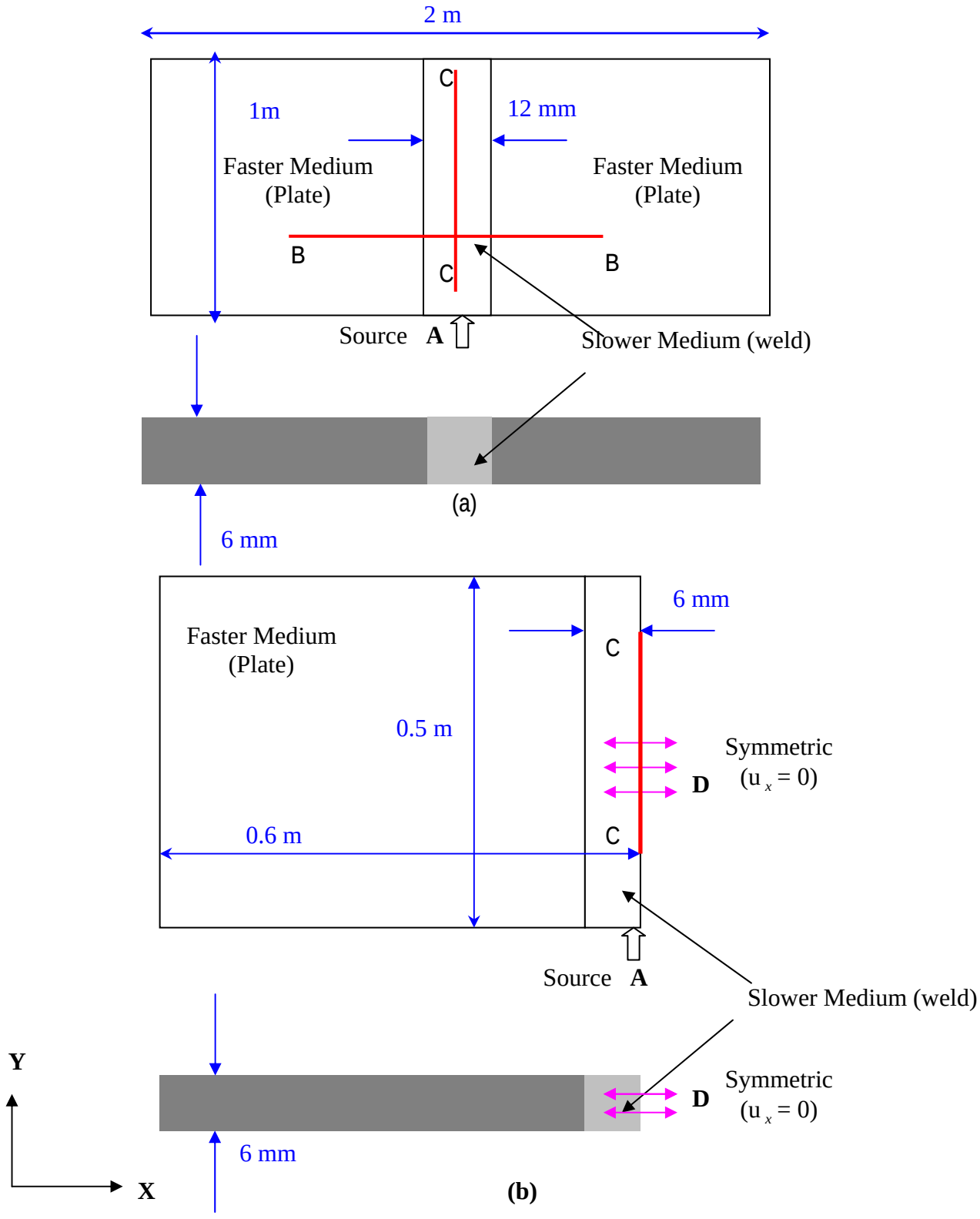

FIGURE 3.7: FE Study using idealized weld, (a). Schematic diagram of system modelled (Not to scale), (b). Schematic diagram of system modelled with symmetric boundary conditions for high frequencies (Not to scale),

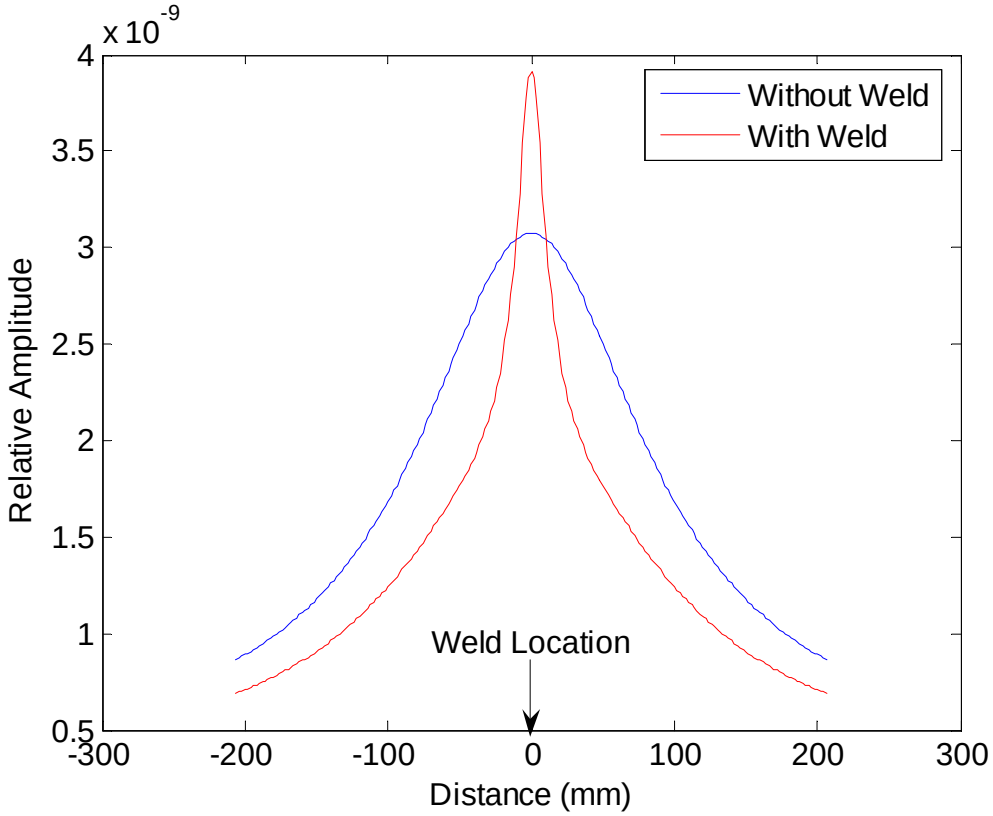

FIGURE 3.8: Amplitudes (max of time signal) for with and without weld cases on line BB shown in Figure 3.7(a)

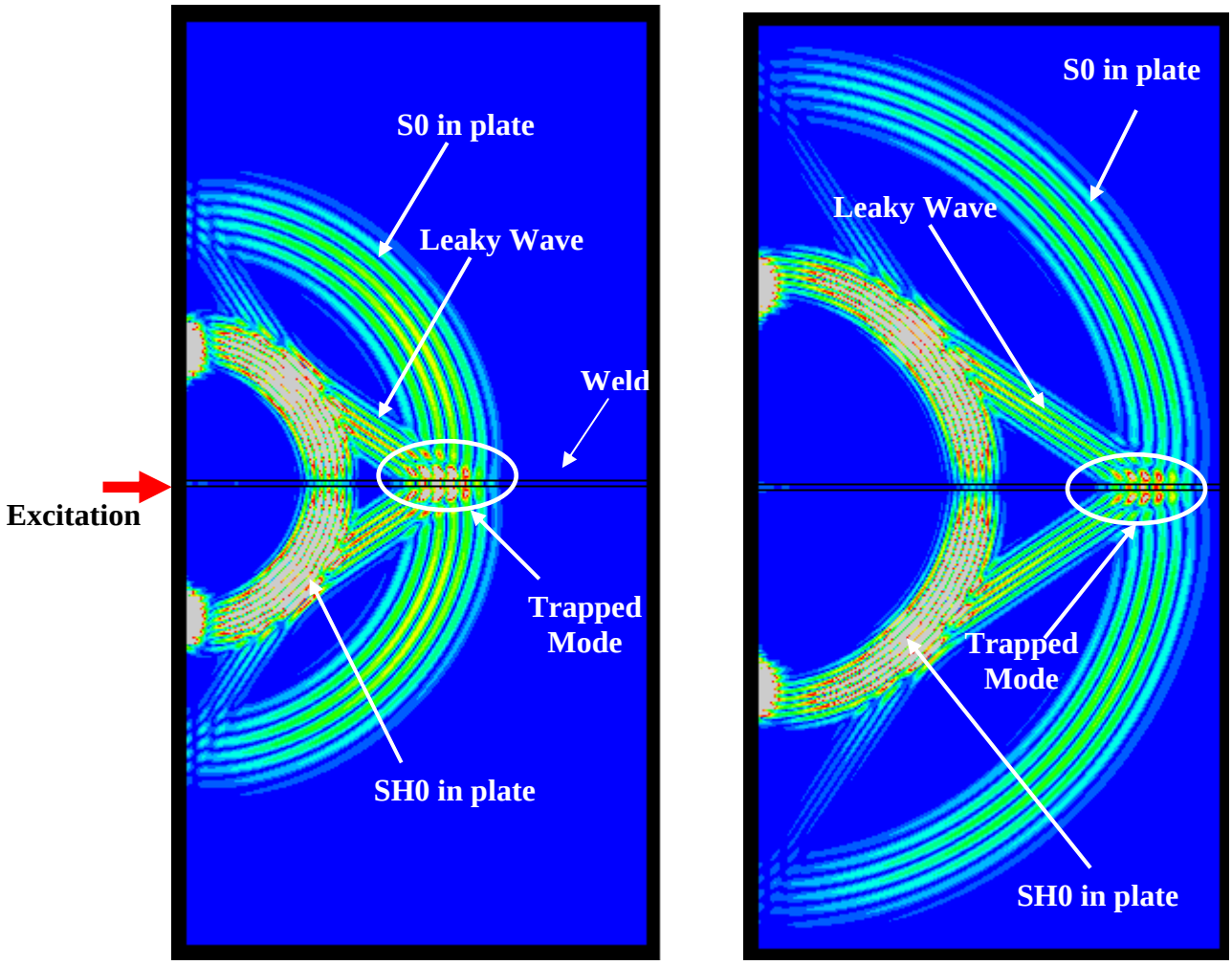

FIGURE 3.9 Contour of magnitude of resultant displacements during the simulation for the model shown in Figure 3.7(a).

(a) At an instant during the simulation, (b) at a later instant during the simulation

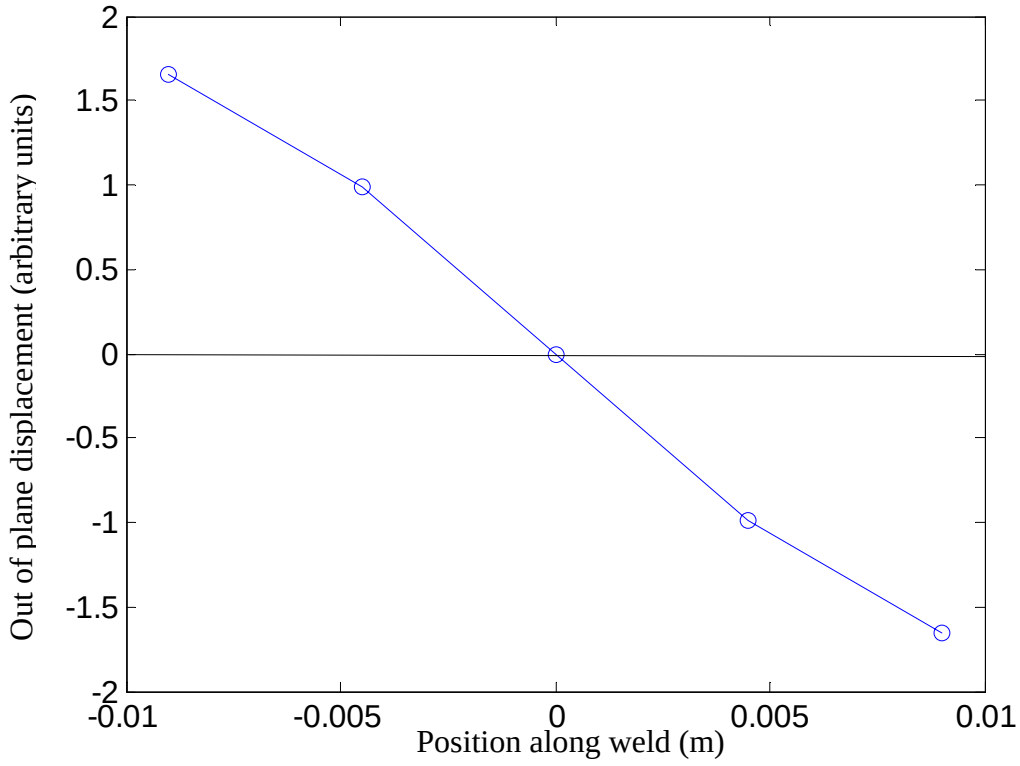

(a)

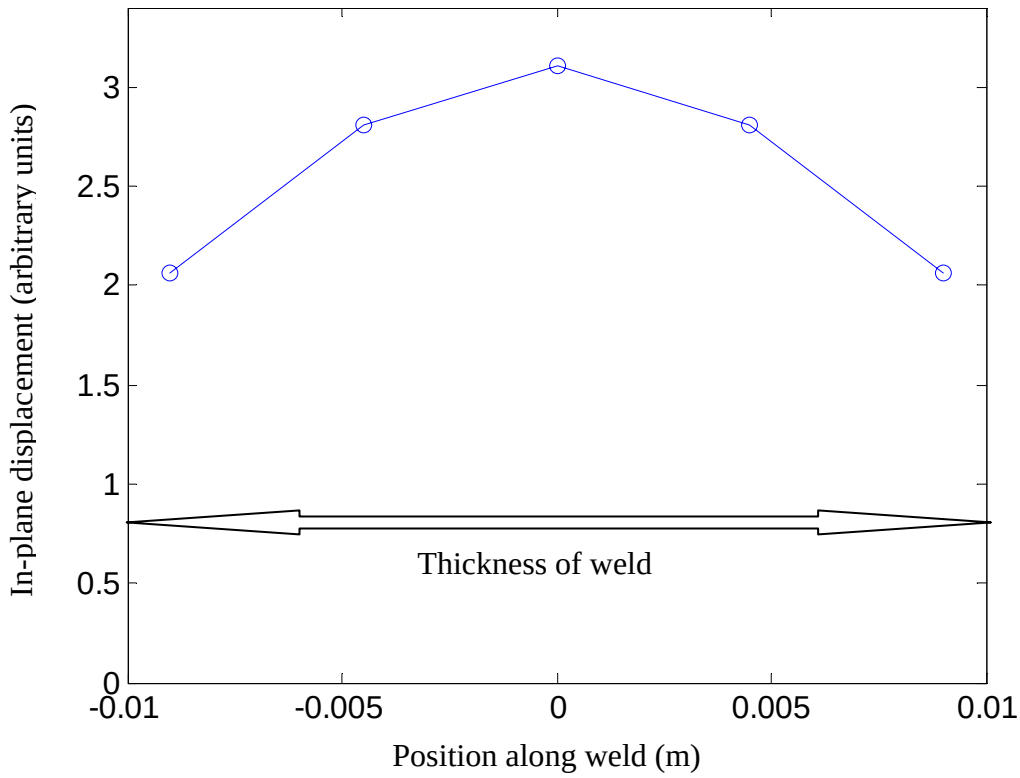

(b)

FIGURE 3.10: Mode shapes of trapped S0-like mode at 100 kHz,

(a) Out of plane displacement, (b) In plane displacement

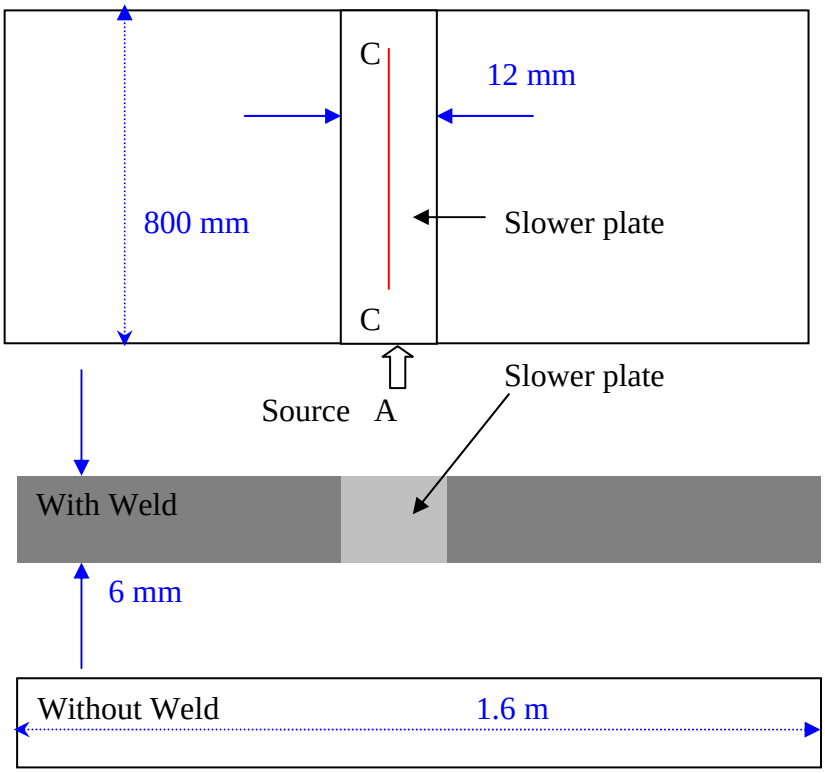

(a)

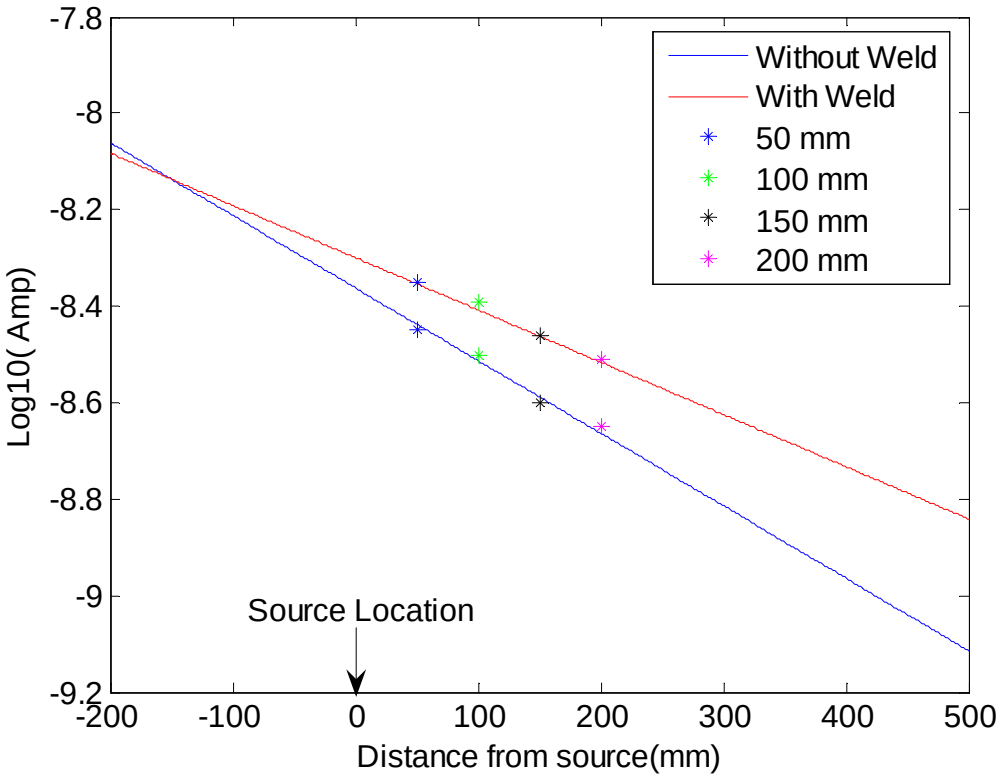

(b)

FIGURE 3.11: FE Study using idealized weld, (a). Schematic diagram of system modeled (Not to scale), (b). Log amplitudes (max of time signal) for with and without weld cases on line CC.

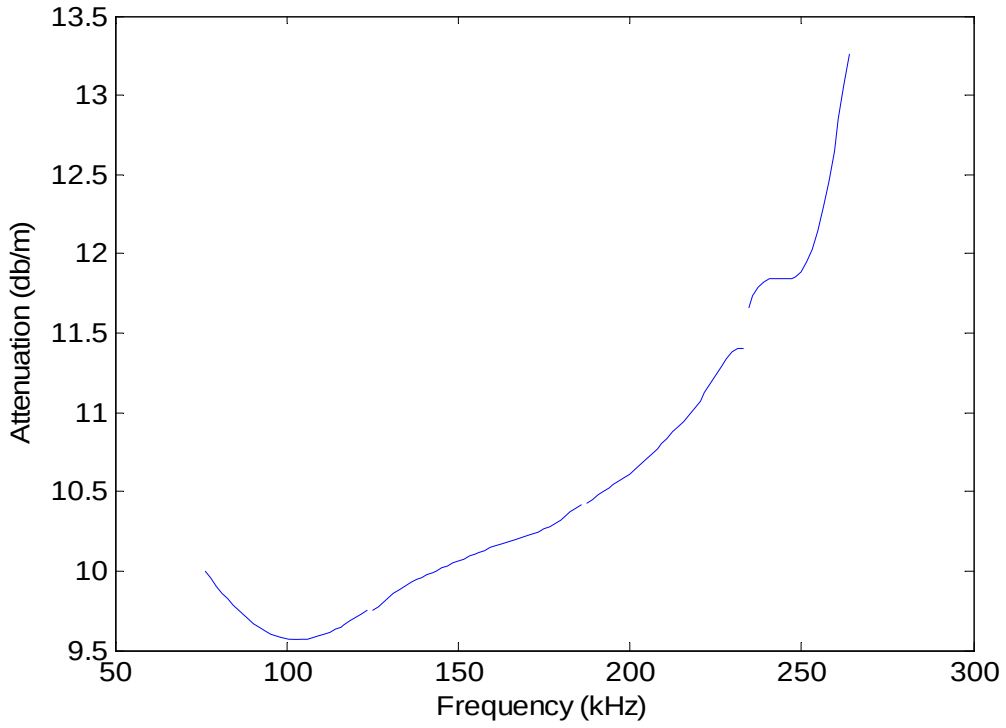

(a)

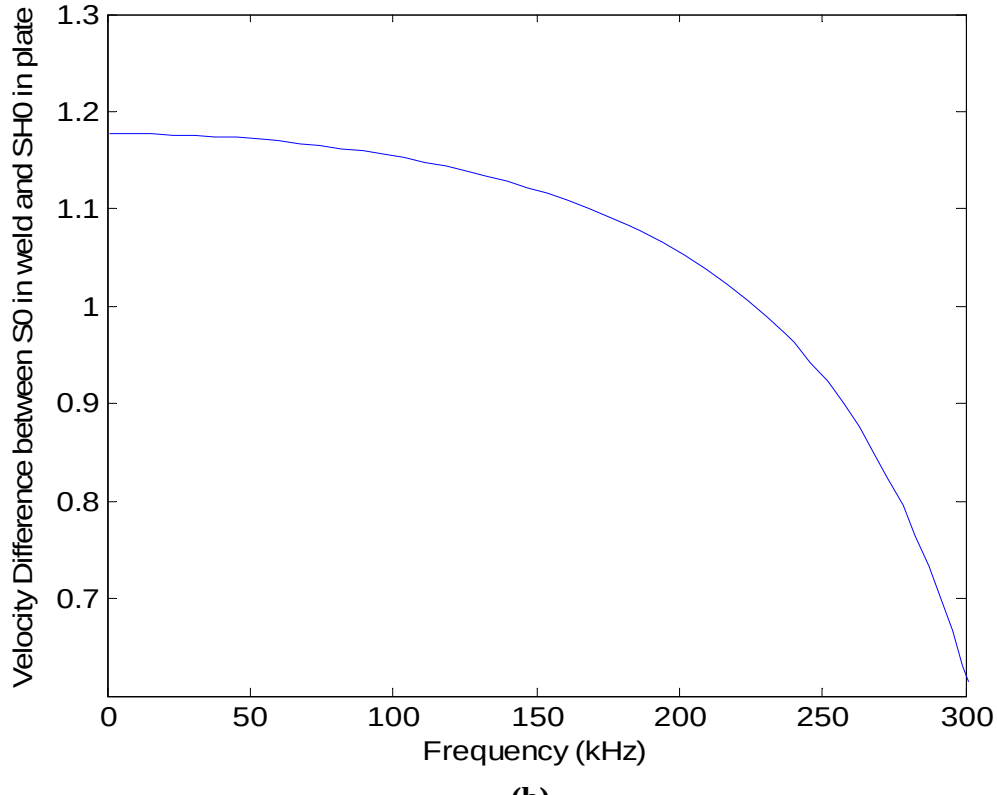

(b)

FIGURE 3.12: (a) Attenuation of the trapped S0-like mode at different frequencies (b) Velocity difference between the S0 mode in the weld and the SH0 mode in the plate at different frequencies

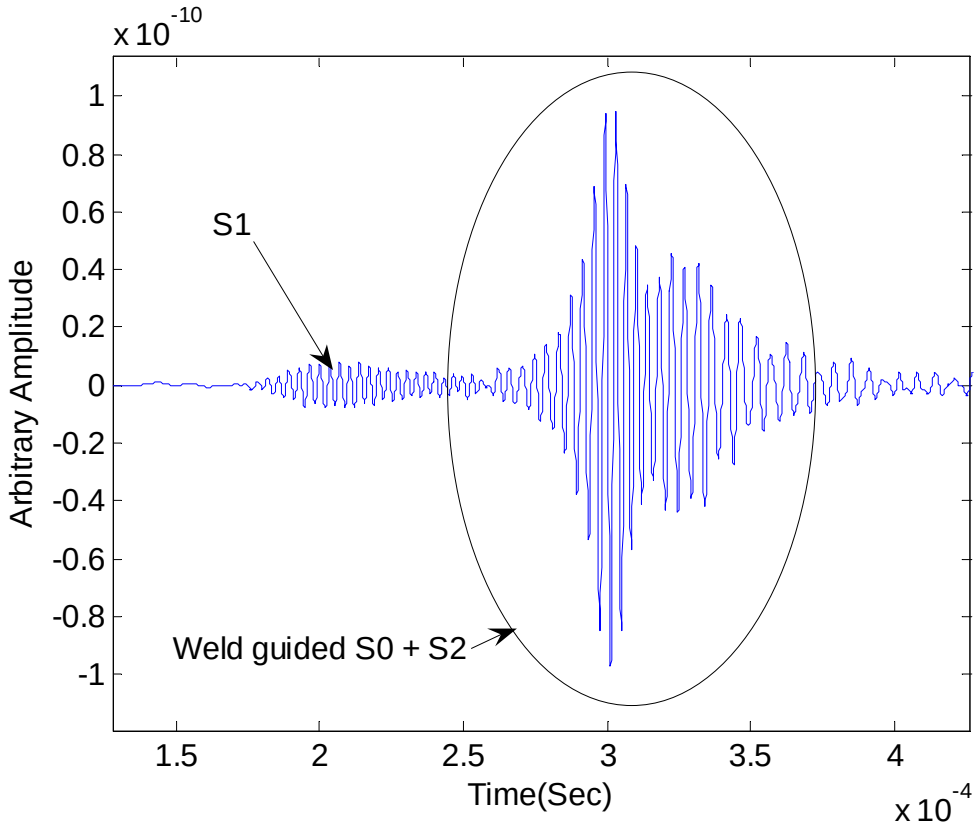

FIGURE 3.13: Typical measured signal for the model shown in Figure 3.7(b), on line 'CC' at the operating frequency of 500 kHz

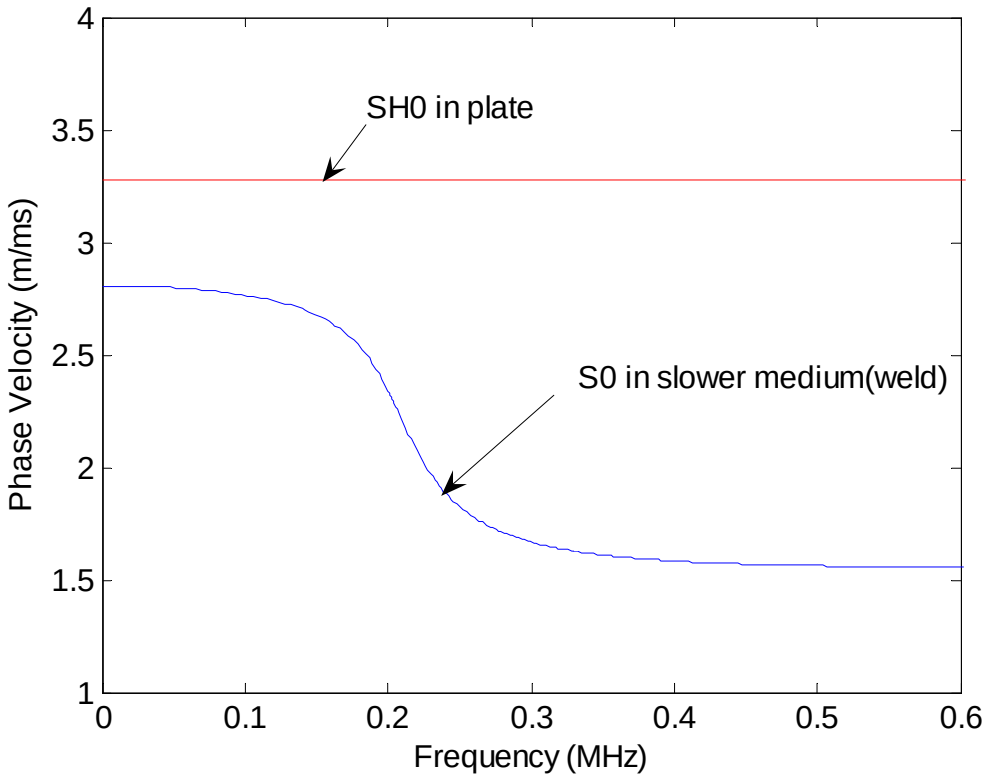

FIGURE 3.14: Phase velocity dispersion curve of S0 mode in a plain plate with properties

(E=216.9 GPa, μ = 0.2865 and density = 30000 kg/ m^3)

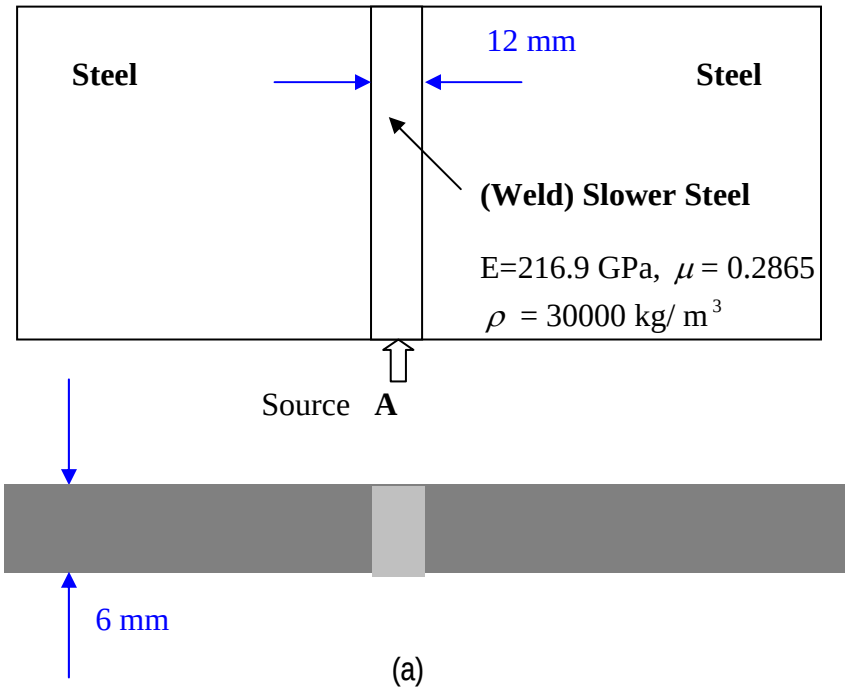

(a)

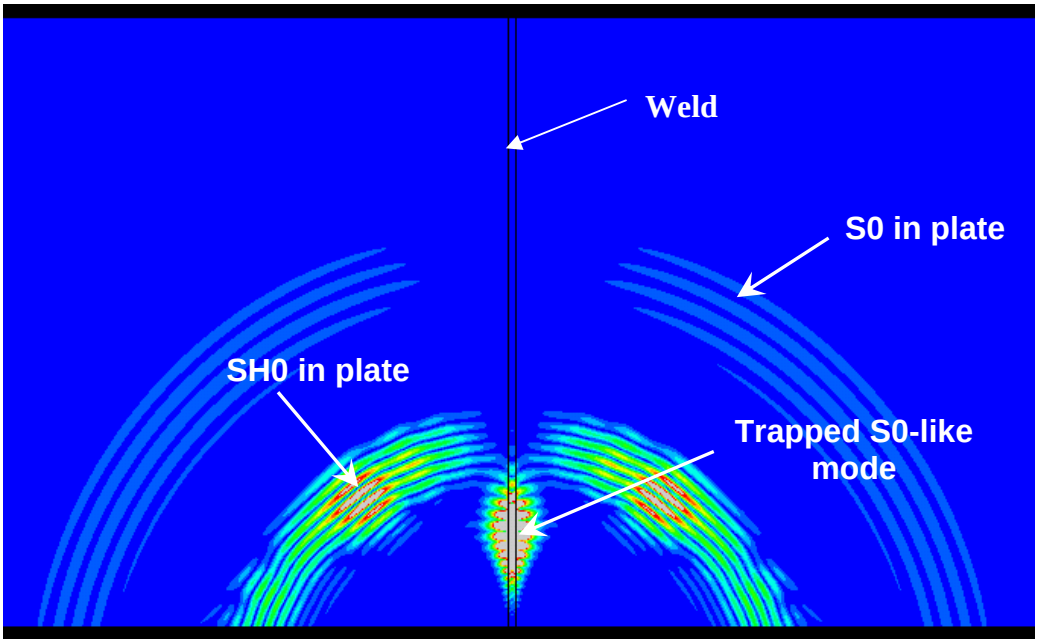

(b)

FIGURE 3.15: FE study of weld embedded between two faster steel plates. (a). Schematic diagram of system modelled (Not to scale), (b)Contour of magnitude of resultant displacement at a chosen time during the simulation

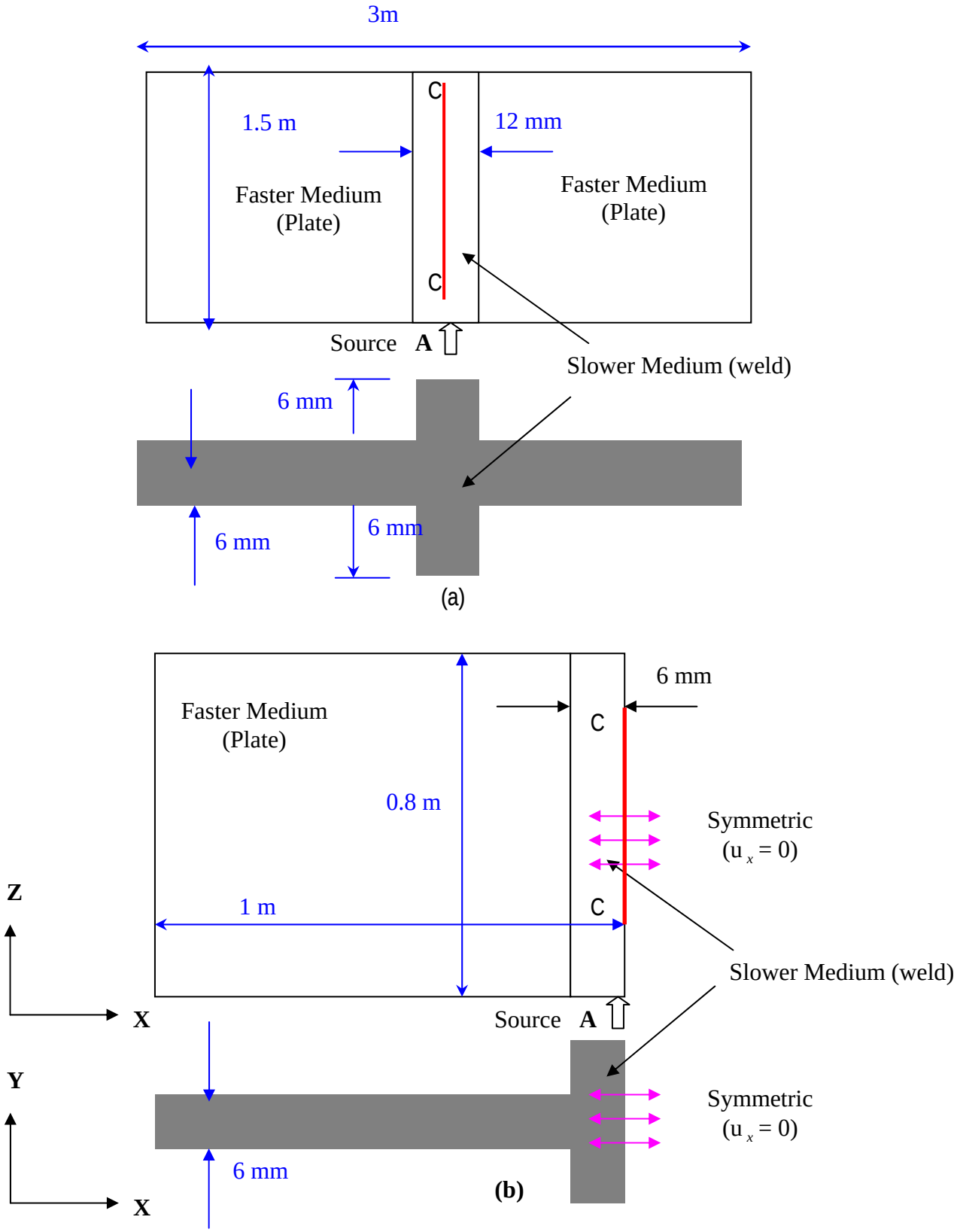

FIGURE 3.16: FE Study of propagation of trapped S0-like when the trapping is caused by the geometry of the weld, (a). Schematic diagram of system modelled (Not to scale), (b). Schematic diagram of system modelled with symmetric boundary conditions for high frequencies (Not to scale),

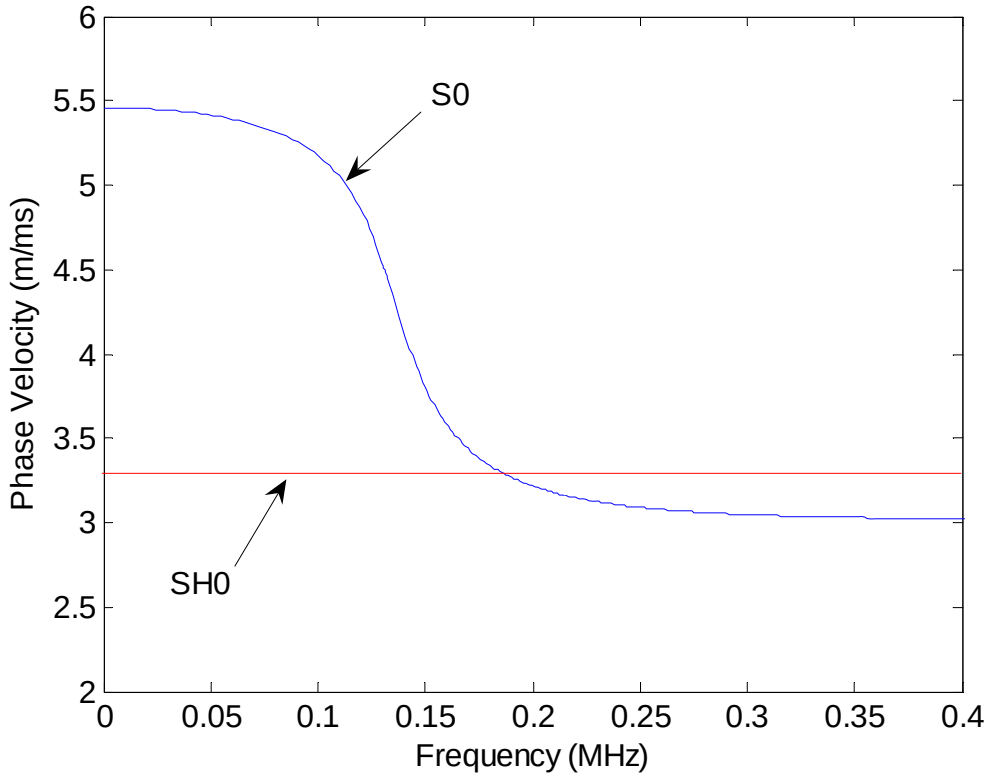

FIGURE 3.17: Phase velocity dispersion curves: S0 in an 18 mm steel plate

And SH0 in a 6 mm plate

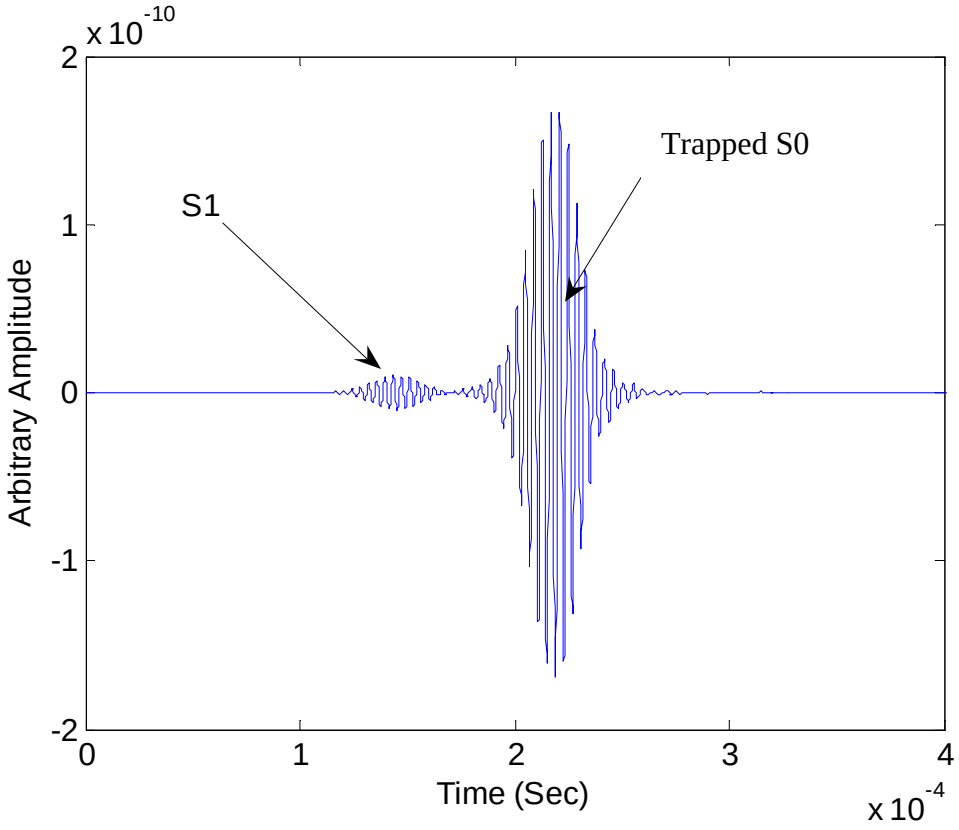

FIGURE 3.18: Typical measured signal at a distance of 500 mm from source for the model shown in Figure 3.16(b)

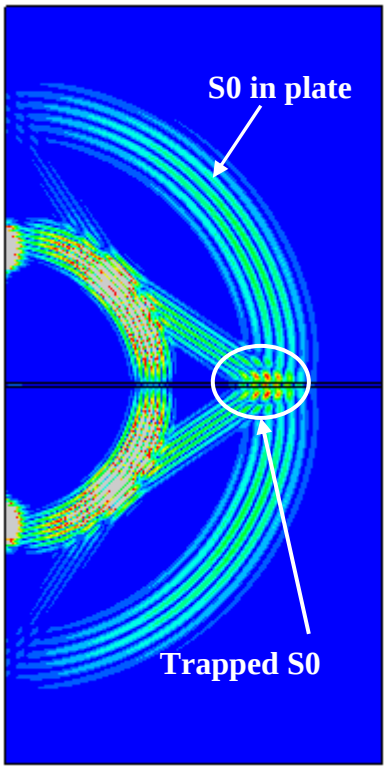

(a)

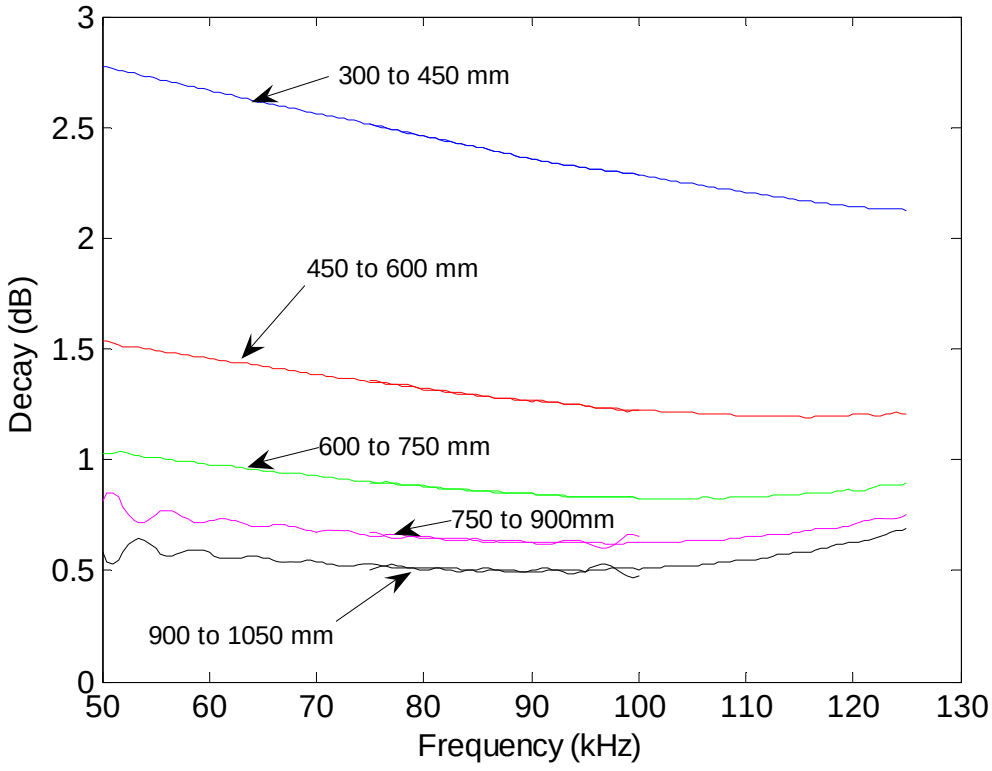

(b)

FIGURE 3.19: (a) Contour of magnitude of resultant displacement at a chosen time during the simulation for the model shown in Figure 3.16(a), (b) Attenuation of the trapped S0-like mode for different frequencies

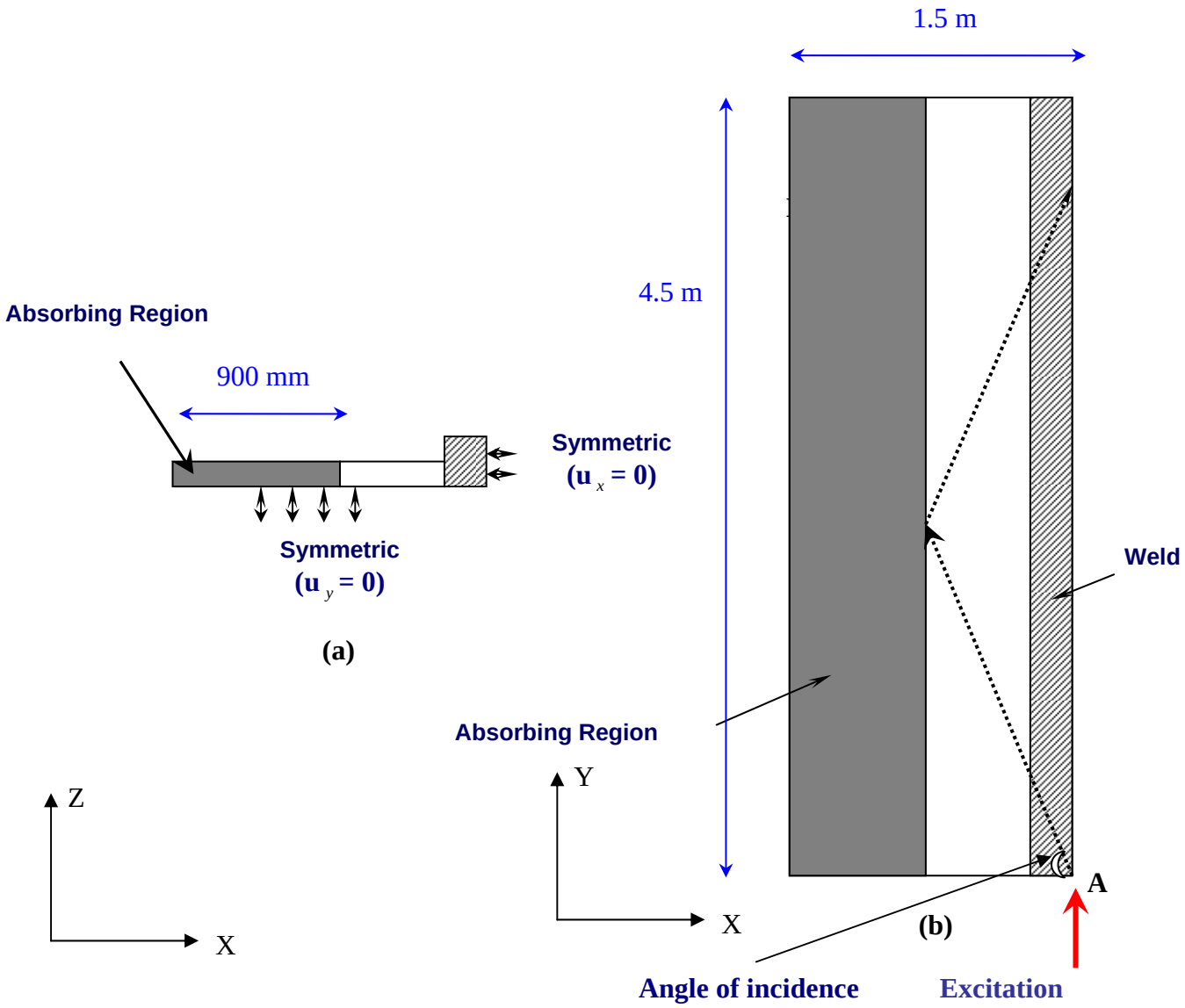

FIGURE 3.20: FE model with absorbing regions to study the attenuation of the trapped S0-like mode. (a) Side View, (b) Top View

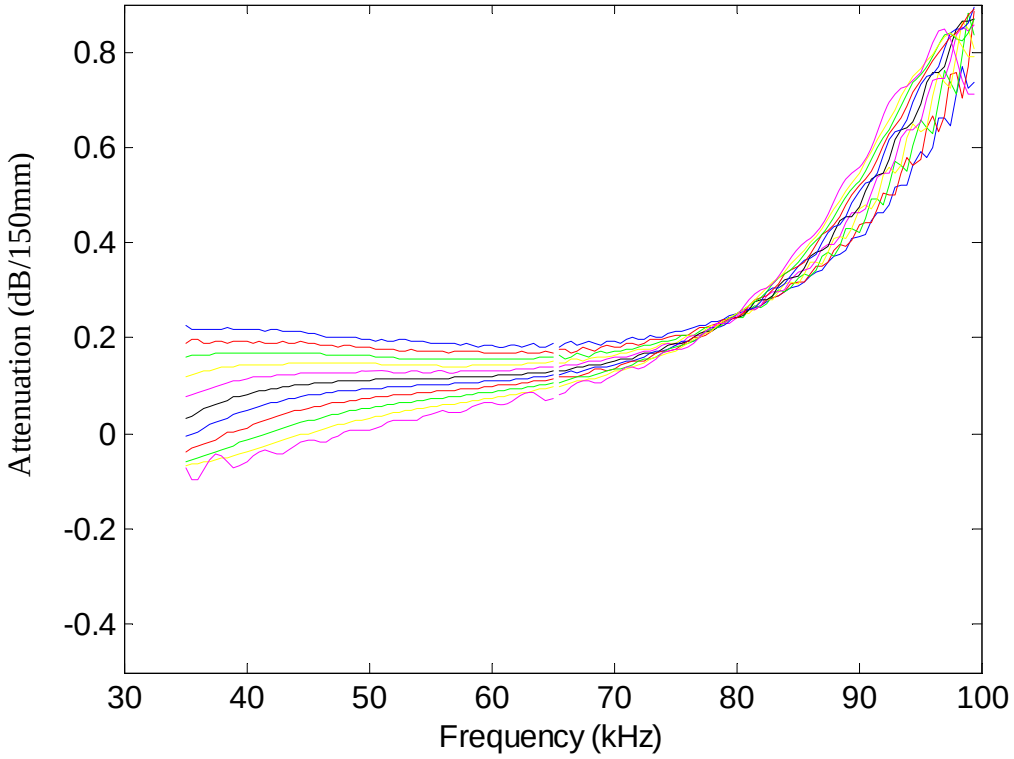

FIGURE 3.21: Attenuation of the trapped S0-like mode for different frequencies (Different curves show attenuations obtained when monitored signals are at different distances) (from 1950 mm to 3600 mm with 150 mm interval)

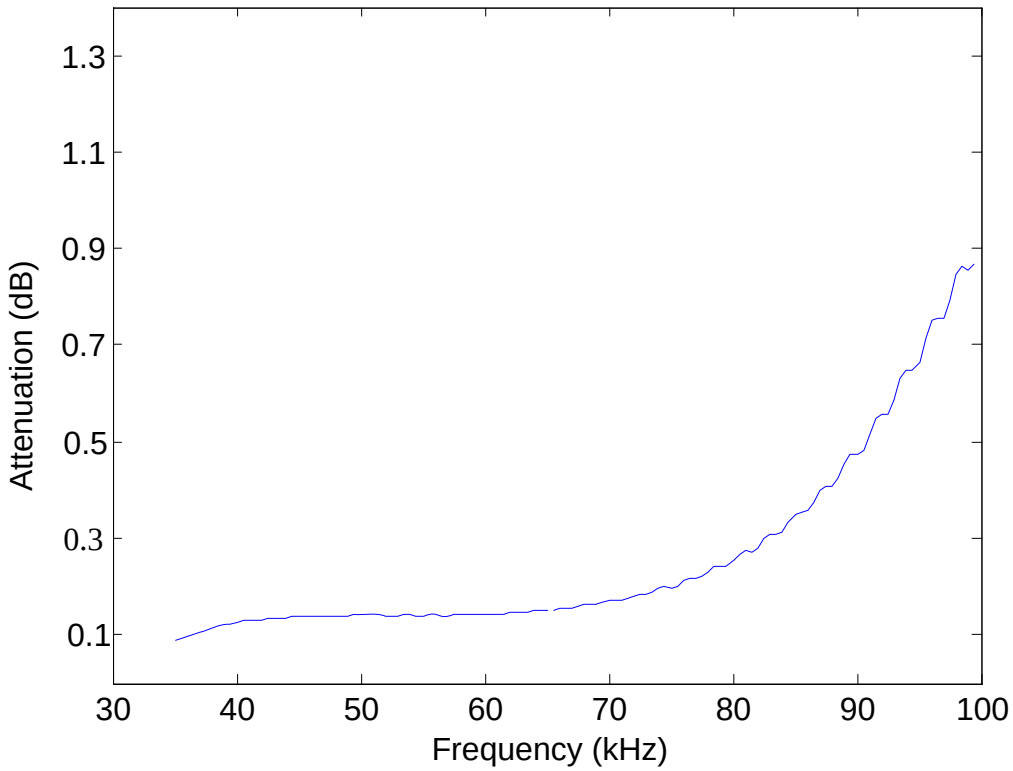

FIGURE 3.22: Average attenuation of the trapped S0-like mode in the model shown in Figure 3.20, for different frequencies

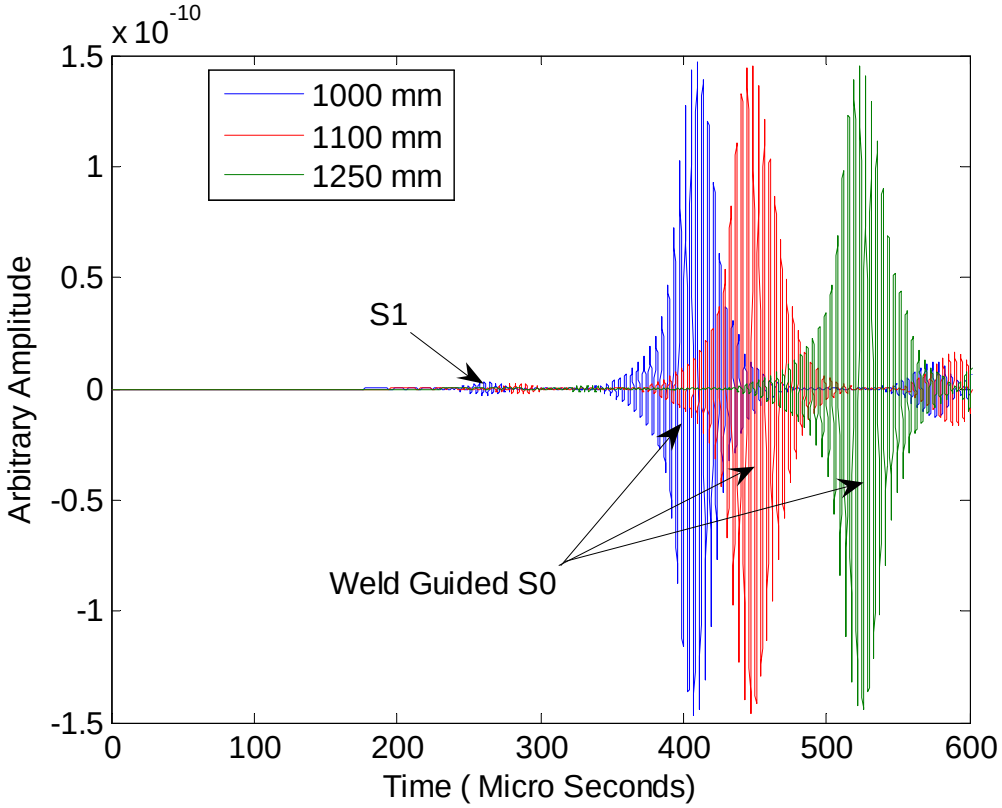

FIGURE 3.23: Typical monitored signals at different distances at 250 kHz

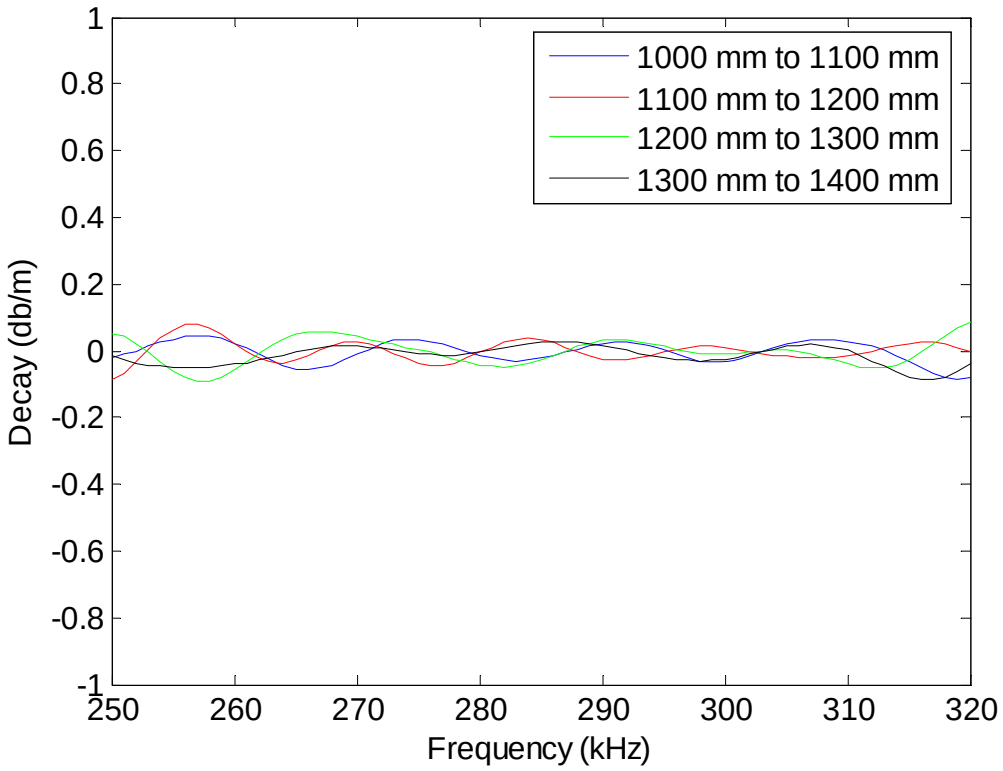

FIGURE 3.24: Attenuation of the trapped S0-like mode in the model shown in Figure 3.20, at high frequencies

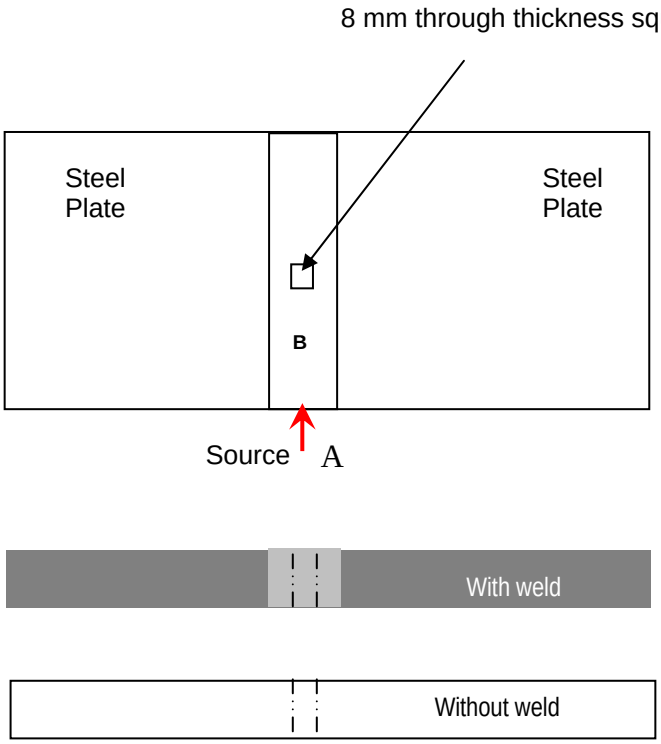

(a)

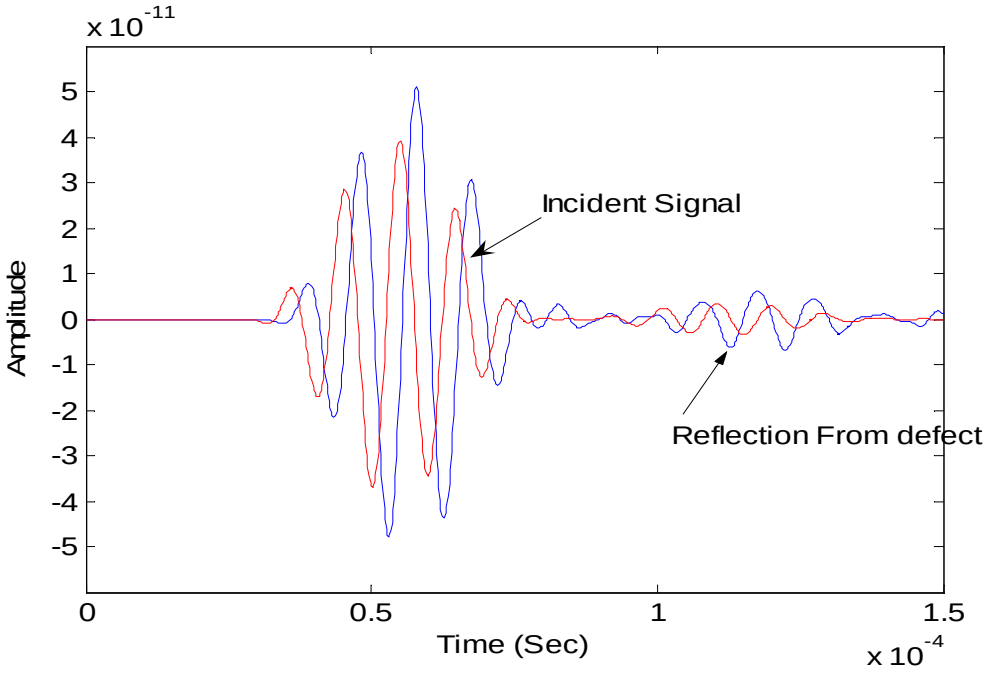

(b)

FIGURE 3.25: Initial Defect Study (a) FE model with defect in the weld (not to scale), (b) Monitored signals at point B. The red line is for a plain plate and the blue line is for the plate with weld

Chapter 4
Study of the trapped S0-like mode using Semi Analytical Finite Element method

4.1 Introduction

The attenuation results of the trapped S0-like mode obtained using 3D finite element simulations, explained in chapter 3, are convincing qualitatively but may not be accurate quantitatively because of the uncertainties related to the performance of the absorbing region at large angles of incidence and also the interference of the trapped S0-like mode with the S0 mode in the plate. Therefore an alternative solution to accurately find the dispersion curves of the trapped S0-like mode in the idealised weld is desirable.

Several methods based on the superposition of bulk waves, including, for example, the transfer matrix method or the surface impedance matrix method[71-73], have been developed in the past for the dispersion equation solution for simple geometries of waveguide such as plates or pipes. However, these methods cannot be used to find dispersion relations of guided modes in structures with arbitrary cross section.

A technique called the semi analytical finite element (SAFE) method has been developed in the recent past to investigate waveguides of arbitrary cross section. This method is also referred to in the literature as the spectral or waveguide finite element methods[74-76]. This method uses a Finite Element representation of the cross-section of the waveguide, with a harmonic description along the propagation direction[74, 75, 77, 78]. The main advantage of the SAFE method is that only the cross section of the waveguide has to be meshed by finite elements[75, 79-81]. This greatly reduces the computational time and can be

used to model large geometries. However the SAFE method is not capable of modelling discontinuities [82-84] and therefore can not be used to model defects. For plane structures of constant thickness, one dimensional SAFE (1D-SAFE) with one dimensional finite elements is used[85]. The use of a one-dimensional finite element mesh was first studied about 30 years ago to describe the cross-sectional deformation of a laminate [86, 87] and the characteristic equation for free wave propagation was expressed as a linear eigenvalue problem in frequency. The complex roots of the dispersion curves were obtained by writing the characteristic equation as an eigenvalue problem in wave number[88]. The linear mesh has been used to investigate the dispersion curves in many cases[89]. In a study of plate edge reflection of Lamb waves, the dispersion curves for elastic plates were determined using the same approach, fixing the wave number and formulating the eigenvalue problem in frequency[90, 91]. 1D-SAFE has also been used to investigate the wave propagation and damping in linear viscoelastic laminates[92].

Two dimensional SAFE (2D-SAFE) has been used to study structures with arbitrary cross section[93]. A rigorous solution of all the roots for waves in an elastic wave guide has been recently reported[94]. The solution finds roots for both propagating and non propagating modes in the wave guide, an important outcome being that necessary results are available for modal composition calculations, for example for the solution of scattering problems. The SAFE method has also been used for infinitely wide structures with periodic changes in geometry or material properties along the width of the model[95]. Wave guides

with damping properties have also been studied using the SAFE method[93]. Some studies have reported on how the SAFE method may be applied easily using standard commercial Finite Element (FE) programs, thus avoiding the necessity to write special FE codes[96]. The SAFE method with absorbing regions has recently been applied to the case of wave modes propagating along a guide of arbitrary cross-section, and radiating into a surrounding fluid or solid medium of infinite extent, the so-called "leaky" waves [99].

In this chapter the semi analytical finite element model with absorbing regions has been used in order to understand the trapped S0-like mode further. This work has been done in collaboration with Dr Michel Castaings, University of Bordeaux, France [97] to build 2D SAFE models. Mr Zheng Fan, a PhD student in the NDT Lab, Imperial College[98], who is specializing in SAFE has created initial SAFE models [127]. The help of these people is highly appreciated. The SAFE modelling of the plate-weld system has been published by Dr Michel Castaings and Prof Mike Lowe in[99]. Their paper mainly concentrates on the SAFE modelling of the plate-weld system and also presents the attenuation dispersion curve of the trapped S0-like mode using the SAFE method. However it does not present a detailed analysis of the trapped S0-like mode and its potential to NDE of long lengths of welds. A thorough mode shape analysis and defect sensitivities, at different frequencies, of the trapped S0-like mode have not been discussed in their paper. The lateral extent, an important feature of the trapped S0-like mode, has also not been discussed.

Chapter 4
Study of the trapped S0-like mode using Semi Analytical Finite Element method

The aim of this chapter is to extend this work and present a detailed analysis of the trapped S0-like mode and explain the reasons for the attenuation characteristics. I also discuss the lateral extent of the trapped S0-like mode, which can be used to detect defects in the region near the weld. The suitable frequency regime for detecting defects in the weld and the suitable frequency regime for detecting defects in the region near the weld are discussed. The attenuation values obtained using 3D finite element models, explained in chapter 3, will be compared with SAFE results.

4.2 Semi-Analytical Finite Element (SAFE) model with absorbing regions to study the trapped S0 mode

4.2.1 SAFE model formulation for the weld geometry.

The SAFE method to find dispersive solutions uses a finite element discretisation of the cross section of the wave guide with displacements along the wave propagation direction described in an analytical fashion as harmonic exponential functions [95]. The 3D weld model shown in figure 4.1(a) has been reduced to a 2D model shown in figure 4.1(b), and the guided waves propagating along the weld are considered. The cross section has been meshed with 2D semi analytical finite elements. These elements are also called spectral elements or spectral finite elements [75-80]. The element used has 3 degrees of freedom per node and the element takes into account the variation of mechanical properties along its depth (along the length of the weld). The formulation of the spectral finite elements can be found in [95]. The displacement vector u_r in the weld is written as [95]

$$u_r(x_1, x_2, x_3, t) = U_r(x_1, x_2)\, e^{i(kx_3 - wt)} \tag{4.1}$$

where 'k' is the wave number along the propagation direction, ω is the angular frequency and t is the time. The equation of dynamic equilibrium is written in the following form of an eigenvalue problem [95].

$$C_{sprq}\frac{\partial^2 U_r}{\partial x_p \partial x_q} + i(C_{s3rp} + C_{spr3})\frac{\partial (kU_r)}{\partial x_p} - kC_{s3r3}(kU_r) + \rho\omega^2 \delta_{sr} U_r \tag{4.2}$$

where the coefficients C_{sprq} are the stiffness moduli. The solution is to find eigenvalues of wave number (k) for a given value of frequency (ω). The general form of the eigenvalue problem is expressed as follows [95]:

$$\nabla.(c\nabla U + \alpha U - \gamma) - \beta\nabla U - aU + \lambda d_a U = 0 \tag{4.3}$$

Each solution at the given frequency will reveal the wave numbers of all the possible modes at that frequency. The dispersion curves are found by repeating the solution for a range of frequencies.

4.2.2 Modelling of absorbing regions in the SAFE model.

The surrounding plates of the plate-weld system are limited by borders and therefore there is a problem with the original SAFE approaches because, however large the surrounding plates are chosen to be, they are still finite. Thus the set of eigenvalues found when solving equation 4.2 represents resonances of the whole bounded system, including the weld and the surrounding plates, and consequently the leaky solutions are not found [99].

In order to suppress the reflections from the free edges of the plates in the SAFE model, an absorbing region is modelled at each side as shown in figure 4.2. The SAFE model shown in Figure 4.2 is 2 m in length and it has absorbing regions of length 800 mm on both sides as shown in the figure. The dimensions of the plate weld system shown in Figure 4.2 are the same as those in QNDE paper [126] and in [99]. The absorbing region has been optimized as explained in chapter 2. The maximum possible wavelength in the system is that of the S0 mode at the lowest frequency of interest. At 50 kHz the wavelength of the S0 mode in the plate is about 100 mm and its projection along the x_1 axis will depend on the angle of incidence, so the optimum length of absorbing region is different for different angles of incidence. For angles of incidence close to 90^o, the projection of wave length along the x-axis is close to infinity. As it is impossible to model infinite lengths of absorbing regions, it is also almost impossible to avoid reflections from the boundaries at large angles of incidence. These reflections again pollute the monitored signal at distances far away from the source.

The length of the absorbing region has been chosen in such a way that there are no reflections from the edge for angles of incidences between 0^o *and* 65^o where the projection of wavelength along the x_1-axis would be between 109 mm and 258 mm. The length of the absorbing region was therefore set to 800 mm. The width of the model was set to 2 m including the absorbing regions.

4.3 Results

The equation 4.2 is solved for frequencies in the range from 50 kHz to 300 kHz. Several solutions *k* are found at each frequency; some representing resonances of the whole system or of the plates, and some corresponding to resonances of the weld joint and representing modes guided along the weld and radiating to infinity in the surrounding plates. The trapped S0-like mode has been identified by plotting the axial component of power flow [99]. The mode shapes of the trapped S0-like mode have been obtained, by monitoring nodes through the thickness (on line 'B' shown in Figure 4.2).

The eigenvalue solution found at the operating frequency of 50 kHz is 57.71-0.076i rad/mm. The phase velocity for this solution is 5.44 m/ms ($vph = \frac{2\pi f}{57.71} = 5.44\, m/ms$) and the attenuation is 0.076 Np/m which is equal to 0.66 dB/m. According to Snell's law [50,51], only modes of the surrounding plates having phase velocities smaller than 5.44 m/ms could be radiated into the plates. The S0 mode in the surrounding plates has a phase velocity of $5.45\, m/ms$ and therefore the S0 mode cannot radiate, while the other two

fundamental modes, A0 and SH0 could. However, the trapped S0-like mode is symmetric with respect to the mid plane of the plates and weld, so the A0 mode, which is anti symmetric, cannot be launched. Therefore, the SH0 mode is the only mode that can leak into the plates, and its radiation must be at an angle equal to $\theta_{rad} = \sin^{-1}(\frac{3.26}{5.44}) = 36.78^{o}$, with respect to the direction normal to the plates- weld interfaces.

Figure 4.3(a) shows the power flow in the x_3 direction. Figure 4.3(b) shows mode shapes through thickness on line 'B' shown in Figure 4.2, where the red curve shows out of plane displacement(x_2) and the blue curve shows in-plane displacement (x_3). Figure 4.3(c) shows amplitudes of the trapped S0-like mode in the x_3 direction on line 'A' shown in Figure 4.2. Figure 4.3(c) shows that the trapped S0-like mode is also present in the region near to the weld at this frequency. The same can also be seen in Figure 4.3(a), where the energy is plotted across the cross section.

The lateral extent (the extent in the x_3 direction, up to the point where the amplitude reaches zero for the first time) of the trapped S0-like mode is about 350 mm, which is approximately equal to 3.2 wave lengths, on both sides of the weld, and the amplitude of the trapped S0-like mode decreases exponentially in the lateral direction as shown in Figure 4.3(c). This suggests that the trapped S0-like mode at 50 kHz can potentially be used to inspect defects in the weld and defects near the weld that are up to a maximum of 3.2 wave lengths from the

weld. However the sensitivity is expected to decrease exponentially as the lateral distance of the defect from the weld increases. The reason for the 3.2λ lateral extent is yet unknown. The oscillations in Figure 4.3(c) are due to the leakage of SH0 into the plate. There are no oscillations at frequencies where there is no leakage into the surrounding plates, which will be shown later in this chapter.

The results at frequencies from 75 kHz to 300 kHz have been calculated in the same way explained above. The power flow and mode shapes for frequencies 75 kHz to 300 kHz have been plotted in Figures 4.4 to 4.13. The lateral extent of the trapped S0-like mode at 75 kHz is about 200 mm (with exponential decay in the lateral direction) on both sides of the weld, which is equal to 2.7 wave lengths on both sides at 75 kHz. This suggests that the trapped S0-lke mode at 75 kHz can potentially be used to inspect defects in the weld and heat affected zones that are up to a maximum of 2.7 wave lengths from the weld. At 100 kHz, the trapped S0-like mode has a lateral extent of 90 mm, which is equal to 1.7 wavelengths at that frequency. Similarly the trapped S0-like mode has a lateral extent of 50mm, equal to 1.2 wavelengths, at 125 kHz and one wave length at 150 kHz. At 175 kHz it has a lateral extent of 0.5 wave length.

At frequencies above 175 kHz, the trapped S0-like mode has no lateral extent. The lateral extent of the trapped S0-like mode decreases as the frequency increases, which suggests that the sensitivity of the trapped S0-like mode to the target defects in the region near the weld decreases as the frequency increases.

Therefore, only the low frequency regime is suitable for inspecting defects in the region near the weld.

The energy becomes more and more concentrated in the centre of the weld with less and less energy near the surface as the frequency increases up to 125 kHz. This can be seen from power flow plots shown in Figure 4.3(a) to 4.6(a) and mode shape plots shown in Figures 4.3(b) to 4.6(b). This suggests that the sensitivity of the trapped S0-like mode to the small surface breaking cracks decreases and the sensitivity to defects in the centre of the weld increases as the frequency increases up to 125 kHz. At frequencies above 125 kHz, the energy starts dispersing towards the surfaces of the weld, which can be seen in Figures 4.7(a) to 4.13(a) and 4.7(b) to 4.13(b). Therefore, the frequencies above 125 kHz may only be used to inspect small surface breaking cracks as the trapped S0-like mode has energy concentrated near the surface of the weld. The defect study is discussed in detail in chapter 6.

Figure 4.14(a) shows the phase velocity dispersion curve for the trapped S0-like mode, found by repeating the SAFE solutions over a range of frequencies. Figure 4.14(b) shows the angle at which SH0 is leaked in to the surrounding plates at different frequencies. The phase velocity of the trapped S0-like mode crosses the phase velocity of the SH0 mode in the plate at a frequency of 200 kHz and hence the trapped S0-like mode is expected to show no SH0 leakage and no attenuation at frequencies above 200 kHz. In Figure 4.15, the phase velocity of the trapped S0-like mode has been compared with the phase velocity of the S0

mode in an 18 mm steel plate. The SAFE solutions indicate that the trapped S0-like mode in the weld is similar to the S0 lamb mode in the 18 mm thick plate. Figure 4.16 shows the attenuation of the trapped S0–like mode due to leakage of energy into the adjacent plates, at different frequencies. The SAFE results in Figures 4.14 and 4.16 have been published in [99]

The trapped S0-like mode attenuates as it leaks SH0 mode into the plate, where the phase velocity of the trapped S0-like mode is greater than SH0 in the plate. The velocity difference of the trapped S0-like mode and the SH0 mode in the plate decreases as the frequency increases up to 175 kHz, so an increased attenuation with frequency up to 175 kHz would be expected. However the geometry of the plate-weld interface also plays a major role in the attenuation of the trapped S0-like mode.

The plates are attached to the centre of the weld, so the energy from the weld can only leak from the centre of the weld. The energy in the weld becomes more and more centre concentrated as the frequency increases up to 125 kHz, so more and more energy can leak into the plates for frequencies up to 125 kHz. At frequencies above 125 kHz, the energy of the trapped S0-like mode starts dispersing towards the surfaces of the weld with less and less energy in the centre. Therefore, less and less energy can leak into the plates at frequencies above 125 kHz, resulting in less attenuation at frequencies above 125 kHz.

When the leaky SH0 mode strikes the edge of the plate at an angle, it reflects the SH0 mode and also a mode converted S0 mode. The absorbing region modelled is capable of absorbing the leaky SH0 mode for angles of incidence up to 80^0. However for angles of incidence between 80^0 and 90^0, it is not possible to avoid S0 reflections from the edge of the plate as the absorbing region is not capable of fully absorbing the SH0 mode between these angles. The reflected S0 mode pollutes the results and therefore the results obtained at 175 kHz are unreliable. The trapped S0-like mode above 200 kHz is slower than SH0 mode in the plate. Therefore, the trapped S0-like mode shows zero attenuation above 200 kHz.

4.4 Comparison of SAFE and 3D FEM results

Figure 4.16 compares the attenuation values of the trapped S0–like mode, obtained using SAFE and 3D FEM. The blue curve shows SAFE results and the red curve shows 3D FEM results. Both 2D SAFE and 3D FEM results are frequency domain calculations and have no attenuation due to dispersion. Both results show an increasing attenuation as the frequency increases, in the low frequency regime, as the velocity difference between the trapped S0-like mode and the SH0 mode in the plate decreases.

Even though the 2D SAFE and 3D FEM results in the low frequency regime are comparable qualitatively, they show a significant amount of variation quantitatively. This is believed to be due to the near field effects in the 3D FEM model as explained in the previous chapter. The SAFE results are believed to be

more accurate than the 3D FEM results in the low frequency regime as SAFE models do not have any near field issues. The SAFE results between 150 kHz and 200 kHz are not reliable because of the S0 reflections, at large angles on incidence, from the absorbing region. 3D FEM is the only option at frequencies where SAFE results are unreliable because of the reflections from the absorbing region.

At high frequencies (above 200 kHz) both 2D SAFE and 3D FEM results are comparable both qualitatively and quantitatively as the trapped S0-like mode and the S0 mode in the plate are well separated in time in the 3D FE model. SAFE method is advantageous over 3D FEM in a way that SAFE method requires less computational resources. However SAFE method is not capable of modelling defects and 3D FEM is the only option for all defect studies.

4.5 Conclusions

From the above studies it is understood that the trapped S0-like mode can potentially be used to inspect long lengths of weld and regions near welds. The attenuation of the trapped S0-like mode increases as the velocity difference between the trapped S0-like mode and SH0 mode in the plate decreases. It has zero attenuation at frequencies where the trapped S0-like mode is slower than SH0 in the plate. The lateral extent of the trapped S0-like mode decreases as the frequency increases. Therefore, the low frequency regime is more suitable for

inspection of defects in the heat affected zones and the high frequency regime for defect inspection in the weld.

The energy of the trapped S0-like mode is concentrated more and more in the centre of the weld as the frequency increases up to 125 kHz. At frequencies above 175 kHz, the wave length of the trapped S0-like mode is less than the width of the weld and the mode is completely guided by the weld caps with no lateral extent in the surrounding plates. At frequencies above 175 kHz the mode behaves like a surface wave and may only be used to detect small surface breaking cracks in the weld. The above studies suggest that the properties of the trapped S0-like mode depend on the geometry of the weld. Therefore, it is necessary to model more realistic geometries of the weld in order to exploit the trapped S0-like mode for NDE of real welds. More realistic welds are studied in the next chapter.

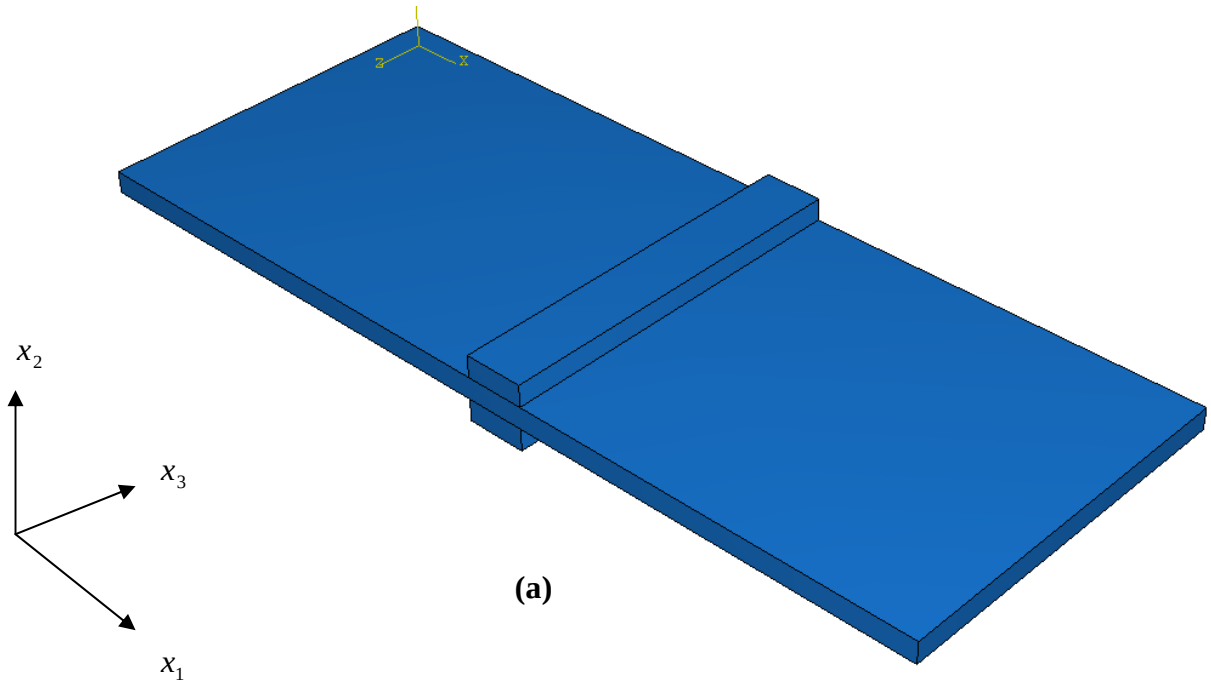

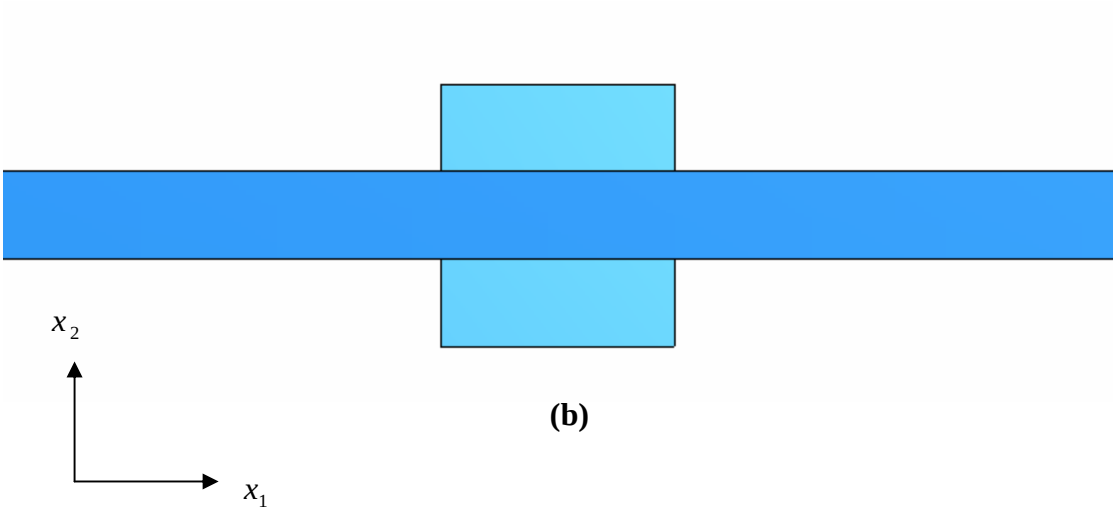

FIGURE 4.1: Idealized weld with thickened region in the middle, (a) 3D model, (b) 2D model

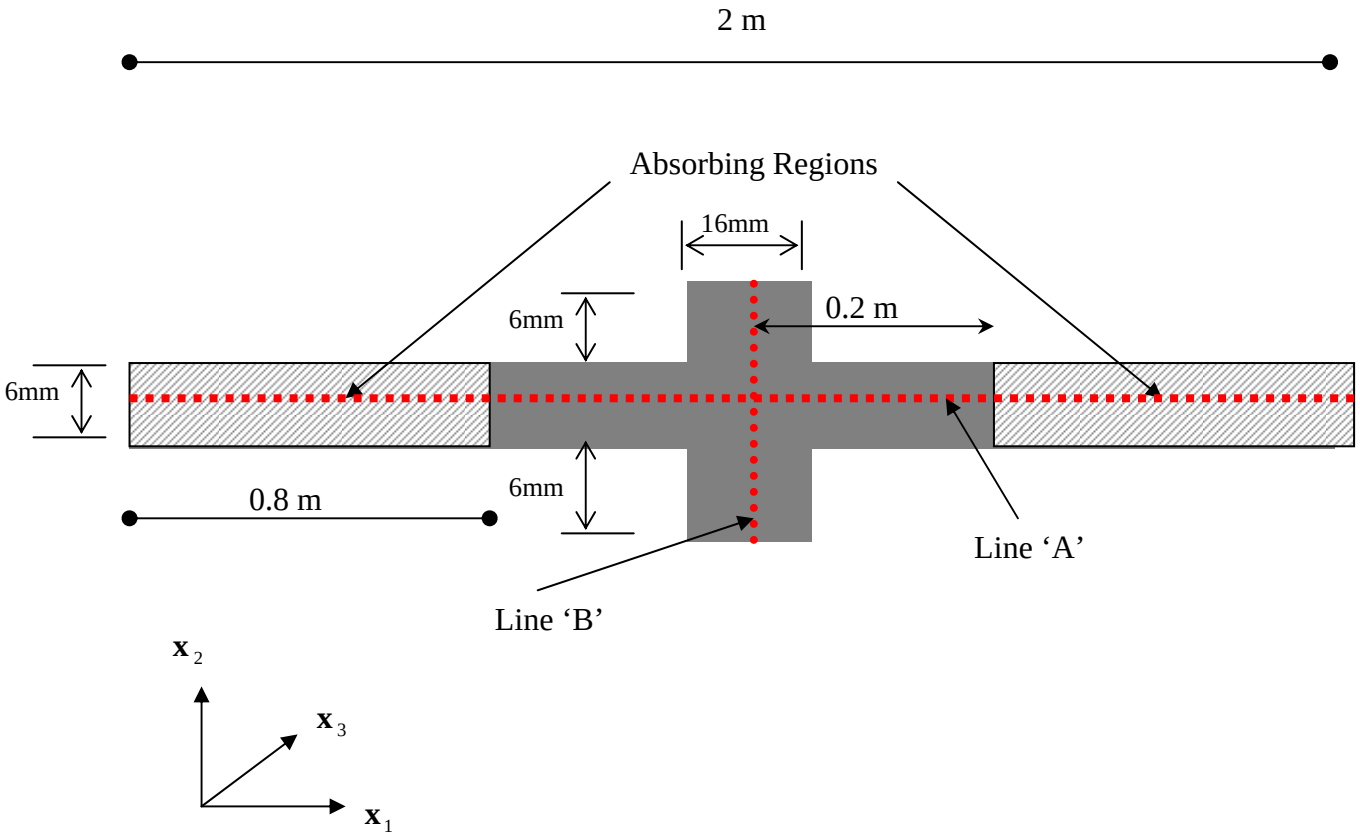

FIGURE 4.2: SAFE model with absorbing regions[99]

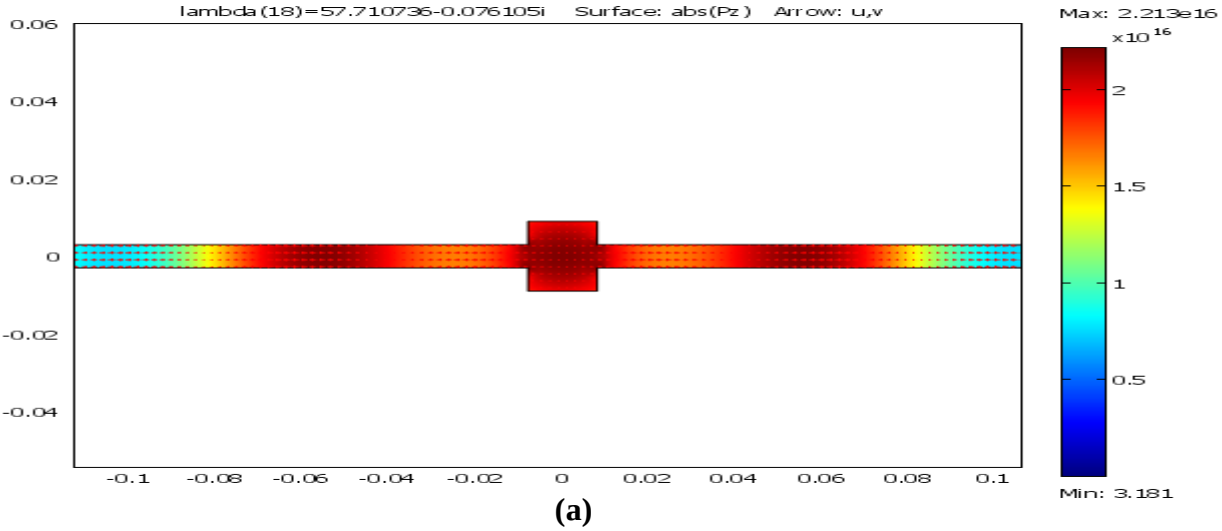

(a)

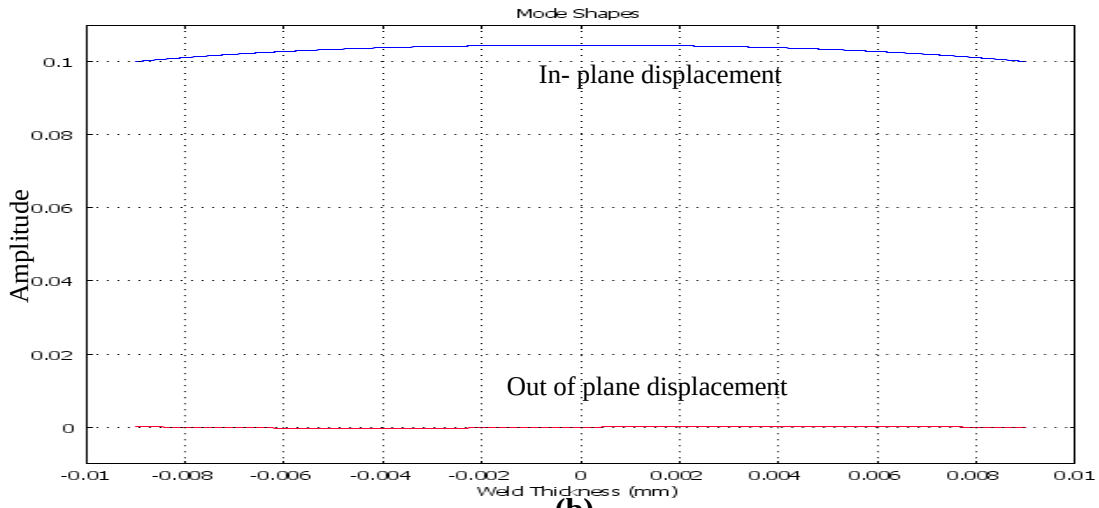

(b)

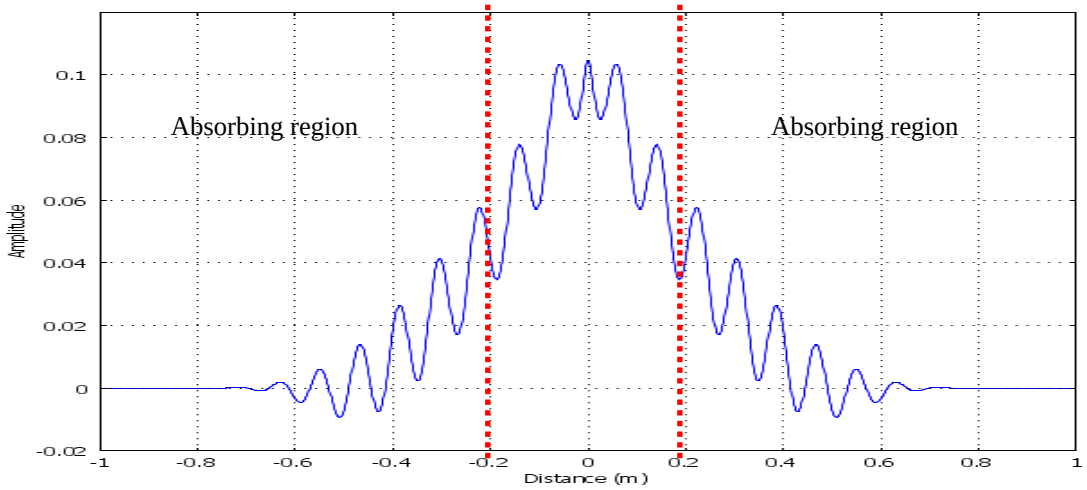

(c)

FIGURE 4.3: SAFE results at 50 kHz, (a) Power flow along the weld, (b) Mode shapes obtained by monitoring nodes through thickness of the weld (c) Amplitudes on line x_1 = -1 m to x_1 = 1 m at x_2 =0.

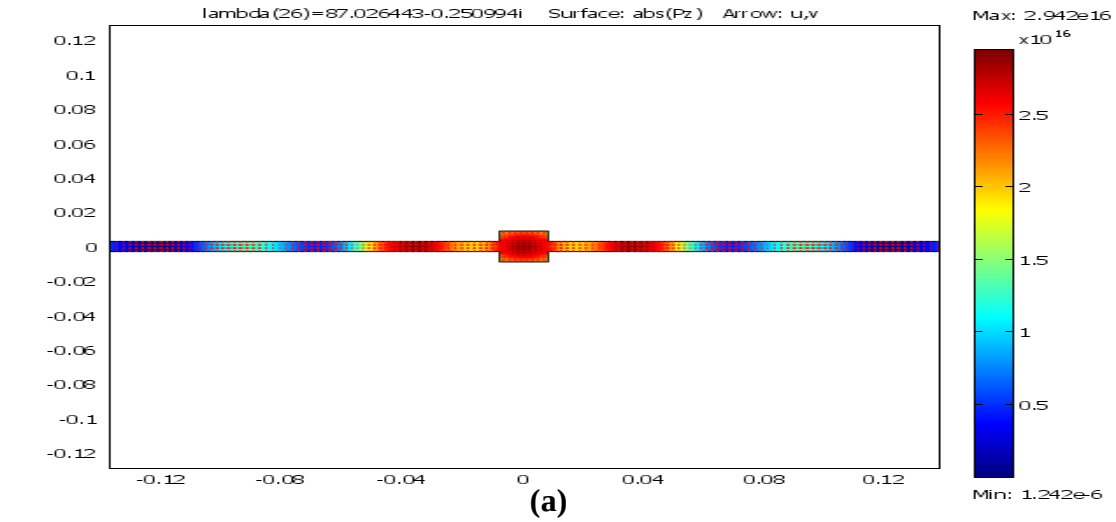

(a)

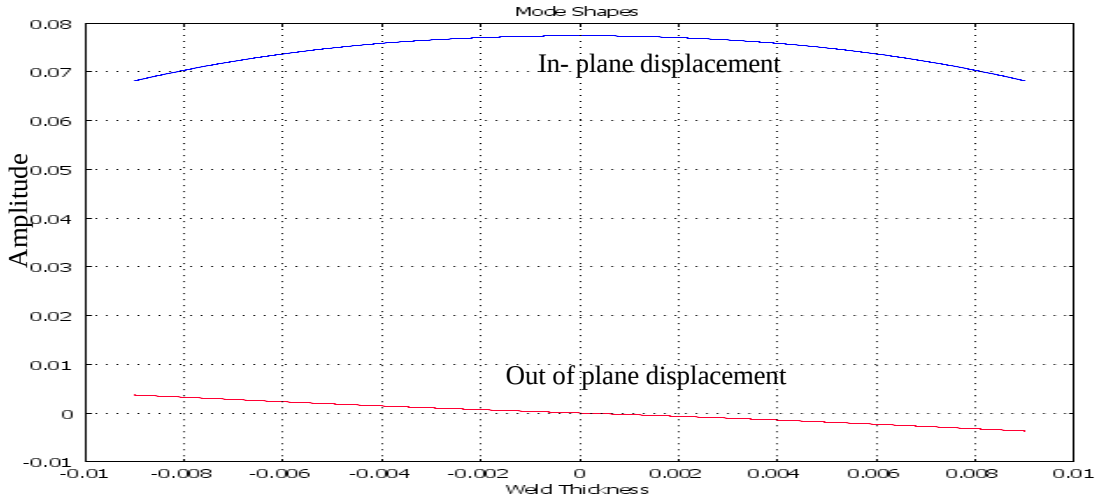

(b)

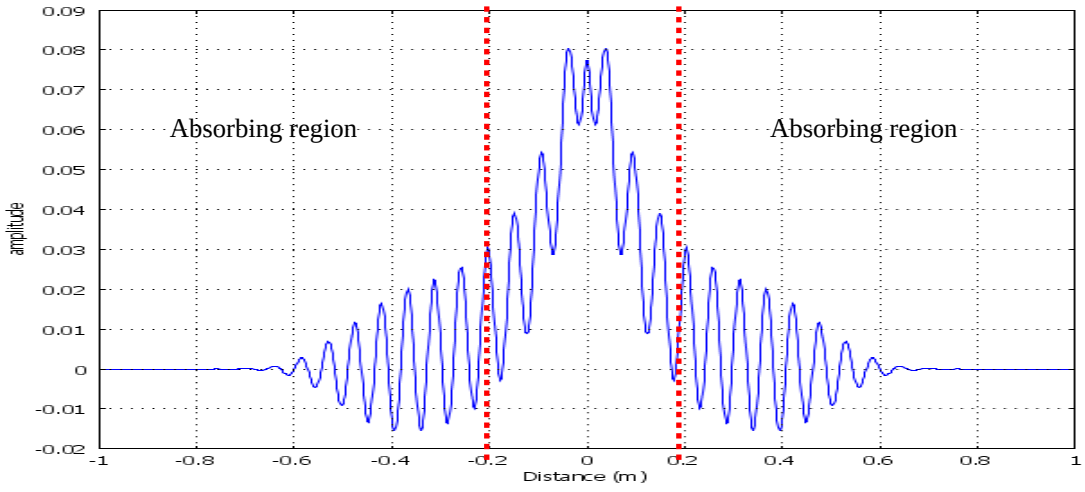

(c)

FIGURE 4.4: SAFE results at 75 kHz, (a) Power flow along the weld, (b) Mode shapes (c) Amplitudes on line x_1 = -1m to x_1 = 1m at x_2 =0.

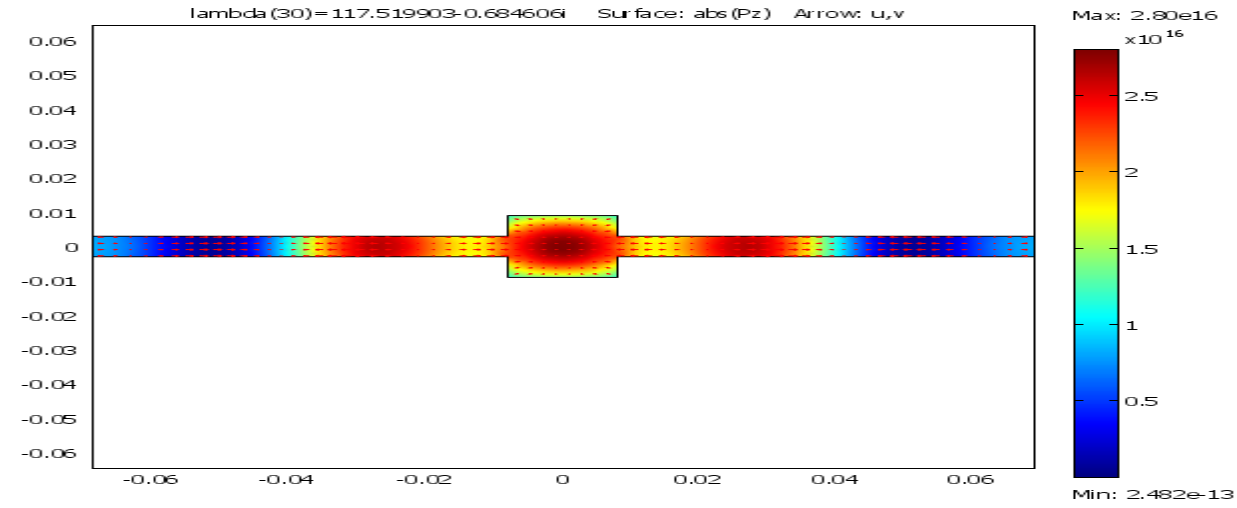

(a)

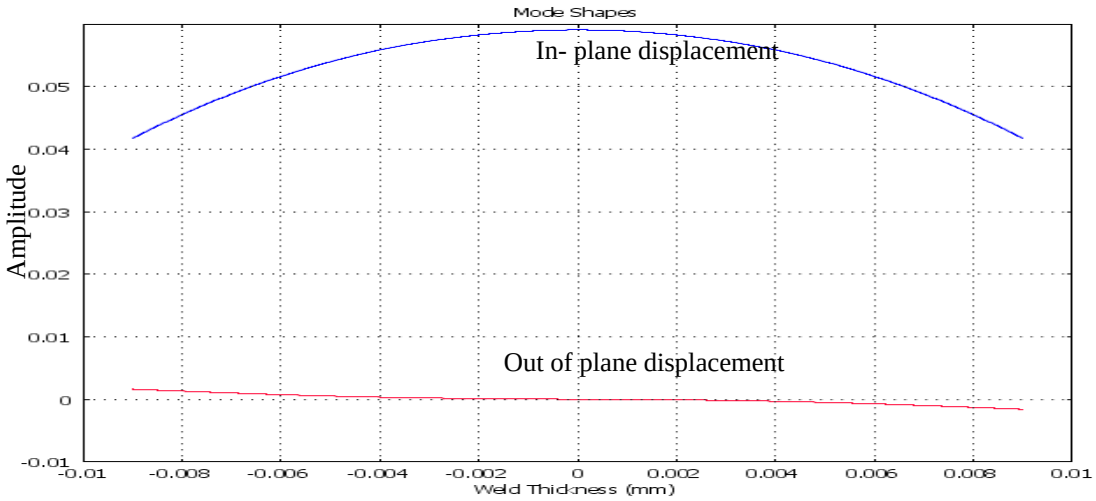

(b)

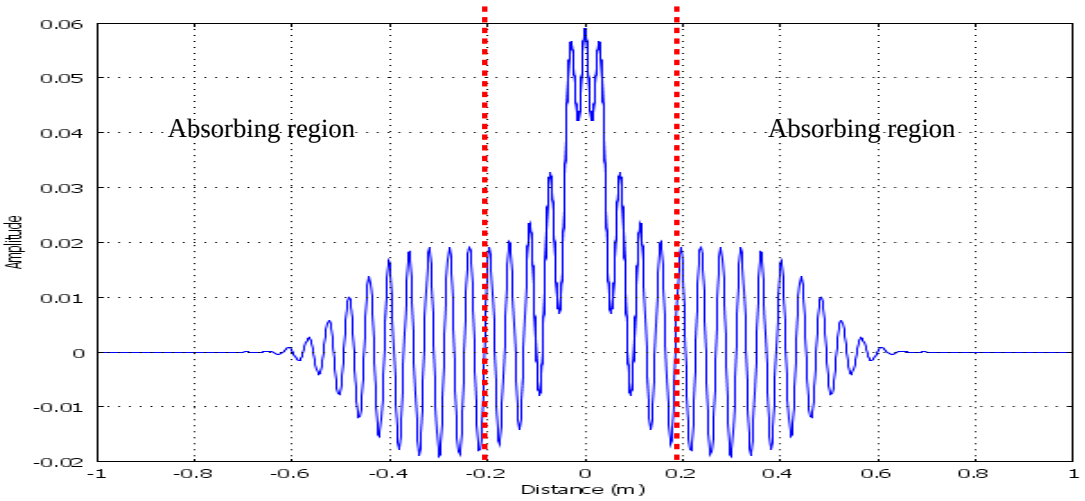

(c)

FIGURE 4.5: SAFE results at 100 kHz, (a) Power flow along the weld, (b) Mode shapes (c) Amplitudes on line x_1 = -1 m to x_1 = 1 m at x_2 =0.

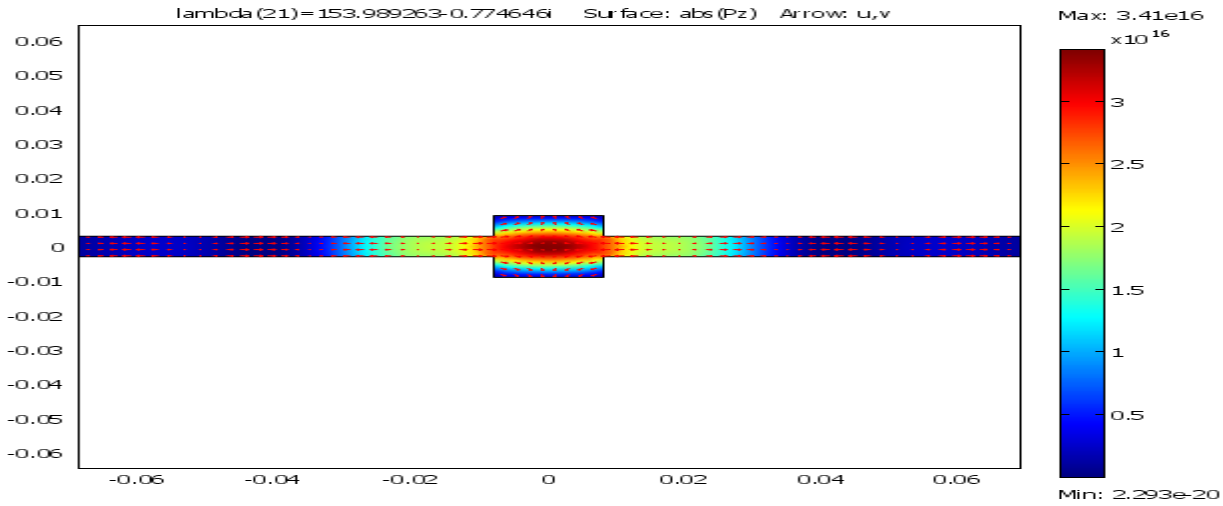

(a)

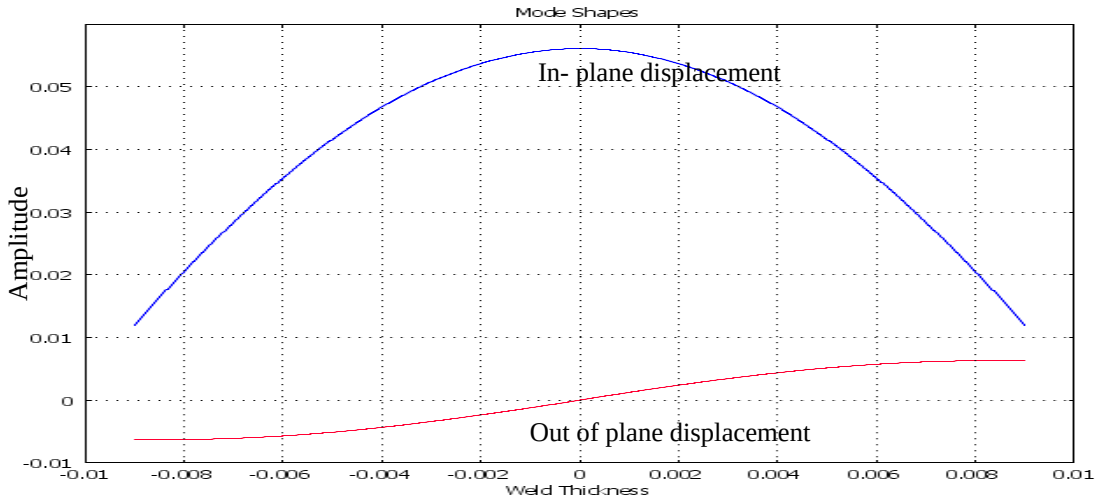

(b)

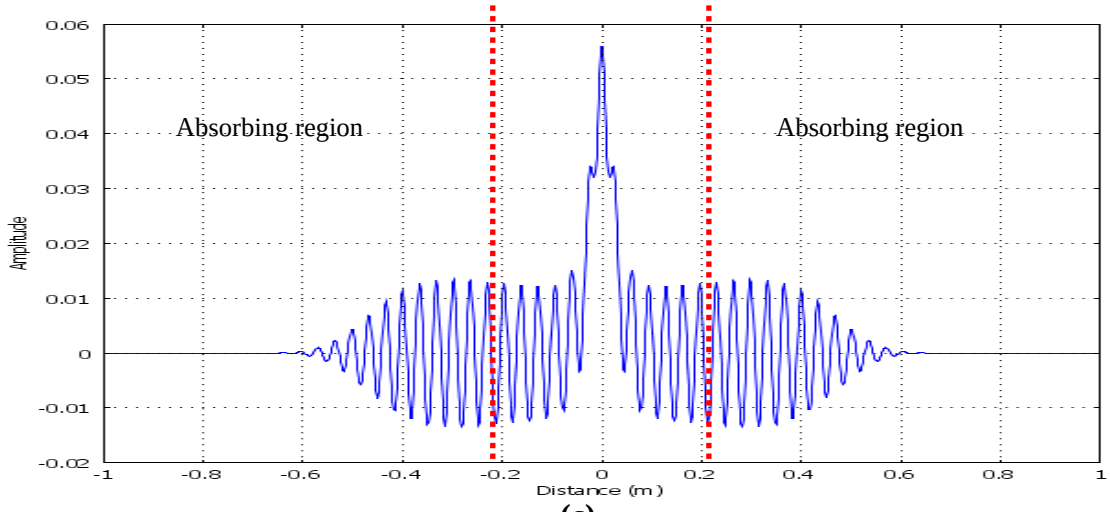

(c)

FIGURE 4.6: SAFE results at 125 kHz, (a) Power flow along the weld, (b) Mode shapes (c) Amplitudes on line x_1 = -1 m to x_1 = 1 m at x_2 =0.

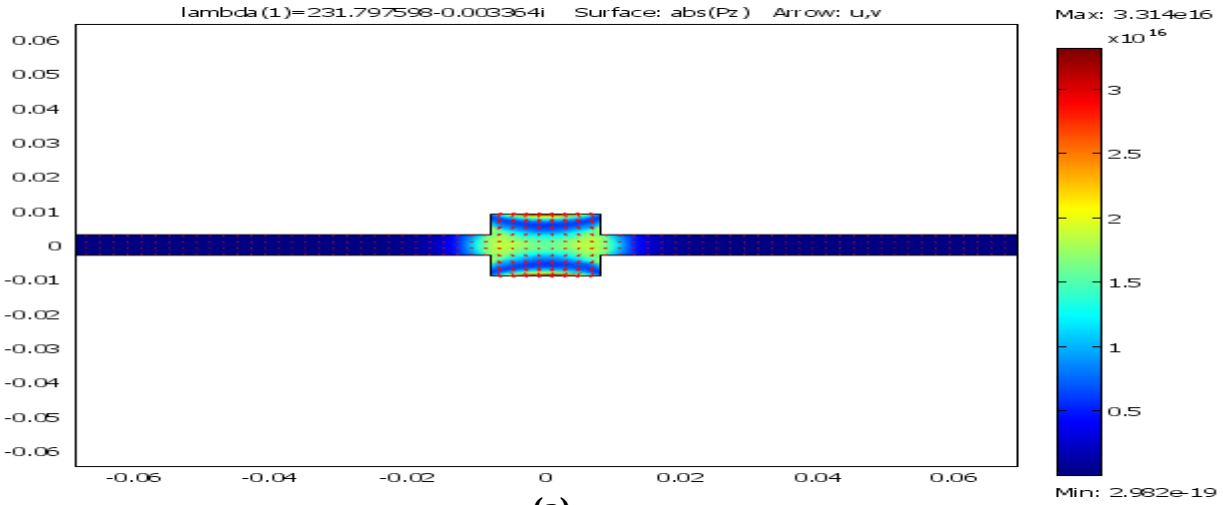

(a)

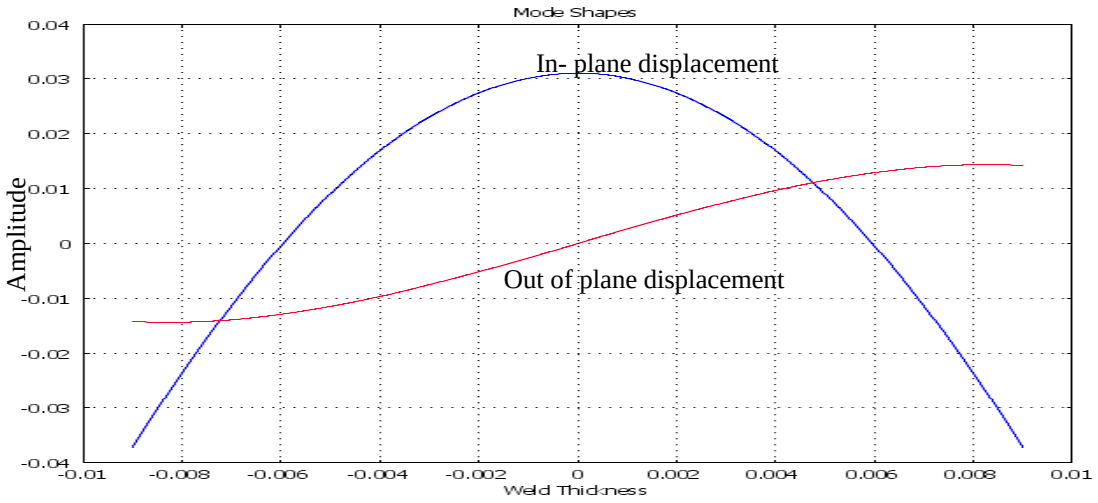

(b)

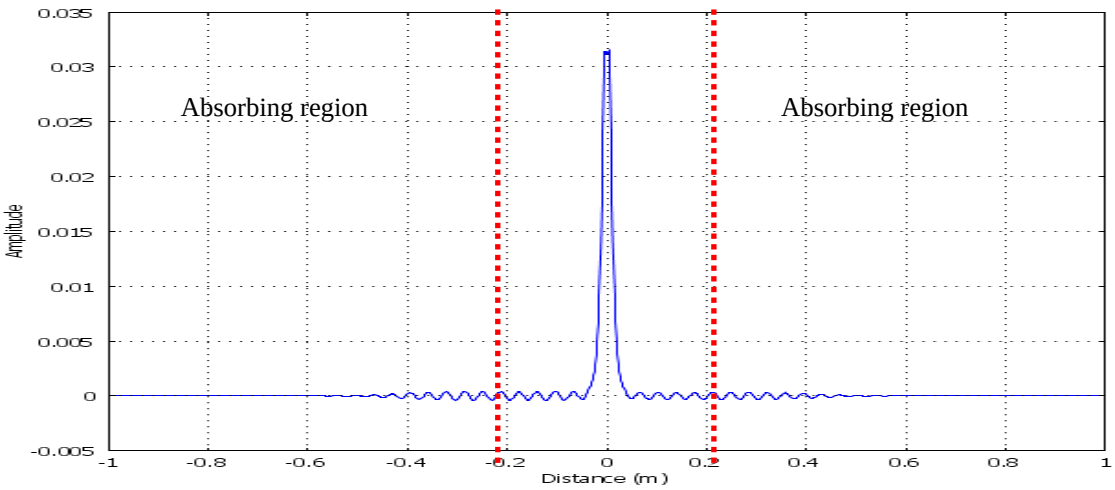

(c)

FIGURE 4.7: SAFE results at 150 kHz, (a) Power flow along the weld, (b) Mode shapes (c) Amplitudes on line x_1 = -1 m to x_1 = 1 m at x_2 =0.

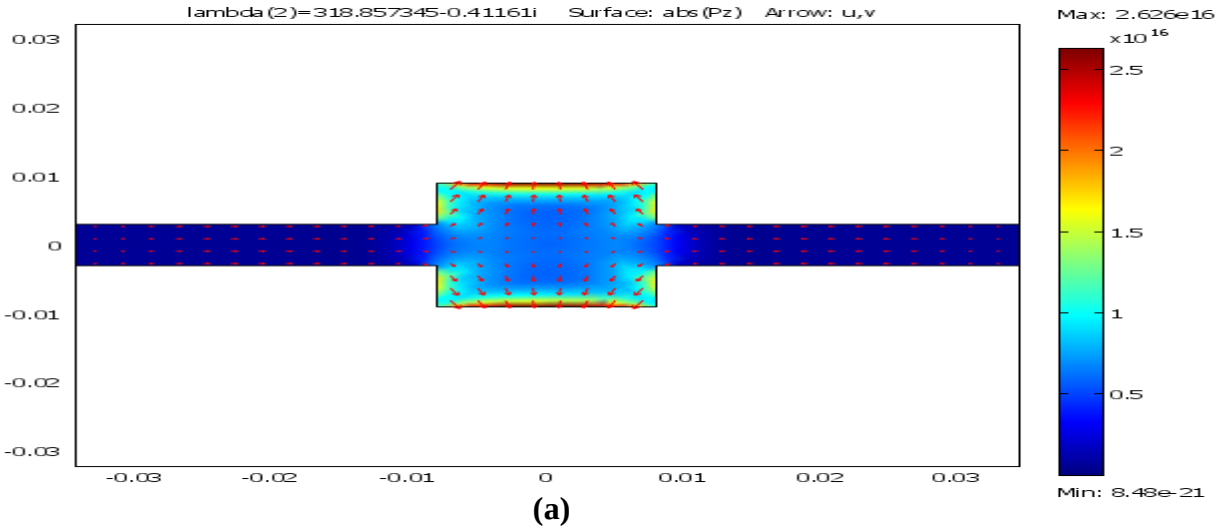

(a)

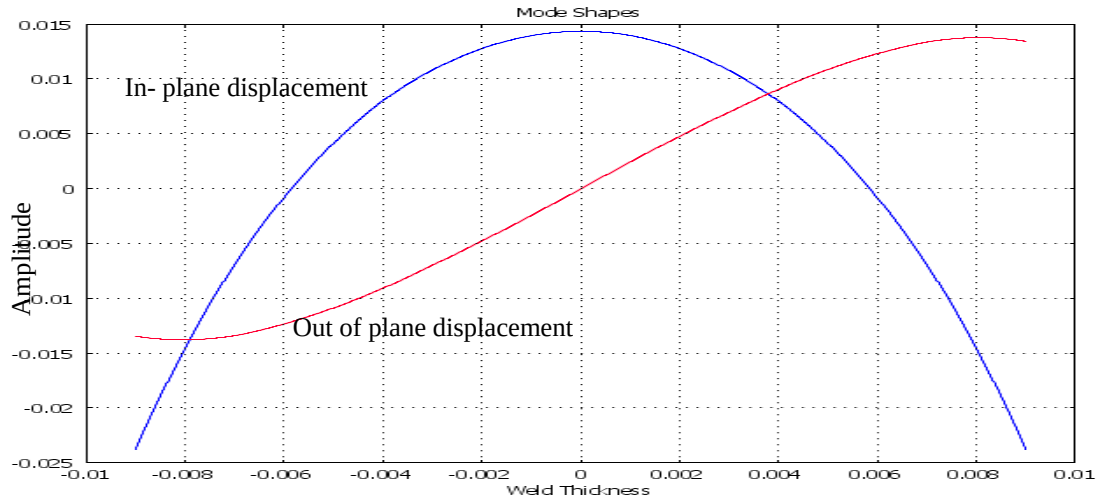

(b)

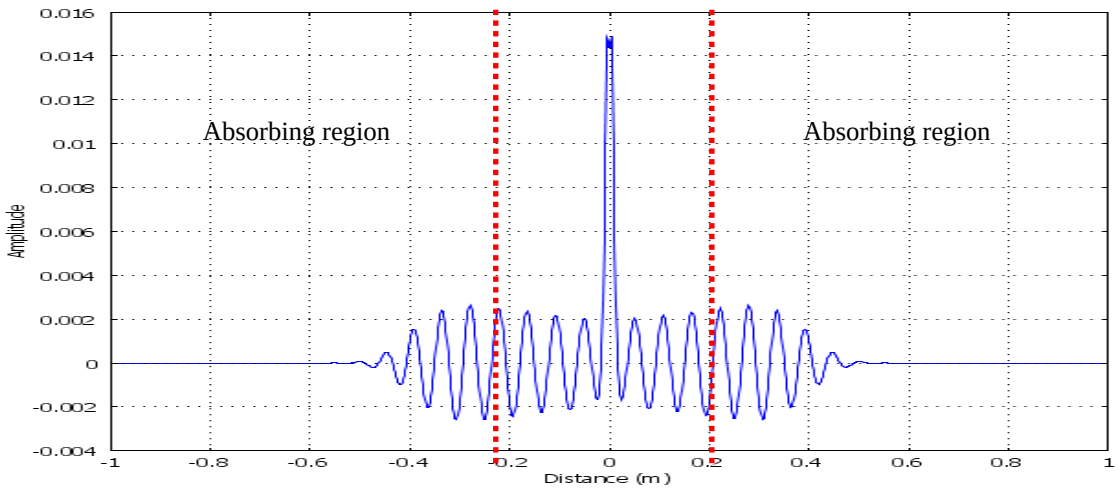

(c)

FIGURE 4.8: SAFE results at 175 kHz, (a) Power flow along the weld, (b) Mode shapes, (c) Amplitudes on line x_1 = -1 m to x_1 = 1 m at x_2 =0.

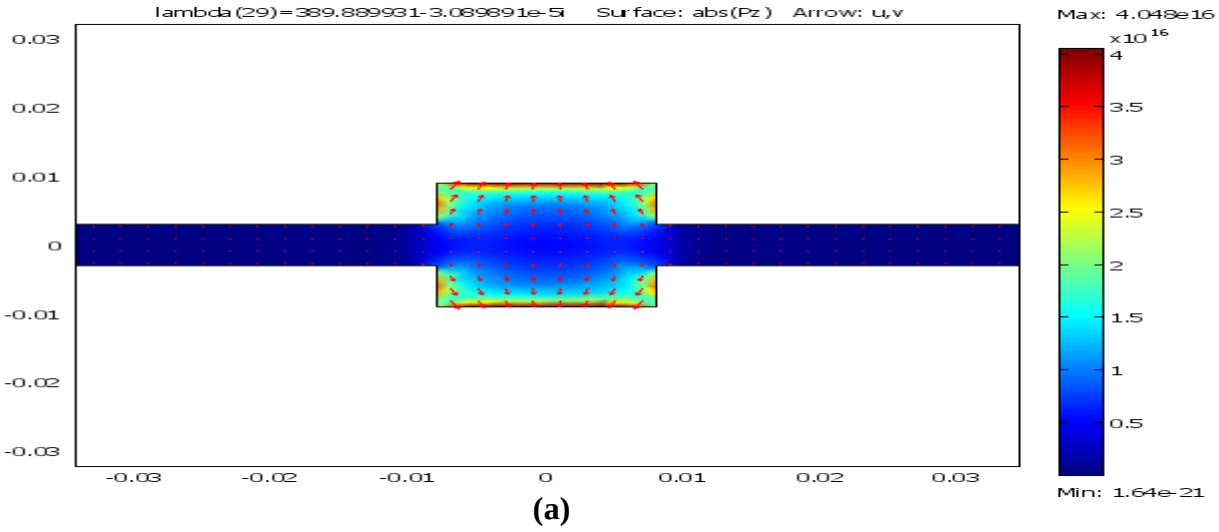

(a)

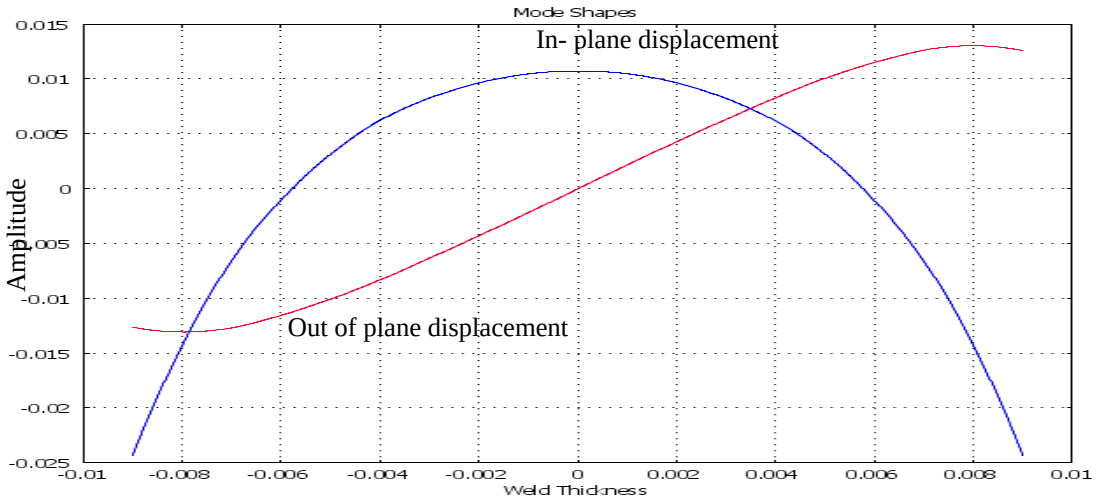

(b)

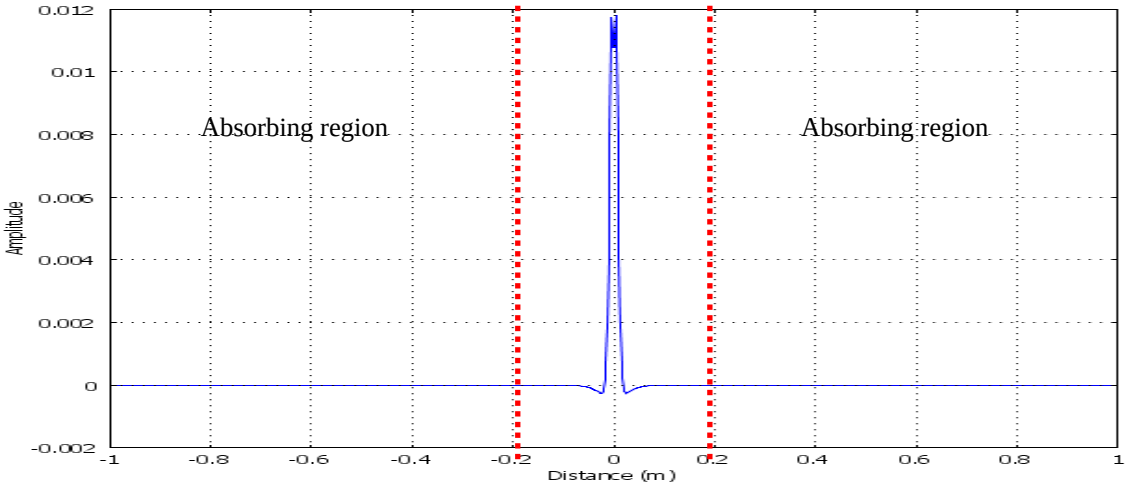

(c)

FIGURE 4.9: SAFE results at 200 kHz, (a) Power flow along the weld, (b) Mode shapes, (c) Amplitudes on line x_1 = -1 m to x_1 = 1 m at x_2 =0.

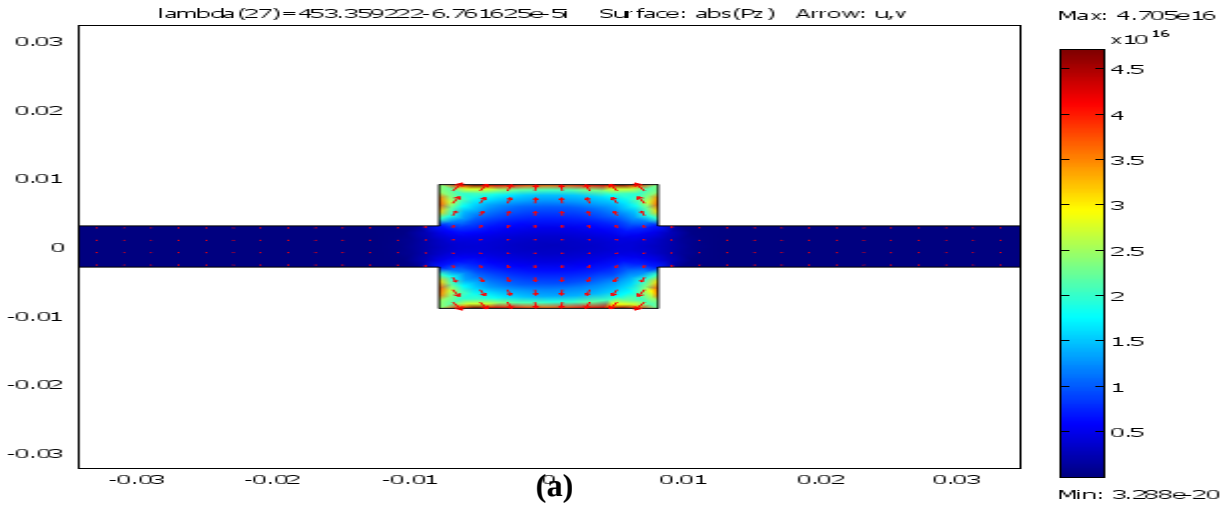

(a)

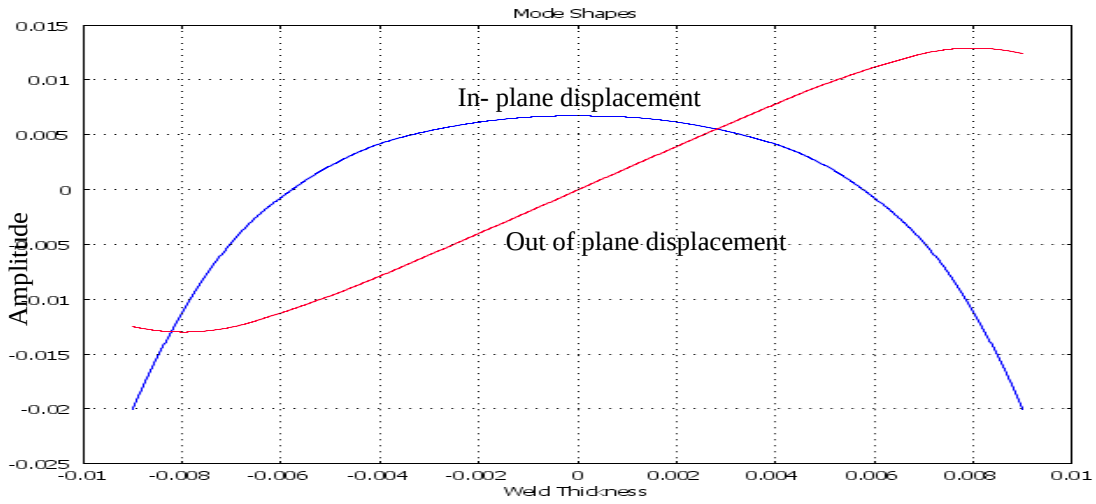

(b)

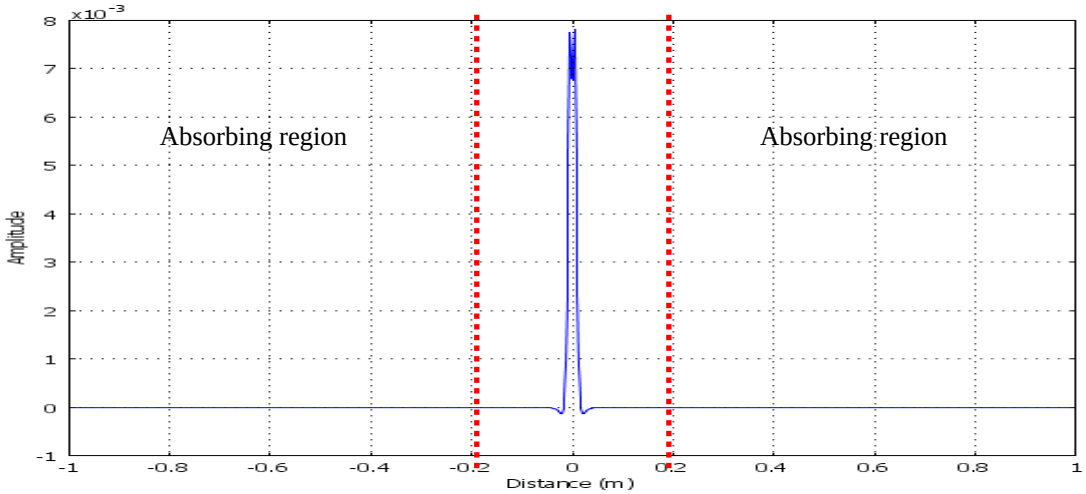

(c)

FIGURE 4.10: SAFE results at 225 kHz, (a) Power flow along the weld, (b) Mode shapes (c) Amplitudes on line x_1 = -1 m to x_1 = 1 m at x_2 =0.

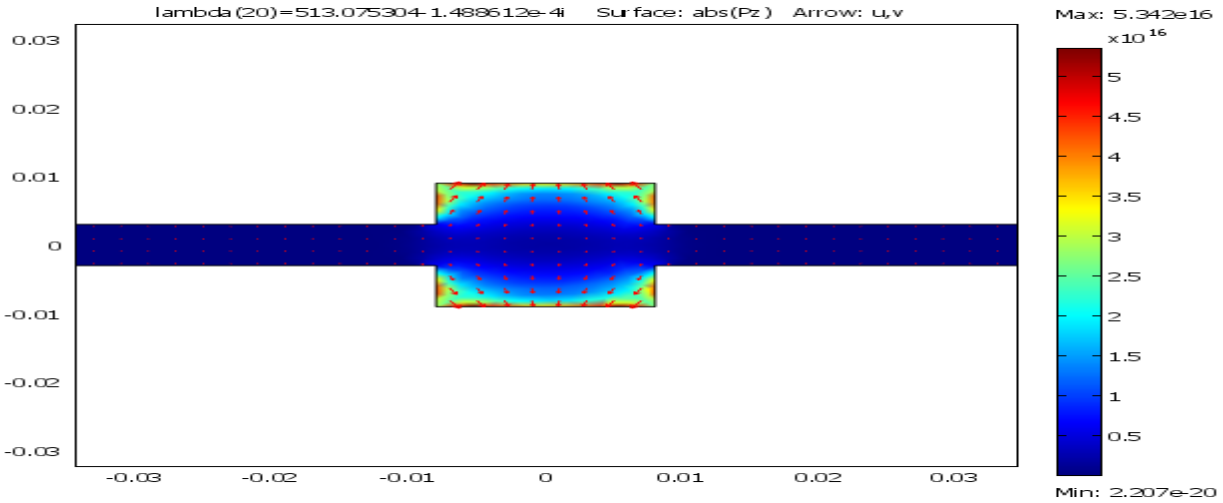

(a)

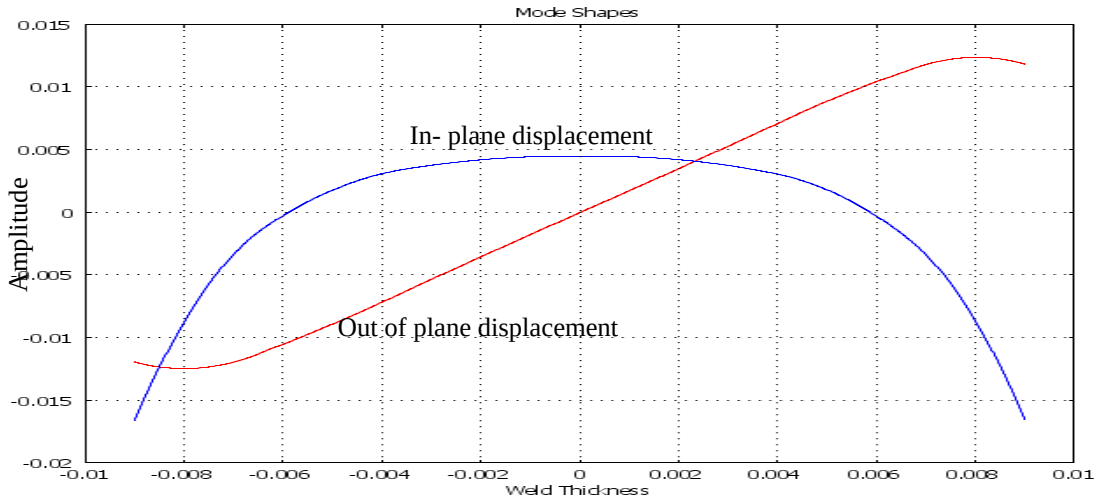

(b)

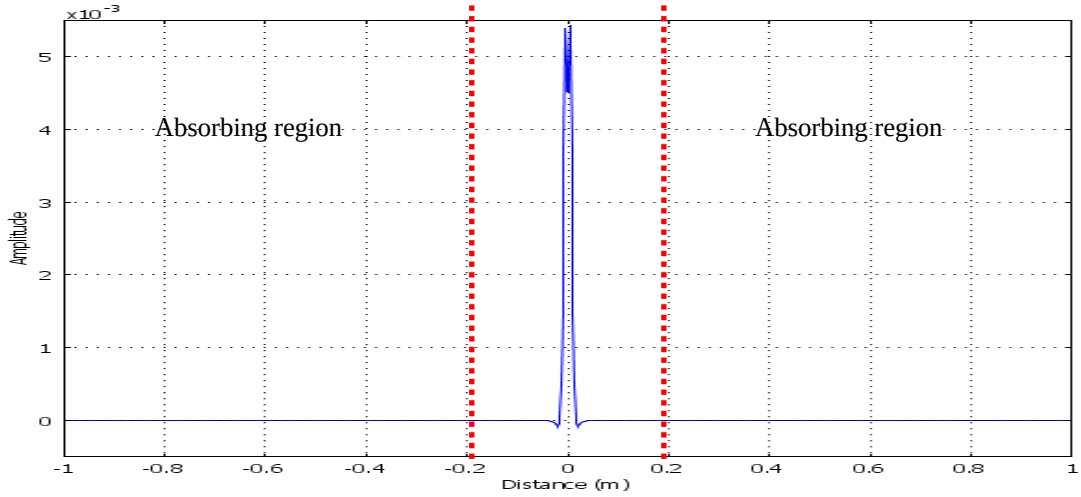

(c)

FIGURE 4.11: SAFE results at 250 kHz, (a) Power flow along the weld, (b) Mode shapes (c) Amplitudes on line x_1 = -1 m to x_1 = 1 m at x_2 =0.

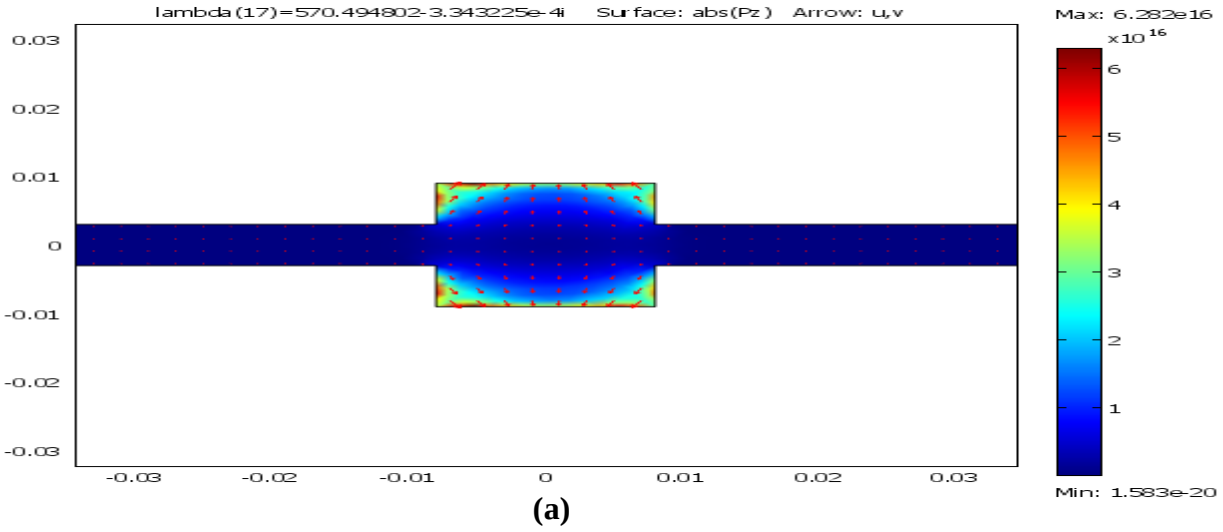

(a)

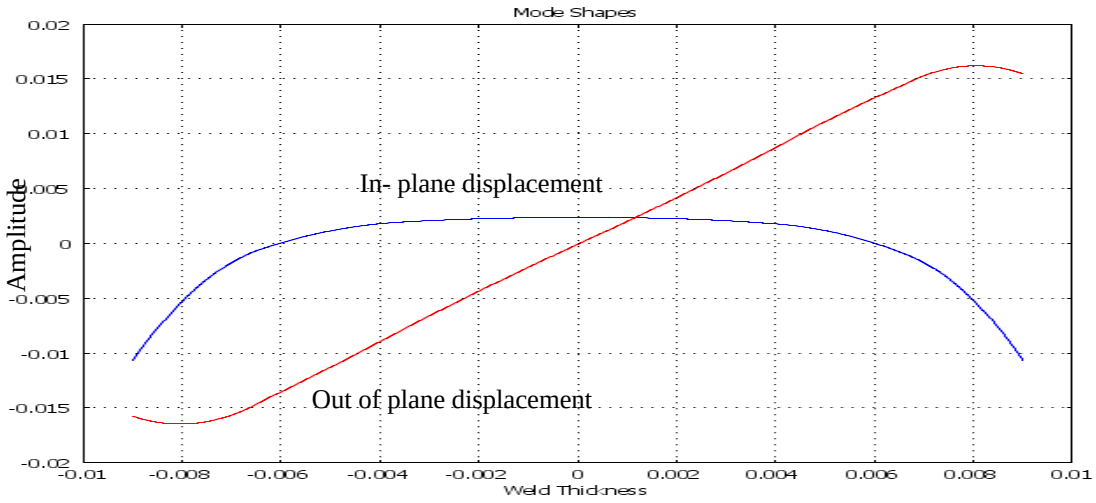

(b)

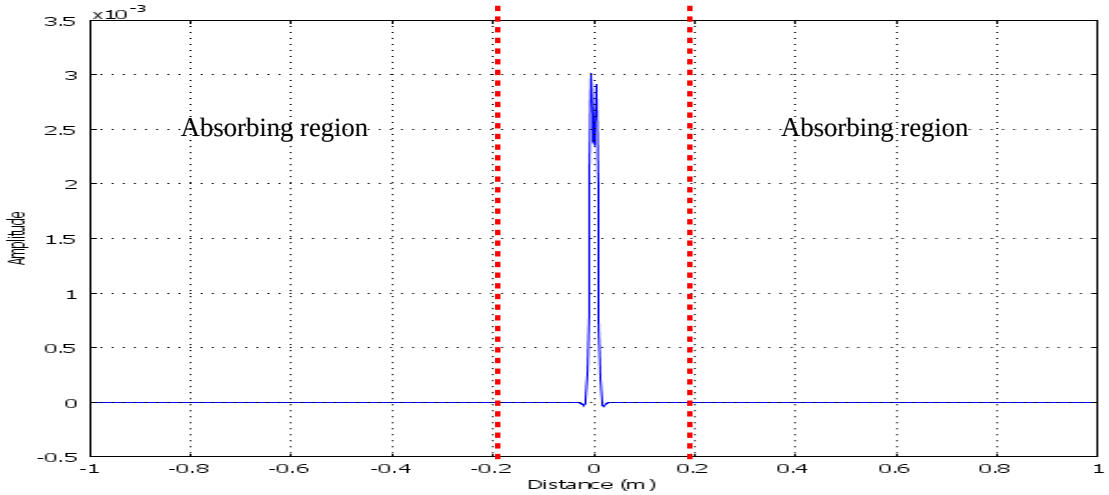

(c)

FIGURE 4.12: SAFE results at 275 kHz, (a) Power flow along the weld, (b) Mode shapes, (c) Amplitudes on line x_1 = -1 m to x_1 = 1 m at x_2 =0.

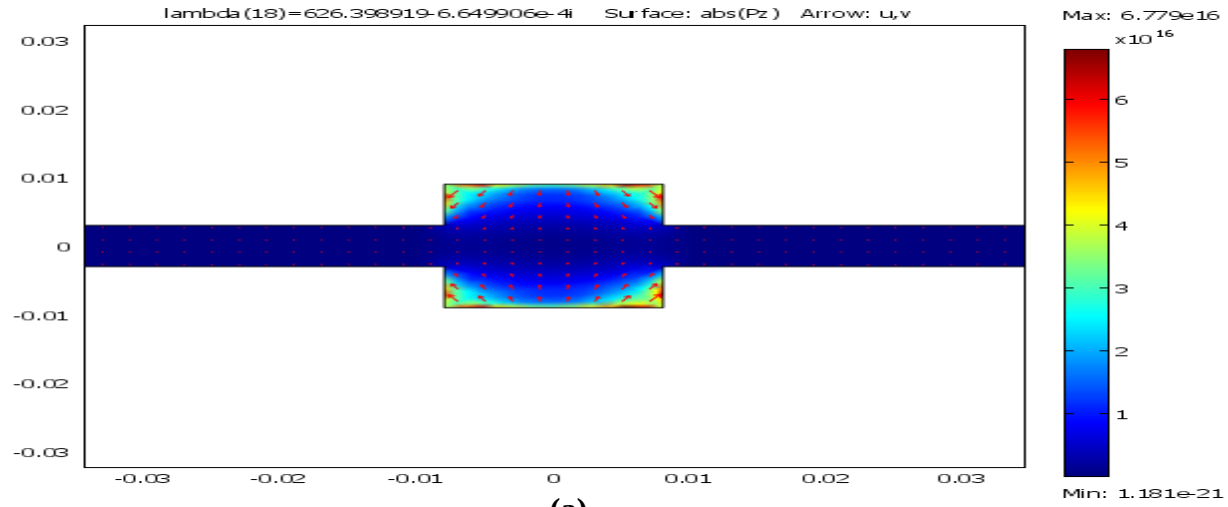

(a)

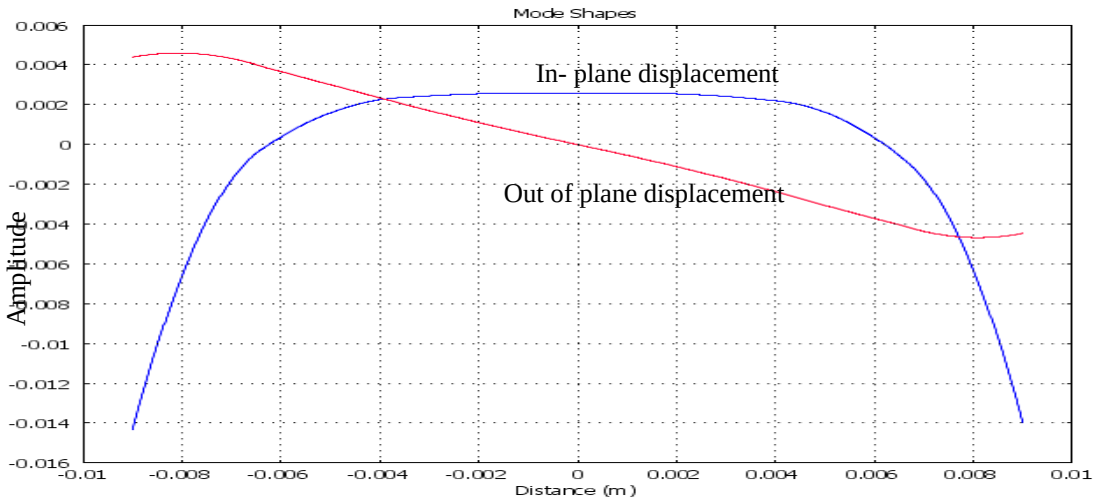

(b)

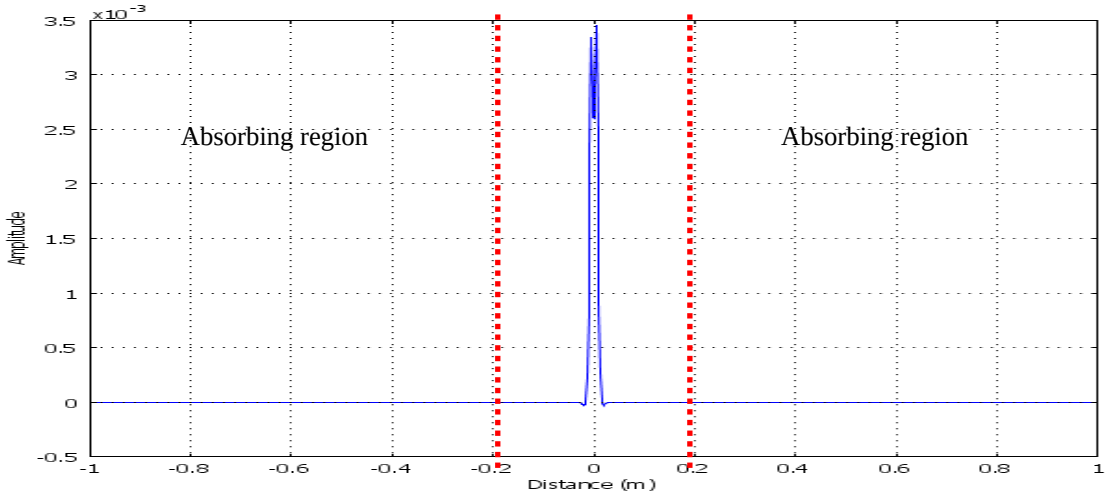

(c)

FIGURE 4.13: SAFE results at 300 kHz, (a) Power flow along the weld, (b) Mode shapes, (c) Amplitudes on line x_1 = -1 m to x_1 = 1 m at x_2 =0.

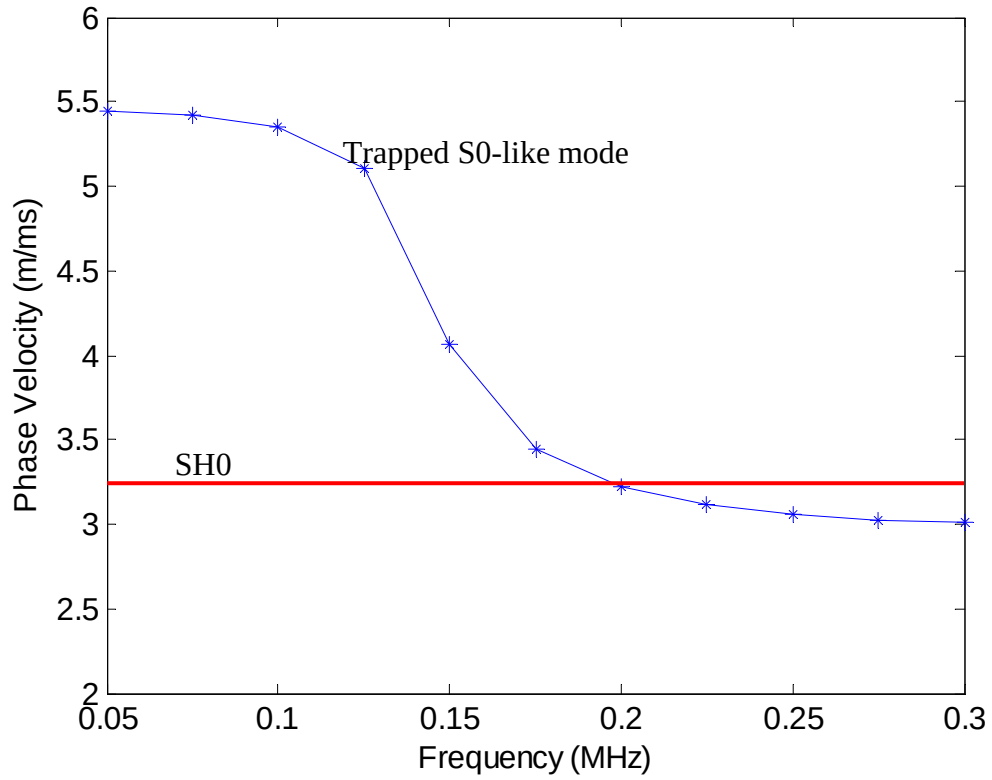

(a)

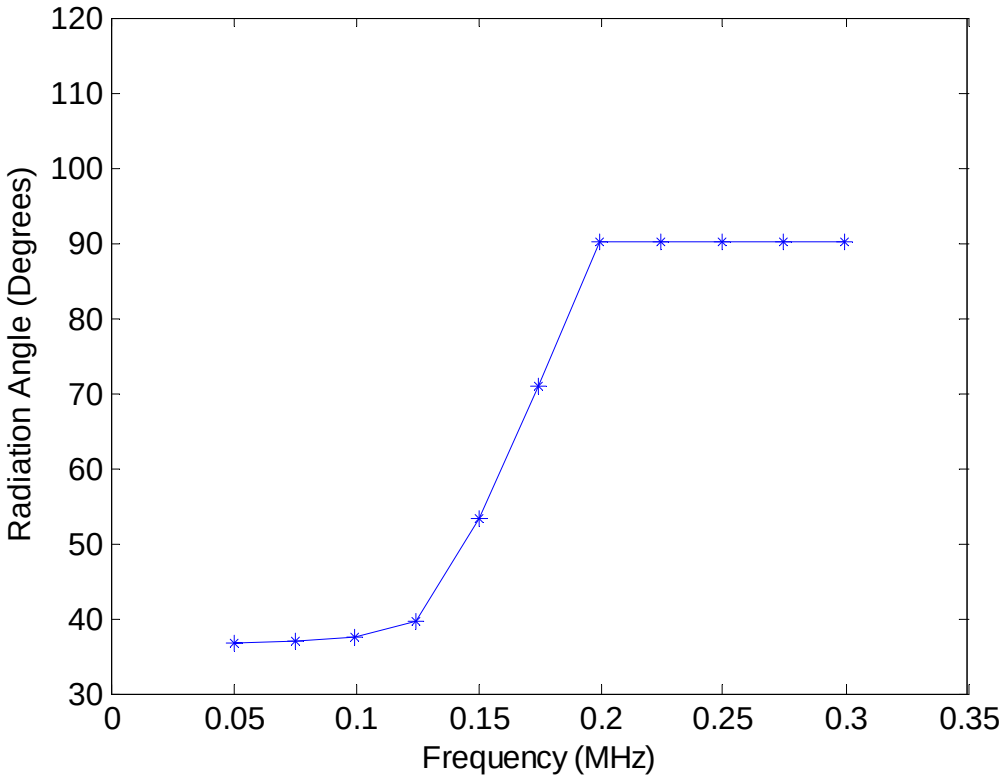

(b)

FIGURE 4.14: (a) Phase velocity of the trapped S0-like mode at different frequencies, (b) Radiation angle of the SH0 mode at different frequencies [99]

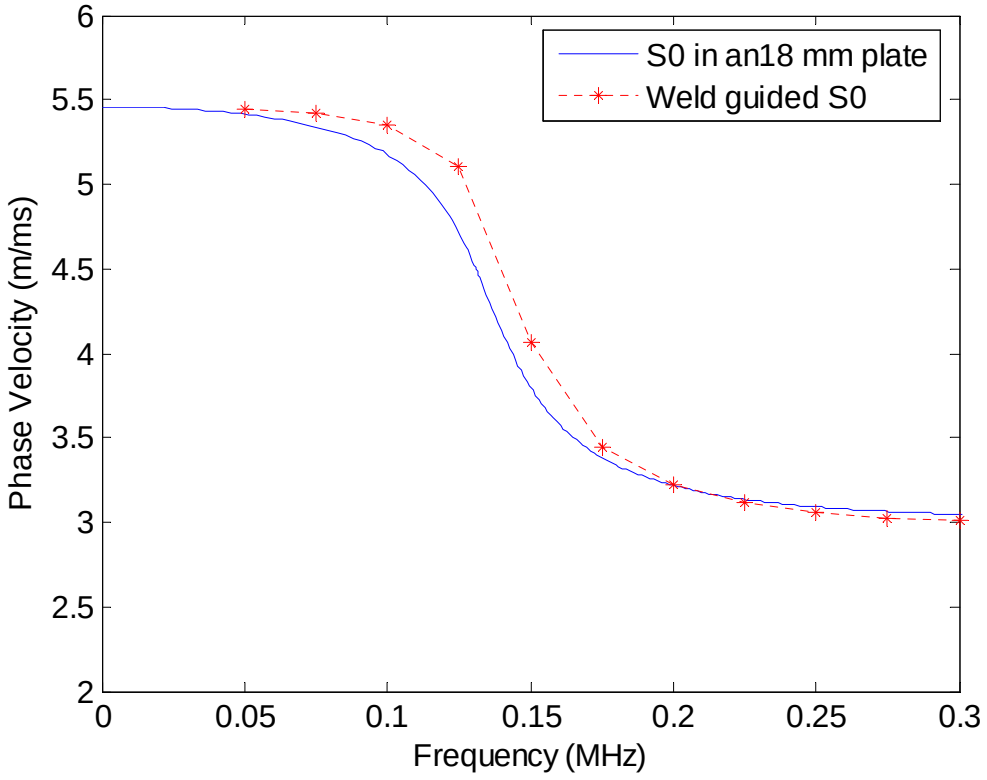

FIGURE 4.15: Comparison of the phase velocity of the trapped S0-like mode with the phase velocity of the S0 mode in an 18 mm steel plate

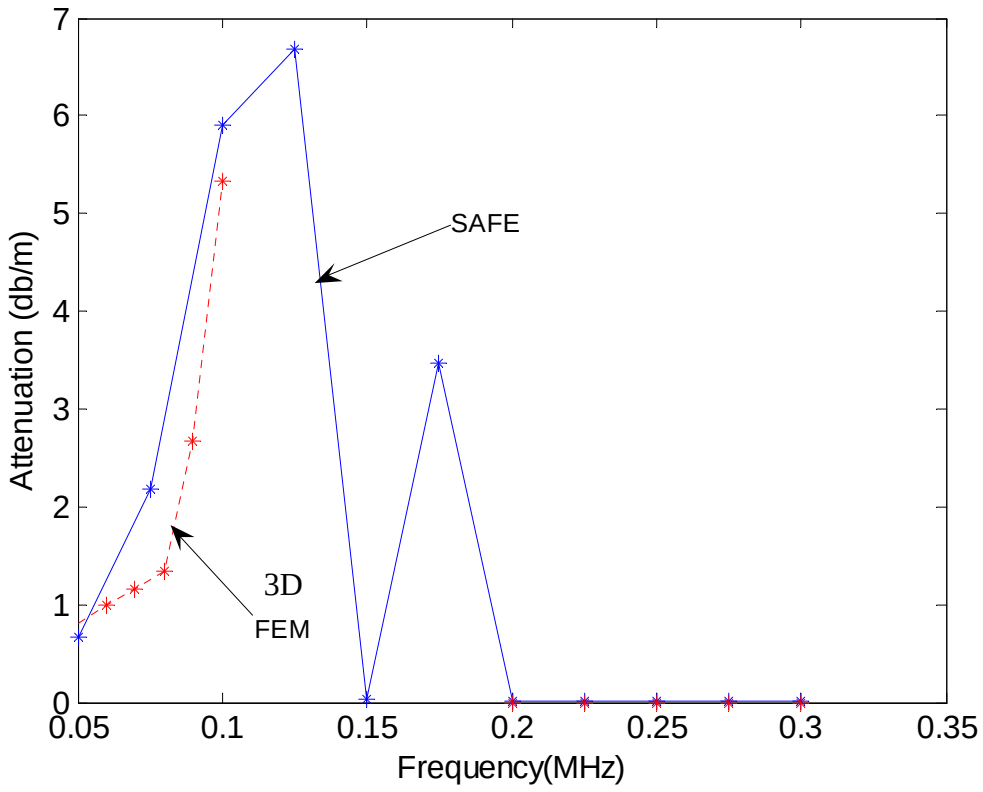

FIGURE 4.16: Attenuation of the trapped S0-like mode at different frequencies. SAFE results are from [99]

Chapter 5
Application of the trapped S0-like mode for real welds

5.1 Introduction

The properties of the trapped S0-like mode are geometry dependent as explained in chapter 4. In order to exploit the trapped S0-like mode for inspection of long lengths of real welds, it is necessary to understand the properties of the trapped S0-like mode in real welds. Real welds have a profile with increasing thickness towards the centre. Figure 5.1 shows an example of a real weld geometry. In the weld geometry shown in Figure 5.1, the weld caps have varying thickness across the profile unlike the idealized weld, discussed in previous chapters, where the weld caps have constant thickness.

In this chapter we examine the attenuation, velocities and mode shapes of the trapped S0-like mode in real welds and discuss its applicability to NDE of long lengths of real welds. 3D Finite element models and Semi Analytical Finite Element(SAFE) models have been used to understand the characteristics of the trapped S0-like mode in real welds and the results have been compared with experimental measurements.

In real welds, the top and bottom weld caps are not normally the same. In these cases the trapped S0-like mode may behave slightly differently. Non symmetric modes, along with symmetric modes are excited if the top and bottom weld caps are not the same as the weld structure is non symmetric. This may slightly complicate the monitored signal because of the interference of all these modes.

The measurement of the signal might also become difficult especially when out-of-plane displacement is measured as the non symmetric modes in general have high out-of plane displacement at low frequencies. At high frequencies, this effect is expected to be minimal as the trapped S0-like mode also has high out-of-plane displacement. However the experimental measurements on real welds, which are explained later in this chapter, have shown that the small non symmetric nature of the real weld geometry has very little effect.

In real welds the weld geometry along the length of the weld is also not normally the same. The non uniform nature of the weld along its length might also slightly change the properties of the trapped S0-like mode as the properties of the trapped S0-like mode are geometry dependent. E.g. a slightly thinner weld cap region along its length can slow the trapped S0 mode in that region and might also lead to reflection and refraction of the wave. At low frequencies this effect is expected to be minimal and at high frequencies this might have a significant effect because of the smaller wavelength at these frequencies. The variation in the properties of the trapped S0-like mode depends on the length scale of the non-uniformity of the weld geometry along the length of the weld. For small non-uniformity scales, the effect is minimal and this will be explained later in this chapter.

In some cases the weld material may also have slightly different material properties and this may also slightly change the properties of the trapped S0-like mode in the weld. In general the same material is used to weld the plates but the properties of the weld material might change slightly because of the thermal effects it undergoes during the welding process.

Symmetric weld caps, with no variation in the weld geometry along the length of the welds have been considered in this chapter as it is very difficult to model the non uniform case. The properties of the weld material are taken to be those of the surrounding plates. It is also assumed that the material damping is zero in both 3D FE and SAFE models. The characteristics of the trapped S0-like mode in real welds are compared with the characteristics of the trapped S0-like mode in idealised welds.

5.2 Semi-Analytical Finite Element (SAFE) model with absorbing regions to study the trapped S0-like mode in real weld.

The real weld model has been studied using the 2D SAFE method in order to understand the trapped S0-like mode in real welds. Mr Zheng Fan, a PhD student in the NDT Lab, Imperial College [98], who is specialising in SAFE has created these SAFE models [127]. The 3D weld model shown in figure 5.2(a) has been reduced to a 2D problem shown in figure 5.2(b), which requires meshing the cross section of the guide only. The modelling of 2D SAFE for real welds has been done in the same way explained in the previous chapter. The model has been meshed with 3-noded triangular elements. Each node has 3 degrees of freedom and the element takes in to account the harmonic propagation in the third direction (along the length of the weld).

The absorbing regions have been modelled as shown in Figure 5.3 in order to suppress the reflections from the edges. The weld has a maximum thickness of 10 mm in the centre and has a width of 12 mm. The plate is 6 mm thick and the weld cap is of maximum thickness 2 mm. These dimensions have been chosen

for 2D SAFE as the experimental weld model, explained in chapter 3, is of approximately these dimensions. The real weld used for experimental measurements has a small variation in the geometry of the top and bottom weld caps and a small amount of non-uniformity along the length of the weld. The small amount of anti symmetric nature of the real weld can potentially generate anti-symmetric modes . These variations have not been considered in either the 2D SAFE or the 3D FE models. The results from 2D SAFE will be compared with 3D Finite element and experimental results later in this chapter.

The absorbing region has been optimised as explained in chapter 2. The maximum possible wave length in the surrounding plates is that of the S0 mode at the lowest frequency of interest. At 50 kHz the wavelength of the S0 mode in the plate is about 100 mm. The optimum length of the absorbing region depends on the wave length projection on to the x-axis. An infinite length of absorbing region is needed in order to absorb the signals at all angles of incidence.

As infinite lengths of absorbing regions are not possible, the length of the absorbing region has been chosen in such a way that there are no reflections from the edge for angles of incidence between 0^0 and 65^0 where the projection of wavelength along the x-axis would be between 100 mm and 250 mm. The length of the absorbing region should be at least three times the maximum wavelength of the signal to be absorbed as explained in chapter 2 and therefore the length of the absorbing region was set to 800 mm. The width of the model was set to 2 m including the absorbing regions.

5.2.1 Results

The equation 4.2 is solved for frequencies in the range from 50 kHz to 500 kHz and the solution corresponding to the trapped S0-like mode has been identified by plotting the axial component of power flow. The attenuation and phase velocity of the trapped S0-like mode at different frequencies has been calculated from its eigenvalue at that particular frequency, in the same way as explained in chapter 4. The mode shapes of the trapped S0-like mode have been obtained, by monitoring nodes through thickness (on line 'B' shown in Figure 5.3) and the lateral extent of the trapped S0-like mode has been found by monitoring nodes on line 'A' shown in Figure 5.3.

Figure 5.4(a) shows the phase velocity of the trapped S0-like mode, calculated by repeating the SAFE solution in real welds at different frequencies. The phase velocity of the trapped S0-like mode is greater than the phase velocity of the SH0 mode in the plate for frequencies up to 400 kHz. As the SH0 mode is the only mode that could leak into the surrounding plates, the trapped S0-like mode is expected to show attenuation because of SH0 leakage for frequencies up to 400 kHz and show zero attenuation at frequencies above 400 kHz as it can not leak SH0 at frequencies above 400 kHz. Figure 5.4(b) shows the leakage angle of the SH0 mode into the plates for different frequencies.

In Figure 5.5, the phase velocity of the trapped S0-like mode has been compared with that for plain plates of different thicknesses. The weld has a maximum thickness of 10 mm and the plate has a thickness of 6 mm. Figure 5.5 shows that

the phase velocity of the trapped S0-like mode is similar to the phase velocity of the S0 mode in 7 mm plain plate at low frequencies up to 200 kHz. Between 200 kHz and 250 kHz the phase velocity of the trapped S0-like mode is close to the phase velocity of the S0 mode in an 8 mm plate. The trapped mode behaves as if in a 9 mm plate at frequencies above 250 kHz. This is due to the larger wave length of the trapped S0 mode at low frequencies and smaller wave length at high frequencies. The trapped S0-like mode is completely guided by the weld at high frequencies, because of the smaller wavelength at these frequencies, which will be explained later in this chapter.

Figure 5.6 shows the attenuation of the trapped S0-like mode due to leakage of energy into the adjacent plates, at different frequencies. The velocity difference between the trapped S0-like mode and the leaky SH0 mode in the plate decreases as the frequency increases up to 400 kHz, so one would expect an increasing leakage and increasing attenuation for frequencies up to 400 kHz. However the SAFE results shown in Figure 5.6 show an increasing attenuation for frequencies up to 350 kHz and decreasing attenuation values at frequencies between 350 and 400 kHz.

The SAFE results between 350 kHz and 400 kHz are unreliable as the absorbing region of the model is not capable of fully absorbing signals at large angles of incidence. The radiation angle of SH0 in to the plates between frequencies 350 and 400 kHz is very high, as we can see from Figure 5.4(b). Therefore the model is not capable of fully absorbing leaky SH0 waves between frequencies 350 and 400 kHz and the unwanted reflected signals from the edges pollute the results

between these frequencies. The zero attenuation above 400 kHz is explained by the Snell-Descartes' law, which does not allow the SH0 mode to be radiated above this frequency because its velocity is greater than that of the trapped S0-like mode propagating along the weld.

As explained in chapter 4, the sensitivity of the trapped S0-like mode to target defects depends on its mode shape at the chosen frequency, so, it is necessary to understand the mode shapes of the trapped S0-like mode at different frequencies. Figure 5.7 to 5.20 show power flows across a cross section of the weld, and mode shapes through thickness and lateral extent of the trapped S0-like mode at different frequencies. Figures 5.7(a)-5.20(a) show power flows in the x_3 direction at different frequencies from 50 kHz to 500 kHz. Figures 5.7(b)-5.20(b) show mode shapes through thickness on line 'B' shown in Figure 5.3, where the red curve shows out of plane displacement and the blue curve shows in-plane displacement. Figures 5.7(c)-5.20(c) show amplitudes of the trapped S0-like mode in the x_3 direction, the lateral extent of the trapped S0 mode, on line 'A' shown in Figure 5.3.

The trapped S0-like mode has a lateral extent of about 440 mm, at 50 kHz, which is equal to 4 wave lengths. However, this lateral extent decreases as the frequency increases for frequencies up to 250 kHz. At frequencies above 250 kHz the trapped S0-like mode has almost no lateral extent because of smaller wavelengths at these frequencies and therefore the trapped S0-like mode is completely guided by the weld. Therefore, one would argue that low frequency

inspection is suitable for inspecting defects both in the weld and defects near the weld whereas high frequency inspection is suitable only for defects in the welds.

The amplitude of the lateral extent of the trapped S0-like mode decreases rapidly as the distance from the weld increases. This suggests that the sensitivity of the trapped S0-like mode also decreases rapidly as the distance of the defect from the weld increases. The oscillations in Figures 5.7(c) to 5.17(c) are due to the leakage of the SH0 mode in to the plate. This can also be confirmed by looking at frequencies where there is no leakage e.g. Figure 5.14 (c) shows no oscillations and the trapped S0-like mode at this point has no leakage and shows zero attenuation, which can be seen in Figure 5.6. This observation is similar to the results observed in the previous chapter.

The energy of the trapped S0-like mode becomes more and more concentrated in the centre of the weld with less and less energy near the surface as the frequency increases up to 250 kHz. This can be seen from power flow plots shown in Figures 5.7(a) to 5.15(a) and mode shape plots shown in Figures 5.7(b) to 5.15(b). This suggests that the sensitivity of the trapped S0-like mode to the small surface breaking cracks decreases and the sensitivity to defects in the centre of the weld increases as the frequency increases up to 250 kHz. At frequencies above 250 kHz, the energy starts dispersing towards the surfaces of the weld, which can be seen in Figures 5.16(a) to 5.20(a) and 5.16(b) to 5.20(b). Therefore, the frequencies above 250 kHz may only be used to inspect small surface breaking cracks as the trapped S0-like mode has energy concentrated near the surface of the weld.

The absorbing regions in the above SAFE model are capable of absorbing waves at angles of incidence between 0^0 and 65^0 only and the small unavoidable reflections at higher angles pollute the results and therefore the SAFE results may not be very accurate for angles of incidence between 0^0 and 65^0. Therefore the un-reliable results at large angles of incidence are unavoidable in 2D SAFE models.

It is possible to monitor the signal in 3D FE models, at points where the angle of incidence is less than 65^0 to calculate the attenuation. However, large 3D finite element models are problematic because of computational limitations as explained in previous chapters. One could model a small FE model and monitor points at locations not far away from the source but this might give errors because of near field effects as explained in chapter 3. An attempt has been made in this chapter by taking a small FE model and the 2D SAFE results have been compared with 3D FE results. A good match of FE and SAFE results suggests that the results obtained from both models are reasonably accurate. The results have also been validated by experimental measurements. However the experimental weld is not uniform and is not expected to produce 100% matching results. The FE and experimental results are explained in the next few sections.

5.3 Study of the Attenuation of the trapped S0-like mode in a real weld using 3D Finite element simulations

5.3.1 Geometry, material properties and FE input data

The properties of the trapped S0-like mode have also been studied using 3D finite element models. The weld geometry has been modelled by removing elements from the mesh as shown in Figure 5.21. An 8 node brick element of 2nd order has been used to mesh the model in 3D. The size of the element should be very small in order to accurately model the weld profile. Therefore, an element size of 0.5 mm, with 4 elements through thickness in the weld cap, has been chosen. Figure 5.21 (a) shows the solid model studied and Figure 5.21(b) shows the mesh of the model in 3D. Figure 5.21(c) shows the side view of the mesh where we can clearly see the weld profile.

A finer mesh should be used for a closer match to the real weld profile, but a finer mesh is not feasible because of the computational limitations. The model shown in Figure 5.21 is 1 m long and 0.5 m wide, so the model would require 26 million nodes and 78 million degrees of freedom, which is impossible because of the computational limitations. Therefore, a quarter model of the model shown in Figure 5.21 is used for the present study and this model is shown in Figure 5.22. This model has 7 million nodes and 21 million degrees of freedom. The near field effects (interference of the trapped S0-like mode with the S0 mode in the plate) explained in chapter 4 are unavoidable in this model.

5.3.2 Results

To study the attenuation of the trapped S0-like mode, the amplitude of the trapped S0-like mode has been monitored at a series of nodes on the weld. Typical monitored time signals, at 325 kHz, at distances 50, 60, 70, 80, 90 mm from the source can be seen in Figure 5.23. Figure 5.24 shows the log of the maximum amplitudes of these monitored signals. A line has been fitted connecting the points shown in Figure 5.24 and the slope of this line has been taken as the attenuation of the trapped mode at that particular frequency.

The same procedure has been repeated for a range of frequencies from 200 kHz to 500 kHz and the values of attenuation at different frequencies have been calculated and plotted as shown in Figure 5.25. The attenuation increases as the frequency increases up to 400 kHz. This is because of the increase in shear leakage as the velocity difference of the trapped S0-like mode and the SH0-mode in the plate decreases for frequencies up to 400 kHz. At frequencies above 400 kHz, the phase velocity of the trapped mode falls below the velocity of SH0 in the plate and therefore can not leak SH0 into the plate, resulting in zero attenuation at frequencies above 400 kHz.

One would expect a smooth increase in the attenuation for frequencies up to 400 kHz as the velocity difference between the trapped S0-like mode and the SH0 mode in the plate varies smoothly. However the attenuation curve shown in Figure 5.25 shows some fluctuations. This could be mainly because of near field effects explained in the previous chapters, as the monitored signals in the 3D FE models are not at distances far away from the source. Larger models are not

possible because of computational limitations and therefore near field effects are unavoidable.

The lateral extent of the trapped S0-like mode at different frequencies has been found by monitoring the signal at different locations on line 'BB' shown in Figure 5.1. The lateral extent is found to decrease as the frequency increases. Figure 5.26 shows amplitudes of the trapped S0-like mode on line 'BB' at two different frequencies. Figure 5.26(a) shows amplitudes of the trapped S0-like mode at a frequency (200 kHz) from the low frequency regime and Figure 5.26(b) shows amplitudes of the trapped S0-like mode at a frequency (400 kHz) from the high frequency regime. The trapped S0-like mode has significant lateral extent at low frequencies and this decreases as the frequency increases.

5.4 Experimental Measurements

Figure 5.27 shows the experimental setup. The test plate comprised two 1m x 2m x 6mm steel plates butt welded together to give a 2m square plate with a weld down the middle. This test plate is the same as that explained in chapter 2. The transducer which was used is a single element immersion transducer and it was mounted on the edge of the plate as shown in Figure 5.27. The plate was excited as shown in Figure 5.27 in the in-plane direction using a 20 cycle tone burst multiplied by a Hanning window.

A tone burst with 50 cycles has been used at high frequencies where the trapped S0-like mode is dispersive. The trapped S0-like mode has been measured on line 'CC' at different locations on the weld using an out of plane laser interferometer

(Polytec OFV 512). Typical measured signals, at different locations on the weld, can be seen in Figure 5.28. The monitored signals show the trapped S0-like mode, reflection from the defect in the heat affected zone and reflections from far edges. The trapped S0-like mode has been gated out for further processing.

Figure 5.29 shows the log of the maximum amplitudes of the monitored signals on line 'CC' at different distances from the source. One would expect a smooth decrease in the amplitude values as the distance from the source increases. However Figure 5.29 shows a non-smooth decreasing curve and this is believed to be due to the non-uniform nature of the weld along its length. A straight line has been fitted connecting the points and the slope of this line has been taken as the attenuation of the trapped mode at that particular frequency. The same procedure has been repeated for a range of frequencies from 200 kHz to 500 kHz and the values of attenuation at different frequencies have been plotted as shown in Figure 5.30. Figure 5.30 also compares attenuation results calculated using finite element simulations with experimental results. The FE results are comparable with experimental results except for small fluctuations at some frequencies in the FE results.

The experimental plate has dimensions of 2m X 1m and has the flexibility to monitor signals at distances far away from the source to avoid near field effects, whereas the FE model has dimensions of 1 m x 0.5 m and monitoring at distances far away from the source is not possible. The weld profile in the FE model is not exactly the same as the real weld. The real weld in the experimental

plate is also not uniform along the length. All these lead to small differences between experimental results and FE results.

Figure 5.31 compares the attenuation of the trapped S0-like mode calculated by 2D SAFE, 3D FE and Experimental measurements. The attenuation calculation using 2D SAFE is a frequency domain calculation and it has no attenuation due to dispersion, whereas the attenuation values calculated from FE and experimental signals are time domain calculations and they have attenuation due to dispersion. Therefore, in Figure 5.31 the attenuation values of 3D FE and experimental signals have been compensated for dispersion for comparison. The amount of amplitude decrease due to dispersion, at a particular frequency and for a particular propagation distance, has been taken from DISPERSE and this value has been used for the above dispersion compensation calculations.

Figure 5.31(a) compares attenuation in the low frequency region and Figure 5.31(b) compares attenuation of the trapped S0-like mode in the high frequency region. Comparison between 300 kHz and 400 kHz is avoided as the 2D SAFE results between these frequencies are unreliable because of unavoidable reflections of the leaky SH0 at large angles of radiation in to the plate. From Figure 5.31, we can see that the SAFE results, experimental results and FEM results are comparable.

5.5 Comparison of Idealised weld and real weld

The trapped S0-like mode shows attenuation because of the SH0 mode leakage into the surrounding plates at frequencies where the trapped S0-like mode is faster than the SH0 mode. At frequencies where the trapped S0-like mode is slower than the SH0 in the plate, the trapped S0-like mode can not leak SH0 in to the plates and therefore results in zero attenuation because of leakage. This phenomenon is the same in both cases. However the trends of the attenuation with frequency are different.

With idealized weld caps as explained in the previous chapter, the attenuation of the trapped S0-like mode increases with frequency up to 125 kHz and decreases at frequencies above 125 kHz. The energy in the weld, for the idealised weld, becomes more and more concentrated at the centre as the frequency increases up to 125 kHz, so more and more energy can leak into the plates for frequencies up to 125 kHz. At frequencies above 125 kHz, the energy of the trapped S0-like mode starts dispersing towards the surfaces of the weld with less and less energy in the centre. Therefore, less and less energy can leak into the plates at frequencies above 125 kHz, resulting in less attenuation at frequencies above 125 kHz. With real weld caps, the attenuation increases for frequencies up to 400 kHz even though the wave starts to behave like a surface wave at frequencies above 275 kHz.

The energy distribution and mode shapes across the cross section of the model are also different. The energy distribution and mode shapes in the real weld case can be seen from Figures 5.7 to 5.20 and from figures 4.3 to 4.13 for the

idealized weld cap case. This can cause a lot of defect sensitivity difference between the real weld model and the idealized weld model.

5.6 Conclusions

The attenuation of the trapped S0-like mode in a real weld increases as the velocity difference between the trapped S0-like mode and the SH0 mode in the plate decreases. It has zero attenuation at frequencies where the trapped S0-like mode is slower than the SH0 mode in the plate. The lateral extent of the trapped S0-like mode decreases as the frequency increases. At high frequencies the trapped S0-like mode behaves like a surface wave with no lateral extent in the surrounding plates. The properties of the trapped S0-like mode in the real weld are different from the properties of the trapped S0 in idealised welds.

The results obtained using experimental measurements and 3D FE models are comparable at all frequencies except for small fluctuations at some frequencies in the 3D FE results. These results (3D FEM and experimental) are comparable with 2D SAFE results at frequencies between 200 kHz to 300 kHz and 400 kHz to 500 kHz. The results from 2D SAFE models are un-reliable between frequencies from 300 kHz to 400 kHz due to the un-avoidable reflections from the absorbing region between these frequencies. The low frequency regime is expected to be suitable for inspection of defects in the weld and defects near the weld, whereas the high frequency regime is expected to be suitable for inspection of small surface breaking cracks in the weld.

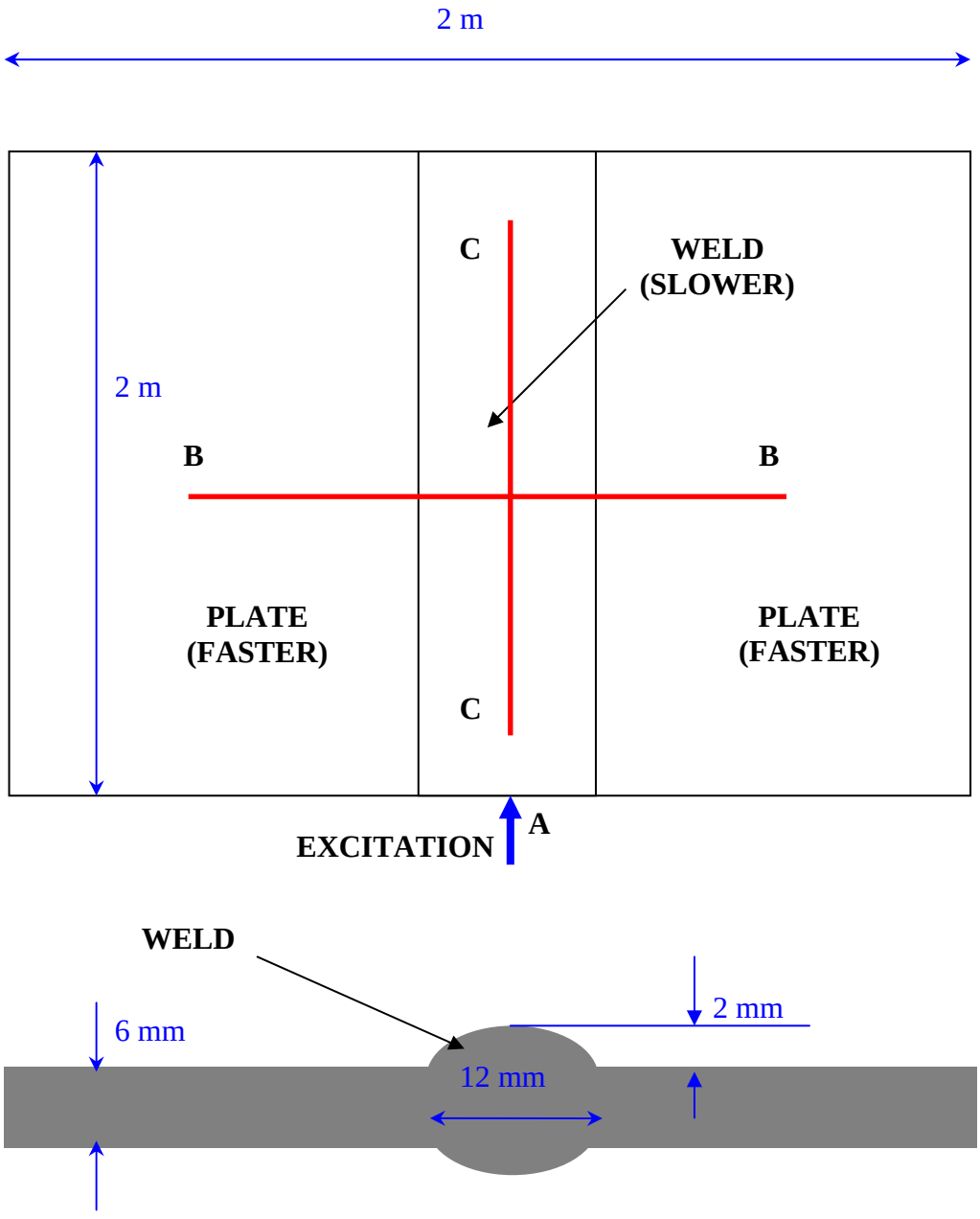

FIGURE 5.1: Geometry of real weld (not to scale)

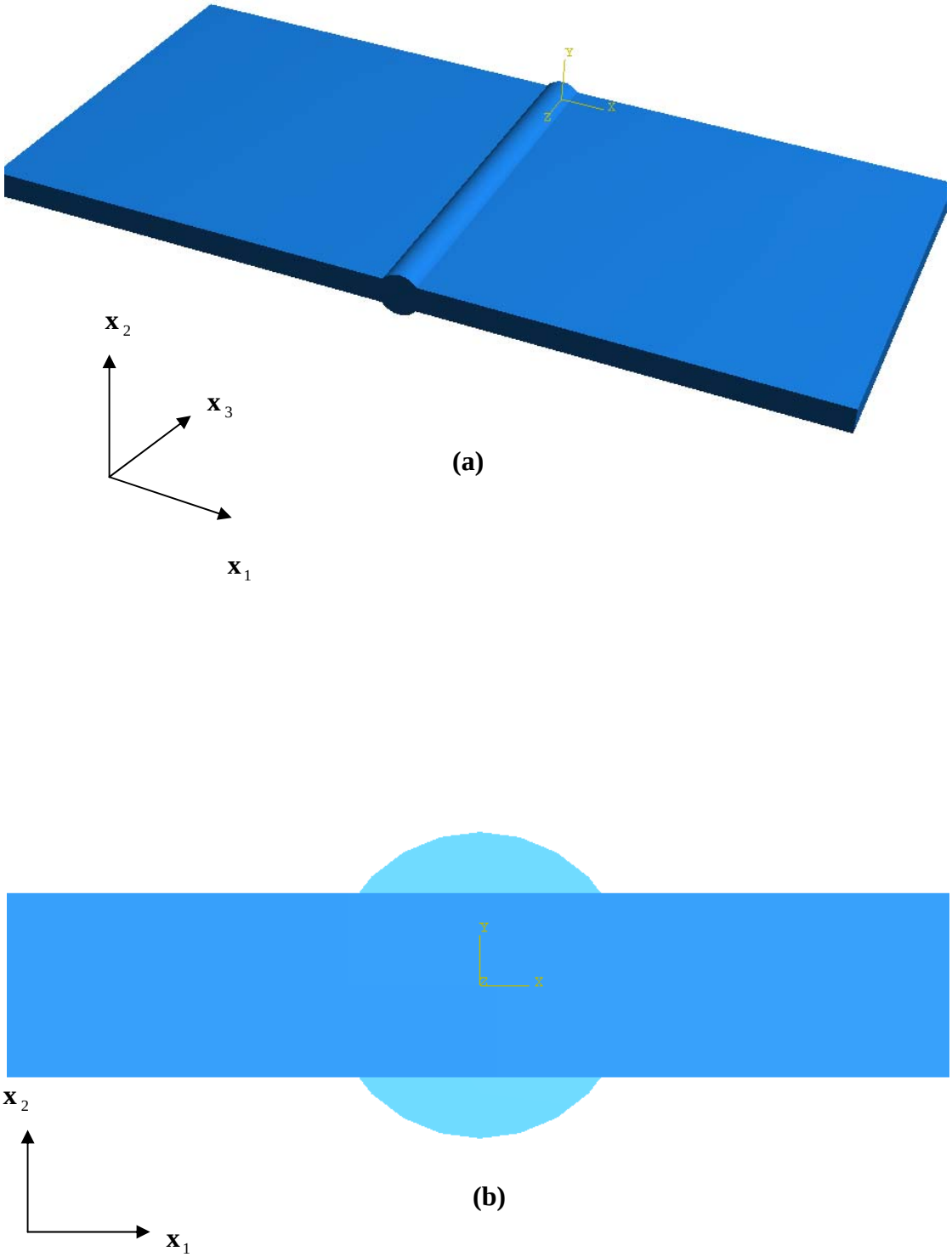

FIGURE 5.2: Real weld (a) 3D model, (b) 2D model

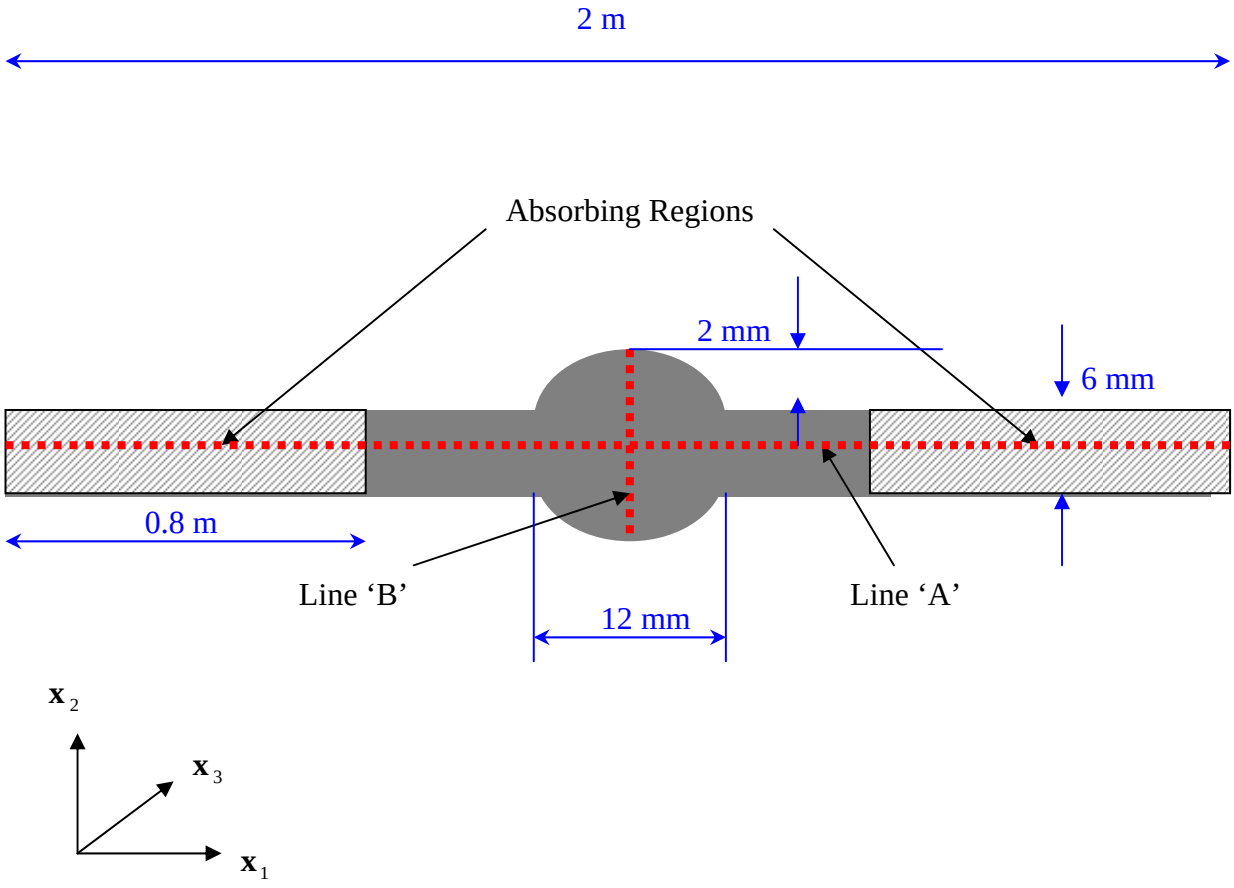

FIGURE 5.3: SAFE model with absorbing regions for the real weld (Dimensions not to scale)

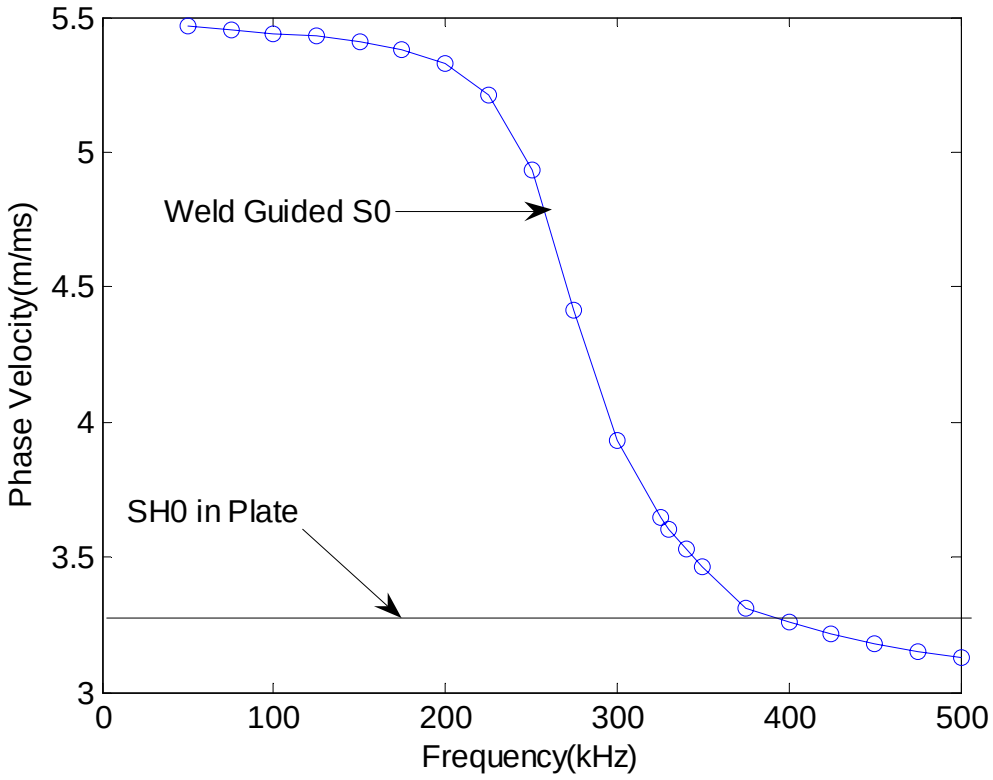

(a)

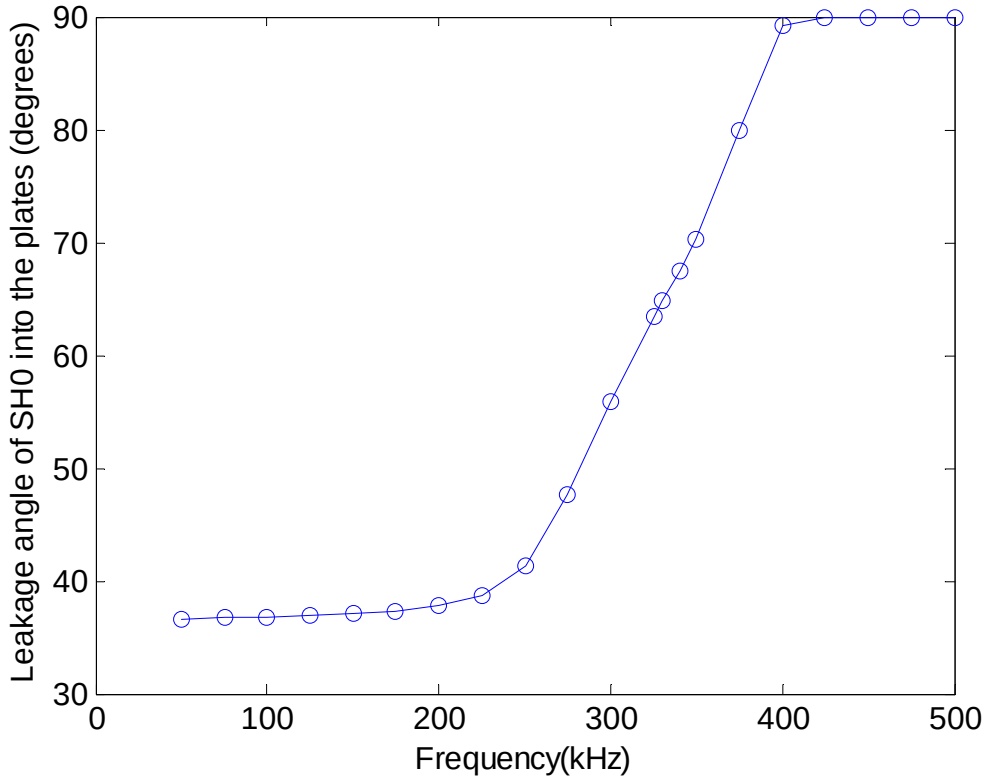

(b)

FIGURE 5.4: (a) Phase velocity dispersion curve of the trapped S0-like mode from 2D SAFE, (b) Leakage angle of the SH0 mode into the plates for different frequencies

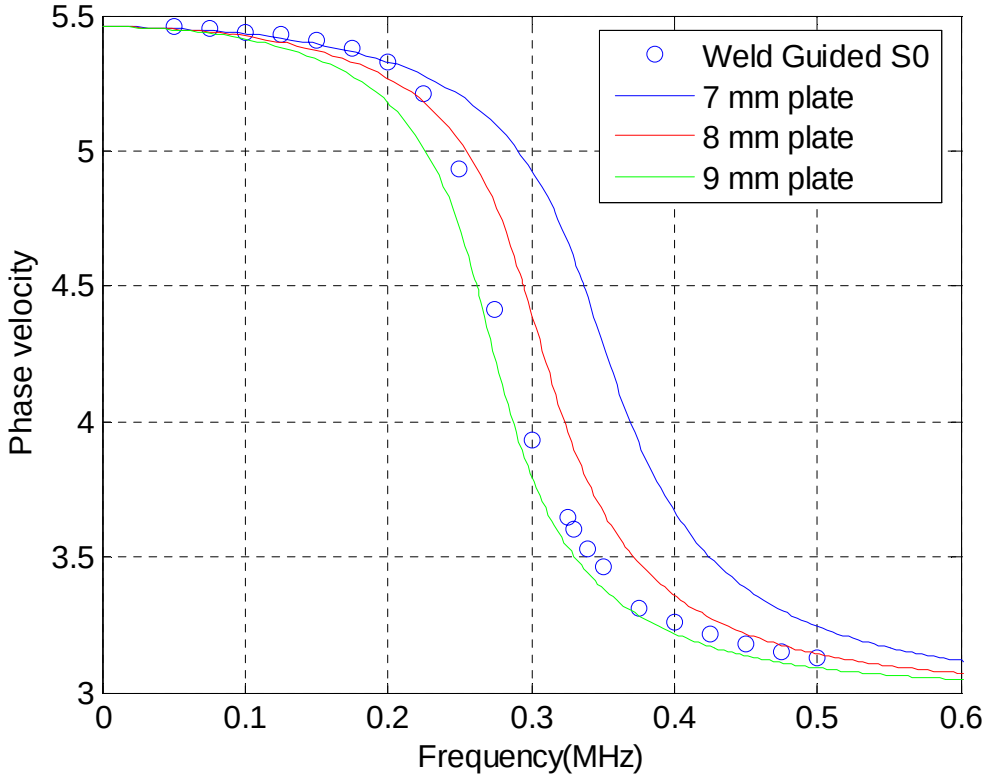

FIGURE 5.5: Phase Velocity of the trapped S0-like mode compared with the phase velocities of plates with different thicknesses at different frequencies

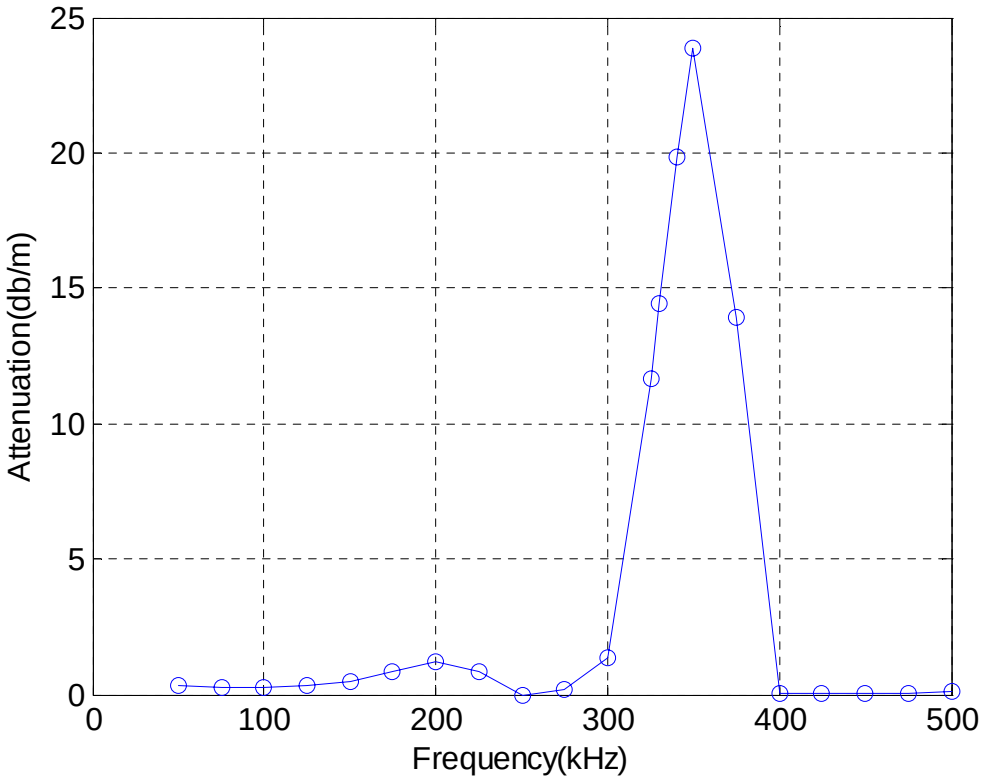

FIGURE 5.6: Attenuation of the trapped S0-like mode calculated from 2D SAFE models

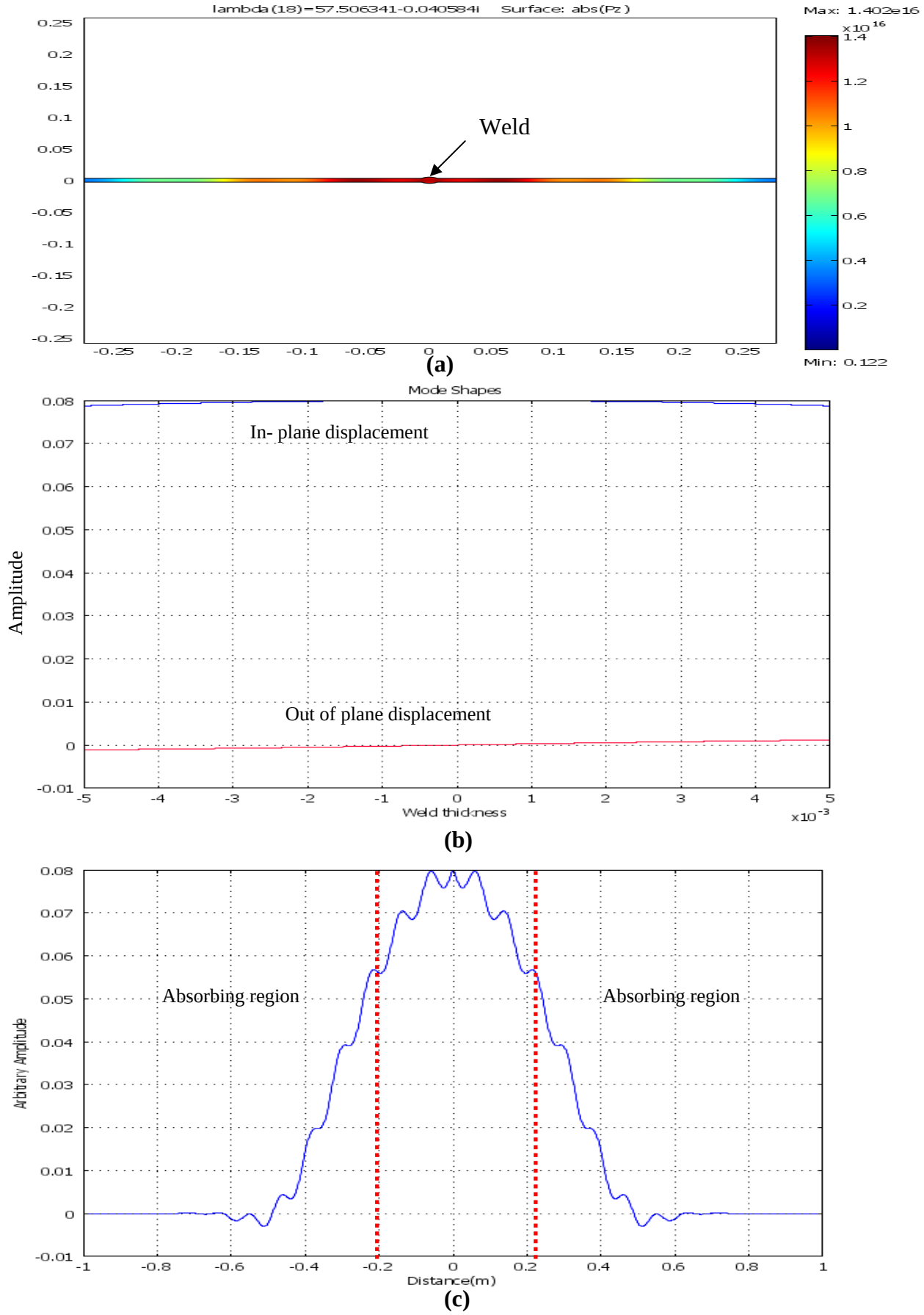

FIGURE 5.7: SAFE results at 50 kHz, (a) Power flow along the weld, (b) Mode shapes, (c) Amplitudes on line x_1 = -1m to x_1 = 1mm at x_2 =0.

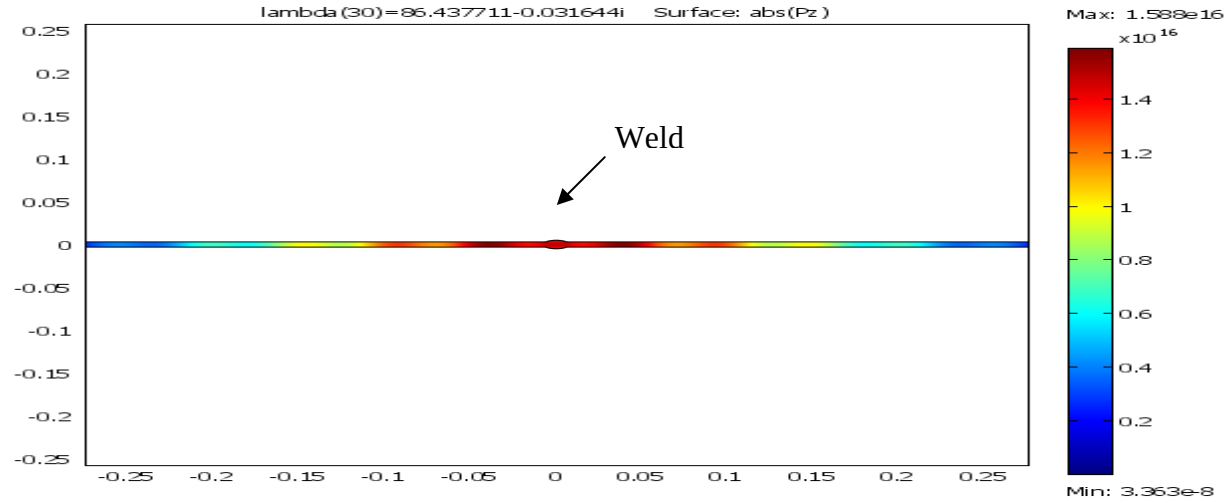

(a)

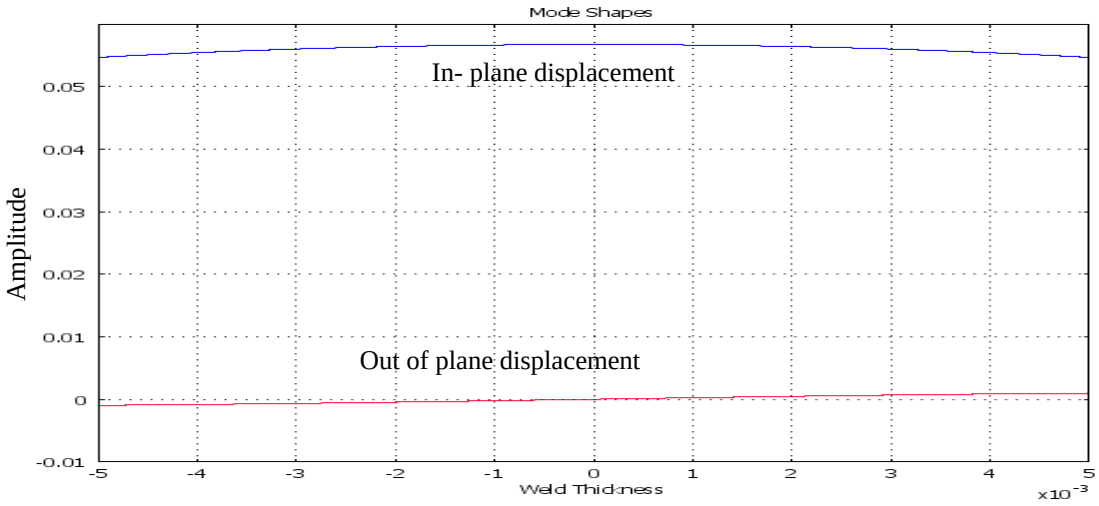

(b)

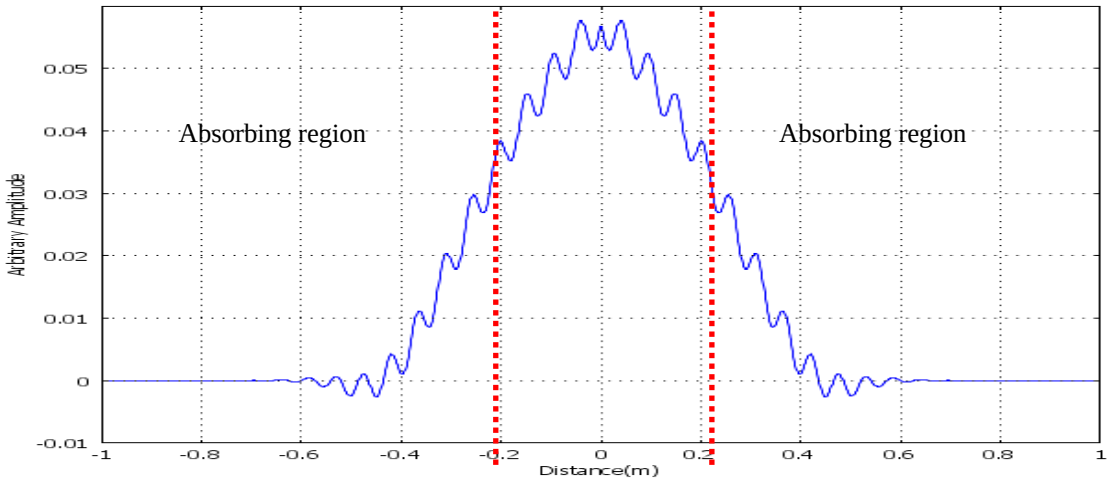

(c)

FIGURE 5.8 : SAFE results at 75 kHz, (a) Power flow along the weld, (b) Mode shapes, (c) Amplitudes on line x_1 = -1m to x_1 = 1mm at x_2 =0.

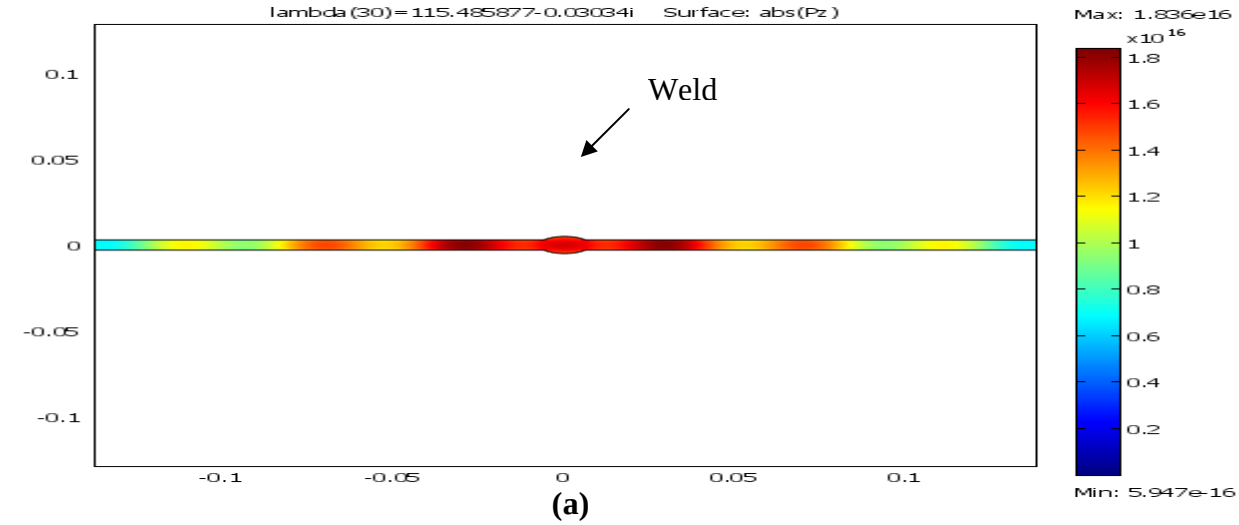

(a)

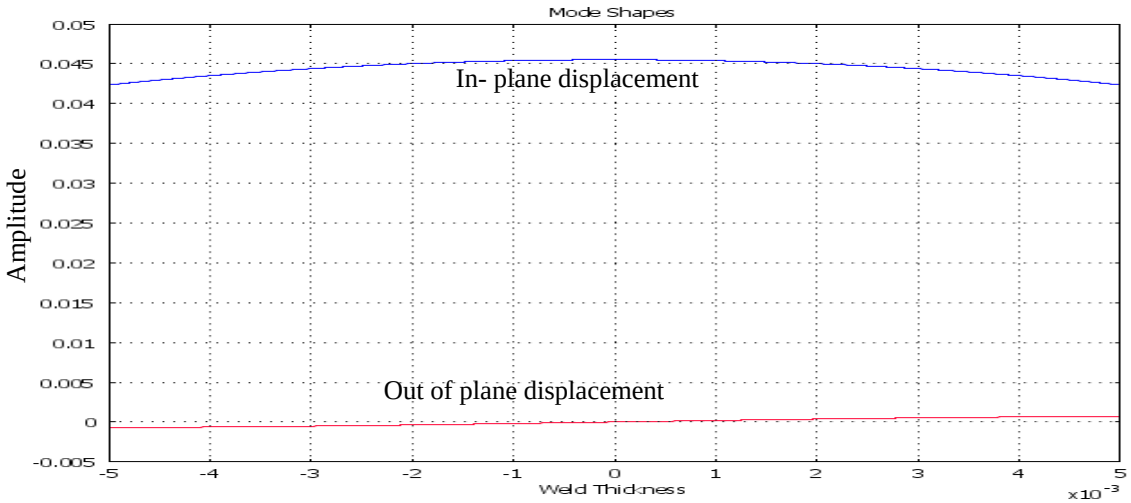

(b)

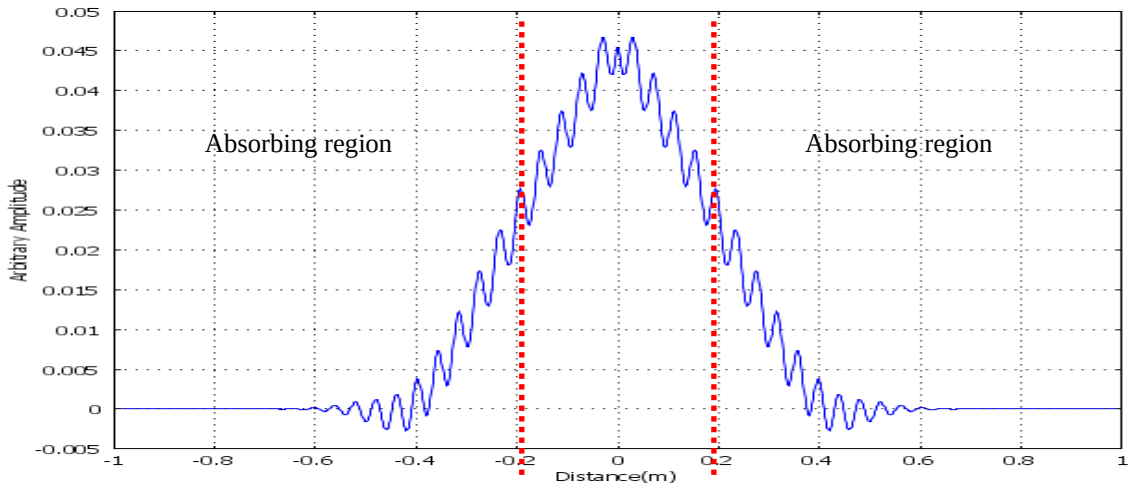

(c)

FIGURE 5.9: SAFE results at 100 kHz, (a) Power flow along the weld, (b) Mode shapes, (c) Amplitudes on line x_1 = -1m to x_1 = 1mm at x_2 =0.

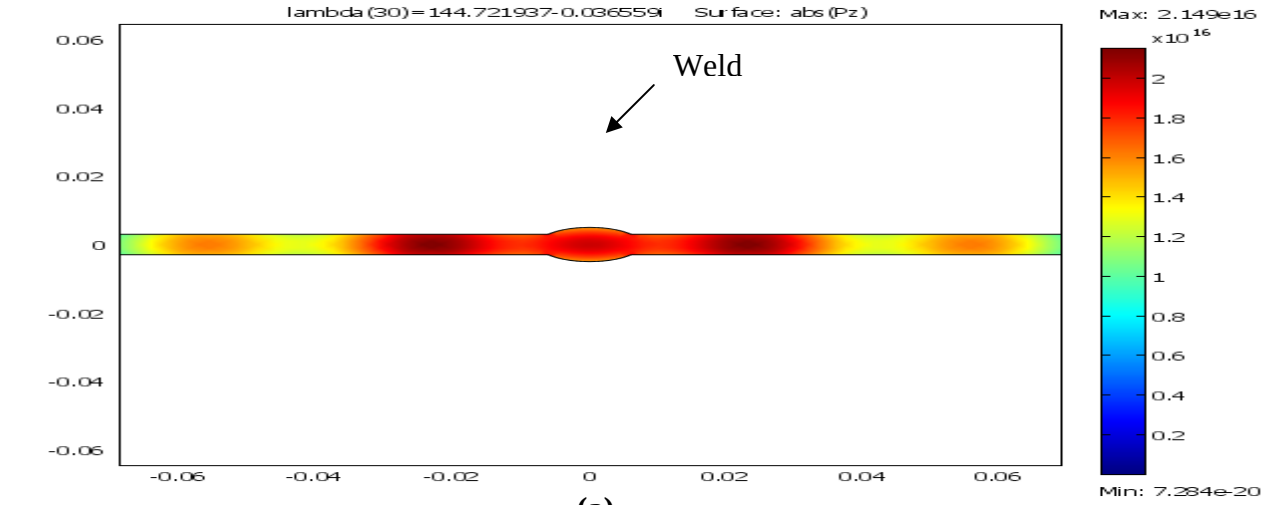

(a)

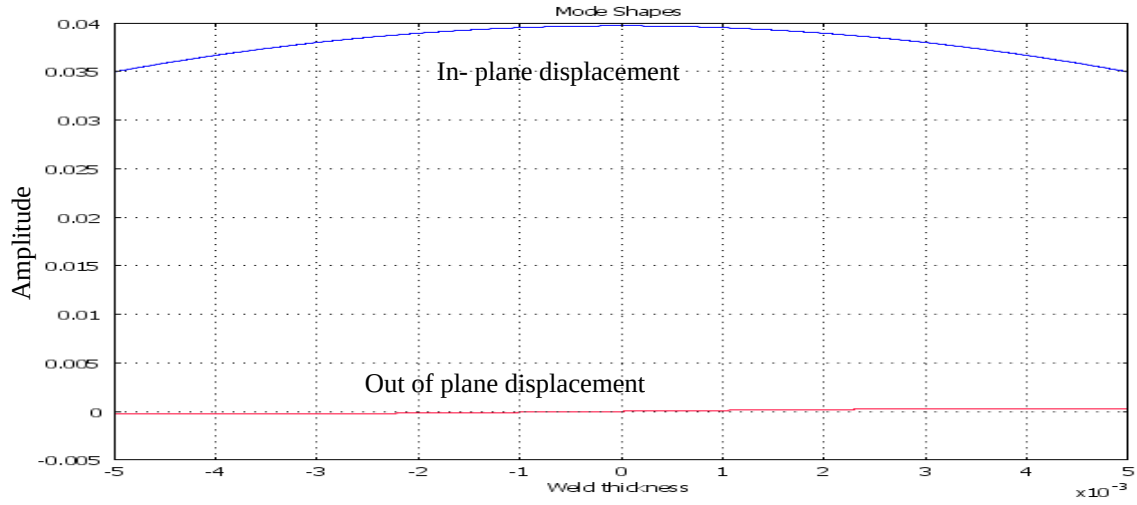

(b)

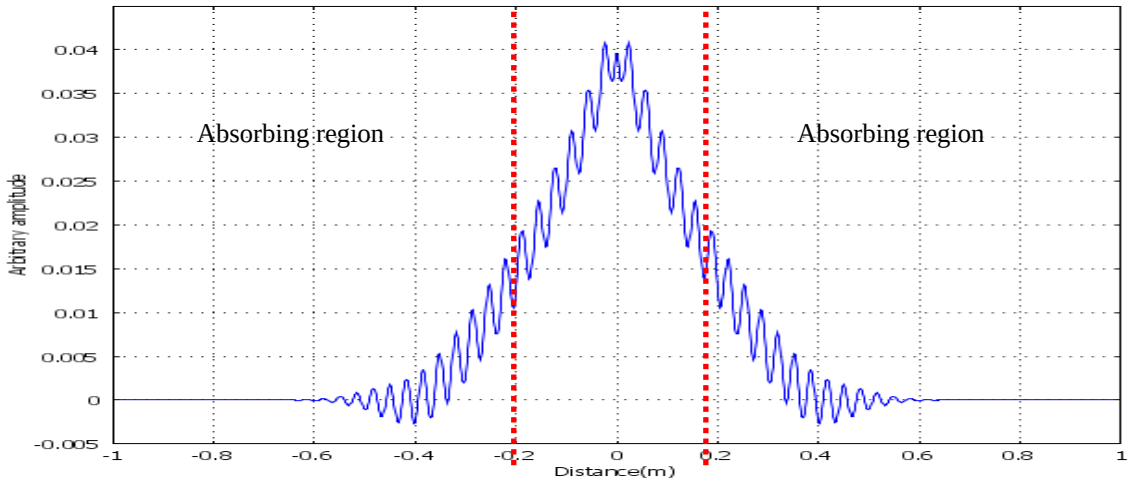

(c)

FIGURE 5.10: SAFE results at 125kHz, (a) Power flow along the weld, (b) Mode shapes, (c) Amplitudes on line x_1 = -1m to x_1 = 1mm at x_2 =0.

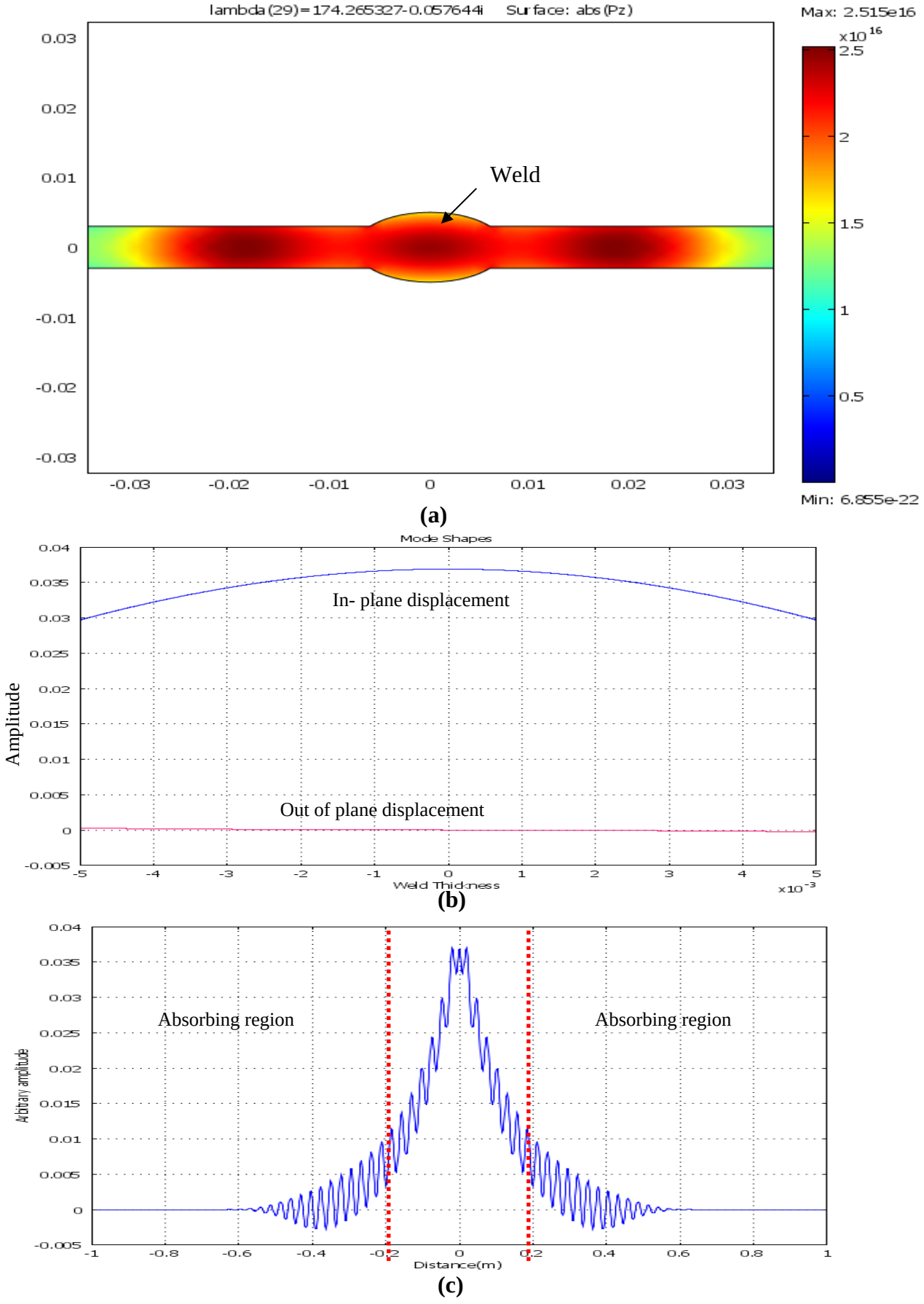

FIGURE 5.11: SAFE results at 150 kHz, (a) Power flow along the weld, (b) Mode shapes, (c) Amplitudes on line x_1 = -1m to x_1 = 1mm at x_2 =0.

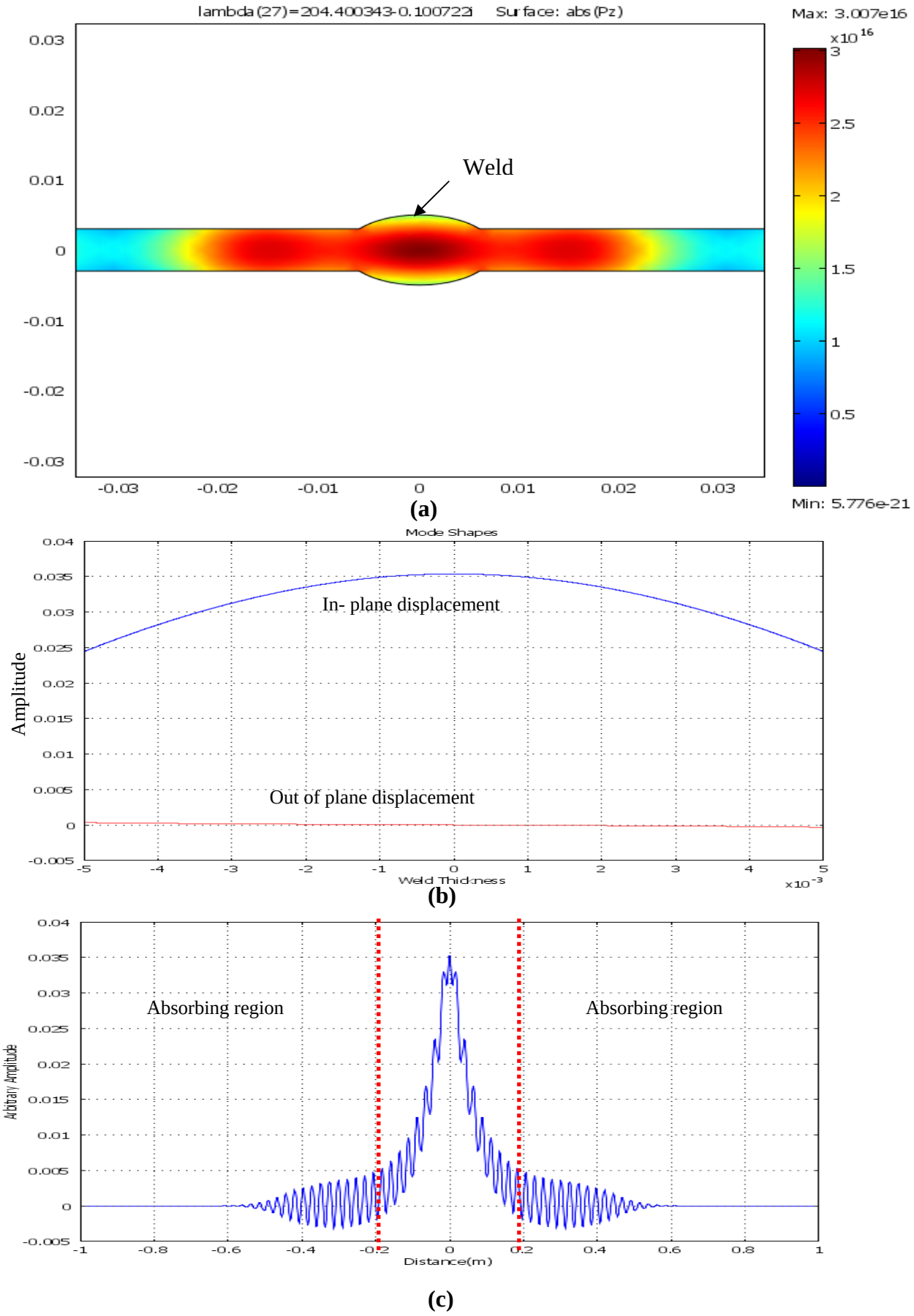

FIGURE 5.12: SAFE results at 175 kHz, (a) Power flow along the weld, (b) Mode shapes, (c) Amplitudes on line x_1 = -1m to x_1 = 1mm at x_2=0.

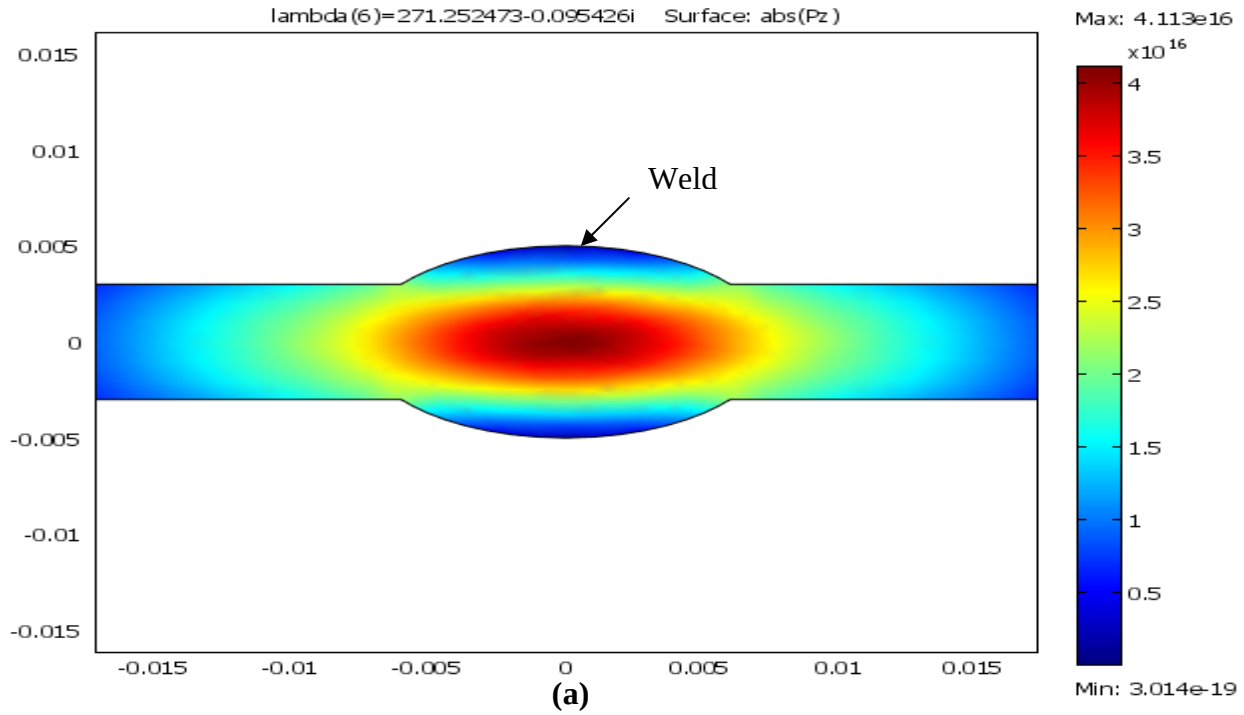

(a)

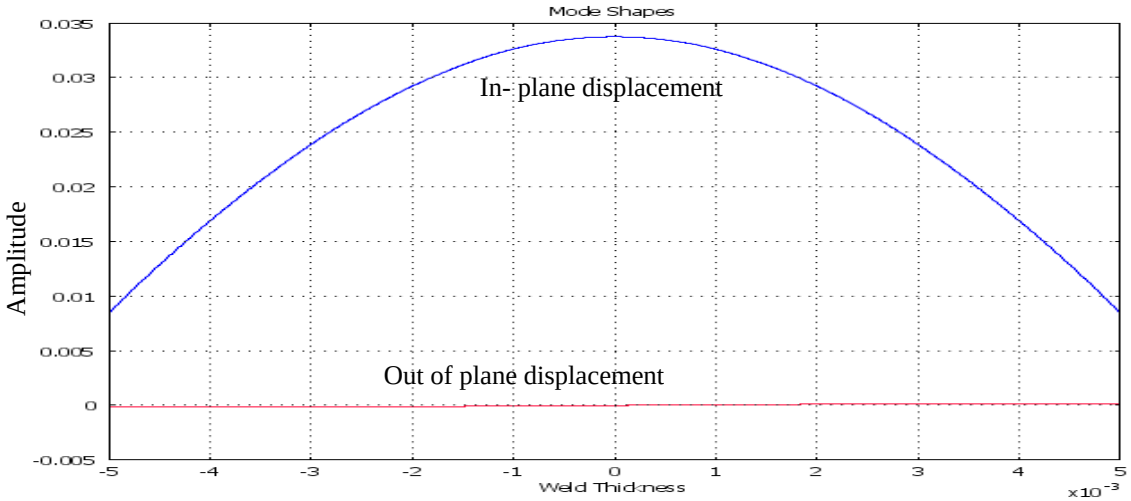

(b)

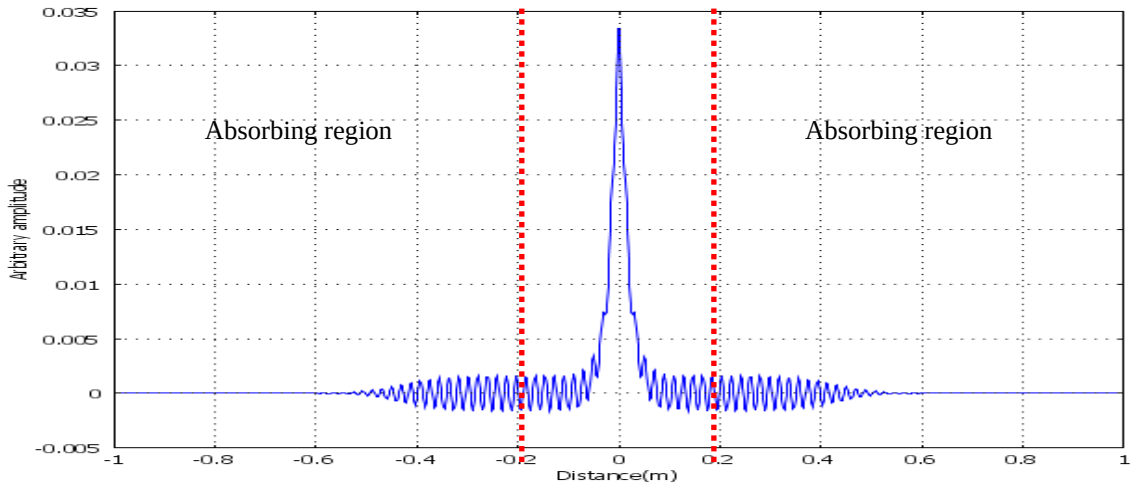

(c)

FIGURE 5.13: SAFE results at 225 kHz, (a) Power flow along the weld, (b) Mode shapes, (c) Amplitudes on line x_1 = -1m to x_1 = 1mm at x_2 =0.166

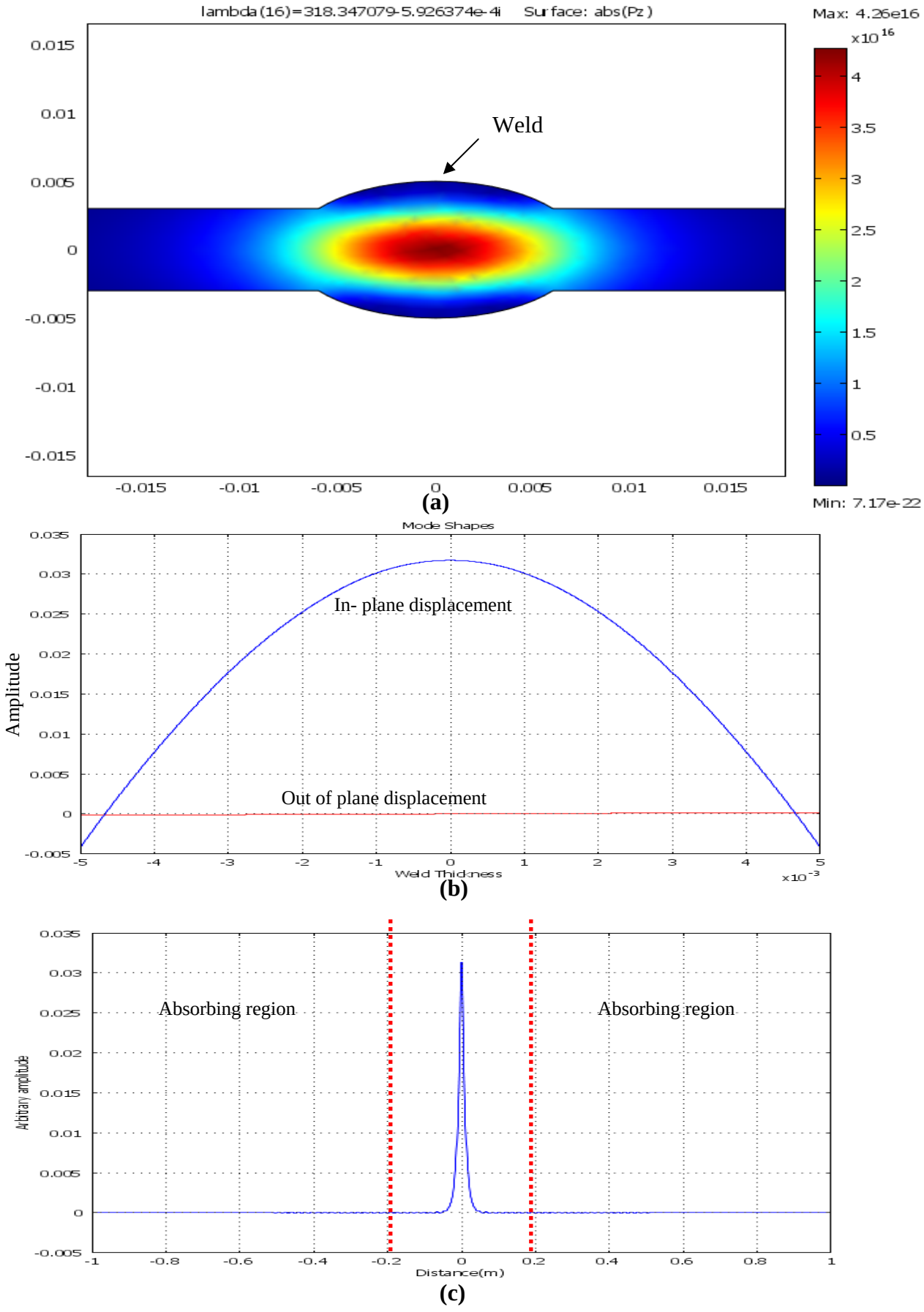

FIGURE 5.14: SAFE results at 250 kHz, (a) Power flow along the weld, (b) Mode shapes, (c) Amplitudes on line x_1 = -1m to x_1 = 1mm at x_2 =0.

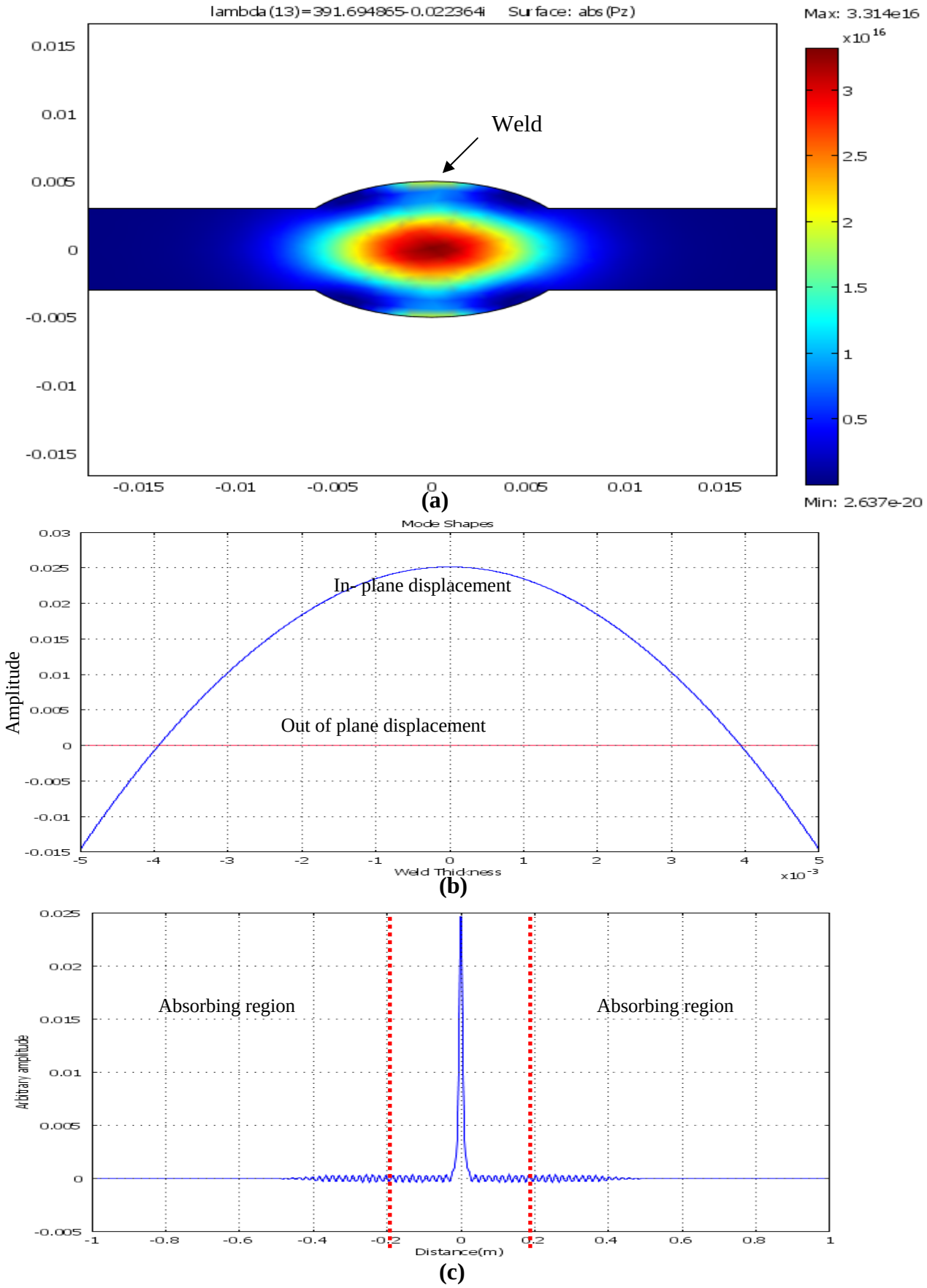

FIGURE 5.15: SAFE results at 275 kHz, (a) Power flow along the weld, (b) Mode shapes, (c) Amplitudes on line x_1 = -1m to x_1 = 1mm at x_2 =0.

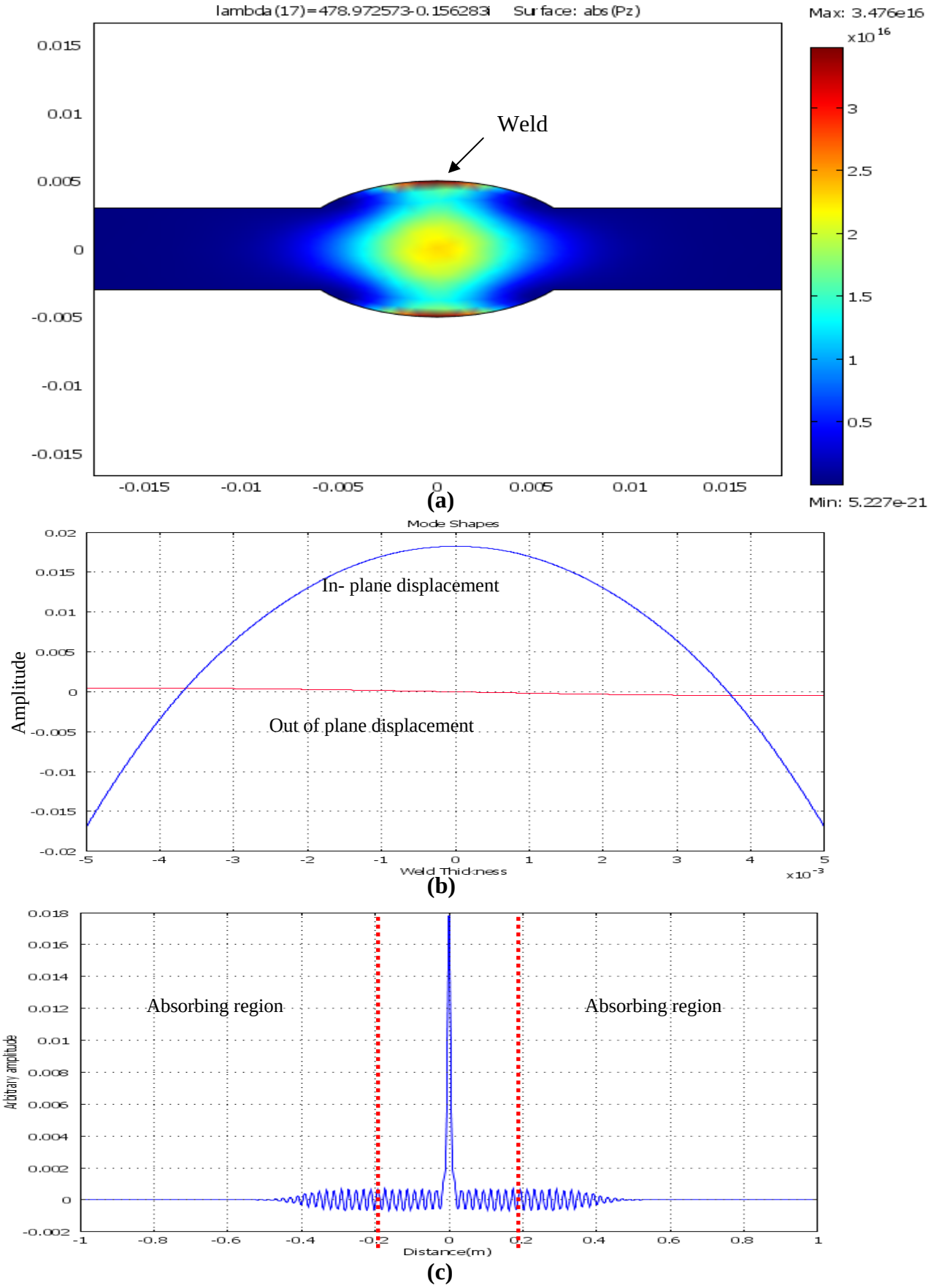

FIGURE 5.16: SAFE results at 300 kHz, (a) Power flow along the weld, (b) Mode shapes, (c) Amplitudes on line x_1 = -1m to x_1 = 1mm at x_2 =0.

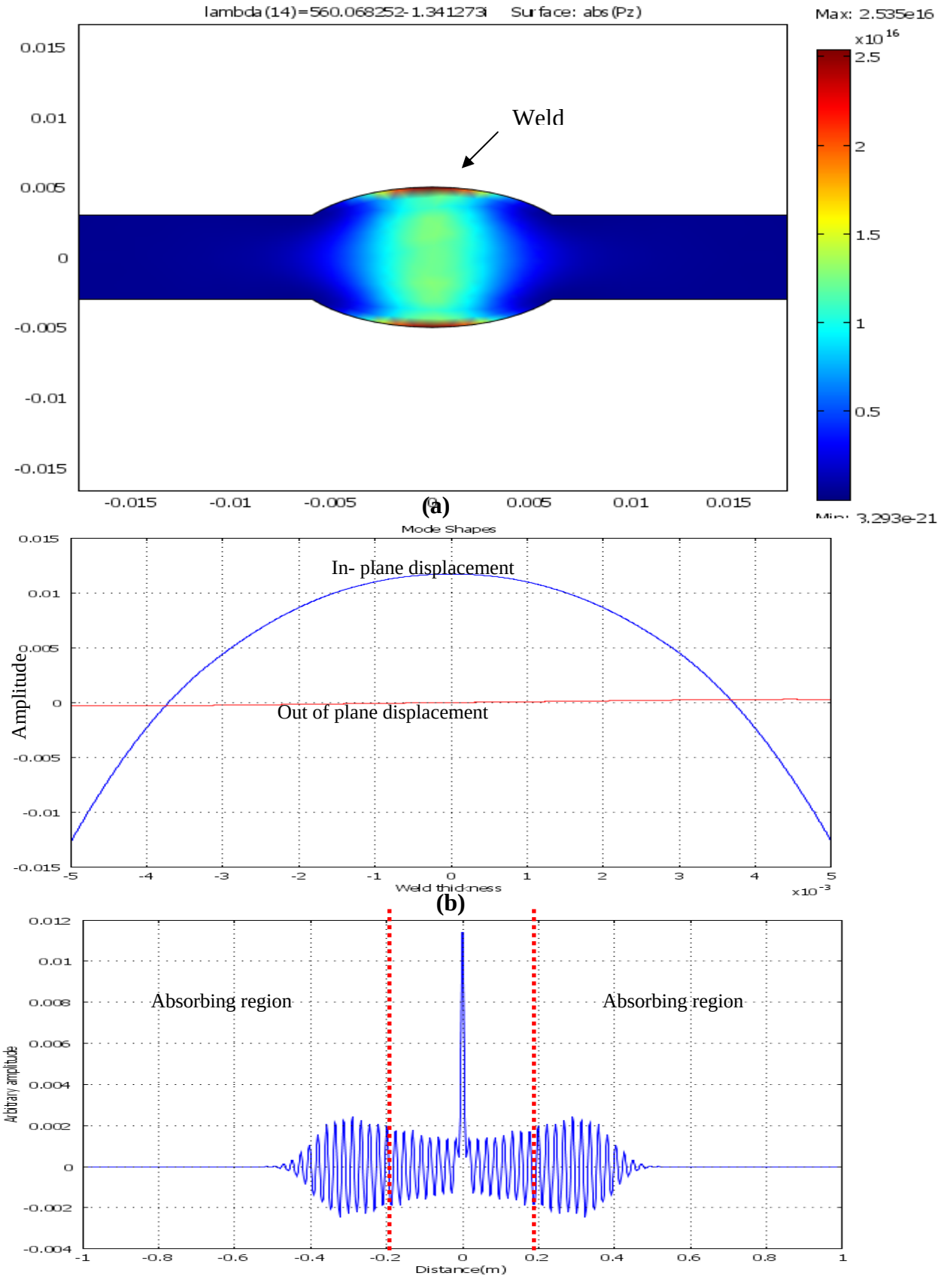

FIGURE 5.17: SAFE results at 325 kHz, (a) Power flow along the weld, (b) Mode shapes, (c) Amplitudes on line x_1 = -1m to x_1 = 1mm at x_2 =0.

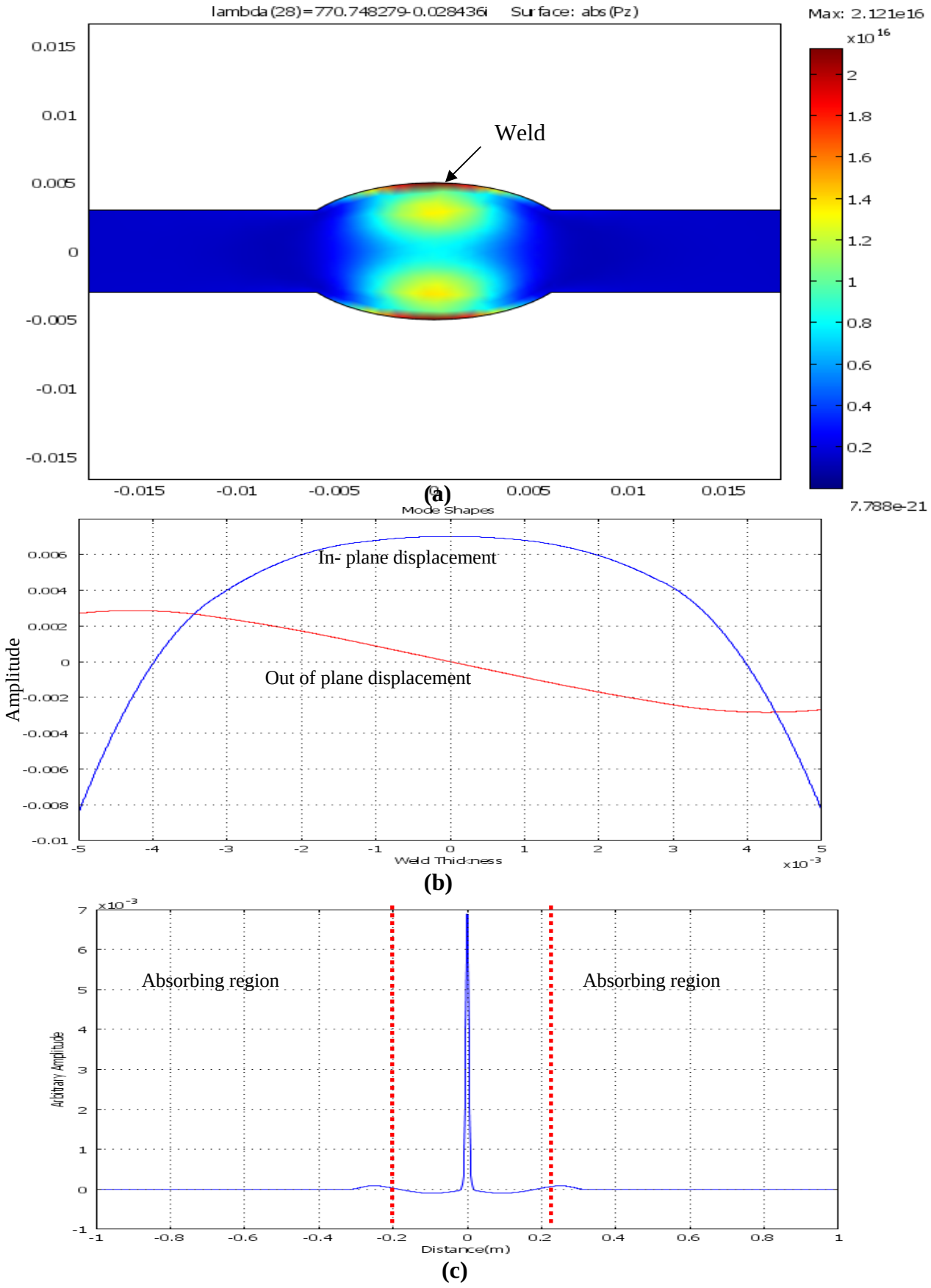

FIGURE 5.18: SAFE results at 400 kHz, (a) Power flow along the weld, (b) Mode shapes, (c) Amplitudes on line x_1 = -1m to x_1 = 1mm at x_2 =0.171

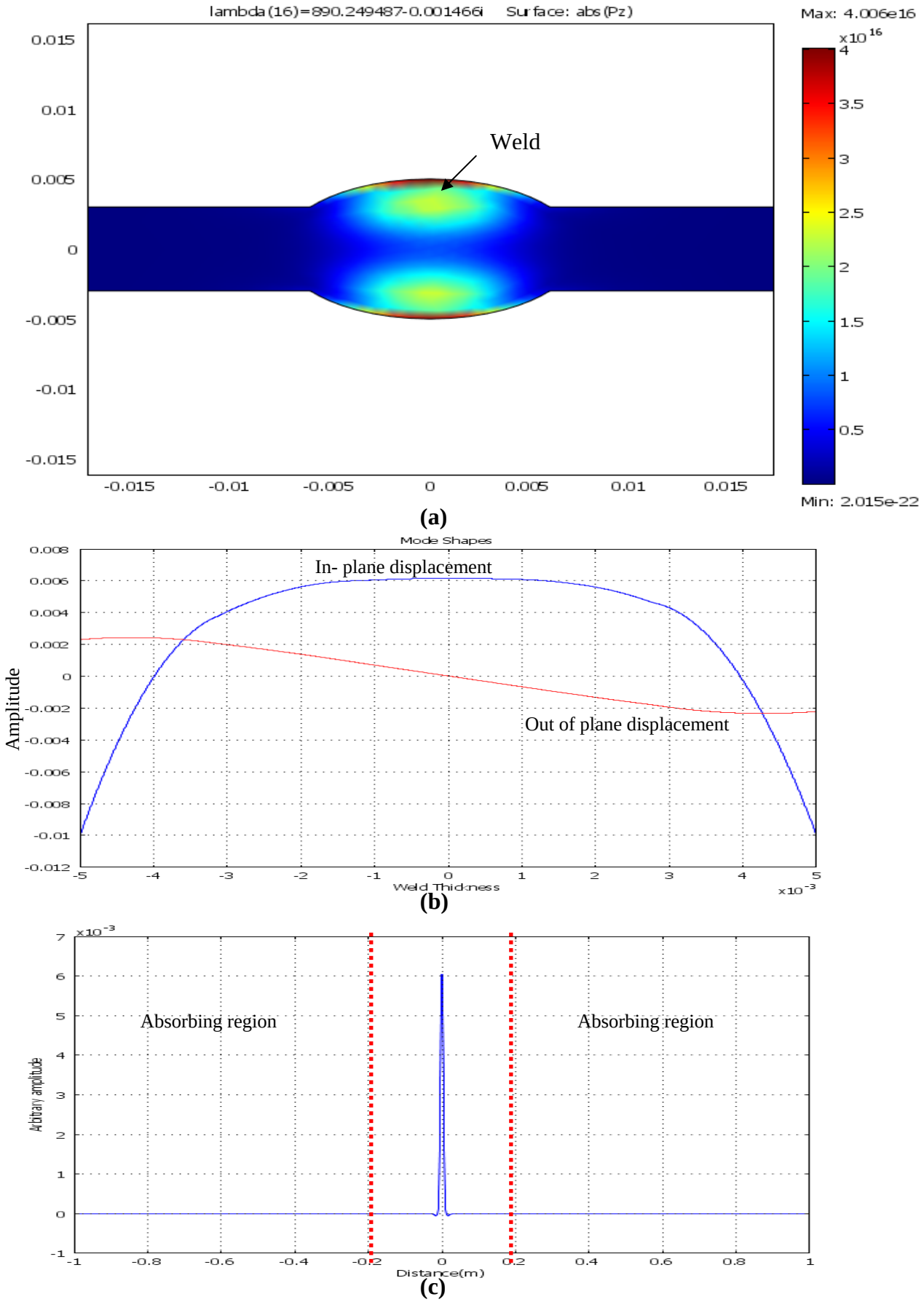

FIGURE 5.19: SAFE results at 450 kHz, (a) Power flow along the weld, (b) Mode shapes, (c) Amplitudes on line x_1 = -1m to x_1 = 1mm at x_2 =0.

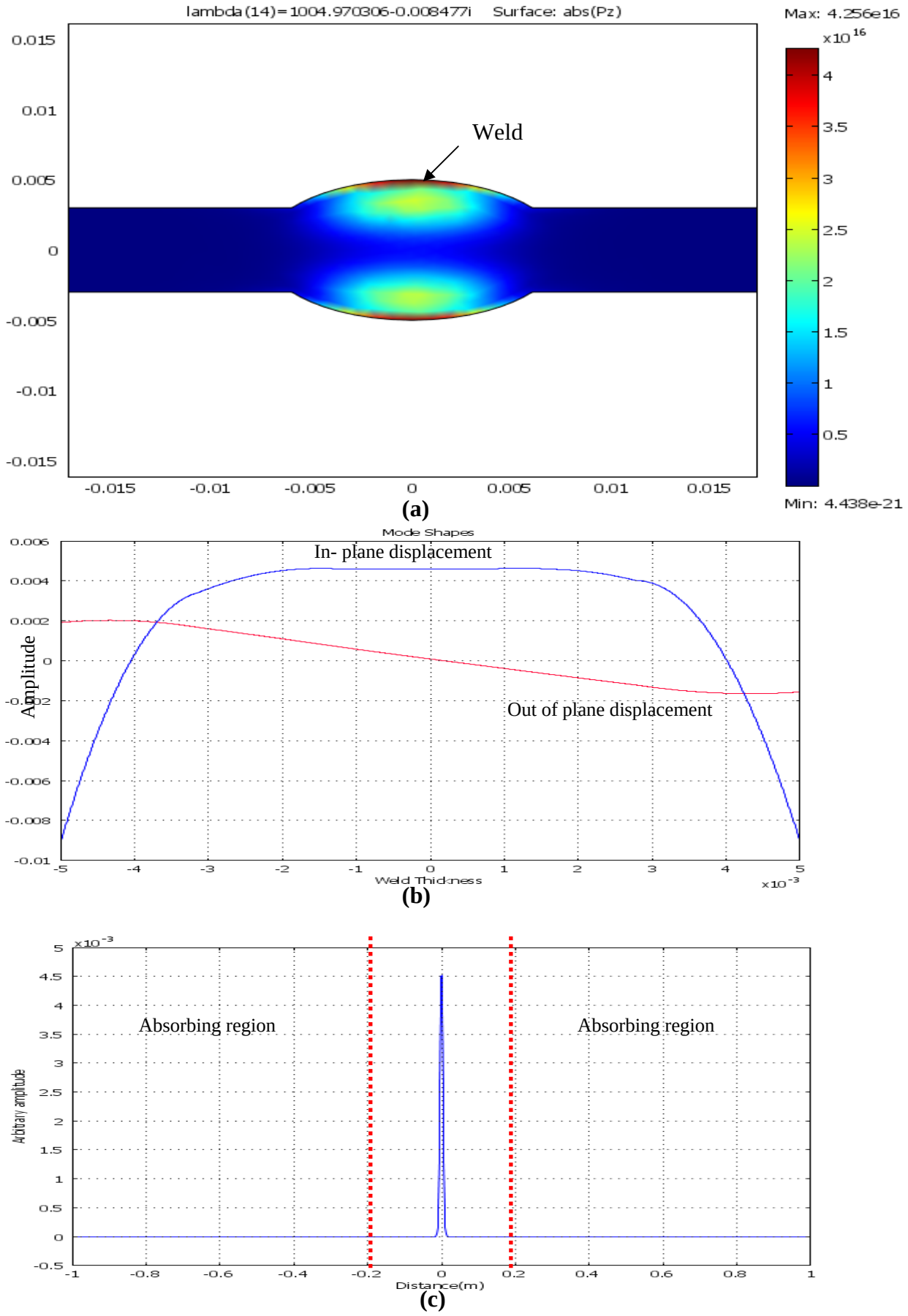

FIGURE 5.20 : SAFE results at 500 kHz, (a) Power flow along the weld, (b) Mode shapes, (c) Amplitudes on line x_1 = -1m to x_1 = 1mm at x_2 =0.

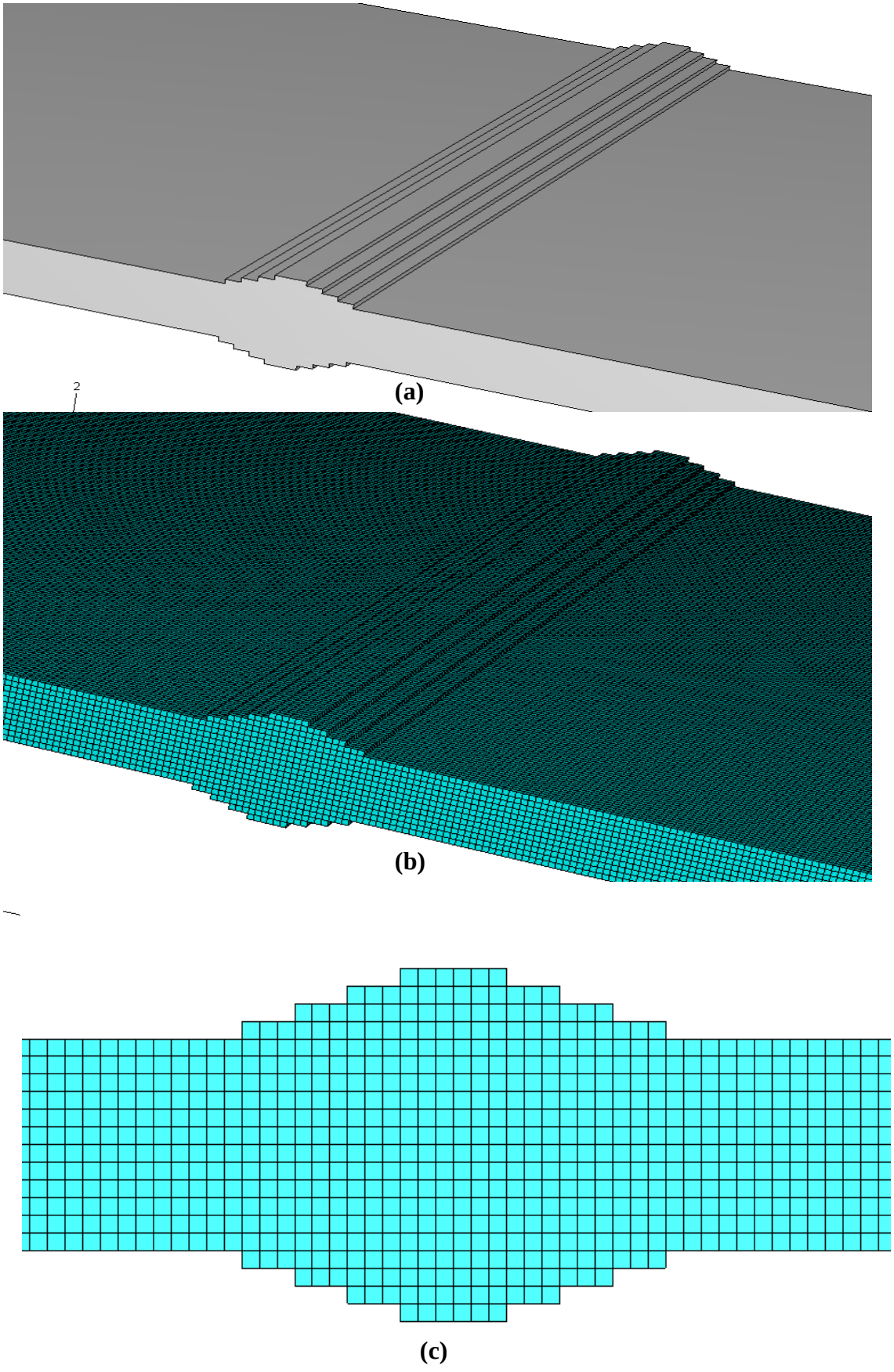

FIGURE 5.21: Finite element model of real weld, (a) Geometry used in FE model (b) 3D mesh, (c) Side view of mesh

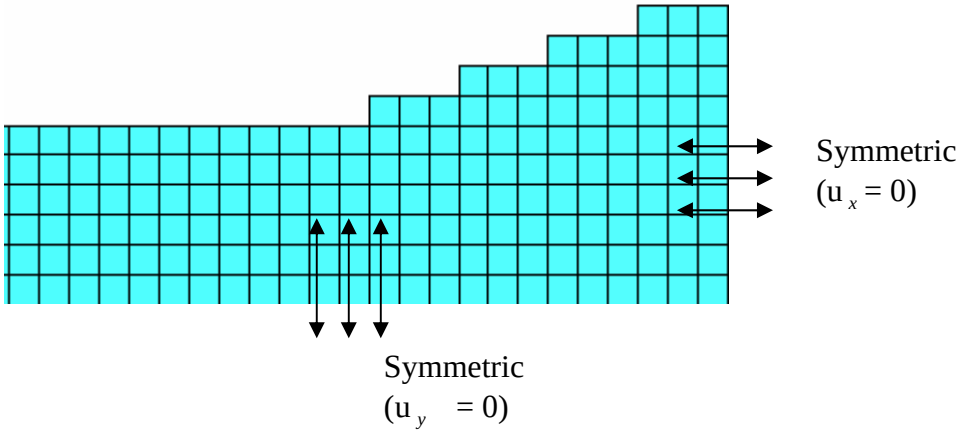

FIGURE 5.22: Side view of the quarter finite element model studied

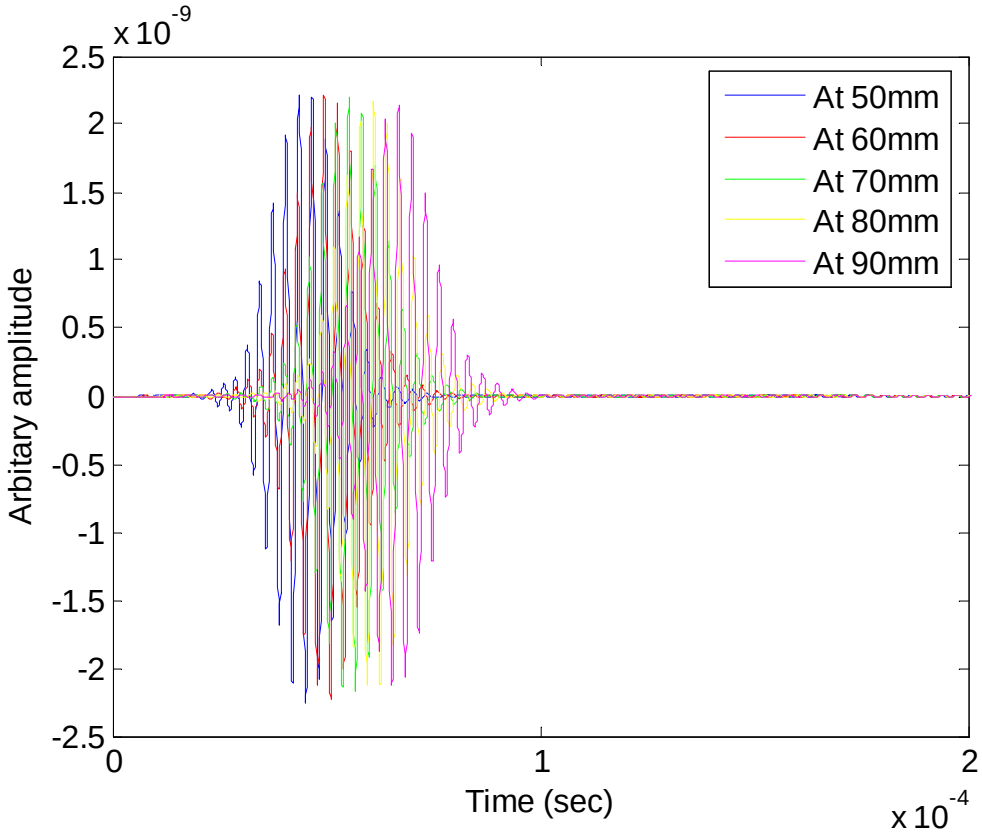

FIGURE 5.23: Typical monitored signals at different distances on line 'CC' at the operating frequency of 325 kHz

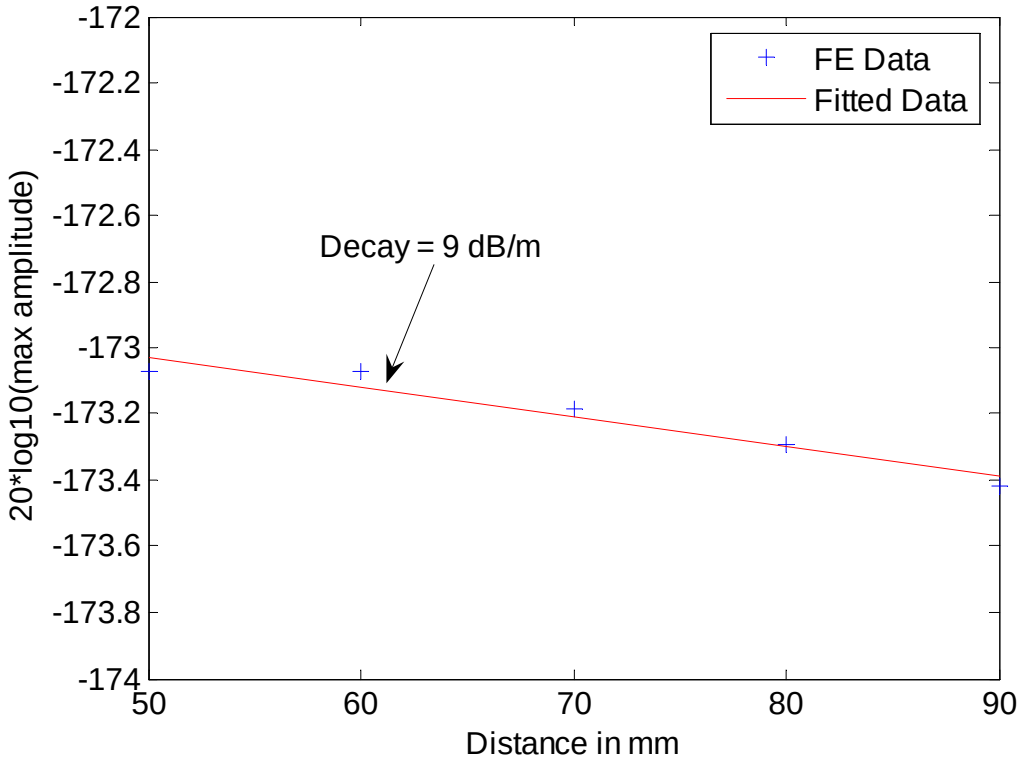

FIGURE 5.24: Log of maximum amplitudes of monitored signals at different distances from the source at 325 kHz

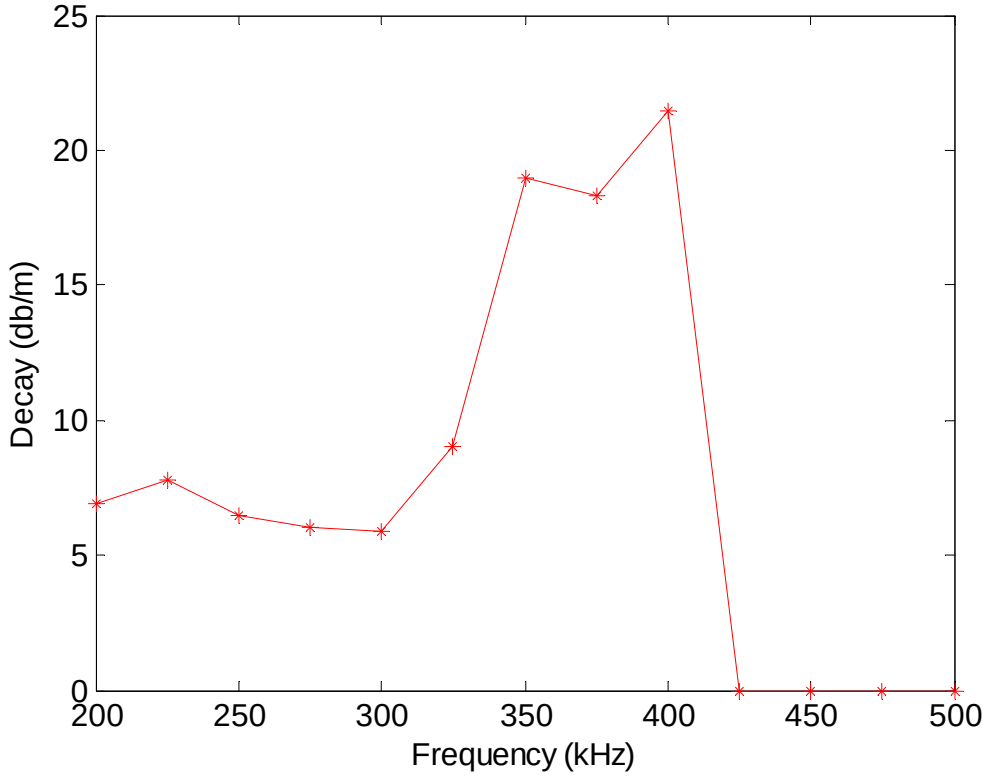

FIGURE 5.25: Attenuation of weld guided mode at different frequencies (Calculated using 3D FE models)

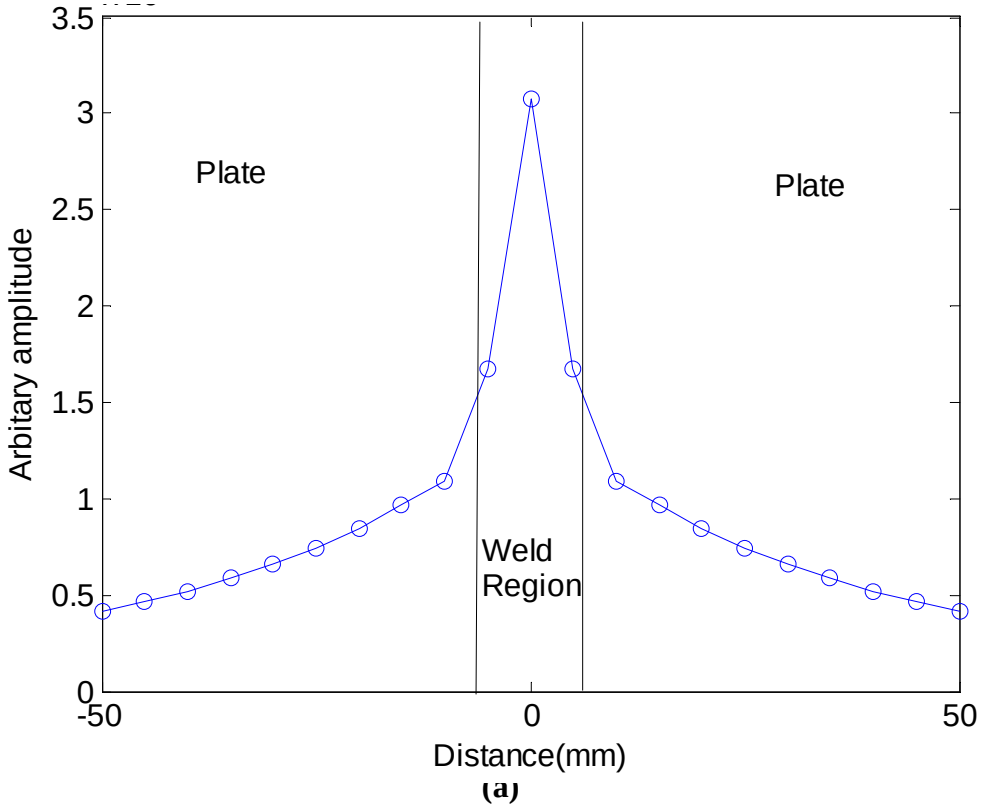

(a)

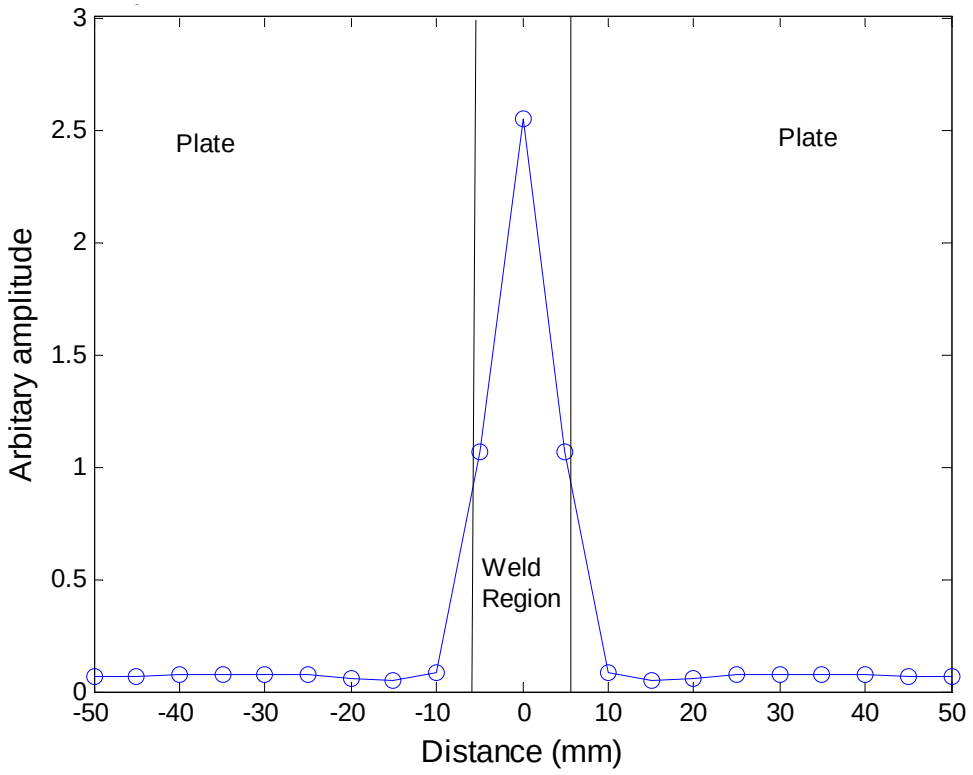

(b)

FIGURE 5.26: Amplitudes of weld guided S0, on line 'BB' shown in Figure 5.1 at frequencies (a) 200 kHz, (b) 400 kHz

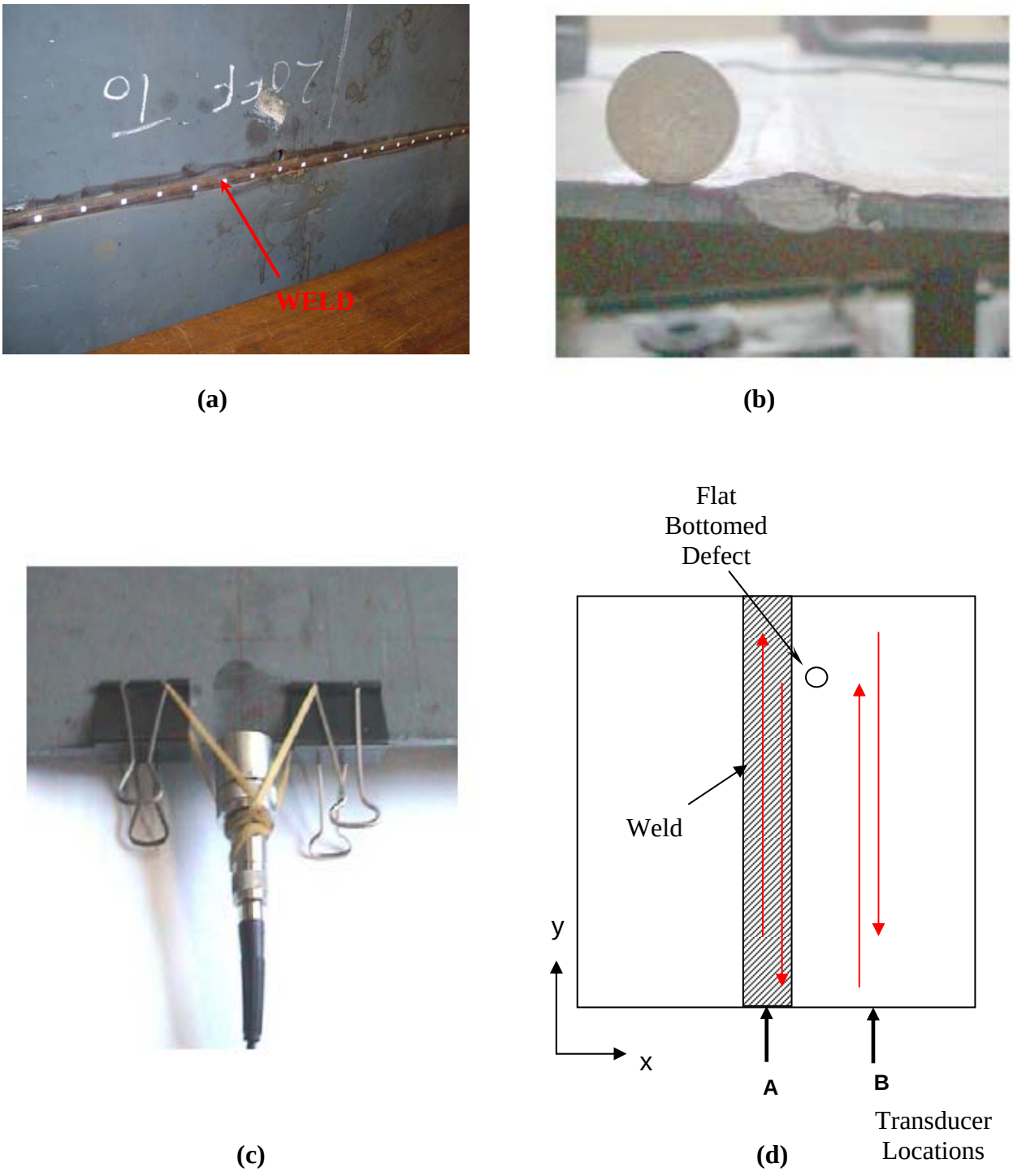

FIGURE 5.27. Experimental Setup, (a) Plate with a butt weld in the middle, (b) Edge of the plate with butt weld, (c) Transducer mounted on the edge of the plate, (d) Schematic diagram of the plate used for experiments [37].

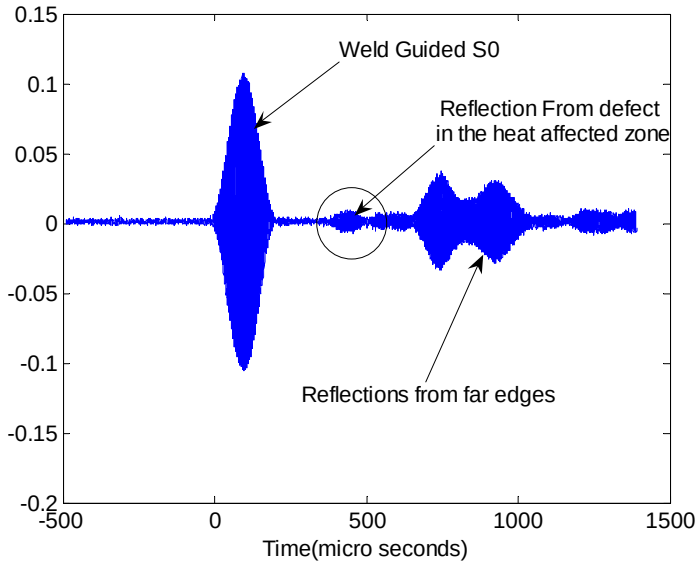

(a)

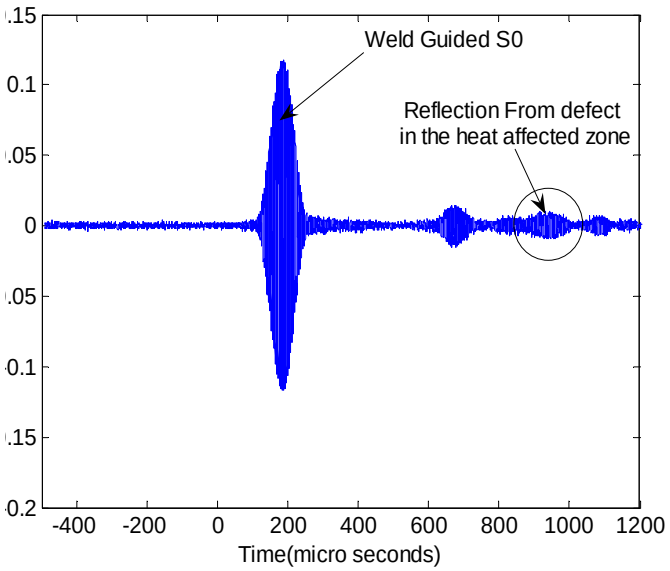

(b)

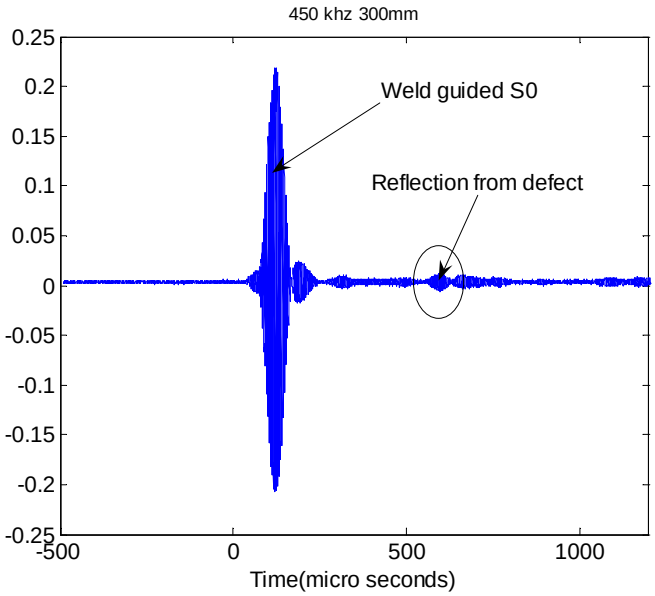

(c)

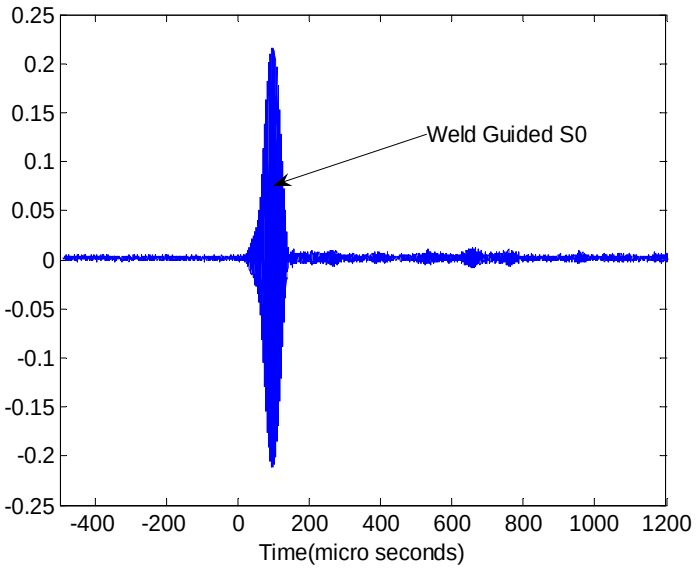

(d)

FIGURE 5.28: Typical monitored signals on line 'CC' at (a) a distance of 400 mm from source at the operating frequency of 225 kHz, (b) a distance of 350 mm and at 350 kHz (c) a distance of 300 mm and at 450 kHz (d) at 250 mm and 500 kHz

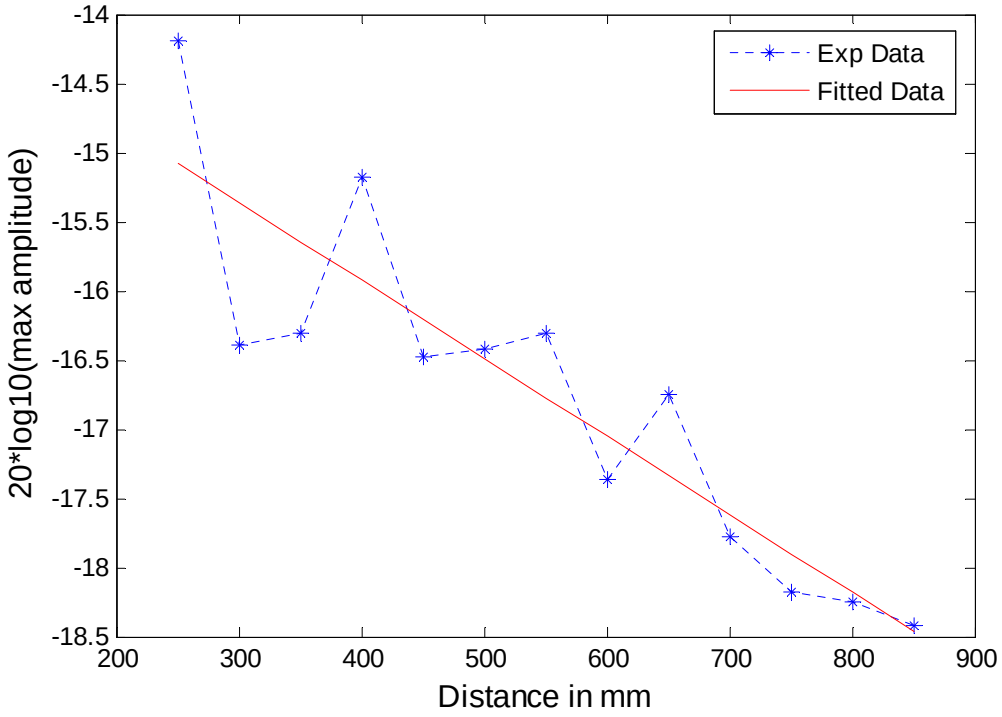

FIGURE 5.29: Log of maximum amplitudes of monitored signals at different distances from the source at 300 kHz (experimental signals)

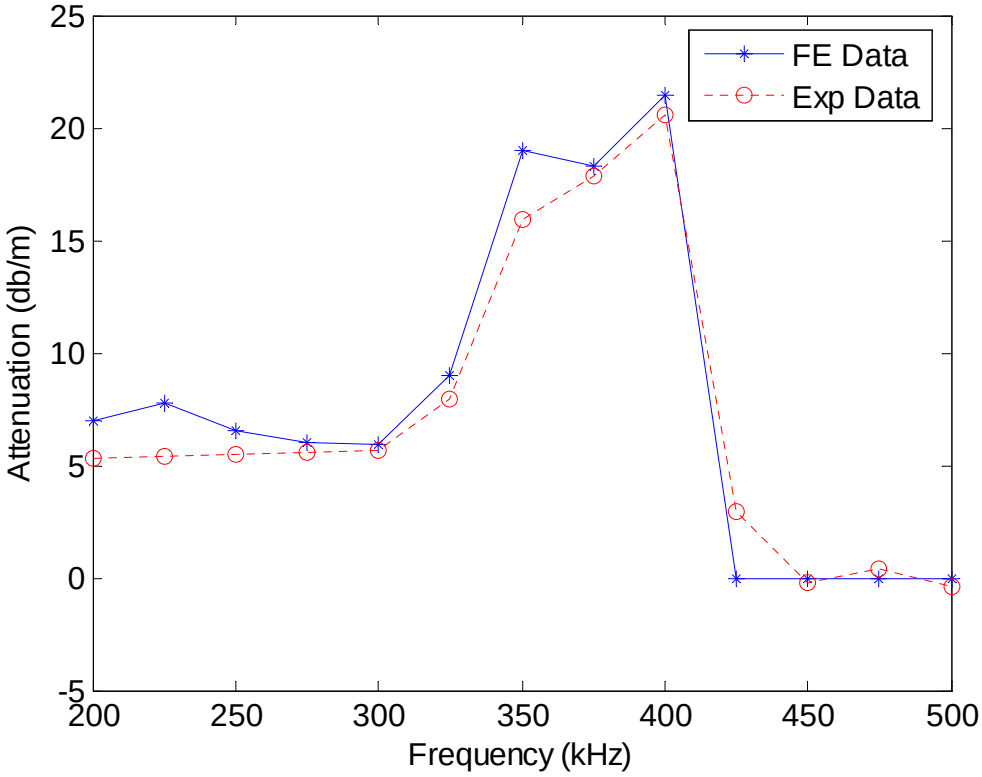

FIGURE 5.30: Attenuation of the trapped S0-like mode in real weld at different frequencies

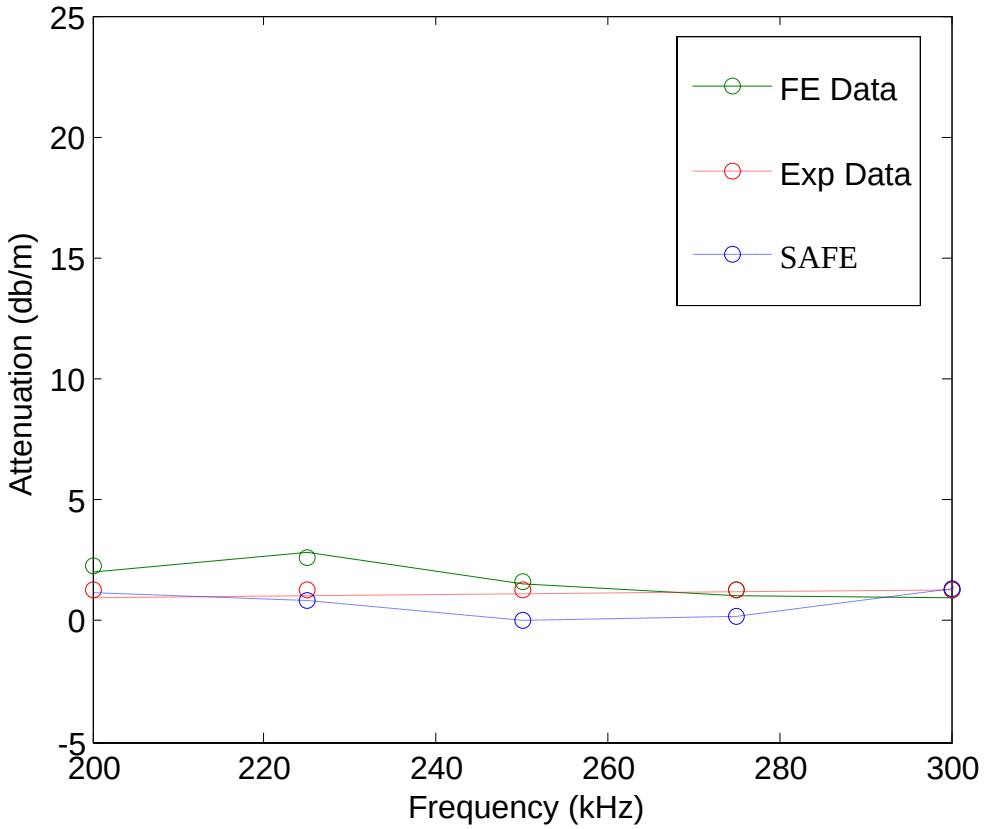

(a)

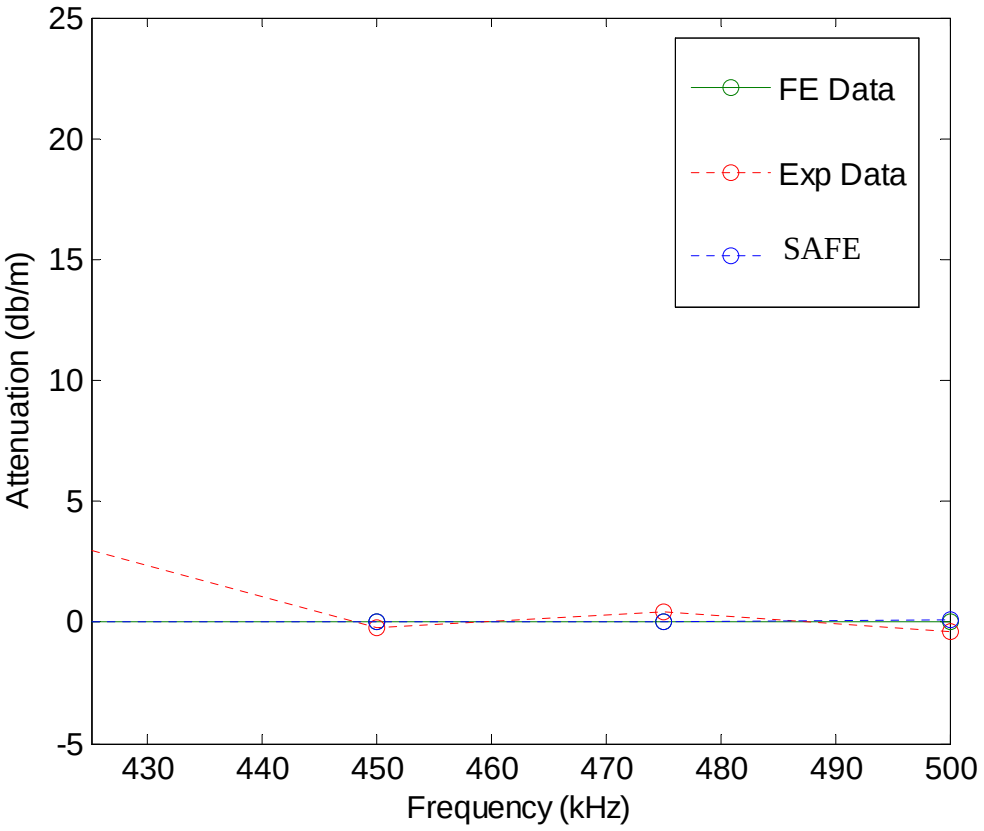

(b)

FIGURE 5.31: Comparison of FE, SAFE and Experimental attenuation values of the trapped S0-like mode in real weld. (a) Comparison at low frequencies, (b) Comparison at high frequencies

Chapter 6
Interaction of the trapped S0-like mode with defects in the weld and in the region near the weld

6.1 Introduction

Initial defect studies, explained in chapter 3, confirmed the sensitivity of the trapped S0-like mode to target defects. However the initial defect studies were mainly on very simplified geometries and the defects were highly simplified too. In real welds, defects are arbitrary in geometry, size, orientation and position. Therefore it is necessary to understand the interaction of the trapped S0-like mode with defects in real welds both qualitatively and quantitatively, in order to fully exploit the trapped S0-like mode for NDE of welds.

When the incident wave reaches the defect, it is reflected and mode converted, and these waves propagate back in the plate. This is called scattering. Scattering is a very wide topic and has been discussed by many authors [49, 104-111] and different models have been developed to understand the reflection and transmission of the guided waves when incident at defects. Strong interaction between the incident wave and the defect is important to find the location and sizing of the defect.

The SAFE, FE and experimental studies conducted on real welds, explained in chapter 5, revealed that the trapped S0-like mode has presence both in the weld and in the region near the weld. However these studies proved that the lateral extent of the trapped S0-like mode in the region near the weld depends upon the geometry of the weld and the wavelength of the trapped S0-like mode. The lateral extent decreases as the wavelength decreases (or as the frequency increases), with almost no lateral extent when the wavelength is less than the

width of the weld. Therefore one could argue that the trapped S0-like mode is sensitive to defects in the region near the weld, only at low frequencies where the trapped S0-like mode is present in the region near the weld.

The trapped S0-like mode in the weld behaves differently in different weld geometries. This can be observed in chapter 4, where the trapped S0-like mode is studied in idealised welds and chapter 5, where the trapped S0-like mode is studied in real welds. The study explained in chapter 5 show that the energy of the trapped S0-like mode becomes more and more concentrated in the centre of the weld with less and less energy near the surface as the frequency increases up to 250 kHz. This suggests that the sensitivity of the trapped S0-like mode to the small surface breaking cracks decreases and the sensitivity to defects in the centre of the weld increases as the frequency increases up to 250 kHz. At frequencies above 250 kHz, the energy starts dispersing towards the surfaces of the weld. Therefore, the frequencies above 250 kHz may only be used to inspect small surface breaking cracks as the trapped S0-like mode has energy concentrated near the surface of the weld.

In this chapter we explain the interaction of the trapped S0-like mode with different kinds of defects, over a range of possible test frequencies, both within the weld and the region near the weld (heat affected zones). Studies have been conducted on cracks, notches, and circular defects. Both part depth and through thickness defects have been studied.

6.2 Interaction of the trapped S0-like mode with defects in the region near the weld

6.2.1 Finite element study of Interaction of the trapped S0-like mode with cracks in the region near the weld

The study of the interaction of the guided wave with cracks is the initial step to understand the defect sensitivity of the guided wave being studied as the cracks are easier to model numerically and also to develop analytical models. Many researchers have studied the interaction of A0, S0 and SH0 [29, 45, 110, 112-117] waves with cracks and these results form the fundamentals to build any defect inspection system using these waves.

The study to understand the defect sensitivity of the trapped S0-like mode has also been started with cracks in this thesis. The interaction of the trapped S0-like mode with defects has been studied numerically using FE models in this chapter as the SAFE method is not capable of modelling discontinuities. Therefore near field effects and other problems explained in the previous chapters with smaller FE models (smaller in the size of the geometry) are unavoidable. Only time domain signals have been used to calculate reflection coefficients to avoid errors in the frequency domain calculations because of near field effects.

The finite element model used for defect study in this chapter is the same model used in chapter 5. The geometry of the weld is shown in Figure 6.1. The plate is 6 mm thick and the weld is 10 mm thick in the centre and 12 mm wide. The varying weld geometry has been modelled by a series of steps as shown in Figure

6.2. A quarter model of the whole system, with symmetric boundary conditions has been chosen to reduce the computational size of the problem. The model has been meshed in the same way explained in the previous chapters.

A through-thickness crack has been introduced in the region near the weld as shown in the Figure 6.1 and Figure 6.2. A crack is defined as a zero width defect and the crack has been modelled by disconnecting nodes. The crack modelled has one end touching the edge of the weld as shown in the Figure 6.1. Two models have been studied separately; one with a 25 mm long crack and one with a 50 mm long crack. Because of the symmetric nature of the model, two cracks one on each side of the weld are modelled.

The model was excited at point 'A', as shown in Figure 6.1, in the in-plane direction to generate the trapped S0-like mode in the weld. When the trapped S0-like mode strikes the crack, some part of the signal is reflected and the reflection from the crack was monitored at point B. A typical monitored signal can be seen in Figure 6.3, where we can clearly see the incident signal and the reflection from the 25 mm long crack. The other signals are due to the crack reflection reaching the edge of the plate and coming back to the monitored location. This has been confirmed by checking the group velocity of the trapped S0-like mode and the distance it travelled.

The amplitude reflection coefficient has been calculated by dividing the maximum amplitude of the reflected signal by the maximum amplitude of the

incident signal. In order to calculate the reflection coefficients over a range of frequencies, from low frequencies to high frequencies, the model has been excited with tone-bursts of different centre frequencies. Figure 6.4 shows the amplitude reflection coefficients for different crack lengths at different frequencies. The amplitude of the reflection from the crack has been compensated for the distance travelled and the attenuation values of the trapped S0-like mode, obtained from SAFE models explained in chapter 5 have been used to calculate the amount of distance compensation.

At an operating frequency of 100 kHz, the wavelength of the trapped S0-like mode is about 50 mm. Therefore, the ratio of crack length to wavelength of the trapped S0-like mode is about 0.5 for the 25 mm long crack and 1 for the 50 mm long crack; this ratio increases as the frequency increases. An increase in the reflection coefficient as the frequency increases would be expected because of the smaller wavelengths at high frequencies, but figure 6.4 shows a decreasing reflection coefficient as the frequency increases. This is mainly due to the decrease in the lateral extent of the trapped S0-like mode as the frequency increases, as explained in chapter 5. The decrease in lateral extent of the trapped S0-like mode can be seen from figures 5.7 to 5.20. A larger extent of the trapped S0 mode strikes the crack at low frequencies, which results in larger reflection coefficients. The extent of the trapped S0 mode that strikes the crack decreases as the frequency increases, resulting in decreased reflection coefficients with the increase in frequency.

Figure 6.4 shows some interesting characteristics of the trapped S0-like mode. At low frequencies, there is a substantial difference between the two reflection coefficients (Reflection coefficient from 25mm crack and reflection coefficient from 50 mm crack) but this difference decreases rapidly as the frequency increases. This is again due to the decrease in lateral extent of the trapped S0-like mode as the frequency increases.

At low frequencies, the trapped S0-like mode has a larger lateral extent and therefore a larger portion of the trapped S0-like mode strikes the 50 mm crack which results in larger reflections coefficients. At high frequencies, a relatively small extent of the trapped S0-like mode strikes the 50 mm crack and therefore results in smaller reflection coefficients at these frequencies even though the crack is bigger. The above results show that the trapped S0-like mode is more sensitive to target defects in the region near the weld, at low frequencies, which is as expected from the mode shape studies explained in chapter 5. The work has been extended to notches and this is explained in the next section.

6.2.2 Finite element study of the interaction of the trapped S0-like mode with notches.

Several researchers have studied the reflection characteristics of guided waves from notches in plates and pipes and the examination of the reflection coefficient as a function of the notch width has identified the important phenomenon of the interference between the reflections from the two sides of a notch [49, 106, 107, 110, 118]. The reflections from a step down (when the

thickness decreases) and step-up (when the thickness increases) have been studied in the past to understand the reflection from a notch [119].

In this thesis, notches with fixed axial extent (width) have been studied using FE simulations. To study the interaction of the trapped S0-like mode, at different frequencies, with notches in the heat affected zones, a through thickness notch of 25 mm length and 3 mm width has been introduced as shown in Figure 6.5. The notch has been modelled by removing elements. The model has been meshed and excited in the same way as explained above and the reflection from the notch has been monitored at point 'B'. The reflection coefficient has again been calculated by dividing the maximum amplitude of the reflected signal with the maximum amplitude of the incident signal.

Figure 6.6 shows the reflection coefficient from the notch for different frequencies and also compares the notch case with the crack case of the same length. The reflection coefficients from the crack differ from the reflection coefficients from a notch. However, both reflection coefficients show the same decreasing trend with frequency. The monitored reflected signal from the notch is composed of two reflected signals; one from the front end of the notch and the other from the back end of the notch, and these two signals overlap on each other and this is the reason for the difference in reflection coefficients for the crack case and notch case. The difference depends upon the notch width and the wavelength of the incident signal. A crack can be approximated to a zero width

notch and a more detailed discussion of the scattering from notches and cracks can be found in [119].

The above study on notches confirms that the trapped S0-like mode is more sensitive to target defects in the region near the weld at low frequencies and therefore the low frequency regime is the best option for inspecting defects in the region near the weld. The interaction of the trapped S0-like mode with circular defects needs to be understood in order to understand the sensitivity of the trapped S0-like mode to corrosion defects. Unfortunately, modelling three dimensional circular defects is not a trivial exercise. A very fine meshing is needed in order to accurately model the defect [111, 120] and this is almost impossible because of computational limitations. Therefore circular defects have only been studied experimentally and are explained in the next section.

6.2.3 Reflection coefficients from circular defects in the region near the weld, calculated from experimental measurements

A flat bottomed circular defect of 20 mm diameter and 3 mm deep (half of the plate thickness) has been drilled in the experimental plate as shown in Figure 6.7. This plate is the same plate used by Sargent [37] for experiments explained in chapter 3. The plate was excited in the same way as explained in chapter 5 and the reflections from the circular defect are monitored at point ‘B’ using a laser interferometer.

Figure 6.8 shows a typical monitored signal. The defect reflects both A0 and S0 as the defect is not symmetric with respect to the mid-plane of the plate. The reflected A0 can not be guided through the weld as it is faster in the weld than the plate. The reflected S0 mode from the defect is guided along the weld. The reflection coefficient has been defined as the ratio of maximum amplitude of the S0 reflection to the maximum amplitude of the incident trapped S0-like mode. The S0 reflection from the circular defect has been identified by checking the group velocity of the trapped S0-like mode and the distance travelled.

Figure 6.9 shows the reflection coefficients from the flat bottomed circular defect at different frequencies. The blue ‘o’ marks show experimental measurements and the blue solid line shows the fitted curve. The fitted curve has been obtained by taking a second degree polynomial that best fits the experimental data. The amplitudes of the reflected signals have been compensated for the distance travelled in the same way explained in the previous chapter and the red solid line show the decay compensated reflection coefficients. The reflection coefficients show a decreasing trend with the increase in frequency as the lateral extent of the trapped S0-like mode decreases as the frequency increases.

The above explained defect studies conducted on cracks, notches and circular defects in the region near the weld show a similar decreasing reflection coefficient trend as the frequency increase and therefore the low frequency regime is suggested for defect inspection in the region near the weld.

6.3 Interaction of the trapped S0 mode with defects in the weld

In this section, we mainly study the interaction of the trapped S0-like mode with defects in the weld. Both cracks and notches have been studied. FE results have also been compared with experimental measurements and finally the frequency regime suitable for inspecting defects in the welds is discussed.

6.3.1 Reflection coefficients from cracks in the weld

Cracks of different depths in the welds have been studied. A 20 percent deep crack is shown in Figure 6.10. A 20 percent deep crack has been defined as two cracks of 10 percent each on both sides of the weld as shown in figure 6.10 and a 40 percent deep crack is defined as two cracks of 20 percent each on both sides of the weld. Cracks on both sides of the weld have been used as it is not possible to model part depth cracks using the quarter models shown in Figure 6.2. The symmetric cracks are used to simplify the modelling even though it is not a realistic case. Cracks on both sides also avoid reflection of anti symmetric modes that complicate the monitored signal. The crack is 12 mm long, which is equal to the width of the weld. The crack has been modelled by disconnecting nodes.

The system has been excited in the same way as explained in previous sections at point ‘A’ in the in-plane direction. The reflection from the crack has been monitored at point ‘B’. A typical monitored signal for a 20 percent crack case can be seen in Figure 6.11. The reflection coefficient has been defined as the ratio of maximum amplitude of the reflected signal to the maximum amplitude of

the incident signal. The reflection coefficients for different crack depths have been plotted in Figure 6.12. The blue curves show reflection coefficients at different frequencies and the red curves show reflection coefficients with decay compensation for the distance travelled.

At low frequencies about 200 kHz there is not much difference between the reflection coefficients from a 20 percent deep crack and 40 percent deep crack when compared to the difference between the 40 percent deep crack and the through thickness crack. This is mainly due to the smaller amount of energy present in the weld cap region at these frequencies as explained in chapter 5. From Figure 5.13(a), we can clearly see that the energy is mainly concentrated in the centre of the weld with less energy in the weld cap. Therefore, a through thickness defect, that covers the centre portion of the weld cap, reflects a large amount of energy, resulting in a larger reflection coefficient.

The reflection coefficient for the through thickness crack increases for frequencies up to the S1 cut-off (300 kHz) because of the increase in crack length to wave length ratio. After the S1 cut-off the crack reflects both S0 and S1. These reflected S0 and S1 modes are both guided by the weld. The reflection coefficient decreases as the frequency increases after the S1 cut-off because of mode conversion into other higher order symmetric modes at these frequencies. The same kind of behaviour can be seen for the 20 percent and 40 percent cracks, where the reflection coefficient increases for frequencies up to the S1 cut-off.

We can see a huge difference in the reflection coefficient, for 20% and 40% cracks, between 200 kHz and 300 kHz. Here, the increase in reflection coefficient is mainly because of two reasons; one being the increase in crack length to wavelength ratio and the other being that the trapped S0-like mode starts behaving like a surface wave as the frequency increases, as explained in the previous chapter. As the energy is mainly present in the weld caps at high frequencies, more energy will be reflected from cracks in the welds at these frequencies and therefore the reflection coefficient from cracks in the weld cap increases. The next section explains the interaction of the trapped S0-like mode with notches in welds.

6.3.2 Reflection coefficients from notches in the weld.

Notches in the welds have also been studied using FE simulations and the results have been compared with experimental measurements. A schematic diagram of the notch in the weld is shown in Figure 6.13(a) and Figure 6.13(b) shows the notch in the experimental plate. The length of the notch is 12 mm, which is equal to the weld dimension and the width of the notch is 3 mm in the FE models. The width of the notch in the experimental case is about 3 mm but the notch is not uniform as we can see from the figure. Finite element simulations have been carried out in the same way explained in the previous section with excitation of the plate at point ‘A’ and monitoring the signal at point ‘B’.

A typical monitored signal from the FE model at the operating frequency of 300 kHz is shown in Figure 6.14(a). Figure 6.14(b) shows a typical measured signal from the experiments. Figure 6.15(a) shows reflection coefficients from the notch, calculated using the FE model, at different frequencies. The trend of the reflection coefficients is similar to the reflection coefficients from the crack case. The reflection coefficient increases with frequency up to 300 kHz (S1 cut-off) as the notch length to wave length ratio increases. At high frequencies the reflection coefficient decreases because of mode conversion into other higher order symmetric modes.

Figure 6.15(b) compares the FE reflection coefficients and the experimental reflection coefficients. Both curves show similar trend with frequency. The small variation in the values may be due to the irregular notch in the experimental plate. We can see a higher difference between the FE and experimental reflection coefficients at high frequencies because of the higher notch width to wavelength ratio at these frequencies.

The studies conducted on notches in the weld confirm that the trapped S0-like mode is more sensitive to target defects in the weld at frequencies around 300 kHz, which is just below the S1 cut-off.

6.4 Conclusions

The above defect studies suggest that low frequency inspection is suitable for inspection of defects both in the weld and in the heat affected zones, whereas higher frequency inspection is suitable for inspection of defects within the weld. The reflection coefficient from defects in the heat affected zones decreases as the frequency increases because of the decrease in the lateral extent of the trapped S0-like mode with increasing frequency.

The reflection coefficient from defects within the weld depends on the mode shape of the trapped S0-like mode at that particular operating frequency. Frequencies where a large amount of energy is concentrated near the surface of the weld are suitable for inspection of small surface breaking cracks. Frequencies where a large amount of energy is concentrated in the centre of the weld are suitable for inspection of large defects that cover the centre portion of the weld. The distance from the defect to the monitoring point matters a lot at frequencies where the trapped S0-like mode has high attenuation. Therefore a low attenuation and high defect sensitive frequency of operation should be chosen to build an effective inspection system using the trapped S0-like mode

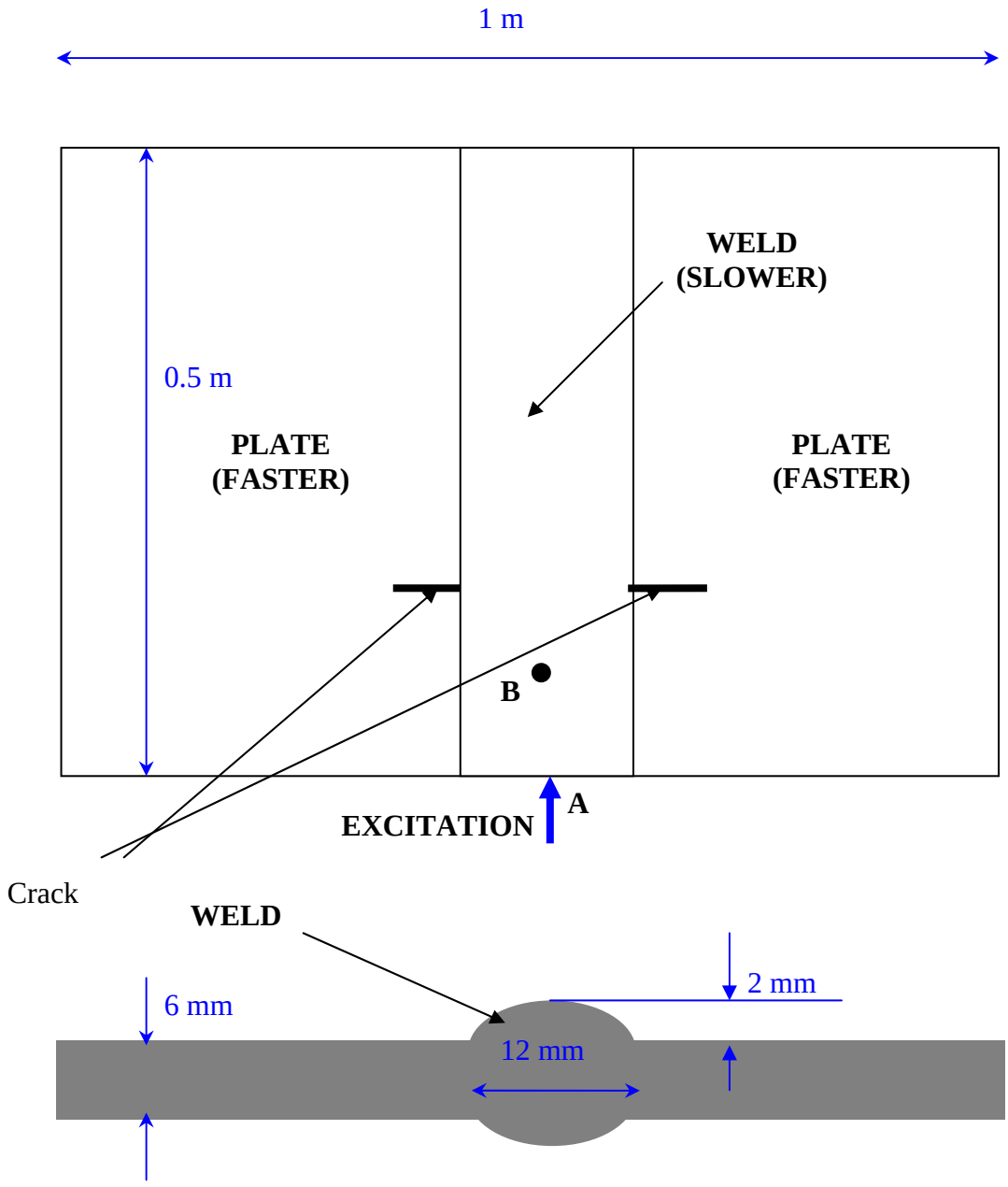

FIGURE 6.1: Geometry of real weld (not to scale)

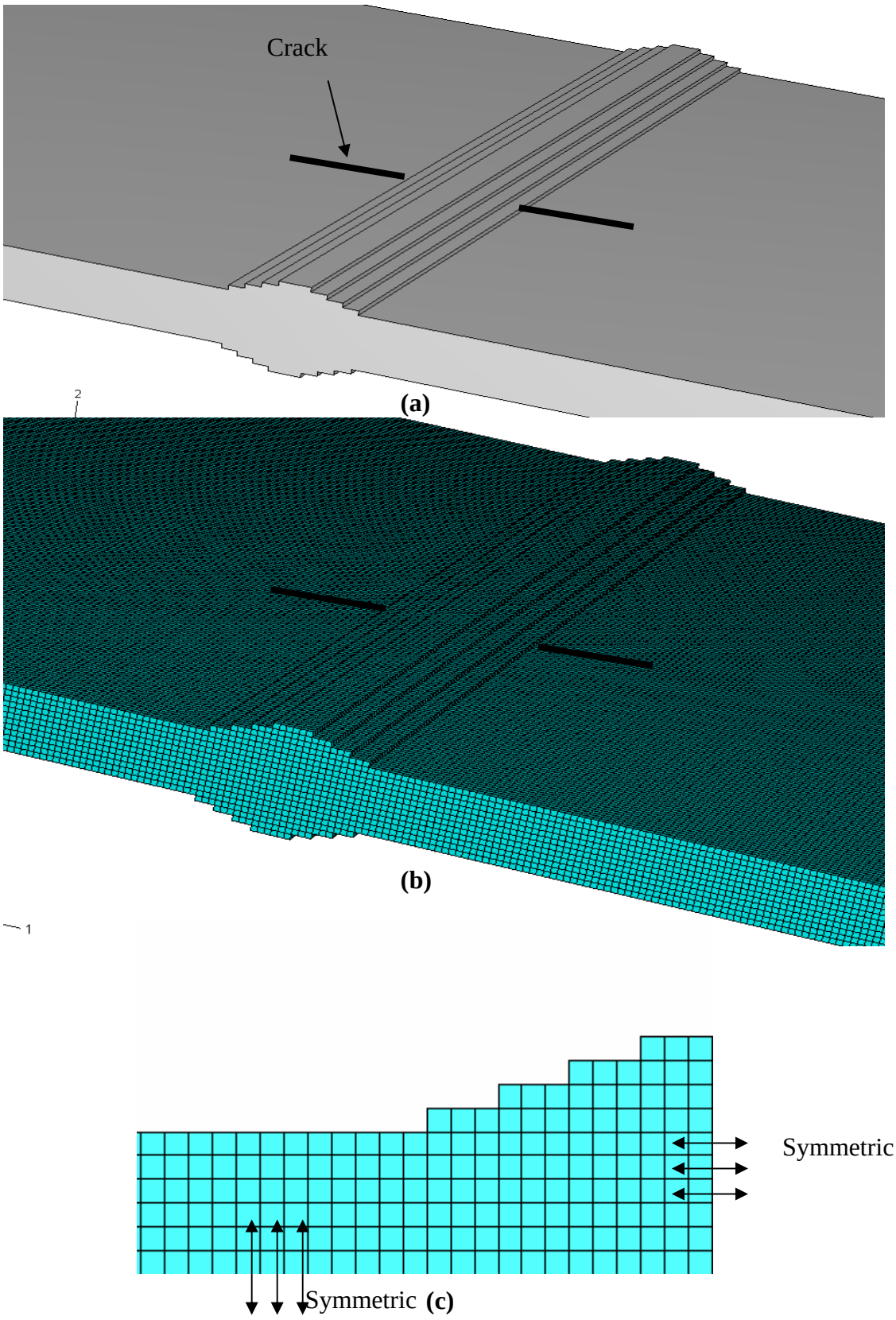

FIGURE 6.2: Finite element model of real weld with crack in the region near the weld, (a) Geometry used in FE model (b) 3D mesh, (c) Side view of the quarter model used

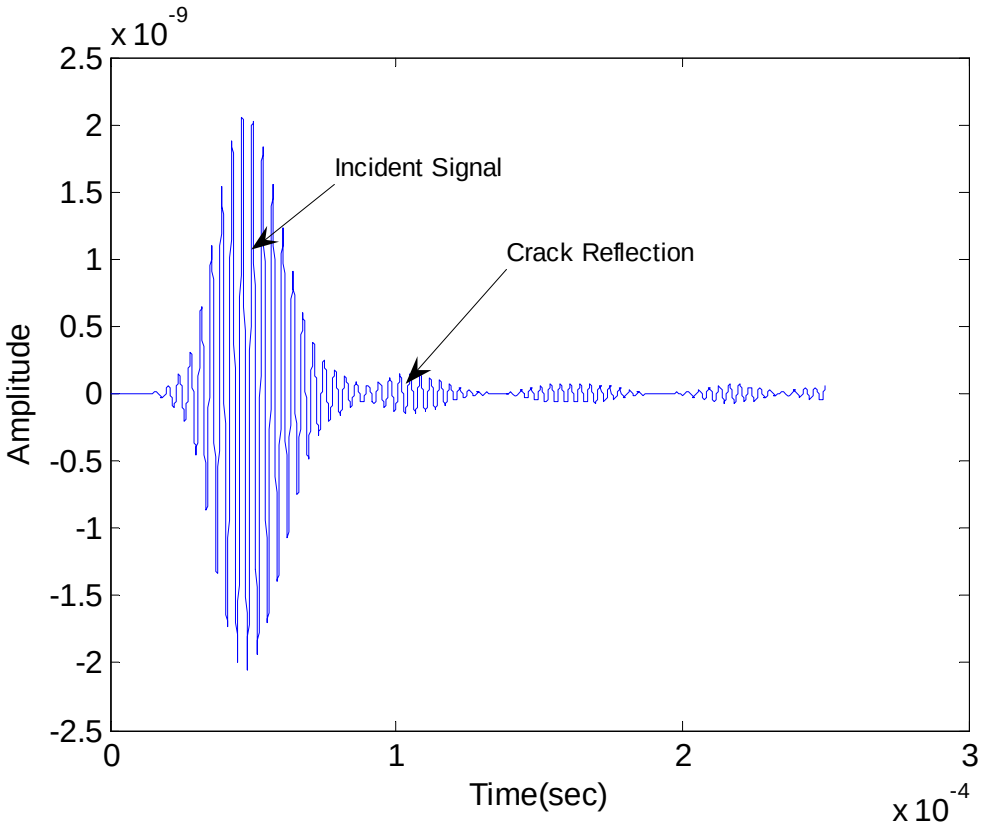

FIGURE 6.3: Typical monitored signal at point 'B' at the operating frequency of 200 kHz

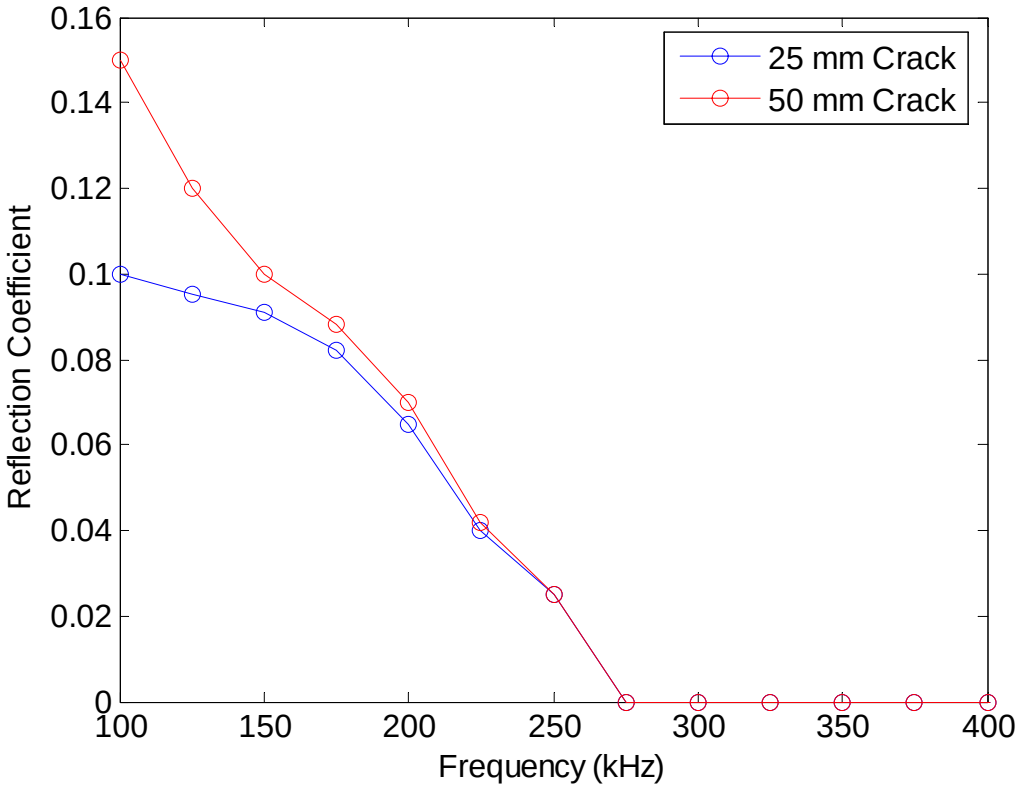

Figure 6.4: Amplitude reflection coefficients from a 25 mm through thickness crack and 50 mm through thickness crack

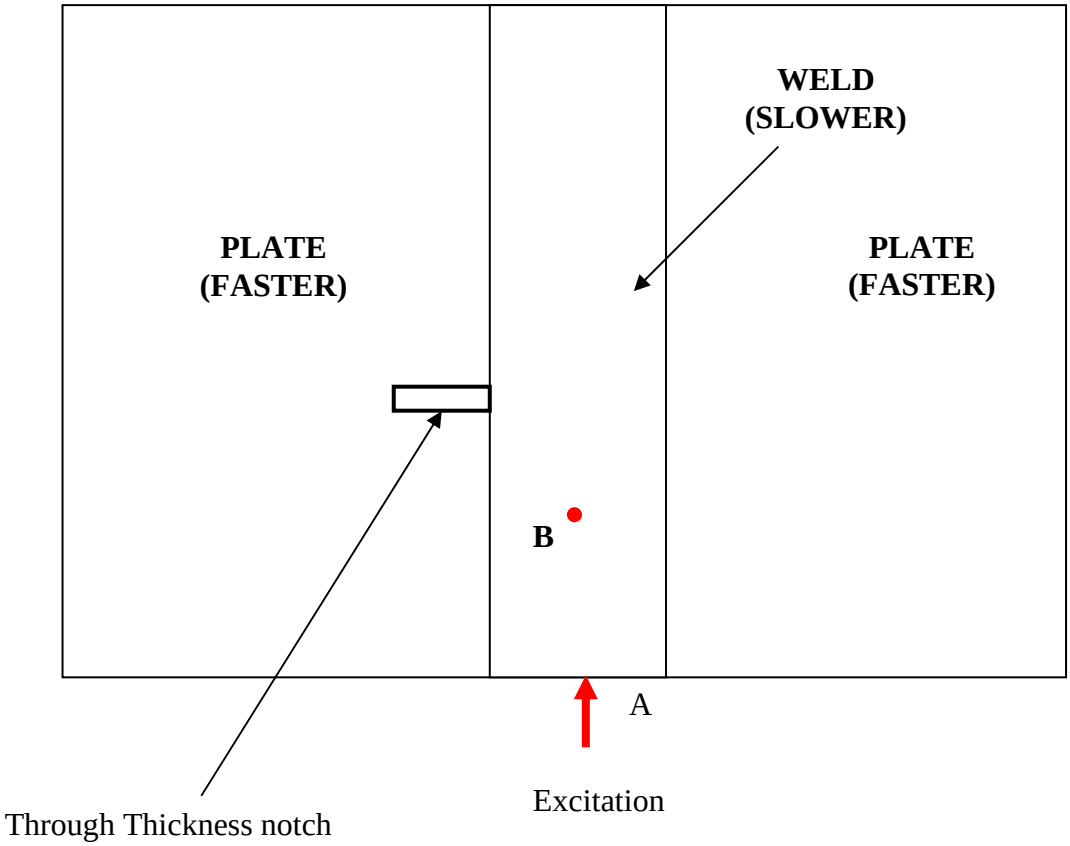

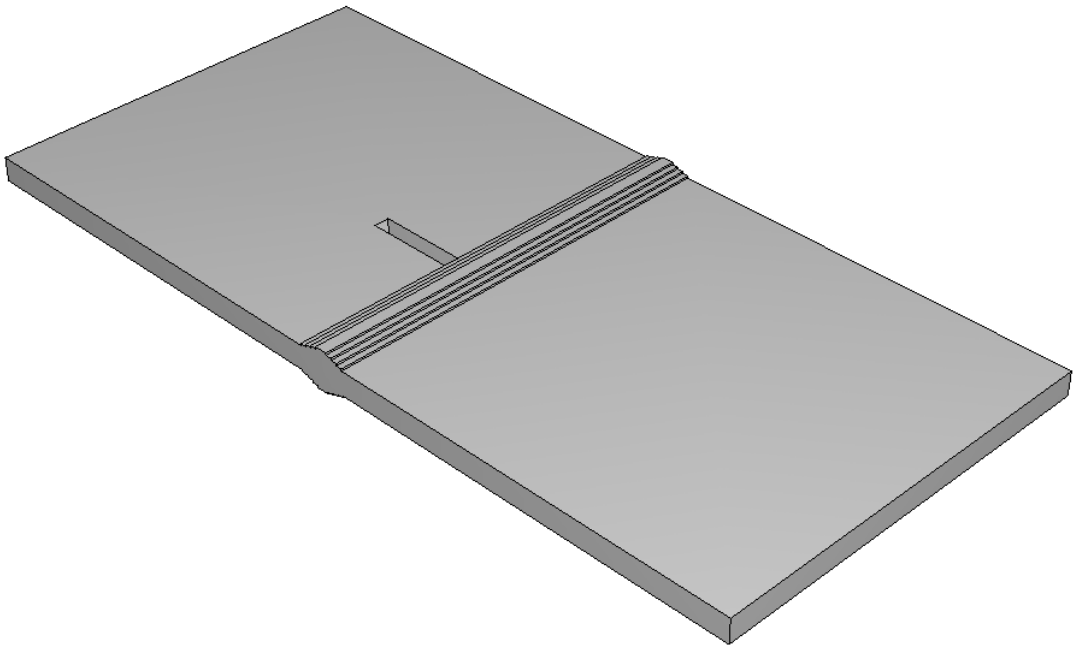

FIGURE 6.5: Finite element model used to study the interaction of weld guided S0 with notches in the heat affected zones.

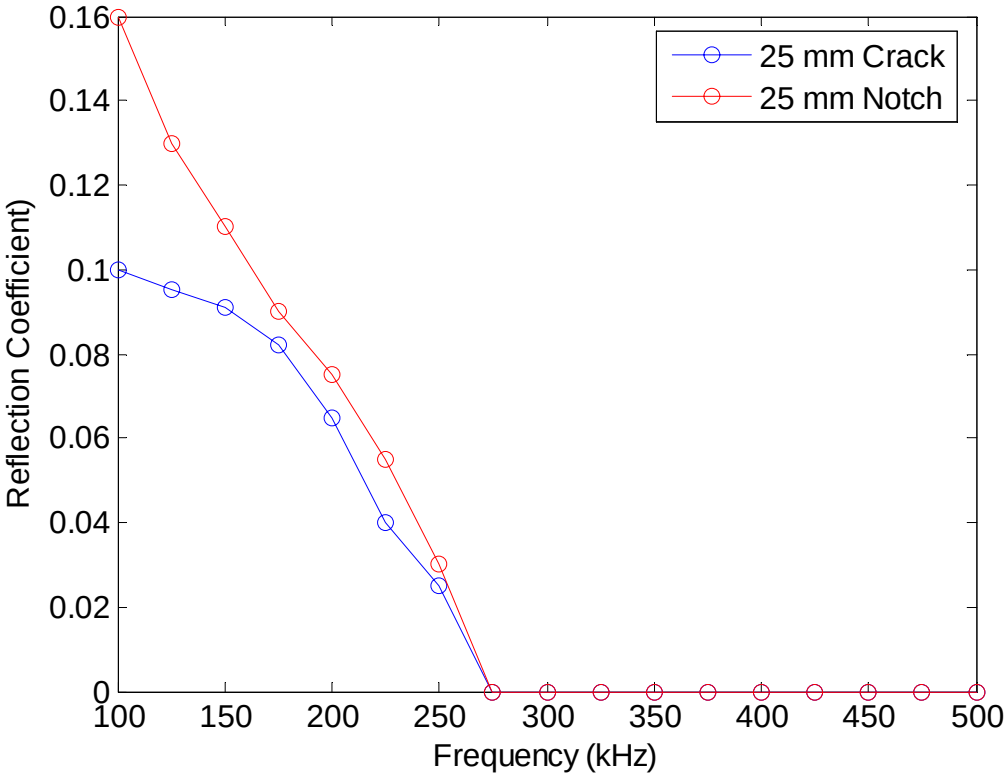

FIGURE 6.6: Comparison of reflection coefficients from a 25 mm crack and 25 mm notch

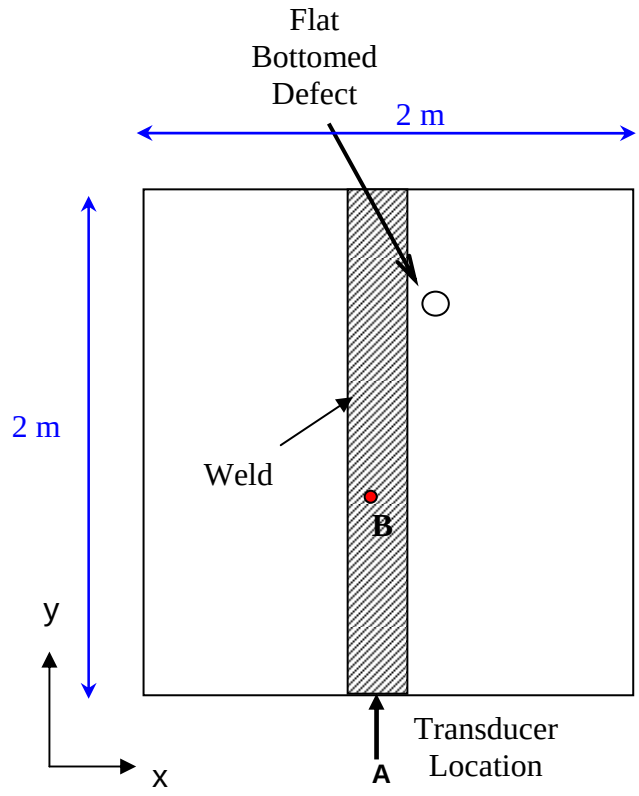

(a)

(b)

FIGURE 6.7: (a) Schematic diagram of the experimental setup, (b) A flat bottomed circular defect near the weld

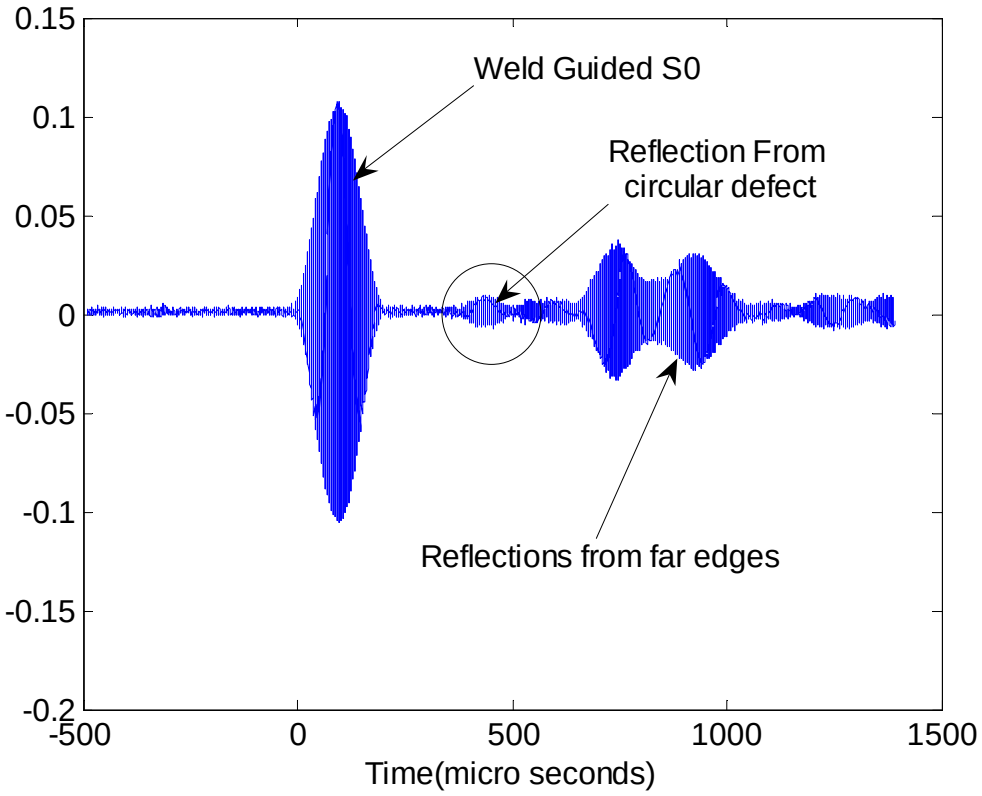

FIGURE 6.8: Typical monitored signal at a distance of 400 mm, at the operating frequency of 225 kHz

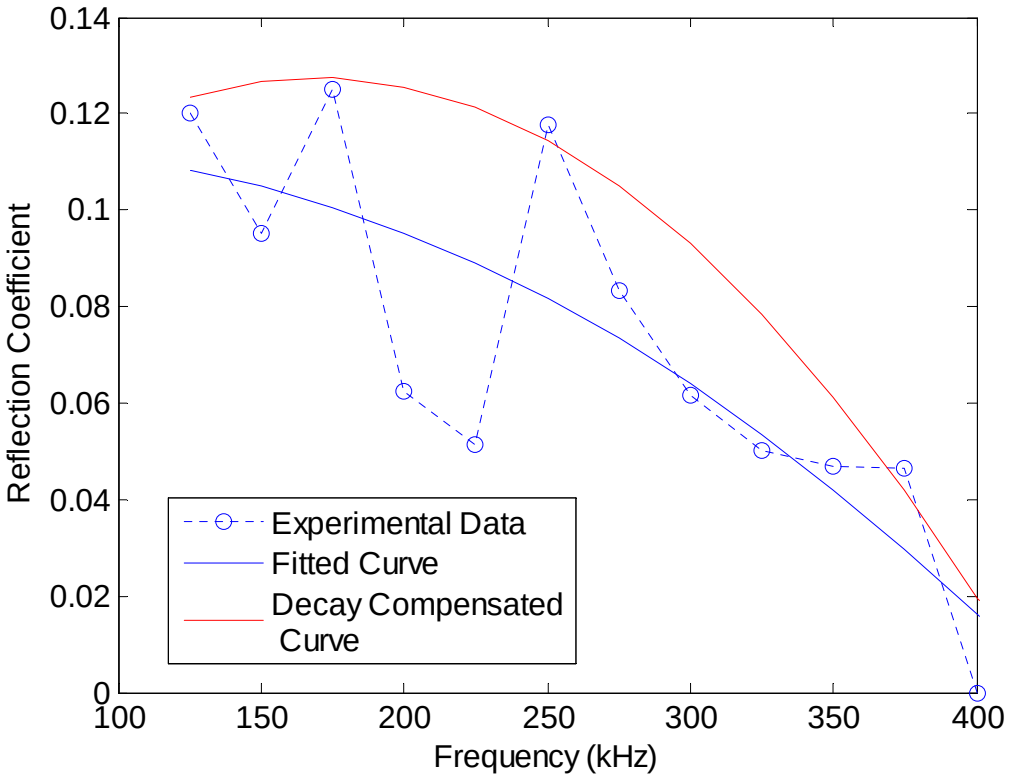

FIGURE 6.9: Reflection coefficient from a flat bottomed circular defect at different frequencies

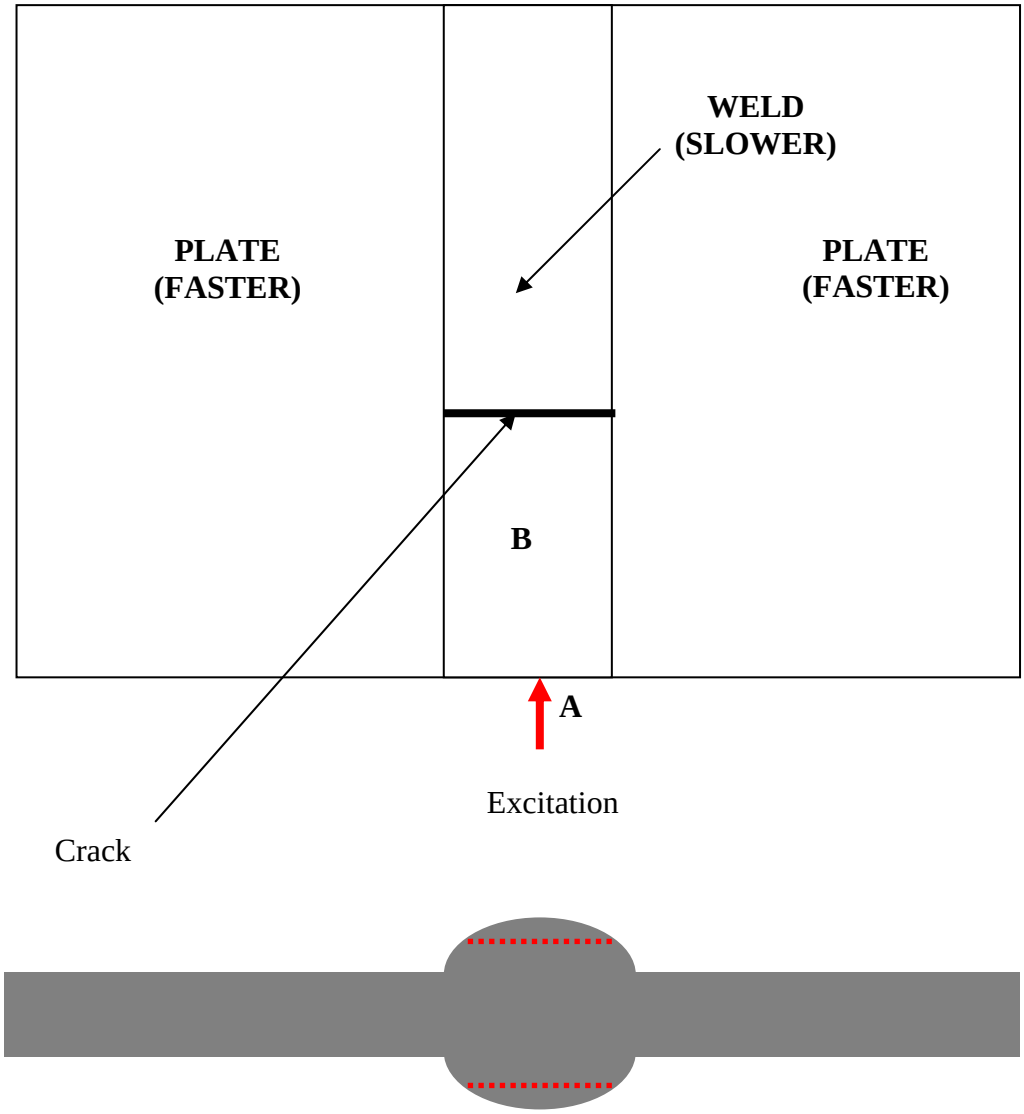

FIGURE 6.10: 20 percent deep crack in weld (not to scale)

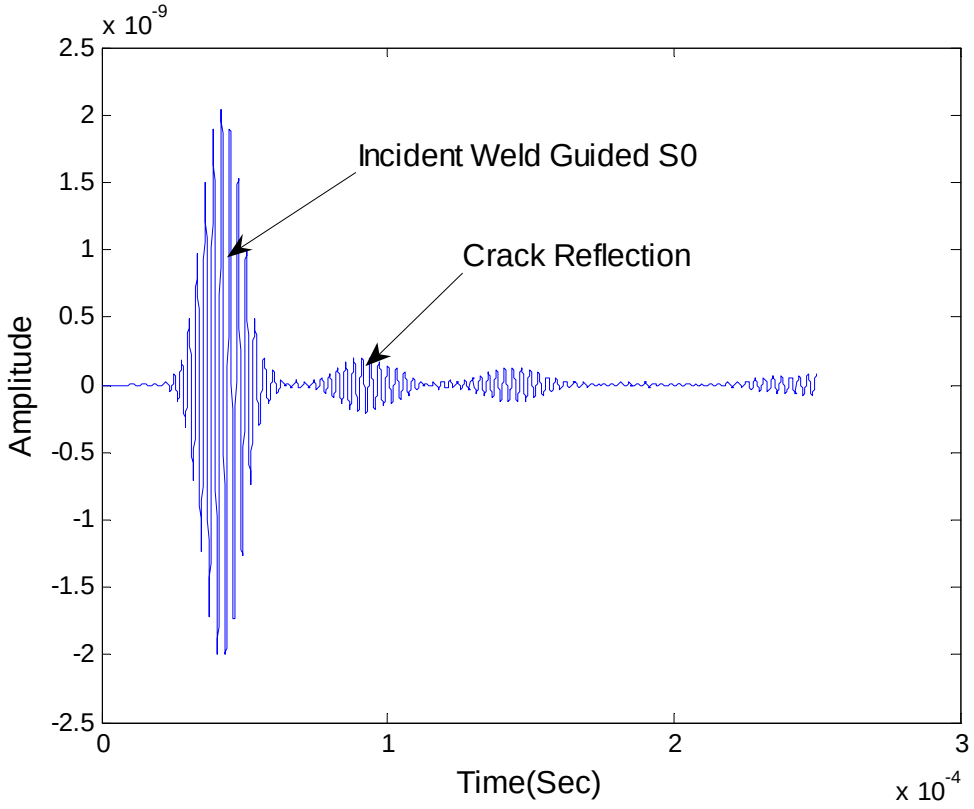

FIGURE 6.11: Typical monitored signal for the model shown in Figure 6.10, at a distance of 50 mm from the source, at the operating frequency of 350 kHz

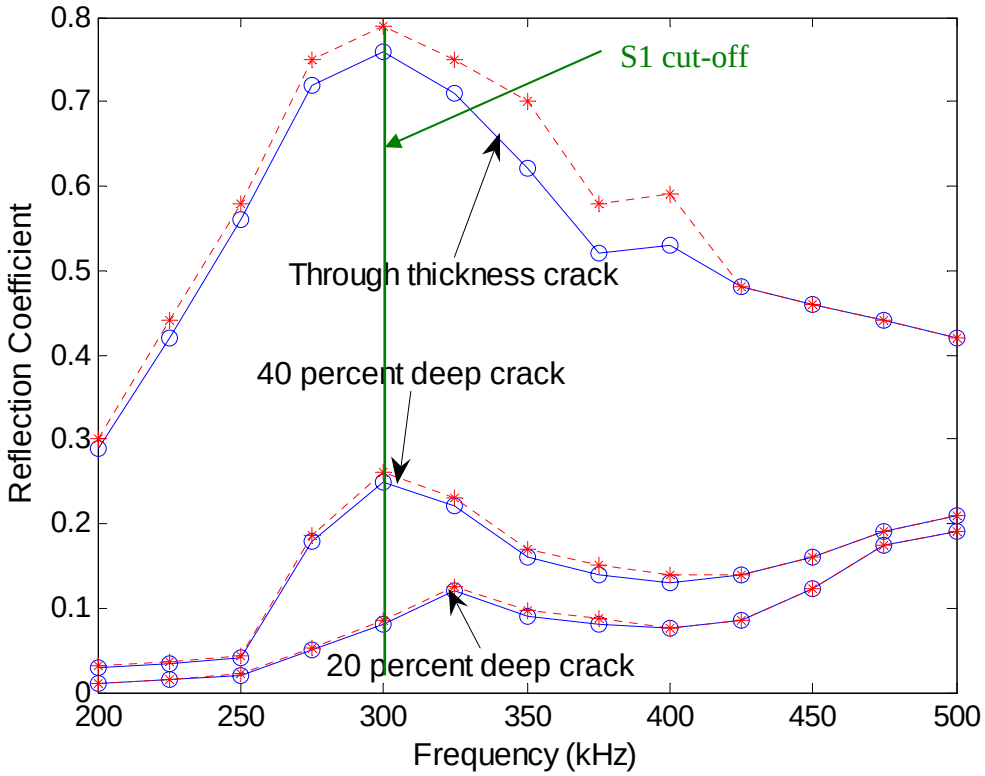

FIGURE 6.12: Reflection coefficients from cracks in the weld at different frequencies

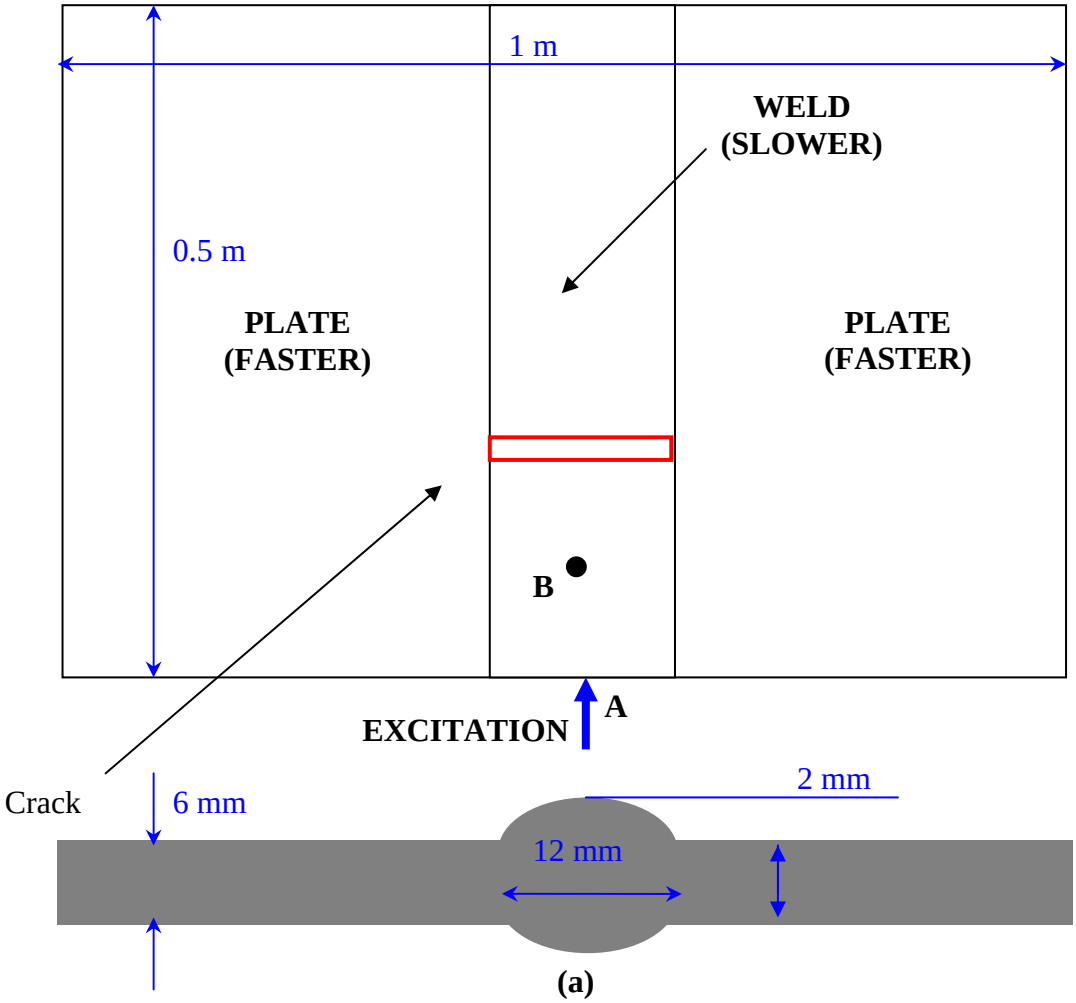

(a)

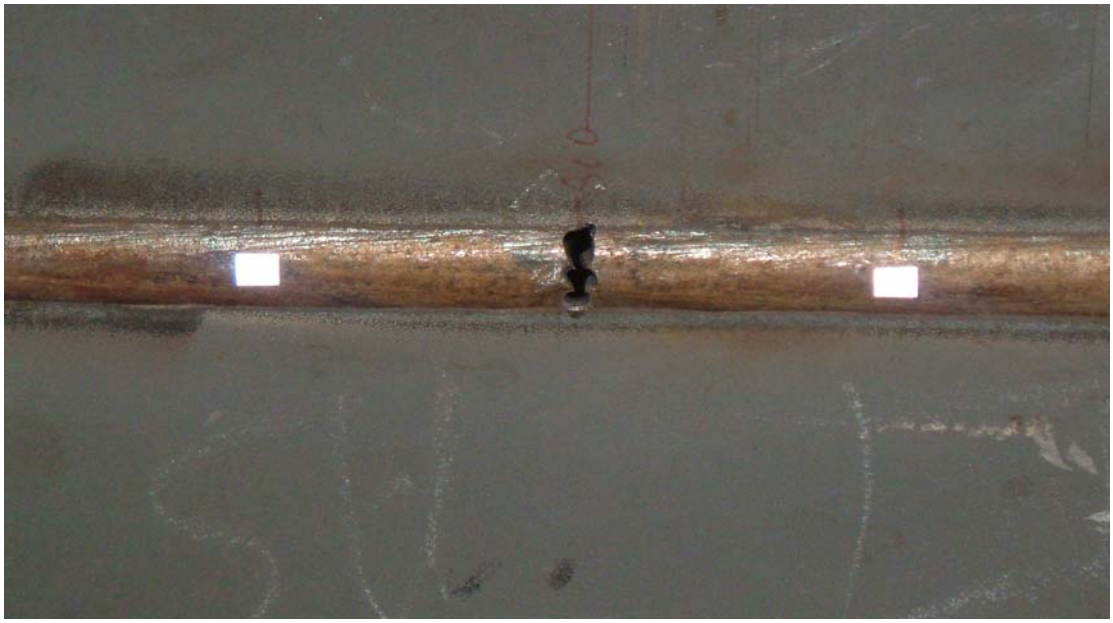

(b)

FIGURE 6.13: (a) schematic diagram of the model with a notch in the weld (b) Experimental plate with the notch in the weld

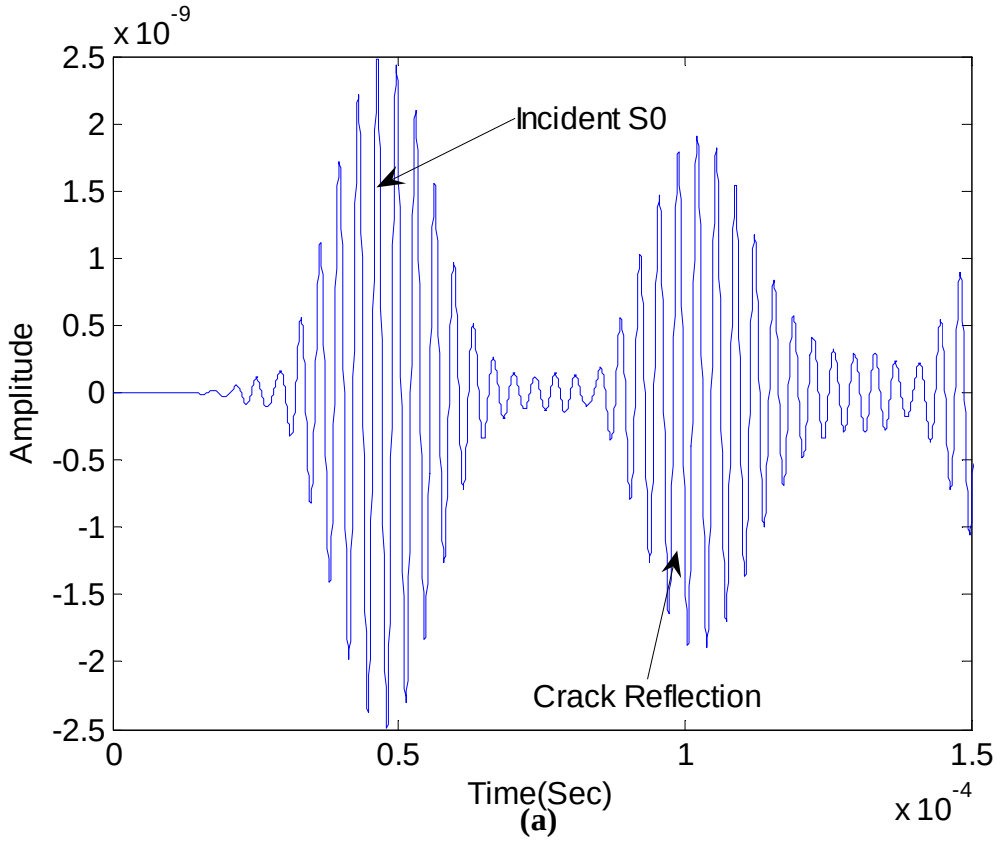

(a)

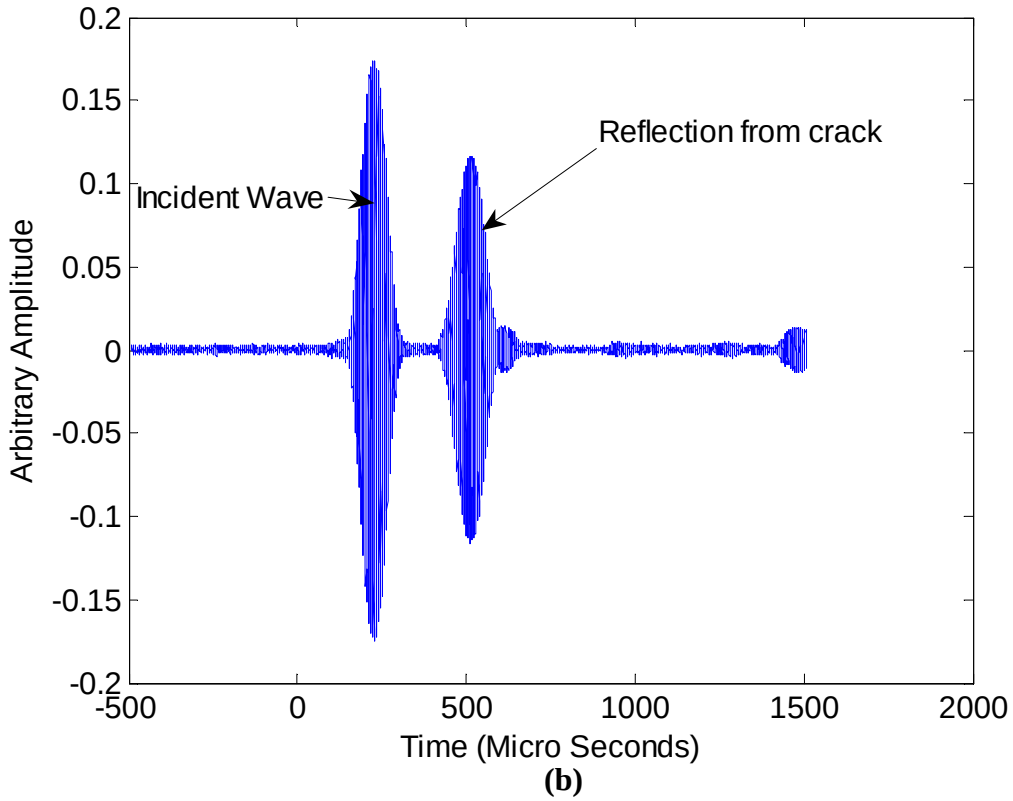

(b)

FIGURE 6.14: (a) Typical monitored signal, from FE model, at point B, 50 mm away from the source, at an operating frequency of 300 kHz
(b) Typical measured signal at an operating frequency of 300 kHz and 400 mm away from the source.

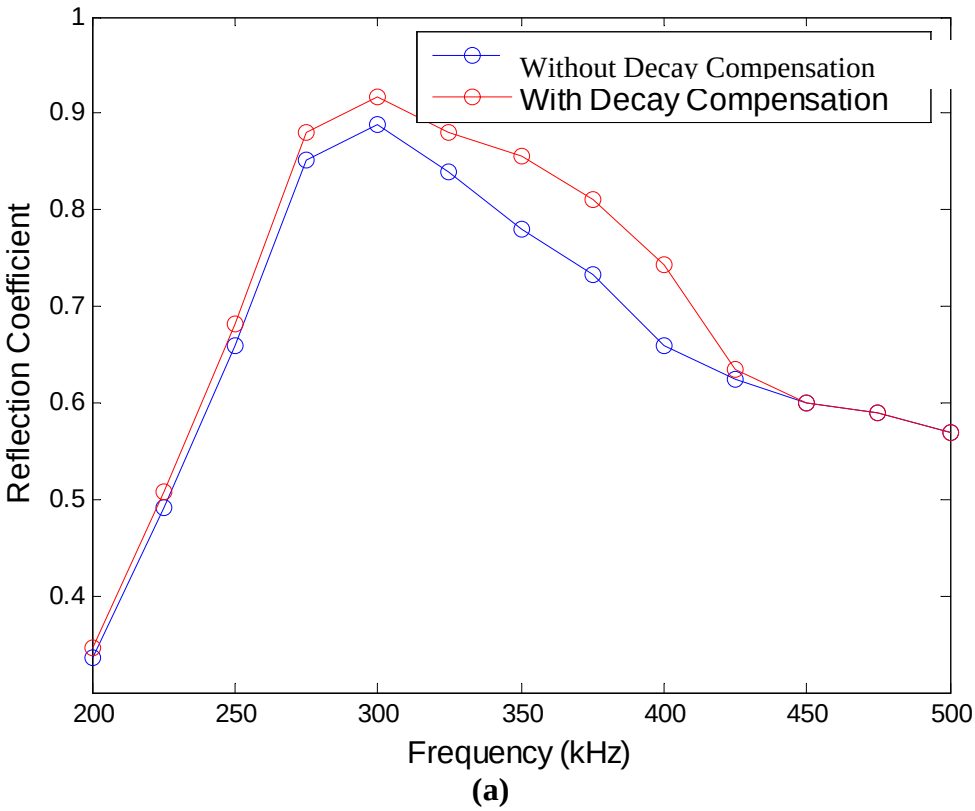

(a)

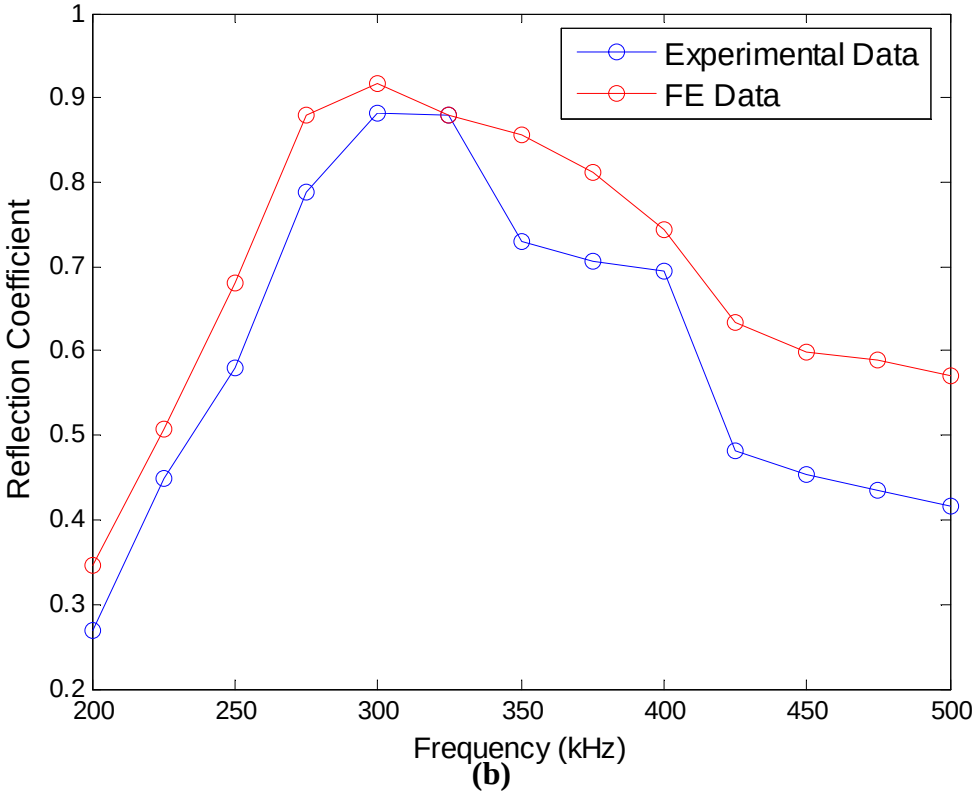

(b)

FIGURE 6.15: (a) Reflection coefficients from the notch in the weld calculated from the FE model, (b) Comparison of FE and Experimental reflection coefficients from the notch in the weld (Reflection coefficients have been compensated for the distance travelled.)

Chapter 7
Conclusions and Future Work

7.1 Conclusions

Experimental observations showed that a compression wave (similar to lamb wave S0) travelling along a weld between two plates is strongly guided by the weld and does not decay as quickly as it would in a plain plate. This phenomenon is attractive for NDE because it may offer the potential to inspect long lengths of welds from a single location. The aim of this thesis is to investigate the reasons for the strong guiding and lesser decay of the S0 mode along the weld between two plates, to discuss the nature of the guiding effect, illustrate the effects and propose its potential for practical NDE of long lengths of welds.

Studies have been conducted on a variety of structures to understand the phenomenon. Numerical, Finite Element and Semi Analytical Finite Element, and Experimental studies revealed the physics behind the phenomenon. Strong guiding and less decay of the S0 mode in the weld between two plates is caused by the geometry of the weld. The S0 mode in the weld is slower than that in the surrounding plates. The S0 mode is trapped in the weld as it is embedded between two faster media, which is analogous to optical waveguides. Studies have been conducted on structures where a slower medium is embedded in a faster medium and from these studies it is understood that a trapped mode is generated in a medium when it is embedded in a faster medium. It is also understood that this trapped mode decays less than S0 mode in a plain plate because of its one dimensional propagation, and can potentially be used to inspect long lengths of slower medium from a single location. This mode is called ‘trapped S0-like’ mode or ‘trapped S0’ mode throughout this thesis as this mode has mode shapes similar to S0 mode in a plain plate.

When a slower medium is embedded in a faster medium, the trapped S0-like mode generated in the slower medium decays as it leaks bulk longitudinal and shear waves in to the surrounding faster medium. The amount of leakage depends upon the impedance difference between the slower medium and its surrounding medium. At frequencies where the phase velocity of the trapped S0-like mode is greater than the bulk longitudinal wave velocity, the trapped S0-like mode leaks both longitudinal and shear waves in to the surrounding plates. At frequencies, where the trapped S0-like mode is slower than bulk longitudinal waves and faster than shear waves, the trapped S0-like mode can only leak shear waves in to the surrounding faster medium. Below the bulk shear wave velocity the trapped S0-like mode cannot leak bulk waves and shows no decay because of leakage. The attenuation of the trapped S0-like mode in the slower medium increases as the impedance difference between the slower medium and the surrounding faster medium decreases.

The trapping of the S0 mode in the slower medium can be achieved by two ways, one being a variation in the material properties between the weld and surrounding plates and the other being variation in geometry between the weld and the surrounding plates. In real welds, the trapping of S0 is caused by the variation in the geometry of the weld and the plates. The thicker weld makes the trapped S0 slower even though there is no significant material property variation between the weld and the plate. The trapped S0 mode in realistic welds attenuated by leakage of the SH0 mode into the surrounding plates. At frequencies where the trapped S0 mode is slower than the SH0 mode in the plate,

the trapped S0 mode cannot leak SH0 mode into the surrounding plates and hence shows no attenuation.

Studies conducted on weld models with idealised weld caps revealed that the geometry of the plate-weld interface also plays a major role in the attenuation of the trapped S0 mode. The energy from the weld can only leak into the surrounding plates from the centre of the weld. At frequencies where the energy is more centre concentrated, more energy can leak into the plates, resulting in high attenuation. At high frequencies where the trapped S0 mode behaves like a surface wave, the energy is more concentrated near the surface of the weld cap and it leaks less energy into the surrounding plates, resulting in low attenuation.

Studies conducted on FE and SAFE models revealed that the trapped S0-like mode is also present in the region near the weld. Therefore it is also possible to detect defects in the region near the weld using the trapped S0-like mode. The amplitude decreases exponentially as the distance from the weld increases. The trapped S0-like mode has a substantial lateral extent at low frequencies and this lateral extent decreases as the frequency increases. At high frequencies, where the wavelength of the trapped S0-like mode is less than the width of the weld, the trapped S0-like mode is contained entirely in within the weld. At high frequencies the trapped S0-like mode behaves like a surface wave with energy mainly concentrated near the surface of the weld cap. Therefore the low frequency regime is suitable for inspecting both the weld and the region near the weld, whereas the high frequency regime is suitable for detecting small surface breaking cracks in the weld.

The sensitivity of the trapped S0-like mode to defects in the region near the weld decreases as the frequency increases because of the decrease in the lateral extent of the trapped S0-like mode with frequency increase. The sensitivity of the trapped S0-like mode to defects in the weld increases as the frequency increases for frequencies up to the S1 cut-off in the weld because of the increase in crack length to wave length ratio. The sensitivity decreases as the frequency increases after the S1 cut-off because of the mode conversion into other higher order symmetric modes at these frequencies.

In conclusion the low frequency regime is suggested for inspecting the region near the weld. At low frequencies, the attenuation of the trapped S0-like mode is also very low and hence one will be able to inspect long lengths of welds from a single location. The high frequency regime where the trapped S0-like mode behaves like a surface wave is suitable for detecting small surface breaking cracks. The sensitivity of the trapped S0-like mode to defects in the weld increases for frequencies up to S1 cut-off and decreases above that. Therefore the frequency regime below S1 cut-off is suggested for potential inspection.

7.2 Future Work

The discovery of trapped modes started a new area of research in the field of guided ultrasonic waves. This thesis presented the discovery of trapped S0-like mode and how it can be exploited to inspect long lengths of welds. The trapped S0-like mode can also potentially be applied to inspect many other geometries where a slower medium is embedded in a faster medium; e.g. adhesive joints and T-joints. It would also be very interesting to see how the trapped modes behaves in a structure that is not symmetric, e.g. lap joint, where the trapped mode generated in the weld can leak both symmetric and anti-symmetric modes into the surrounding plates and this study is necessary to exploit the trapping phenomenon for inspecting structures that are not symmetric.

The trapped S0-like mode can also potentially be used to inspect stiffeners, e.g. stiffeners in an aircraft fuselage, from a single location. It would also be very interesting to see how the higher order modes can be trapped in the slower medium and if they could be used to exploit for NDE.

Appendix A
Use of Shell elements for modelling of the A0 mode at low frequencies in large 3D geometries

A 4 noded doubly curved general purpose shell element with finite membrane strains which uses Mindlin plate theory [121-124] has been investigated, for modelling A0 at low frequencies, in order to reduce the computational size of the 3D geometry. Studies have been carried out on a steel plate. A steel plate has been modelled using both shell elements and solid elements separately and the results obtained are compared to validate shell model with solid model.

Figure A.1 (a) shows a steel plate modelled with shell elements and Figure A.1 (b) shows a steel plate, having same dimensions of the model shown in figure A.1 (a), modelled with solid elements. The solid model has 8 elements through its thickness. Symmetric boundary conditions have been applied on edges A on both plates as shown in the Figure A.1. Both plates have been excited on edges B using a five cycle tone burst with a centre frequency of 20 kHz-mm and the output has been monitored at point C, at a distance of 100 mm from excitation.

The monitored signals have been compared as shown in figure A.2(a). A zoomed version of figure A.2(a) is shown in figure A.2(b). From figure A.2(b), it is clear that shell model is giving results with 0.25% error in amplitude and 0.5% error in velocity which shows that shell elements can be used to model A0 at low frequencies. At 20 kHz-mm, the A0 mode has nearly zero in-plane displacement and constant out-of-plane displacement through thickness. However, the in-plane displacement increases as the frequency increases and the out-of-plane displacement varies through thickness. Therefore it is necessary to study the

frequency range of accuracy of shell model as the shell element doesn't support amplitude variation through thickness.

To understand the frequency range of accuracy of the shell model, the phase velocity dispersion curve of the A0 mode for a 1 mm steel plate shown in figure A.1(a), using the Amplitude Spectrum method [125], has been obtained. The phase velocity curve obtained from shell model has been compared with the phase velocity dispersion curve of the A0 mode for a 1 mm steel plate from DISPERSE as shown in figure A.3. From Figure A.3, it is clear that both curves converge at very low frequencies (below 30 kHz) with 95-99% accuracy. The frequency region in which the shell elements give comparable results with solid elements has been shown in figure A.3. Therefore shell elements are suitable for modelling the A0 mode at frequencies below 30 kHz-mm.

Mesh convergence study has also been conducted to know how many number of shell elements per wavelength, have to be used to obtain accurate results. A 1mm thick steel plate has been modelled as shown in figure A.1(a) with different numbers of elements per wavelength ranging from 5 to 50. The results of the shell elements have been compared with the model that is meshed with solid elements. The solid model has 10 elements per wave length. Figure A.4 shows percentage error, compared to solid model, in amplitude for different number of elements per wavelength. From figure A.4, we can say that shell models with 10 to 15 elements per wavelength give results with 5% to 3% error. So, more than

15 elements per wavelength gives results that are comparable to models with solid elements.

In conclusion, we can say that the shell elements can only be used to model the A0 mode at low frequencies, where the in-plane displacement is almost zero and the out-of-plane displacement is constant through thickness. Shell elements can not be used to model modes at frequencies where the displacements vary through thickness.

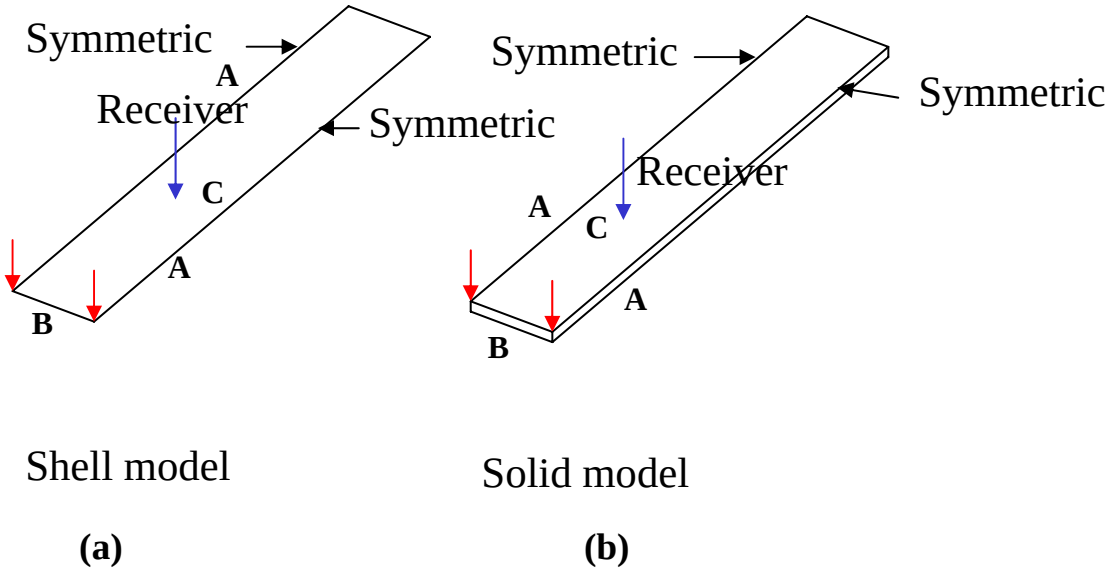

FIGURE A.1: Modelling domains used for validation of Shell elements for modelling A0 wave propagation in 3D plate structures, (a) Shell model, (b) Solid model

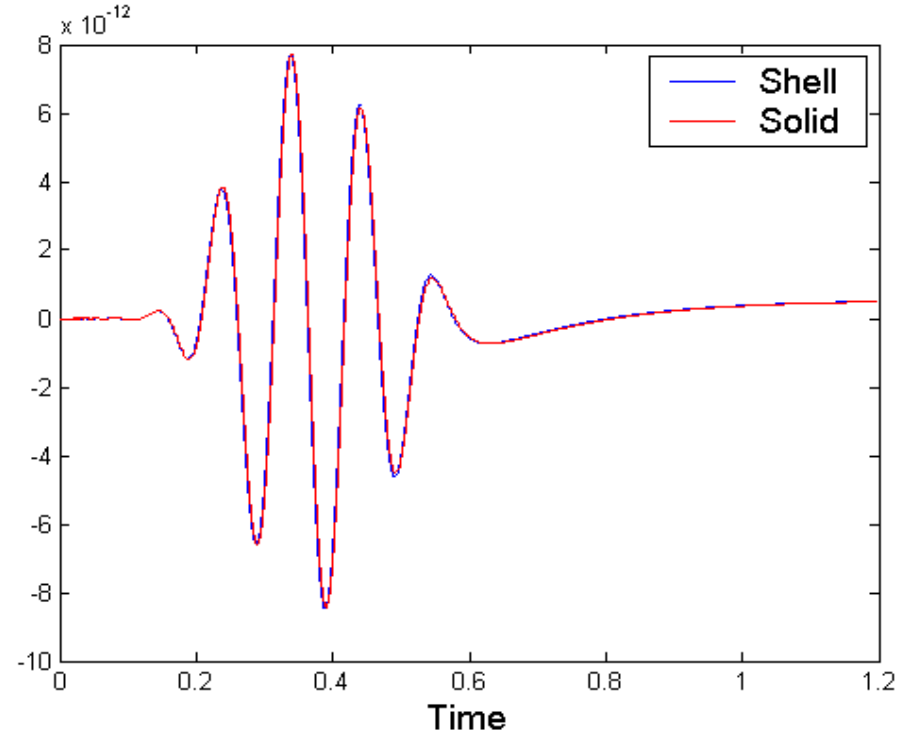

(a)

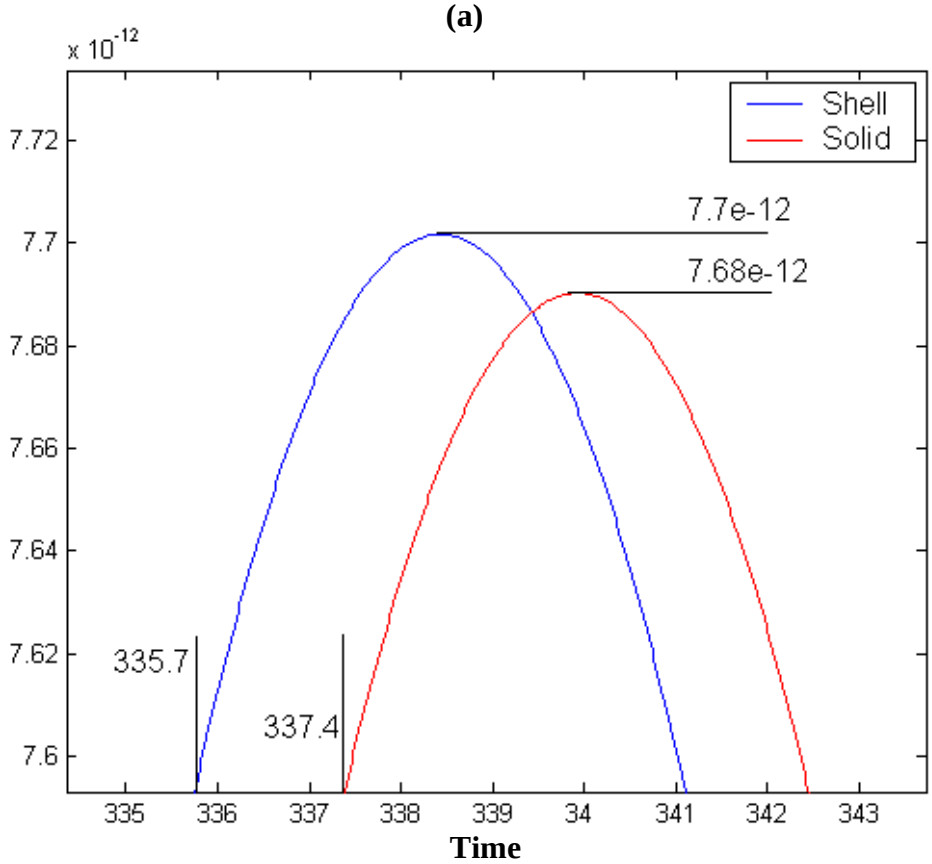

(b)

FIGURE A.2: (a) Predicted Signals for Shell and Solid models at a distance of 100 mm from source, (b) zoomed version of figure A.2 (a)

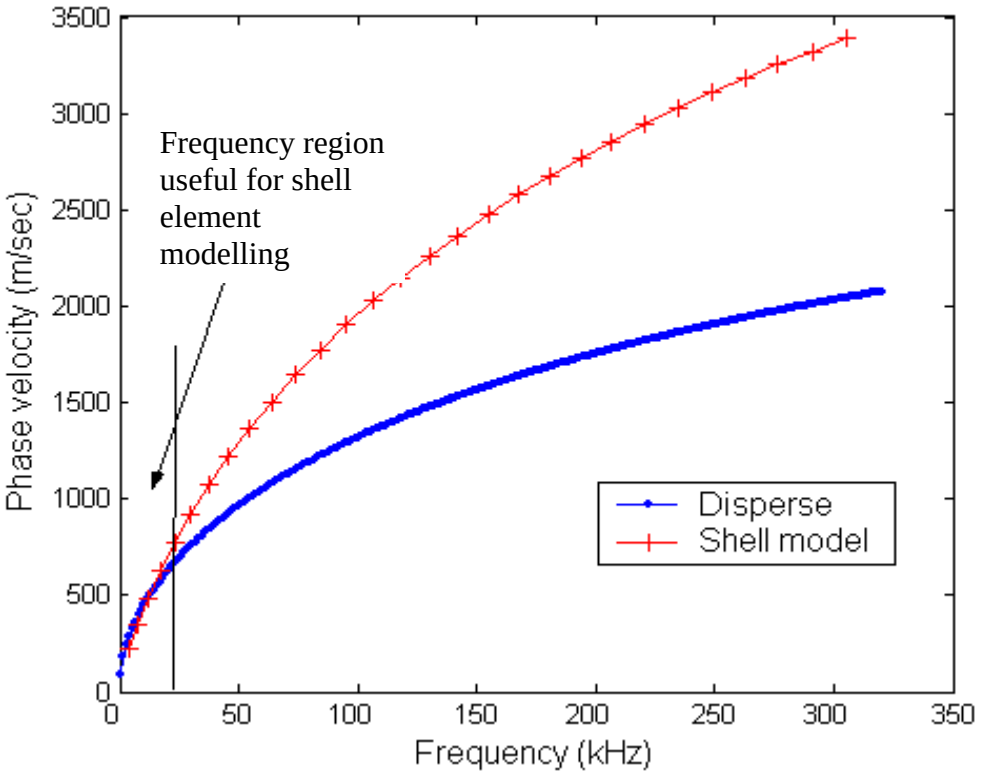

FIGURE A.3: Frequency range of accuracy of shell model for a 1mm steel plate

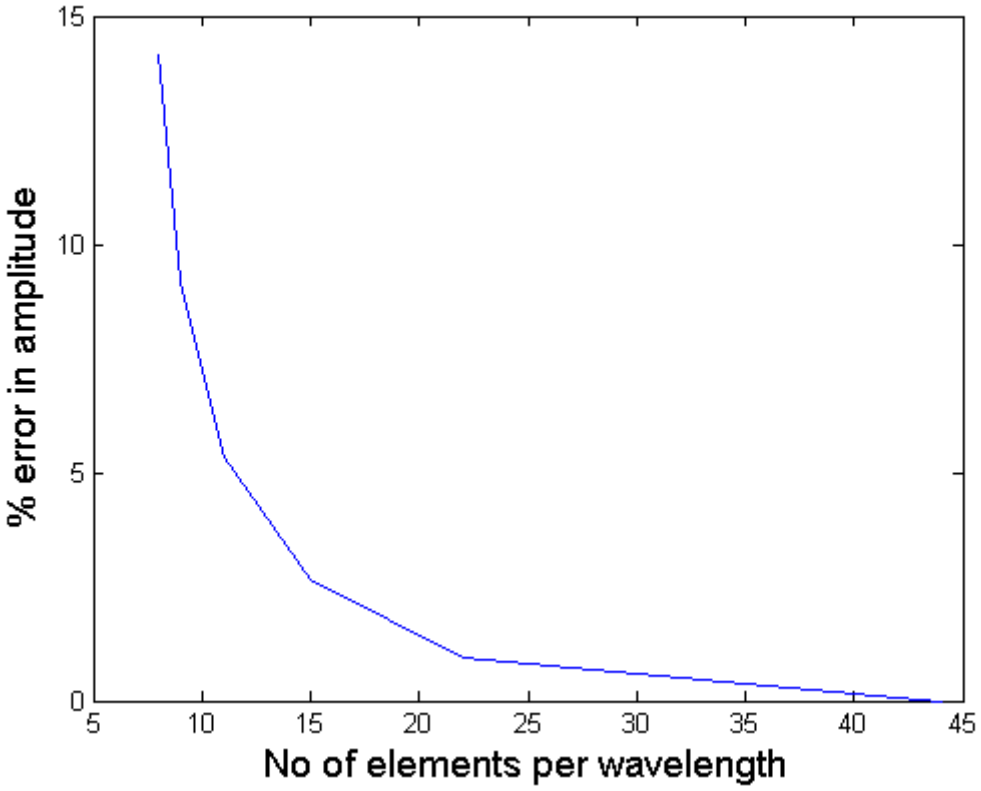

FIGURE A.4: Mesh convergence study of shell elements: percentage error in amplitude vs. number of elements per wave length plot

References

1. Ong, P.S., Anderson, W. L., Cook, B.D., and Subramanyan, R., A *novel x-ray technique for inspection of steel pipes.* Journal of Non-Ddestructive Evaluation, 1994. 13(4): p. 165-173.

2. Sun, Y.S., Qu, M.X., Si, J.T., Lu, C.T., Zhou, X.Y. and Atherton, D.L. *Improvements in remote-field eddy current probe structure.* Materials Evaluation, May 1992: p. 600-64.

3. Sun, Y., Jiatun Si Cooley, D., Han, H.C., Udpa, S., Lord, W., Minxing Qu., Meijuan Chen, Yang Zhao., *Efforts towards gaining a better understanding of the remote field eddy current phenomenon and expanding its applications.* IEEE Transaction on Magnetics, 1996. 32: p. 1589-1592.

4. Stalenhoef, J.H.J., Raad, J.A.D., *MFL and PEC Tools for Plant Inspection*. Insight, 2000, 42(2): p. 74-77.

5. Atherton, D.L., *Magnetic inspection is key to ensuring safe pipelines.* Oil and Gas Journal, 1989. 87(32): p. 52-61.

6. Plotnikov, A.C., *Stress effects and magnetic NDE methods for pipeline inspection: a study of interacting defects.* Insight, 2002. 44(2): p. 74-79.

7. Rose, J.L., *Recent Advances In Guided Wave NDE*. IEEE Ultrasonic Symposium, 1995: p. 761-770.

8. Alleyne, D. and Cawley, P. *Long range propagation of Lamb waves in chemical plant pipework*, Materials Evaluation. 1997. p. 504-508.

9. Lamb, H. *On waves in an elastic plate*. Proceedings of Royal Society of London Series A, 1917, 93(648): p. 114-128

10. Brekhovskikh, L.M., *Waves in layered media*. 1980, Academic Press, New York.

11. Rose, J.L., *Ultrasonic waves in solid media*. 1999, Cambridge University Press, Cambridge, U.K.

12. Lowe, M.J.S, *Matrix techniques for modelling ultrasonic waves in multilayered media.* IEEE Transactions on Ultrasonics, Ferroelectrics and Frequency Control, 1995. 42(4): p. 525-542.

13. Lowe, M.J.S., Pavlakovic, B.N. and Cawley, P. *Guided wave NDT of structures: a general purpose computer model for calculating waveguide properties*. Proceedings of Workshop on Structural Health Monitoring. 2001, p. 880

14. Wilcox, P., Lowe, M.J.S. and Cawley, P. *An EMAT array for the rapid inspection of large structures using guided waves*, Review of Progress in QNDE. 2003, p. 814-821.

15. Szilard, J., *Ultrasonic Testing*. 1980, New York: John Wiley & Sons.

16. Dalton, R.P., Cawley, P. and Lowe, M.J.S. *The potential of guided waves for monitoring large areas of metallic aircraft fuselage structure.* Journal of Non-Destructive Evaluation, 2001. 20(1): p. 29 - 46.

17. Dalton, R.P., Cawley, P. and Lowe, M.J.S. *Propagation of guided waves in aircraft structure*. Review of Progress in QNDE. 2003, p. 225-232.

18. Worlton, D., *Experimental confirmation of Lamb waves at megacycle frequencies.* Journal of Applied Physics, 1961. 32(6): p. 967-971.

19. Alleyne, D.N. and Cawley, P. *The interaction of Lamb waves with defects.* IEEE Transactions on Ultrasonics, Ferroelectrics and Frequency control, 1992. 39(3): p. 381-397.

20. Rose, J.L., Pelts, S.P. and Li, J. *Quantitative guided wave NDE.* Proceedings of the 15th World Conference on Non-Destructive Testing. 2001, p. 1 - 5.

21. Adams, R.D., Brownjohn, J.M.W. and Cawley, P. *The detection of defects on GRP lattice structures by vibration measurements.* NDT & E International, 1991. 24: p. 123-134.

22. Chimenti, D. E. and Safaeinili. A. *Exploiting guided waves for materials characterization in plates*. Proceedings of the 14th World Conference on Non-Destructive Testing. 1996, p. 237-240

23. Allin, J.M., Cawley, P and Lowe, M.J.S. *Adhesive disbond detection of automotive components using first mode ultrasonic resonance.* NDT & E International, 2003. 36: p. 503 - 514.

24. Dewen, P.N. and Cawley, P. *Ultrasonic determination of the cohesive properties of bonded joints by measurement of reflection coefficient and bondline transit time.* Journal of Adhesion, 1993. 40: p. 207-227.

25. Alleyne, D., *Rapid long range inspection of chemical plant pipe work using guided wave.* Insight, 2001. 43(2): p. 93 - 96.

26. Lowe, M.J.S., Alleyne, D.N. and Cawley, P. *Defect detection in pipes using guided waves.* Ultrasonics, 1998. 36: p. 147 - 154.

27. Cawley, P., *Practical long range guided wave testing: applications to pipes and rails.* Materials Evaluation, 2003(January): p. 66 - 74.

28. Alleyne, D.N., Cawley, P., Lank, A. M. and Mudge, P. J., *The Lamb wave inspection of chemical plant pipework.* Review of Progress in QNDE, 1997. 16: p. 1269-1276.

29. Rose, J.L., Jiao, D., and Spanner, J. *Ultrasonic guided wave NDE for piping.* Materials Evaluation, 1996: p. 1310 - 1313.

30. Barshinger, J., Rose, J.L. and Avioli, M.J. G*uided wave resonance tuning for pipe inspection.* Journal of Pressure Vessel Technology, 2002. 124: p. 303 - 310.

31. Cawley, P., *The rapid non-destructive inspection of large composite structures.* Composites, 1994. 25: p. 351-357.

32. Lowe, M.J.S., *Plate waves for the NDT of diffusion bonded titanium*, PhD thesis, 1993, Mechanical Engineering, Imperial College of Science Technology and Medicine, London.

33. Lowe, M., G. Neau, and Deschamps, M. *Properties of guided waves in composite plates and implications for NDE*. Review of Progress in QNDE, 2004. 23: p. 214-221.

34. Wilcox, P.D., Cawley, P and Lowe, M.J.S. *A signal processing technique to remove the effect of dispersion from guided wave signals*. Review of progress in QNDE, 2001, p. 555-562.

35. Wilcox, P., Cawley, P and Lowe, M.J.S. *Mode and transducer selection for long range lamb wave inspection.* Journal of Intelligent Material Systems and Structures, 2001. 12(August): p. 553-565.

36. Alleyne, D., *The use of guided waves for rapid screening of chemical plant pipework.* Journal of the Korean Society for Nondestructive Testing, 2002. 22(6): p. 589 - 598.

37. Sargent, J.P., *Corrosion detection in welds and heat-affected zones using ultrasonic Lamb waves*, Insight. 2006. p. 160-164.

38. Huber, J.C., G*etting down to the basics of fiber-optic transmission.* R&D Magazine, 1994: p. 115-118.

39. Per, W., Bertil, G., *High-order difference methods for waves in discontinuous media.* Journal of Computational and Applied Mathematics, 2005. 192(1): p. 142-147.

40. Tadeu, A., Godinhoa, L., Antónioa, J. and Mendesa, P.A, *Wave propagation in cracked elastic slabs and half-space domains—TBEM and MFS approaches.* Engineering Analysis with Boundary Elements, 2007: 31(7). p. 819-835

41. Kuhlemeyer, R.L., *Finite element method accuracy for wave propagation problems.* Journal of the Soil Mechanics and Foundations Division, 1973. 9(5): p. 421-427.

42. Jianga, L., *A finite element solution of plane wave propagation in inhomogeneous linear viscoelastic solids.* Journal of Sound and Vibration, 1995. 184(3): p. 429-438.

43. Zienkiewicz, O.C., *The Finite Element Method*. 1977, London: McGraw Hill.

44. Bathe, K.J., *Finite element procedures*. 1996: Englewood Cliffs, New Jercey: Prentice Hall.

45. Alleyne, D.N. and Cawley, P. *The quantitative measurement of Lamb wave interaction with defects*, Ultrasonics International. 1991. p. 491-494.

46. Wrobel, L.C., *The Boundary Element Method*. 2002: Wiley; 1 edition.

47. Ihlenburg, F., *Finite Element Analysis of Acoustic Scattering*. 1 edition. 1998: Springer.

48. Alleyne, D.N., *The nondestructive testing of plates using ultrasonic lamb waves*, PhD thesis, 1991, Mechanical Engineering, Imperial College of Science Technology and Medicine: London.

49. Demma, A., Cawley, P and Lowe, M.J.S. *Scattering of the SH0 mode from geometrical discontinuities in plates*, Review of Progress in QNDE, 2003, p. 149-156.

50. Auld, B.A., *Acoustic fields and waves in solids*., 1990, Florida: Robert E. Krieger Publishing Company.

51. Graff, K.F., *Wave Motion in Elastic Solids*. 1975, Oxford: Clarendon Press.

52. Drozdz, M., Cawley, P., *Modeling bulk and guided wave propagation in unbounded elastic media using absorbing layers in commercial FE packages*, Review of Progress in QNDE, 2007, p. 87-94.

53. Hosten, B. and Castings, M.. *Validation at lower frequencies of the effective elastic constants measurements for orthotropic composite materials*. Review of Progress in QNDE, 2007,

54. Givoli, D., *High-order local non-reflecting boundary conditions: a review*. Wave Motion, 2004. 39(4): p. 319-326.

55. Bettess, P., *Infinite elements*. 1992: Penshaw Press.

56. Miller, A.J. *The application of integral equation methods to the numerical solution of some exterior boundary value problems*. Proceeding of the Royal Society of London Series A 323. 1971, p. 965-977

57. Givoli, D, *Non-reflecting boundary conditions for elastic waves*. Wave Motion, 1990. 12: p. 261-279.

58. Liu G.R., *A non-reflecting boundary for analyzing wave propagation using the finite element method.* Finite Elements in Analysis and Design, 2003. 39(5): p. 403-417.

59. Israeli, M., Orszag, S.A, *Approximation of radiation boundary conditions.* Journal of Computational Physics, 1981. 41: p. 115-135.

60. Sochacki, J.R.K., George, J., Fletcher, W.R., and Smithson, S., *Absorbing boundary conditions and surface waves.* Geophysics, 1987. 52(1): p. 60-71.

61. Berenger, J.P., *A perfectly matched layer for the absorption of electromagnetic waves,* Journal of Computational Physics, 1994. 114(2): p. 185-200.

62. Drodz, M., *Personal communication with Drodz M, NDT Lab, Imperial College London*. 2006.

63. Sommerfeld, A., *Partial Differential Equations in Physics*. 1949, New York: Academic press.

64. Liu, G.R., *A non-reflecting boundary for analyzing wave propagation using the finite element method,*. Finite Elements in Analysis and Design, 2003. 39(5-6): p. 403 - 417.

65. Madja, B.E., *Radiation boundary conditions for acoustic and elastic waves.* Communications in. Pure and Applied. Mathematics., 1979. 32(2): p. 313–357.

66. Bayliss, A., *Radiation Boundary Conditions for Wave-Like Equations.* Communications in. Pure and Applied. Mathematics., 1980. 33: p. 707-725.

67. Givoli, J.B., *Exact Non-reflecting Boundary Conditions.* Journal of computational physics, 1989. 82(172-192).

68. Givoli, D., *High-order nonreflecting boundary conditions without high-order derivatives.* Journal of Computational Physics, 2001. 170(2): p. 849-870.

69. Pavlakovic, B.N., *Leaky guided ultrasonic waves in NDT*, PhD thesis, 1998, Mechanical Engineering, Imperial College of Science Technology and Medicine: London.

70. *ABAQUS v6.6 Analysis User's Manual*. 2005: http://www.simulia.com/.

71. Lowe, M.J.S., *Matrix techniques for modeling ultrasonic waves in multilayered media.* IEEE Transactions on Ultrasonics, Ferroelectrics and Frequency control, 1995. 42(4): p. 525 - 542.

72. Lowe, M.J.S., *Plate waves for the NDT of diffusion bonded titanium*, PhD thesis, 1992, Mechanical Engineering, Imperial College of Science Technology and Medicine: London.

73. Shuvalov, A.L., Poncelet, O., and Deschamps, M., *General formalism for plane guided waves in transversely inhomogeneous anisotropic plates.* Wave Motion, 2004. 40(4): p. 413-426.

74. Vinod, K.G., *Free vibration and wave propagation analysis of uniform and tapered rotating beams using spectrally formulated finite elements.* International Journal of Solids and Structures, 2007. 44(18-19): p. 5875-5893.

75. Doyle, J.F., *A spectrally formulated finite element for longitudinal wave propagation.* International Journal of Analytical and Experimental Modal Analysis, 1988. 3: p. 1-5.

76. Krawczuk, M.P., *Analysis of longitudinal wave propagation in a cracked rod by the spectral element method.* Computers & Structures, 2002. 80(24): p. 1809-1816.

77. Doyle, J.F., *Spectrally formulated finite element for flexural wave propagation in beams.* International Journal of Analytical and Experimental Modal Analysis, 1990. 5: p. 13-23.

78. Desceliers, C., Grimal, Q., Haiat, G. and Naili, S., *A time-domain method to solve transient elastic wave propagation in a multilayer medium with a hybrid spectral-finite element space approximation.* Wave Motion, 2007: p. In Press.

79. Gopalakrishnan, A.C.a.S., *A spectrally formulated finite element for wave propagation analysis in layered composite media.* International Journal of Solids and Structures, 2004. 41(18-19): p. 5155-5183.

80. Pawel Kudela, A.Z., Marek Krawczuk and Wieslaw Ostachowicz, *Modelling of wave propagation in composite plates using the time domain spectral element method.* Journal of Sound and Vibration, 2007. 302(4-5): p. 774-777.

81. Gopalakrishnan, D.R.M.a.S., *A spectral finite element for analysis of wave propagation in uniform composite tubes.* Journal of Sound and Vibration, 2003. 268(3): p. 429-463.

82. Oliveira, S.P., Seriani, G., *Dispersion analysis of spectral element methods for elastic wave propagation.* Wave Motion, 2007: p. In Press.

83. Chakraborty, A., *Wave propagation in anisotropic media with non-local elasticity.* International Journal of Solids and Structures, 2007. 44(17): p. 5723-5741.

84. Ostachowicz, W.M., *Damage detection of structures using spectral finite element method.* Computers & Structures, 2007: p. In Press.

85. P. Kudela, M.K.a.W.O., *Wave propagation modelling in 1D structures using spectral finite elements.* Journal of Sound and Vibration, 2007. 300(1-20): p. 88-100.

86. Dong, R.N.a.S., *High frequency vibrations and waves in laminated orthotropic plates.* Journal of Sound and Vibration, 1973. 30(1): p. 33-44.

87. Dong, S. and R. Nelson, *On natural vibrations and waves in laminated orthotropic plates.* Journal of Applied Mechanics, 1972: p. 739-745.

88. Huang, S.D.a.K., *Edge vibrations in laminated composite plates.* Journal of Applied Mechanics, 1985. 52: p. 433–438.

89. Xi, Z.C., Liu, G.R., Lam, K.Y., and Shang, H.M, *Dispersion and characteristic surfaces of waves in laminated composite circular cylindrical shells.* Journal of the Acoustical Society of America., 2000. 108(5): p. 2179-2186.

90. Jose M. Galan, R.A., *Numerical simulation of Lamb wave scattering in semi-infinite plates.* International Journal for Numerical Methods in Engineering, 2001. 53(5): p. 1145 - 1173.

91. Abascal, J.M.G.a.R., *Lamb mode conversion at edges. A hybrid boundary element–finite-element solution.* The Journal of the Acoustical Society of America, 2005. 117(4): p. 1777-1784.

92. Shorter, P.J., *Wave propagation and damping in linear viscoelastic laminates.* The Journal of the Acoustical Society of America, 2004. 115(5): p. 1917-1925.

93. Ivan Bartoli, A.M., Francesco Lanza di Scalea, and Erasmo Viola, *Modeling wave propagation in damped waveguides of arbitrary cross-section.* Journal of Sound and Vibration, 2006. 295(3-5): p. 685-707.

94. Weaver, R.L., Damljanovic, V., *Propagating and evanescent elastic waves in cylindrical waveguides of arbitrary cross section.* The Journal of Acoustical Society of America, 2004. 115(4): p. 1572-1581.

95. M. V. Predoi, M.C., B. Hosten, C. Bacon, *Wave propagation along transversely periodic structures.* Journal of the Acoustical Society of America, 2007. 121(4): p. 1935-1944.

96. Wilcox, P., Evans, M., Dilient, O., Lowe, M. and Cawley, P. *Dispersion and excitability of guided acoustic waves in isotropic beams with arbitrary cross section*. Review of Progress in QNDE. 2002, p. 203-210

97. Castaings, M., *Personal Communication with Dr Michel Castings, University of Bordeaux, France*. 2006.

98. Fan, M.Z., *Personal Communication with Mr Zheng Fan, a PhD student in the NDT Lab, Imperial College, London.* 2007.

99. Castaings, M., Lowe, M..J.S, *Finite element model for waves guided along solid systems of arbitrary section coupled to infinite solid media.* Journal of Acoustical Society of America, In Press.

100. Simonetti, F., *Sound propagation in lossless waveguides coated with attenuative materials*, PhD Thesis, 2003, Department of Mechanical Engineering, Imperial College of Science Technology and Medicine: London.

101. Simonetti, F. and Cawley, P. *On the nature of shear horizontal wave propagation in elastic plates coated with viscoelastic materials,*

Proceedings of the Royal Society of London. Series A, Mathematical, Physical and Engineering Sciences, 2004. 460: p. 2197-2221.

102. Simonetti, F., *Lamb wave propagation in elastic plates coated with viscoelastic materials.* Journal of the Acoustical Society of America, 2004. 115(5): p. 2041-2053.

103. Simonetti, F. and Cawley, P., *A guided wave technique for the characterisation of highly attenuative viscoelastic materials.* Journal of Acoustical Society of America, 2003. 114(1): p. 158 - 165.

104. Diligent, O., Lowe, M.J.S., Cawley, P. and Wilcox, P., *Reflection of the S0 lamb mode from a part-depth circular defect in a plate, when the incident wave is created by a small source,* Review of progress in QNDE, 2003, p. 197-204

105. Aristegui, Cawley, P and Lowe, M.J.S., *Reflection and mode conversion of guided waves at bends in pipes*. Review of progress in QNDE, 2000. p. 209-216

106. Demma, A., Cawley, P and Lowe, M.J.S., *Scattering of the fundamental shear horizontal mode from steps and notches in plates.* Journal of Acoustical Society of America, 2003. 113(4): p. 1880-1891.

107. Demma, A., et al., *The reflection of guided waves from notches in pipes: a guide for interpreting corrosion measurements.* NDT&E International, 2004. 37: p. 167-180.

108. Demma, A.C., Cawley, P and Lowe, M.J.S., *Mode conversion of longitudinal and torsional guided modes due to pipe bends,* Review of Progress in QNDE, 2001, p. 172-179.

109. Pialucha, T.P, *The reflection coefficient from interface layers in adhesive joints*. PhD Thesis, 1992, Department of Mechanical Engineering, Imperial College of Science Technology and Medicine: London.

110. Demma, A., Cawley, P. and Lowe, M.J.S., *The reflection of the fundamental torsional mode from cracks and notches in pipes.* Journal of Acoustical Society of America, 2003. 114(2): p. 611-625.

111. Diligent, O., M.J.S. Lowe, and P. Cawley, *Reflection and scattering of the S0 Lamb mode from 3-D circular defects in plates.* Review of progress in QNDE, 2002. 21: p. 231 - 238.

112. Alleyne, D., Cawley, P and Lowe, M.J.S.. *The inspection of chemical plant pipework using lamb waves: defect sensitivity and field experience*. Review of progress in *QNDE*. 1996. p.1859-1866

113. Beard, M.D., Cawley, P and Lowe, M.J.S., *Development of a guided wave inspection technique for rock bolts.* Insight, 2002. 44(1): p. 19 - 25.

114. Adams, R.D. and Cawley, P., *A review of defect types and nondestructive testing techniques for composites and bonded joints.* NDT International, 1988. 21(4): p. 208-221.

115. Beard, M.D., Lowe, M.J.S and Cawley, P., *Inspection of Rockbolts using Guided Ultrasonic Waves*. *Review of Progress in QNDE*. 2001. p. 1156-1163

116. Rose, J.L., Avioli, M.J and Song, W., *Application and potential of guided wave rail inspection.* Insight, 2002. 44(6): p. 353 - 358.

117. Koshiba, M., Karakida, S. and Suzuki, M., *Finite-element analysis of lamb wave scattering in an elastic plate waveguide.* IEEE Transactions On Sonics And Ultrasonics, 1984. SU-31(1): p. 18-25.

118. Alleyne, D.N., Lowe, M.J.S and Cawley, P., *The reflection of guided waves from circumferential notches in pipes.* Journal of Applied Mechanics, 1998. 65: p. 635 - 641.

119. Demma, A., *The interaction of guided waves with discontinuities in structures*, PhD thesis, 2003, Department of Mechanical Engineering, Imperial College of Science Technology and Medicine: London.

120. Diligent, O., and Lowe, M.J.S., *Reflection of the s_0 Lamb mode from a flat bottom circular hole.* Journal of the Acoustical Society of America, 2005. 118(5): p. 2869-2879.

121. Mindlin, R.D., *Influence of rotatory inertia and shear flexural motions of isotropic, elastic plates.* Journal of Applied Mechanics, 1951: p. 31-38.

122. Mindlin, R.D. *Waves and vibrations in isotropic, elastic plates.* First Symposium on Naval Structural Mechanics. 1960: 123(4), p. 417-420.

123. Mindlin, R.D. and Medick, M.A., *Extensional vibrations of elastic plates.* Journal of Applied Mechanics, 1959: p. 561 - 569.

124. Mindlin, R.D., Schacknow, A. and Deresiewicz, H., *Flexural vibrations of rectangular plates.* Journal of Applied Mechanics, 1956: p. 430-436.

125. Pialucha, T., Guyott, C.C.H and Cawley, P., *Amplitude Spectrum Method For The Measurement Of Phase Velocity.* Ultrasonics, 1989. 27: p. 270-279.

126. Juluri, N., Cawley, P., Lowe, M.J.S., *Guiding of ultrasound by a welded joint in a plate*, Review of Progress in QNDE. 2007. p. 1079-1086

127. Fan, M.Z., *Personal Communication with Mr Zheng Fan, PhD transfer report, NDT Lab, Mechanical Engineering, Imperial College, London.* 2007.